The PomXYZ cell division regulators self-organize on the nucleoid to position cell division at midcell in the rod-shaped bacterium *Myxococcus xanthus*

Dissertation

zur Erlangung des akademischen Grades
des Doktors der Naturwissenschaften
(Dr.rer.nat.)

dem Fachbereich Biologie
der Philipps-Universität Marburg
vorgelegt

von
Dominik Schumacher
aus Arnsberg

Marburg (Lahn), Dezember 2015

Die Untersuchungen zur vorliegenden Arbeit wurden von Oktober 2011 bis August 2015 am Max-Planck-Institut für terrestrische Mikrobiologie unter der Leitung von Prof. Dr. MD Lotte Søgaard-Andersen durchgeführt.

Vom Fachbereich Biologie der Philipps-Universität Marburg

als Dissertation angenommen am 25.03.2015

Erstgutachter:	Prof. Dr. MD Lotte Søgaard-Andersen
Zweitgutachter:	Prof. Dr. Martin Thanbichler
Drittgutachter:	Prof. Dr. Hans-Ulrich Mösch
Viertgutachter:	Prof. Dr. Renate Renkawitz-Pohl
Fünftgutachter	Prof. Dr. Michael Bölker

Tag der mündlichen Prüfung: 31.03.2016

Die während der Promotion erzielten Ergebnisse wurden zum Teil in folgenden Originalpublikationen veröffentlicht:

Treuner-Lange, A., Aguiluz, K., van der Does, C., Gómez-Santos, N., Lenz, P., Harms, A., **Schumacher, D.**, Hoppert, M., Kahnt, J., Muñoz-Dorado, J. & Søgaard-Andersen, L. (2013). PomZ, a ParA-like protein, regulates Z-ring formation and cell division in *Myxococcus xanthus*. Mol. Microbiol. 87, 235-253.

Harms, A., Treuner-Lange, A., **Schumacher, D.** & Søgaard-Andersen, L. (2013). Tracking of chromosome and replisome dynamics in *Myxococcus xanthus* reveals a novel chromosome arrangement. PLoS Genet. 9, e1003802.

Schumacher, D., Bergeler, S., Harms, A., Vonck, J., Huneke, S., Frey, E., & Søgaard-Andersen, L. (2016). PomXYZ proteins self-organize on the nucleoid to regulate cell division (in preparation).

Meiner Familie

Table of contents

Abbreviations

ATP/ADP	Adenosin tri-/diphosphate
a.u.	Arbitrary unit
BACTH	Bacterial Adenylate Cyclase-based Two Hybrid
bp	Base pair
CTT	Casitone Tris medium
DIC	Differential interference contrast
EDTA	Ethylenediaminetetraacetic acid
eYFP	Enhanced yellow fluorescent protein
FRAP	Fluorescence recovery after photobleaching
GFP	Green fluorescent protein
GTP/GDP	Guanosine tri-/diphosphate
h	Hour
HEPES	2-[4-(2-hydroxyethyl) piperazin-1-yl] ethanesulfonic acid
IPTG	Isopropyl β-D-1-thiogalactopyranoside
Km	Kanamycine
l	Litre
mCherry	Monomeric Cherry (red fluorescent protein)
mDa	Megadalton
min	Minute
kDa	Kilodalton
m-	milli-
µ-	micro-
M	Molarity (mol * l^{-1})
n-	nano-
pH	Negative decimal logarithm of the hydrogen ion activity
SDS-page	Sodium dodecyl sulfate polyacrylamide gel electrophoresis
sec	Second
Tc	Tetracycline
TEMED	*N*,*N*,*N*′,*N*′-Tetramethylethane-1,2-diamine
TEM	Transmission electron microscopy
Tris	2-Amino-2-hydroxymethyl-propane-1,3-diol
v/v	Volume per volume
w/v	Weight per volume
WT	Wild type
X-gal	5-Brom-4-chlor-3-indoxyl-β-D-galactopyranosid

1 Abstract

Accurate positioning of the division site is essential to produce daughter cells with the correct size, and chromosome content. Generally, the first known event of bacterial cell division is the accumulation of FtsZ at the incipient cell division site to form the circumferential, ring-like structure Z-ring. In bacteria, positioning of the division site occurs at the level of formation of the FtsZ-ring. While the cytokinesis machinery is conserved throughout bacteria, the mechanisms to position the Z-ring are diverse. The rod-shaped social bacterium *Myxococcus xanthus* divides precisely by binary fission at midcell but it lacks all the known systems that regulate Z-ring formation in other bacteria. Instead two novel regulators PomX and PomY together with the ParA ATPase PomZ stimulate formation and positioning of the Z-ring at midcell.

PomXYZ interact and form a complex that associates with the nucleoid to translocate towards the mid-nucleoid, which coincides with midcell before nucleoids have segregated, by biased random motion. At the mid-nucleoid, at midcell, the PomXYZ complex undergoes constrained motion, not leaving midcell.

Our experimental data show that cluster localization at midcell is independent of FtsZ and that clusters localize at midcell before Z-rings form. By contrast cluster localization at midcell depends on the ATPase PomZ, its associated ability to hydrolyze ATP and its ability to bind non-specifically to DNA. ATP-hydrolysis by PomZ is stimulated by PomX as well as by PomY in the presence of DNA, demonstrating that PomZ is the first ParA ATPase in which ATP-hydrolysis is stimulated by two ATPase activating proteins (AAP's). We show that interference with ATP-hydrolysis, by mutational analysis, affects cluster translocation towards midcell. PomZ on its own interacts with the nucleoid and recruits a complex of PomX and PomY to the nucleoid. By FRAP experiments we show that PomZ is highly dynamic in the PomXYZ complex, where ATP-hydrolysis takes place and on the nucleoid.

Our experimental data support a flux-based mechanism for the positioning of the PomXYZ complex by the ParA ATPase PomZ. In this model, the diffusive random PomZ dynamics on the nucleoid result in diffusive fluxes of PomZ on the nucleoid from either side into the PomXYZ cluster. These fluxes scale with the cellular asymmetry of the cluster within the cell and convert this cellular asymmetry into a PomZ concentration gradient over the PomXYZ complex. This gradient together with the PomZ-associated ATP-hydrolysis translocates the complex towards the higher concentration of PomZ to midcell. At midcell, which coincides with middle of the nucleoid, the diffusive PomZ fluxes equalize, resulting in constrained motion. To understand the molecular details of ATP-hydrolysis, a previously identified *pomX*^{K13A,R15A} mutant was analyzed for its defect in PomXYZ-dependent positioning of the cell division site. Our *in vivo* and *in vitro* data show that the PomX$^{K13A;R15A}$ variant has a defect in stimulating PomZ ATP-hydrolysis, strongly suggesting that the N-terminal part of PomX interacts with PomZ to stimulate ATP-hydrolysis, similar to other ATPase activating proteins.

In summary we identified two novel cell division regulators that work in concert with PomZ to position and promote cell division at midcell. Our data provides insights into the function of ParA-ATPases, which in this case is PomZ, and reveal that the PomXYZ system is a novel system that positions cell division at midcell most likely by recruiting the Z-ring to the incipient cell division site.

2 Zusammenfassung

Die genaue Positionierung der Zellteilungsebene ist von größter Wichtigkeit um Tochterzellen von normaler Größe und komplettem genetischen Material zu produzieren. Erstes Anzeichen einer kommenden Zellteilung ist die Akkumulation von FtsZ in der erscheinenden Zellteilungsebene. In Bakterien wird die Positionierung der Zellteilungsebene auf der Ebene der Produktion und der Positionierung des FtsZ-Rings reguliert. Während der Multi-Protein-Komplex, der die Zellteilung ausführt, höchst konserviert ist unter allen bekannten Bakterien, sind die Mechanismen, die die Zellteilungsebene positionieren häufig unterschiedlich und nur wenig verstanden. In the letzten Jahren wurden viele neue Mechanismen entdeckt, um die Produktion des Z-ringes zeitlich und räumlich zu regulieren und auf die Zellmitte zu beschränken.

Das Stäbchen-förmige, soziale Bakterium *Myxococcus xanthus* teilt sich präzise in der Zellmitte in einem Prozess der binäre Zellteilung genannt wird, besitzt aber keine, der aus anderen Bakterien bekannten Systeme, um die Positionierung und die Produkion des Z-Rings zu regulieren. Stattdessen haben wir zwei neue Zellteilungsregulatoren entdeckt, die zusammen mit der ParA-ähnlichen ATPase PomZ die Formierung des Z-Rings verstärken und dessen Positionierung regulieren. PomXY und PomZ bilden einen intrazellulären Komplex, der selbst-organisierend ist und sich in *M. xanthus* mit dem Kernäquivalent, dem Nukleoid, assoziiert. Dieser Komplex bewegt sich in einer zufälligen, aber gerichteten Bewegung zu dessen Mitte, die mit der Zellmitte übereinstimmt, solange die Chromosomen noch nicht voneinander segregiert wurden. Angekommen in der Mitte des Nukleoids verändert sich die Bewegung des Komplexes in eine eingeschränkte Bewegung und der Komplex verlässt die Mitte nicht mehr. Unsere experimentellen Daten zeigen, dass die Bewegung des Komplexes in die Zellmitte unabhängig von der Anwesenheit von FtsZ ist und zudem, dass sich PomXYZ Komplexe in der Zellmitte positionieren bevor sich ein FtsZ-Ring gebildet hat. Die Positionierung des PomXYZ Komplexes in der Zellmitte ist von der ATPase PomZ abhängig und von dessen Fähigkeit ATP zu hydrolysieren und unspezifisch mit DNA zu interagieren. Unsere Daten zeigen, dass PomX und PomY die ATP-Hydrolyse von PomZ in Anwesenheit von unspezifischer DNA stimulieren, was in der Zelle der Situation im PomXYZ Komplex ähnelt. Damit zeigen wir, dass PomZ die erste ParA-ähnliche ATPase ist, die zwei ATPase-aktivierende Partner Proteine besitzt. Wir zeigen weiterhin durch die Erzeugung von gezielten Mutanten, dass die Bewegung des PomXYZ Komplexes in die Zellmitte von der ATP-Hydrolyse von PomZ abhängig ist. PomZ interagiert mit dem Nucleoid und durch FRAP Experimente konnte gezeigt werden, dass PomZ sehr dynamisch auf der DNA ist und sich durch laterale Diffusion über die DNA bewegt. Des Weiteren zeigen FRAP Experimente, dass ein dynamischer Austausch von PomZ Molekülen im PomXYZ Komplex stattfindet in dem auch ATP-Hydrolyse in der Zelle stattfindet. Unsere Daten deuten auf einen PomZ-Fluss basierenden Mechanismus hin, für die Bewegung und Positionierung des PomXY Komplexes auf der DNA. In diesem Modell skaliert der diffuse PomZ-Fluss auf jeder Seite des PomXYZ Komplexes auf dem Nukleoid mit der zellulären Asymmetrie des Komplexes und wandelt diese Asymmetrie in einen lokalen PomZ Proteingradienten entlang des PomXYZ Komplexes um. Basierend auf der ATP-Hydrolyse von PomZ bewegt sich der Komplex in Richtung der höheren PomZ Konzentration zur Zellmitte. In der Mitte des Nukleoids angekommen gleicht sich der diffuse PomZ-Fluss auf den Seiten des Komplexes aus, was den PomZ Gradienten entlang des PomXYZ Komplexes ausgleicht und zu

einer zufälligen, aber eingeschränkten Bewegung in der Zellmitte führt. Um die molekularen Details der ATP-Hydrolyse von PomZ zu verstehen, wurde die kürzlich identifizierte *pomX*$^{K13A;R15A}$ Mutante auf ihren Defekt in der PomXYZ-abhängigen Positionierung der Zellteilungsebene hin überprüft. Unsere *in vivo* und *in vitro* Daten zeigen, dass das substituierte PomX$^{K13A;R15A}$ einen Defekt in der Aktivierung der ATP-Hydrolyse von PomZ zeigt. Das wiederum deutet stark darauf hin, dass der N-terminale Bereich von PomX mit PomZ interagiert um die ATP-Hydrolyse zu stimulieren.

Zusammengefasst haben wir zwei neue Zellteilungsregulatoren identifiziert, die in Verbindung mit der ParA-ähnlichen ATPase PomZ die Positionierung der Zellteilungsebene regulieren und Zellteilungen in der Mitte auf normaler Frequenz stimulieren. Unsere Daten anhand von PomZ geben neue Einsichten in die Funktionsweise von ParA-ähnlichen ATPasen und zeigen, dass das komplett neue PomXYZ System die Positionierung der Zellteilungsebene sehr wahrscheinlich durch die Rekrutierung des FtsZ-Rings in die Zellmitte reguliert.

3 Introduction

The bacterial cell cycle is composed of several steps from the duplication of the genetic material and its segregation to the daughter cells upon cell division. A basic but very complex challenge in each cell cycle is the spatio-temporal regulation of these processes. Therefore, special control mechanisms have been developed and identified that regulate the activity of these essential processes within the cellular space (Thanbichler, 2010, Treuner-Lange & Sogaard-Andersen, 2014).

3.1 The divisome and the positioning of the cell division site

3.1.1 FtsZ and the production of the divisome

A key process for most bacteria is cell division and its correct positioning, in order to generate viable progenies of similar size and the same chromosome content. To do so, bacterial cells have to cope with several critical events such as chromosome replication and segregation and couple these events temporally to the initiation of cell division (Thanbichler, 2010). In bacteria, cell division initiates with the accumulation of FtsZ (**f**ilamentous **t**emperature **s**ensitive) (Hirota *et al.*, 1968) at the incipient cell division site, where it polymerizes into the circumferential ring-like structure, called the Z-ring (Bi & Lutkenhaus, 1991). Formation of this Z-ring is essential to directly or indirectly recruit all the downstream components of the cell division machinery that in total form the divisome and thereby guides the localization and synthesis of the constriction (Addinall & Lutkenhaus, 1996). FtsZ is highly conserved among bacteria and is further found in a variety of archaea and in some eukaryotic organells like mitochondria and plastids. However, it is absent in *Chlamydiae* and *Planctomycetes*, suggesting that FtsZ-independent cell division mechanisms have evolved in bacteria (Bernander & Ettema, 2010). Several archaea use an FtsZ-unrelated system for cell division, called the Cdv system (for **c**ell **div**ision), which shows high similarity to the ESCRT machinery that is involved in endosomal sorting of proteins in eukaryotes (Lindas *et al.*, 2008, Raiborg & Stenmark, 2009, Samson *et al.*, 2008, Samson *et al.*, 2011).

Structurally, FtsZ is a prokaryotic homolog of eukaryotic tubulin and displays some similar features (Lowe & Amos, 1998). FtsZ is a GTPase like tubulin that polymerizes into GTP-dependent linear protofilaments and hydrolyses GTP in a cooperative and self-activating manner (Mukherjee & Lutkenhaus, 1994, Oliva *et al.*, 2004, Scheffers & Driessen, 2001). Although FtsZ forms a variety of GTP-dependent filamentous structures *in vitro,* the exact architecture of the Z-ring is still elusive. Recently, several different studies using a variety of experimental approaches, such as super-resolution microscopy, electron cryotomography and *in vitro* reconstruction, suggest that the Z-ring is not a continuous ring structure, but consists of several smaller filaments that attach to each other laterally (Holden *et al.*, 2014, Li *et al.*, 2007, Loose & Mitchison, 2014, Osawa *et al.*, 2008, Osawa *et al.*, 2009, Szwedziak *et al.*, 2014). However, the Z-ring is not a static structure but undergoes constant remodelling as observed by FRAP experiments (Anderson *et al.*, 2004, Stricker *et al.*, 2002). Although insights into the native structure were provided by different studies, if and how FtsZ generates force to constrict the cell envelope is debated and different mechanisms have been proposed (Li *et al.*, 2013, Osawa *et al.*, 2009, Szwedziak *et al.*, 2014). Because FtsZ is able to constrict vesicles, in a GTP-

hydrolysis dependent manner, the idea that FtsZ itself can provide force for the constriction is still persistent (Osawa *et al.*, 2008, Osawa *et al.*, 2009).

Generally, bacterial cell division initiates with the polymerization of FtsZ into the Z-ring at the incipient cell division site. This process is crucial for the formation of the cell division machinery, a macromolecular protein complex that is recruited to the cell division site by FtsZ to performe cytokinesis. This multiprotein complex, called the divisome, drives the constriction of the inner membrane, is required for the local production and the remodeling of the cell wall material and invaginates the outer membrane of Gram negative bacteria during cell division. The divisome consists of a set of core-components, which are conserved in nearly all bacteria and some additional accessory proteins that are less conserved. These proteins will be introduced in the following part.

In *E. coli*, *B. subtilis* and *C. crescentus* the assembly of the divisome occurs in two temporally splitted steps. First the production and stabilization of the Z-ring and secondly the consecutive recruitment of late divisome components, after a short period of maturation (Aarsman *et al.*, 2005, Gamba *et al.*, 2009, Goley *et al.*, 2011). Around a dozen essential core proteins are recruited to the divisome that together incorporate several functions during cell division. These functions can be assessed to the (1) stabilization of the Z-ring and its association with the inner membrane by FtsA (ZipA, ZapA FzlA) (Addinall & Lutkenhaus, 1996, Hale & de Boer, 1999, Small *et al.*, 2007, Goley *et al.*, 2010), (2) coordination of cell division with chromosome segregation by FtsK (Wu & Errington, 1994, Yu *et al.*, 1998a, Yu *et al.*, 1998b), (3) remodeling and synthesis of peptidoglycane by FtsW, FtsI and AmiC (Bernhardt & de Boer, 2003, Boyle *et al.*, 1997, Daniel *et al.*, 2000), (4) invagination of the outer membrane by the Tol-Pal complex (Yeh *et al.*, 2010) and finally (5) stabilization of the divisome components and activation of downstream activities by FtsQ, FtsL, FtsB and FtsN (Buddelmeijer & Beckwith, 2004, Gerding *et al.*, 2009, Moll & Thanbichler, 2009) (Figure 1 A).

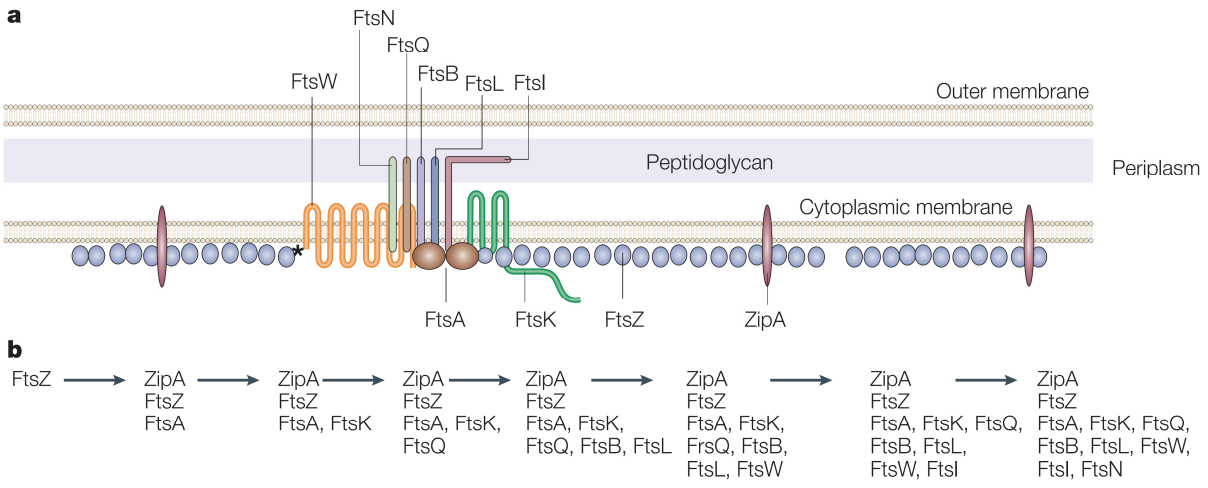

Figure 1: Model of the assembly oft he divisome in *E. coli*
(a) Model of the core components of the *E. coli* divisome. (b) Model of the assembly pathway of the *E. coli* divisome. (Margolin, 2005)

In *E. coli*, the Z-ring is connected to the inner cell membrane via two proteins, ZipA and FtsA that are both essential for cell division. In absence of one of them Z-rings are formed in between segregated nucleoids, but their abundance is reduced (Hale & de Boer, 1997, Pichoff & Lutkenhaus,

2002). Both bind to the extreme C-terminus of FtsZ (Hale & de Boer, 1999, Mosyak *et al.*, 2000). Because a substitution in FtsA bypasses the need for ZipA, FtsA is suggested to play the key role in stabilizing FtsZ at the inner cell membrane (Pichoff & Lutkenhaus, 2005). After the assembly of the Z-ring the downstream components of the divisome are recruited in an FtsZ/FtsA-dependent manner (Goehring *et al.*, 2006). In *E. coli* the recruitment event seems to be hierarchical, but proteins show a high degree of interdependency for their localization at the Z-ring (Figure 1 B) (Karimova *et al.*, 2005). The FtsZ/FtsA/ZipA complex recruits FtsK, the membrane bound DNA-translocase, which can rescue trapped DNA in the septum (Bigot *et al.*, 2005). Besides that, in *B. subtilis* a fundamental function of FtsK is the connection of cytokinesis to membrane invagination (Fleming *et al.*, 2010). FtsK is required for the recruitement of the FtsQ/B/L stability complex. The function of these components is not completely understood, however their presence is crucial for divisome maturation and they may function to link Z-ring formation to peptidoglycane synthesis (Goehring & Beckwith, 2005). FtsI and FtsW are part of the the peptidoglycane synthesis machinery with a specific function in septum specific synthesis of cell wall material (Typas *et al.*, 2012). Finally, the arrival of the late cell division protein FtsN at the divisome, which activates the function of FtsI in peptidoglycane synthesis and recruitment of other cell wall remodelling enzymes, was suggested to be the signal for triggering constriction of the divisome (Gerding *et al.*, 2009, Gerding *et al.*, 2007).

In addition to the essential core proteins of the divisome other non-essential accessory proteins were identified that stimulate Z-ring formation and bundle FtsZ filaments or promote their formation *in vitro*. Some of these proteins are ZapA and ZapB (Fts**Z** **a**ccessory **p**roteins) which were identified in *B. subtilis* and *E. coli*, respectively, FzlA and FzlC (**F**ts**Z** **l**ocalized proteins) from *C. crescentus* and SepF, which was found in *B. subtilis* (Ebersbach *et al.*, 2008b, Goley *et al.*, 2010, Gueiros-Filho & Losick, 2002, Hamoen *et al.*, 2006).

By contrast to the proteins that become incorporated into the divisome to fulfill essential functions within the process of cytokinesis a variety of other proteins influence FtsZ and its assembly into the Z-ring. In *B. subtilis* an integral membrane protein EzrA (**e**xtra **Z**-**r**ing protein **A**) was identified to negatively influence Z-ring formation. Lack of EzrA increases Z-ring formation and induces the formation of multiple Z-rings at midcell and the cell poles. Deletion in *ezrA* lowers the critical FtsZ concentration needed for Z-ring formation (Levin *et al.*, 1999). In line with this, overexpression of *ezrA* results in a block of Z-ring formation and by addition interferes with FtsZ filament formation *in vitro* (Haeusser *et al.*, 2007, Haeusser *et al.*, 2004). Based on the observation that EzrA colocalizes with FtsZ at the divisome it was suggested that it has an additional function *in vivo* by keeping the Z-ring dynamic (Haeusser *et al.*, 2007). Another Z-ring destabilizing factor is the ATPase subunit ClpX, the substrate recognition complex of the ClpXP protease complex (Haeusser *et al.*, 2009, Weart *et al.*, 2005). Overexpression of ClpX blocks cell division and Z-ring formation in *B. subtilis* by an unidentified mechanism and in *E. coli* ClpXP directly interacts with FtsZ to regulate polymer dynamics and to degrade FtsZ (Camberg *et al.*, 2009), suggesting that ClpXP modulates Z-ring assembly in a variety of bacteria (Weart *et al.*, 2005).

Systems have been identified that regulate Z-ring formation under certain stress conditions, such as nutrient limitation and DNA-damage (Bi & Lutkenhaus, 1993, Huisman & D'Ari, 1981, Mukherjee *et al.*, 1998, Weart *et al.*, 2007). *B. subtilis* was shown to utilize a novel mechanism to

couple Z-ring formation to growth rate by limiting Z-ring assembly under low nutrient conditions. The terminal sugar-transferase UgtP was identified to associate with the divisome, regulated by the availability of UDP-glucose (Weart *et al.*, 2007).

The DNA-damage induced SOS-response activates the expression of SulA in *E. coli* that inhibits Z-ring formation and promotes its disassembly once formed. SulA blocks FtsZ assembly into the Z-ring by blocking the C-terminal domain that is crucial for self-interaction of FtsZ, thereby sequestering FtsZ for its incorporation into the Z-ring (Cordell *et al.*, 2003, Huisman *et al.*, 1984, Justice *et al.*, 2000, Trusca *et al.*, 1998).

In summary the Z-ring is under the regulation of several factors that either promote or destabilize it *in vivo*. However, most of the mentioned factors work when the Z-ring is formed or only under certain stress conditions.

In comparison to these proteins, formation of the Z-ring and its localization, which dictates the localization of the cell division site, is under continuous regulation by systems that position the Z-ring at the correct place.

3.1.2 Spatial regulation of division site placement in bacteria

In the last years several systems have been identified and studied in details and were found to block Z-ring formation all over the cell body with the exception of the incipient cell division site (de Boer *et al.*, 1989, Thanbichler & Shapiro, 2006, Woldringh *et al.*, 1991, Woldringh *et al.*, 1990). On the other hand, recently several systems were shown to determine the position of the Z-ring and subsequent cell division by recruiting FtsZ to a specific localization (Fleurie *et al.*, 2014, Holeckova *et al.*, 2015, Willemse *et al.*, 2011). These systems will be discussed further in detail.

Correct positioning of the cell division site is a prerequisite to ensure faithful transmission of genetic information from the mother cell to the daughter cells, producing cells of correct size with similar chromosome content. The question how bacteria achieve the correct localization of the cell division site with high precision is still a fundamental question, as systems that regulate Z-ring localization are diverse compared to the cell division machinery itself. The best studied systems are the Min-system in *E. coli* and *B. subtilis* that work in concert with nucleoid occlusion, performed by SlmA and Noc, respectively, and the MipZ/ParB-system found in *C. crescentus*.

The first evidence that cell division site placement is regulated came from the identification of the “minicell” operon consisting of *minCDE*. Mutant’s carrying mutations in the *minCDE* operon are viable, but produce cells of variable sizes including minicells that lack DNA (de Boer *et al.*, 1991, de Boer *et al.*, 1989, de Boer *et al.*, 1992). The Min-system works around the negative regulator MinC that was shown to inhibit FtsZ assembly into filaments *in vitro* and to confer a cell division block if overexpressed *in vivo* (Hu & Lutkenhaus, 1999, Hu *et al.*, 1999). MinC is a cytoplasmic protein that inhibits cell division throughout the cell body resulting in a strong filamentation phenotype, when expressed alone (de Boer *et al.*, 1992). MinC interacts with MinD and is sequestered away from the cytoplasm to the cell membrane by the ATP-dependent membrane association of MinD (de Boer *et al.*, 1991). This membrane association of dimeric MinD is mediated via a flexible amphipathic helix in the MinD C-terminus (Szeto *et al.*, 2003, Szeto *et al.*, 2002). Nevertheless, sequestering MinC from the

cytoplasm to the membrane does not form a functional Min-system. Spatial specificity is given by the so-called topology-factor MinE. MinE is recruited to the membrane by MinD-ATP and induces the dynamic oscillatory movement of the MinD-MinC complex from pole to pole. MinE forms a ring-like structure called the E-ring, accumulating at the edge of the MinD-MinC zone that extents from the pole (Raskin & de Boer, 1997). By stimulating ATP-hydrolysis of MinD, MinE chases MinD off the membrane together with the MinC inhibitor. By some mechanism MinD-MinC associate again with the membrane at the most distant location, at the opposite cell pole, and together recruit MinE (Figure 2). By this polar recruitment of the MinCD inhibitory complex and its MinE induced pole-to-pole oscillation, the highest concentration of the cell division inhibitor complex over time occurs at the cell poles where cell division is inhibited. The lowest concentration, on the other hand, is at midcell, creating a zone that is permissive to Z-ring formation (Raskin & de Boer, 1999b, Hu & Lutkenhaus, 1999, Hu & Lutkenhaus, 2001, Raskin & de Boer, 1999a).

Similarly, the Min-system was also found in a variety of other bacteria and was observed to inhibit polar cell divisions in *B. subtilis.* However, the mechanism to achieve this was shown to be different. While the *E. coli* Min-system consists of three proteins MinCDE, in *B. subtilis* the Min-system lacks a MinE homolog, but incorporates DivIVA and the connector protein MinJ (Bramkamp *et al.*, 2008, Marston *et al.*, 1998). The function of MinE in *B. subtilis* is at least partially fulfilled by DivIVA, as it binds to negatively curved membranes and recruits the MinCD inhibitor complex to the cell poles via MinJ (Lenarcic *et al.*, 2009, van Baarle & Bramkamp, 2010). In contrast to the oscillatory pole-to-pole dynamics in *E. coli*, the MinCD complex is stably attached to the cell poles, where it inhibits polar cell divisions (Bramkamp *et al.*, 2008, Edwards & Errington, 1997, Marston *et al.*, 1998, Patrick & Kearns, 2008). The MinCD/MinJ/DivIVA system in *B. subtilis* was recently analysed in detail by expression of fluorescently labeled versions of MinC under the control of its native promoter from the endogenous site (Gregory *et al.*, 2008). Contrarily to earlier observations the *B. subtilis* Min-proteins were found to predominantly localize to the incipient cell division site and MinC showed membrane associated, lateral motion towards the new midcell. Based on the Δ*minC* phenotype, which includes minicell formation at midcell, and based on its newly analysed localization it was suggested that MinC prevents multiple cell divisions at midcell, by promoting divisome disassembly during the late cell division (Gregory *et al.*, 2008, van Baarle & Bramkamp, 2010). These data suggest that despite the strong similarities of the Min-systems, the mode of action might be different from organism to organism.

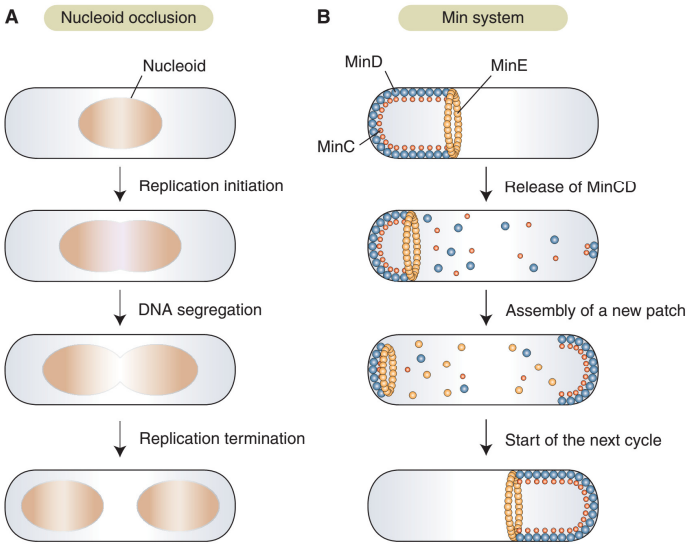

Figure 2: Model for the combined work of the Min-system and nucleoid occlusion in *E. coli*.
(A) SlmA (here shown in brownish colour) associates with the nucleoid asymmetrically, leaving the terminus region free from binding. During chromosome replication and segregation a SlmA-free nucleoid region is formed at midcell where the Z-ring can form. **(B)** Model for the dynamic localization of the Min-system in *E. coli*. MinD is indicated as blue dots, MinC as red dots and MinE as yellow dots. (Picture was obtained from Thanbichler, 2010)

The second regulation mechanism that works in concert with the Min-system in *E. coli* and *B. subtilis* is based on the finding that the nucleoid itself has influence on the correct positioning of the cell division site and was first analysed in *E. coli* (Woldringh *et al.*, 1991, Woldringh *et al.*, 1990). The idea was that by some mechanism the nucleoids were protected from dissection by the divisome by preventing Z-ring formation over the nucleoids. Further insights came when the first nucleoid occlusion proteins SlmA (**s**ynthetic-**l**ethal with **m**in) and Noc (**n**ucleoid **oc**clusion) were identified in *E. coli* and *B. subtilis*, respectively (Bernhardt & de Boer, 2005, Wu & Errington, 2004). Being not essential under normal growth conditions, deletion of either protein resulted in the dissection of the nucleoid if DNA-metabolism or cell division was perturbed (Bernhardt & de Boer, 2005, Wu & Errington, 2004). As seen by the name, a *slmA* deletion in absence of the Min-system resulted in a synthetic-lethal phenotype with strong cell elongation. It was suggested that the complete deregulation of FtsZ localization leads to inappropriate accumulations of FtsZ that only rarely assemble into a functional Z-ring to perform cell division (Bernhardt & de Boer, 2005). Both SlmA and Noc bind specific SlmA-binding (SBS) and Noc-binding sites (NBS) (Cho *et al.*, 2011, Tonthat *et al.*, 2013, Wu *et al.*, 2009). As observed by fluorescence microscopy SlmA and Noc both associate with the nucleoids *in vivo*, but their localization is not homogenous. Consistently, NBS and SBS are also not found homogenously over the nucleoid (Cho *et al.*, 2011, Wu *et al.*, 2009). Because NBS and SBS were found all over the chromosome with the exception of the terminus region it was suggested that nucleoid occlusion by SlmA and Noc, in addition to protecting the nucleoid, also gives temporal information to Z-ring formation, as they do not allow Z-ring formation early during replication but only late, shortly before nucleoids are segregated (Wu *et al.*, 2009). Indeed SlmA binds to DNA and it perturbs FtsZ filament formation *in vitro* (Bernhardt & de Boer, 2005, Tonthat *et al.*, 2013). Recent data suggest that DNA-bound Noc multiprotein complexes recruit DNA to the cell membrane and that this DNA-Noc-membrane interaction is crucial for correct function of the protein. Because of the inability to find an

interaction between Noc and FtsZ an indirect mechanism for the nucleoid occlusion effect was suggested, in which the decreased space between nucleoid and membrane, results in physical block of Z-ring formation over the nucleoids, thereby combining the function of the Min-system and nucleoid occlusion to guide Z-ring formation to midcell (Adams *et al.*, 2015).

In the asymmetrically dividing α-proteobacterium *C. crescentus* cell division is regulated and positioned at midcell by the work of MipZ, a MinD-related P-loop ATPase and its interaction partner ParB (Thanbichler & Shapiro, 2006). Unlike MinD, MipZ itself is a negative regulator of Z-ring formation as it enhances GTP-hydrolysis by FtsZ and leads to the formation of small curved FtsZ filaments *in vitro* (Thanbichler & Shapiro, 2006). Although MinD and MipZ are related proteins, their mode of action is different. MipZ cycles between a monomeric ADP-bound and a dimeric ATP-bound state (Kiekebusch *et al.*, 2012). Monomeric MipZ is recruited to the stalked cell pole by its interaction to ParB, which itself is kept, bound to the *oriC,* at the cell pole in a PopZ-dependent manner (Bowman *et al.*, 2010, Ebersbach *et al.*, 2008a, Thanbichler & Shapiro, 2006). It has been suggested that ParB stimulates the dimerization of MipZ, as it predominantly interacts with the monomeric form (Kiekebusch *et al.*, 2012). As a result of chromosome replication and the ParAB*S*-dependent chromosome segregation of the *oriC* to the opposite cell pole, where it is attached to a newly synthesized patch of PopZ (Bowman *et al.*, 2010, Ebersbach *et al.*, 2008a), MipZ follows ParB, localizing at both cell poles (Thanbichler & Shapiro, 2006). Importantly MipZ does not only localize in a cluster at the cell poles but forms a gradient, with the highest concentration of MipZ at the poles, extending towards midcell (Figure 3) (Kiekebusch *et al.*, 2012, Thanbichler & Shapiro, 2006). The molecular details leading to the steady-state gradient of MipZ have been identified recently (Kiekebusch *et al.*, 2012). In this model, monomeric ADP-bound MipZ is recruited to the cell poles in a ParB-*parS*/PopZ-dependent manner, where ATP-binding and dimerization predominantly takes place. Because dimeric MipZ has low affinity for ParB it is released from the ParB-*parS* complex and associates with the nucleoid. The nucleoid, in turn, stimulates ATP-hydrolysis which creates a MipZ gradient along the nucleoid with decreased concentration of MipZ the further the distance from the cell pole is (Kiekebusch *et al.*, 2012). MipZ directly couples positioning of the Z-ring to chromosome replication and segregation, only forming a bi-directional gradient with the lowest concentration of MipZ at midcell in longer cells that have initiated duplication and segregation of the *oriC* (Kiekebusch *et al.*, 2012, Thanbichler & Shapiro, 2006).

Of note the best studied systems that position cell division at midcell, which are the Min-system that works together with the nucleoid occlusion effect of SlmA and Noc and the MipZ/ParB-system, work by means of negative regulation that guide FtsZ-ring formation away from non-permissive sites. Recently several studies showed that the correct localization of the Z-ring is not negatively regulated in all bacteria.

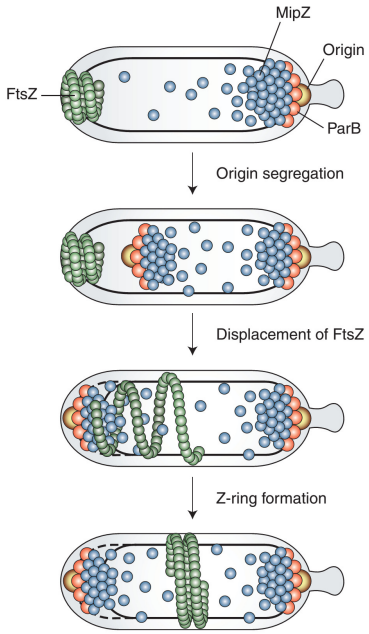

Figure 3: Model for MipZ-dependent positioning of the FtsZ-ring in *C. crescentus*.
In a newly divided stalked cell FtsZ (green) is located at the new pole, whereas MipZ (blue) forms a uni-directional gradient from the old pole with the highest concentration near the ParB-bound *parS* sequences at the *oriC*. MipZ follows ParB-*parS* during chromosome segregation to the new cell pole, thereby creating a bi-directional gradient and replacing FtsZ to midcell, where cell division takes place (Picture was obtained from Thanbichler & Shapiro, 2006).

In *Streptomyces coelicolor* cell division site placement is dictated by the localization of the *Streptomycetes*-specific proteins SsgA and SsgB (Willemse *et al.*, 2011). *S. coelicolor* is a filamentously growing organism in which FtsZ-based cell division is not essential for viability. Indeed, *ftsZ* as well as *ftsQ* could be deleted and cells displayed normal growth behaviour with the exception that they were not able to undergo developmental sporulation, but only compartmentalized their cytoplasm without cell fission (McCormick & Losick, 1996, McCormick *et al.*, 1994). At the onset of sporulation-dependent cell division in the aerial hyphae of *S. coelicolor* SsgB forms SsgA-dependent foci along the cell body that in the later stages of cell division perfectly colocalize with FtsZ in a ladder-like structure (Schwedock *et al.*, 1997, Willemse *et al.*, 2011). It was shown that localization of FtsZ depends on presence of SsgB, which in turn depends on the presence of SsgA. But the other way around SsgB and SsgA localize correctly in the absence of FtsZ. This dependency was consistent with the finding that SsgA, SsgB and FtsZ are within the same molecular complex as observed by *in vivo* interaction studies (Willemse *et al.*, 2011). Similar to ZapA in *E. coli* and FzlC in *C. crescentus*, SsgB stimulated the formation of FtsZ filaments *in vitro*, suggesting that SsgB not only recruits FtsZ to the incipient division site but also stimulates Z-ring formation (Willemse *et al.*, 2011). Of note, how SsgA together with its interaction partner SsgB finds the right place for cell division is unknown and needs to be analysed further.

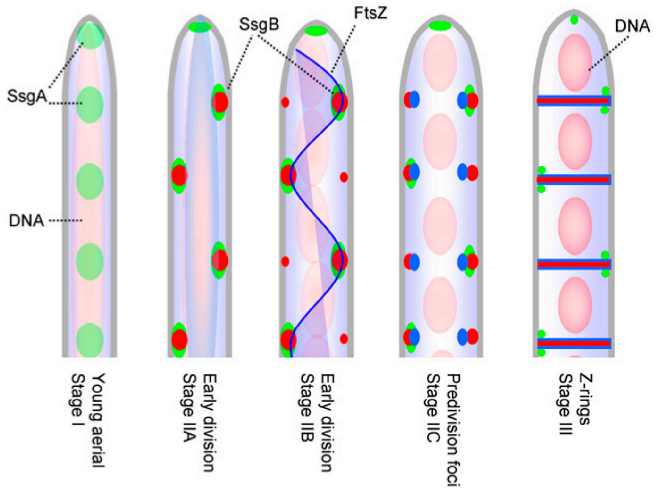

Figure 4: Model for SsgA/B-dependent regulation of cell division during sporulation in *S. coelicolour*. At the onset of sporulation in aerial-hyphae SsgA (green) localizes in distinct foci along the cell body. It recruits SsgB (red) by direct interaction, which in turn recruits FtsZ (blue). All three proteins form a ladder-like pattern, but only SsgB and FtsZ form circumferential rings which leads to multiple cell division events along the hyphae (Picture was obtained from Willemse *et al*., 2011).

Recently an additional positive regulation system was identified in *Streptococcus pneumoniae*. A membrane protein called MapZ (**m**id-cell-**a**nchored **p**rotein **Z**) or LocZ (**loc**alization at midcell of Fts**Z**) was independently identified by two groups to be required for the correct spatial localization of the Z-ring at midcell (Fleurie *et al.*, 2014, Holeckova *et al.*, 2015). Lack of MapZ results in cell division and cell morphology defects. Cells divide at the same frequency as WT cells and furthermore produce Z-rings at same frequency, but the Z-rings formed, are not at midcell and are often tilted compared to the cell axis. A Δ*mapZ* mutant produces anucleate minicells similar to a Δ*min* mutant in *E. coli* and *B. subtilis* (de Boer *et al.*, 1989, Fleurie *et al.*, 2014, Holeckova *et al.*, 2015). MapZ consists of an N-terminal cytoplasmic domain and C-terminal periplasmic domain. Both are required for proper function, but only the N-terminal domain interacts with FtsZ *in vivo* and *in vitro* (Fleurie *et al.*, 2014). In newborn cells MapZ and FtsZ colocalize at midcell in a ring-like structure. Upon peptidoglycan synthesis MapZ duplicates into two rings that are passively pushed apart by cell elongation, while FtsZ remains at midcell where peptidoglycan synthesis occurs. It is suggested that MapZ via its C-terminal domain is associated with the peptidoglycan and therefore it is fixed to the future cell division site from the moment the MapZ ring duplicates (Fleurie *et al.*, 2014). As cells grow, a third MapZ ring occurs that colocalizes with FtsZ at midcell until cells separate. During cell constriction, which is regulated by phosphorylation of MapZ by two kinases, FtsZ relocates to the two new midcells in the daughter cells (Figure 5) (Fleurie *et al.*, 2014). In contrast to SsgB MapZ does not stimulate filament formation by FtsZ and consistently does not stimulate Z-ring formation *in vivo* (Fleurie *et al.*, 2014, Willemse *et al.*, 2011). Therefore MapZ is suggested to be only a spatial regulator for Z-ring formation and couples cell elongation to Z-ring recruitment to the incipient cell division site (Fleurie *et al.*, 2014).

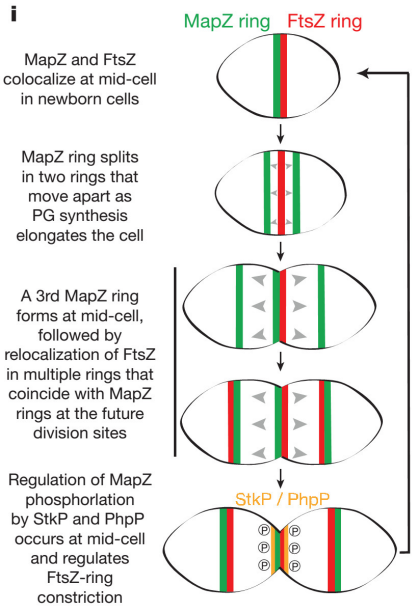

Figure 5: Model for MapZ/LocZ-dependent positioning of cell division in *S. pneumoniae*.
MapZ (green) and FtsZ (red) colocalize as rings in newborn cells. MapZ-rings, which are associated with the cell membrane and most likely cell wall are duplicated and moved apart by lateral cell wall growth. When MapZ-rings locate at ¼ and ¾ of the cell length a third ring occurs at midcell together with FtsZ. FtsZ performs cell division at midcell and concurrently relocates towards the MapZ-rings in the quarter positions. The midcell MapZ/FtsZ-ring constricts during cell division, which is most likely regulated by phosphorylation of MapZ. (Picture was obtained from Fleurie *et al*., 2015)

Corynebacterium glutamicum lacks the Min-system, the MipZ/ParB-system as well as the SsgAB system and MapZ and divides very irregular compared to other rod-shaped bactera (Letek *et al.*, 2008a, Letek *et al.*, 2008b). In a study of the function of ParA-like P-loop ATPases in *C. glutamicum*, the P-loop ATPase PldP (**P**arA-**l**ike **d**ivision **p**rotein) was identified (Donovan *et al.*, 2010). Lack of PldP results in the formation of anucleate minicells as observed in absence of the ParAB*S* system. However, only ParA is important for the correct localization of ParB and for chromosome segregation, while PldP is not. Based on that and on its localization at the incipient cell division site PldP was suggested to be a spatial regulator of cell division in *C. glutamicum*. How PldP defines midcell and its function in cell division are not understood (Donovan *et al.*, 2010).

The Min-system is well studied and quite conserved among a variety of bacterial species but in the recent years several new mechanisms were identified that are partially described above. These new mechanisms may include several novel and species-specific proteins such as in the case of SsgB and MapZ, but their mode of action may be adopted by other unrelated proteins or be evolved independently in different bacteria.

3.2 The versatile Mrp/MinD superfamily of P-loop ATPases

Mrp/MinD ATPases do not solely work in the regulation of cell division but display a high degree of diversity in their function. The Mrp/MinD superfamily of P-loop ATPases belongs to the SIMIBI (for **si**gnal recognition GTPases, **Mi**nD and **Bi**oD) group of NTPases and consists of several subfamilies that possess different cellular functions. To these subfamilies belongs the Mrp subfamily, the MinD subfamily with its close relatives MotR/FlhG, the ParA/Soj subfamily, the NifH subfamily and finally the ArsA subfamily of ATPases as well as the subfamily of MipZ and the ParC subfamily (Kiekebusch *et*

al., 2012, Leipe *et al.*, 2002, Ringgaard *et al.*, 2011). From now on I will refer to these proteins as ParA/MinD ATPases. The superfamily shares a common deviant Walker A motif (or P-loop) with the consensus GKGGhGK[ST] including a third conserved glycine residue and the synapomorphic KGG signature. By addition the superfamily lacks specificity for GTP over ATP by strong variation in the [NT]KxD motif, which in P-loop GTPases determines the specificity for GTP (Bourne *et al.*, 1991, Leipe *et al.*, 2002). Besides these common features P-loop ATPases of the ParA/MinD family show a high degree of diversity in their function. Mrp proteins are multi-drug-resistance proteins and are membrane bound ABC-transporters (Rosen, 2002). Similarly, ArsA proteins are arsenite stimulated ATPases *in vitro*, that together with ArsB, an integral membrane protein, form an ATP-dependent arsenic resistance exporter (Rosen *et al.*, 1988a, Rosen *et al.*, 1988b, Tisa & Rosen, 1990).

Unlike these two proteins, ParA/MinD ATPases can be involved in positioning of different cellular complexes and thereby regulating functions like cell division, as in the case of MinD (de Boer *et al.*, 1991) and MipZ (Thanbichler & Shapiro, 2006), or flagella localization and function as in case of FlhG/MotR (Schuhmacher *et al.*, 2015, Balaban & Hendrixson, 2011, Campos-Garcia *et al.*, 2000, Kusumoto *et al.*, 2006).

Recently, ParA/MinD ATPases were identified that are involved in regulation of chemotaxis in *Vibrio cholerae* and *Rhodobacter sphaeroides,* named ParC and PpfA, respectively (Ringgaard *et al.*, 2011, Roberts *et al.*, 2012, Thompson *et al.*, 2006). Lack of these ParA/MinD P-loop-ATPases results in reduced chemotactic behaviour. On top of that, one of the best studied group of P-loop ATPases is the ParA/Soj subfamily. This group includes ParA-ATPases involved in chromosome and plasmid partitioning as well as P-loop ATPases that are involved in regulation of initiation of chromosome replication (Murray & Errington, 2008, Ptacin *et al.*, 2010).

3.3 Plasmid partitioning systems

A major challenge of each cell is the duplication and faithful segregation of the genetic material before cell division. While high-copy plasmids are suggested to randomly segregate before cell division, by being excluded from the nucleoid area and accumulation at the cell poles (Reyes-Lamothe *et al.*, 2014), it became clear that low copy plasmids have to be actively segregated in order to maintain them stably in the population. Three types of bacterial DNA segregation machineries have been identified that work around actin-like ATPases, P-loop ATPases or tubulin-like GTPases (Ebersbach & Gerdes, 2001, Ebersbach & Gerdes, 2004, Larsen *et al.*, 2007, Moller-Jensen *et al.*, 2002). All these systems consist of an NTPase, a DNA-binding protein and a centromere-like region that is bound by the DNA-binding protein. Besides these similarities the systems show strong differences.

Actin-like segregation systems were identified by the identification of the *parMRC* locus that is required for stable inheritance of the R1 plasmid of *E. coli* (Gerdes *et al.*, 1985). It consists of an actin-like ATPase ParM, the DNA-binding protein ParR and a centromeric region *parC* (Gerdes & Molin, 1986). ParM binds both ATP and GTP, but its affinity for ATP is higher, and it further shows ATPase activity *in vitro* (Galkin *et al.*, 2009, Jensen & Gerdes, 1997). The mechanism by which ParM proteins segregate plasmid DNA depends on the ability of ParM to form ATP-dependent filaments in presence of ParR and *parC*. ParM was observed to form filament bundles *in vitro* (Moller-Jensen *et al.*, 2003,

Moller-Jensen *et al.*, 2002, Salje *et al.*, 2009). Compared to actin, ParM forms a left-handed two-filament helix (Orlova *et al.*, 2007, Popp *et al.*, 2008). Similar to tubulin, ParM filaments display rounds of assembly and disassembly with the incorporation of subunits at their ends, whereas the filament mid-parts are undynamic as observed by FRAP (Garner *et al.*, 2007). Because ParM filaments are produced in presence of ATP, but its ATPase is cooperative, they disassemble fast. However, disassembly is prevented by being capped by the ParRC complex at the filament ends (Salje & Lowe, 2008). Because ParM filaments can attach to ParRC complexes with both ends and furthermore move them apart *in vivo* as well as *in vitro,* a pushing mechanism was proposed for this plasmid partitioning system (Garner *et al.*, 2007).

In contrast to the ParMRC system some plasmids, which have been discovered in *Bacillus thuringensis* and *Bacillus anthracis,* carry the genes for the TubZRC system that is required for their efficient segregation (Larsen *et al.*, 2007). TubZ is related to tubulin and it is a GTPase that forms filaments *in vivo* and *in vitro* (Fink & Lowe, 2015, Larsen *et al.*, 2007). In the current model, TubRC complexes attach to the shrinking minus end of the TubZ filament. Based on filament de-polymerization from the minus end, the TubRC complex follows the shrinking filament. By this mechanism, together with the treadmilling-like pattern that TubZ filaments show *in vivo* and *in vitro,* plasmid partitioning is performed (Fink & Lowe, 2015).

The third group of systems that segregate plasmid DNA as well as chromosomal DNA in bacteria is the ParAB*S* systems. Although it is maybe the most widespread and the most studied system, the exact mechanism for the segregation process is still unknown. The ParA's of this group can be sub-divided into large and small ParA's, depending on the presence of a N-terminal DNA-binding motif or its absence (Gerdes *et al.*, 2000). While large ParA's have only been found on plasmids, small ParA's were identified on plasmids and on chromosomes (Gerdes *et al.*, 2000, Livny *et al.*, 2007). Typical examples of large ParA's are encoded on the famous plasmids F and P1 from *E. coli* and are called SopA and ParA, from the SopAB*C* and ParAB*S* system, respectively (Friedman & Austin, 1988, Niki & Hiraga, 1997). A member of the group of small ParA's is ParA from pB171 of *E. coli*. Although, on the sequence and structure level different, both types of ParA's show a similar behaviour *in vivo* and *in vitro* and are thought to function similarly.

Early on, the observation was made that plasmids in the presence of a functional partitioning system localized over the nucleoid area (Niki & Hiraga, 1997). Meanwhile more about the positioning mechanism is known. ParB proteins bind to their corresponding centromeric DNA-sequences (*parS*/*sopC*) and form a nucleoprotein complex. These complexes were shown to extent from the centromeric sequences further on the DNA (Rodionov *et al.*, 1999) and interact with ParA *in vivo* and *in vitro*. ParA's generally show low intrinsic ATPase activity, that is stimulated by interaction with the ParB*S* complex and/or DNA (Barilla *et al.*, 2007, Castaing *et al.*, 2008, Davis *et al.*, 1992, Pratto *et al.*, 2008). For some ParA's it was shown that they form filaments in presence of ATP (Barilla *et al.*, 2005, Bouet *et al.*, 2007, Ebersbach *et al.*, 2006, Lim *et al.*, 2005). This polymerization is generally stimulated by DNA whereas it is blocked by DNA in case of SopA (Bouet *et al.*, 2007). In the presence of ParA a single plasmid cluster is often at midcell over the nucleoid, whereas two plasmid clusters are equally spaced at the ¼ and ¾ position over the nucleoid. In comparison, in the absence of ParA, they are randomly distributed and sometimes excluded from the nucleoid (Ringgaard *et al.*, 2009). This

localization correlates with the localization of ParA on the nucleoid (Ebersbach & Gerdes, 2001, Ebersbach *et al.*, 2006, Lim *et al.*, 2005, Ringgaard *et al.*, 2009). ParA's occur in cells as an ADP-bound monomer that upon ATP-binding is able to dimerize and interact with the nucleoid. ATP-hydrolysis as well as DNA-binding by the ParA-ATPase is required for its function (Castaing *et al.*, 2008, Hester & Lutkenhaus, 2007, Leonard *et al.*, 2005). *In vivo*, ParA's form cloud-like structures that extent from the nucleoid edges at the cell poles until they reach a ParB-bound plasmid. When ParA interacts with the ParB/plasmid complex, the cloud structure begins to "retract" and the ParB/plasmid complex follows the "retracting" ParA structure. During the "retraction" and the ParB/plasmid motion towards the cell pole a new ParA structure is formed on the opposite cell half. Several rounds of extension and retraction occur during the cell cycle (Ringgaard *et al.*, 2009, Lim *et al.*, 2005, Ietswaart *et al.*, 2014). By this mechanism multiple plasmids are kept equally spaced on the nucleoid (Ringgaard *et al.*, 2009, Ietswaart *et al.*, 2014). Based on this observation a "filament pulling" mechanism was proposed (Ringgaard *et al.*, 2009, Lim *et al.*, 2005, Ebersbach *et al.*, 2006), in which a ParB-bound plasmid follows the "retracting" ParA filament over the nucleoid, leaving a ParA-depleted area behind. The filament grows by polymerization in presence of ATP and retracts by ParB/*parS* induced ATP-hydrolysis of ParA (Ringgaard *et al.*, 2009). Interestingly, this mechanism does not only explain the equipositioning of the plasmids, but furthermore explains how mechanical force may be generated to "pull" on the plasmid DNA.

For the partitioning of plasmids other mechanisms were proposed recently based on *in vitro* reconstruction experiments and the finding that not all ParA-ATPases form filaments. Furthermore SopA was reported to form filaments *in vivo* and *in vitro*, but did not produce these in *in vitro* reconstruction experiments (Vecchiarelli *et al.*, 2014a, Vecchiarelli *et al.*, 2013b, Hwang *et al.*, 2013, Bouet *et al.*, 2007). The "diffusion-ratchet" mechanism was suggested to explain plasmid motion and its directionality, which is crucial for partitioning (Vecchiarelli *et al.*, 2014a, Vecchiarelli *et al.*, 2013b, Vecchiarelli *et al.*, 2010, Hwang *et al.*, 2013). It was observed that single ParB/SopB molecules or ParB/*parS*-bound (SopB/*sopC*-bound) particles colocalize with dimeric P1 ParA-ATP (SopA-ATP of the F-plasmid) on an artificial DNA carpet and create a local ParA/SopA depletion zone. (Vecchiarelli *et al.*, 2013a, Hwang *et al.*, 2013). SopB complexes showed lateral motion on the SopA-bound DNA carpet and during this motion a depletion-zone of SopA was observed "behind" the SopB/*sopC* complex. Importantly, these depletion zones were not directly refilled by SopA. It was suggested that binding of SopB/*sopC* to dimeric ATP-bound SopA on the DNA-carpet induced ATP-hydrolysis and releases monomeric ADP-bound SopA from the DNA, creating a depletion zone behind the SopB/plasmid complex. Based on the biochemical properties of ParA's, it can not directly re-bind but homogenously disperses in the flow cell. Together with slow lateral diffusion of SopA on the DNA carpet, this leads to this SopA-depleted area, which only slowly refills. (Vecchiarelli *et al.*, 2014a, Vecchiarelli *et al.*, 2015). These observations led to the "diffusion-ratchet" model for the function of ParABS systems *in vivo*, in which ParB-bound plasmids associate with dimeric ATP-bound ParA on the nucleoid. This interaction to ParA leads to stimulation of ATP-hydrolysis by ParA and its release from the nucleoid. It results in a ParA-depletion zone around the ParB-bound plasmid. The ParB/plasmid complex will dissociate from the nucleoid, and because ParA does not directly refill the depletion zone on the nucleoid, the ParB/plasmid complex diffuses in the cytoplasm in the confined

area between the nucleoid and the membrane. In an initial random diffusion it will attach to dimeric, ATP-bound ParA on the nucleoid, leaving the depletion zone behind. This cycle is repeated and leads to ParB/plasmid motion. Because the ParB/plasmid complex leaves a depletion zone behind, the complex will predominantly attach to ParA "in front" of the ParB/plasmid complex, which in the end results in a directional motion along the ParA concentration gradient on the nucleoid (Vecchiarelli *et al.*, 2014a, Vecchiarelli *et al.*, 2013b, Vecchiarelli *et al.*, 2010, Hwang *et al.*, 2013). This model explaines how plasmid motion becomes directional. An implication of this model is that ParB/plasmid motion strongly depends on diffusion, for displacement. Recently the "diffusion-ratchet" model was re-defined to explain plasmid cargo motion by a "chemophoresis force" (Vecchiarelli *et al.*, 2015, Vecchiarelli *et al.*, 2014b). In this model, which was tested, by analyzing the SopAB*C* system *in vitro* and *in silico*, plasmids are bound by several ParB molecules that have low affinity for ParA on the nucleoid. However, the cumulative binding of these multiple ParB's to several ParA molecules directs plasmid motion to areas of increased binding of ParB to ParA. In other words, the ParB/plasmid complex moves along a chemical potential gradient, the ParA gradient. The motion is suggested to be promoted by the decreased free energy that comes from the higher number of ParA-ParB interactions. The more ParB molecules bind to ParA along the gradient the lower the free energy is. In this model the change in free energy is directly translated into the chemophoresis force (Vecchiarelli *et al.*, 2015).

Besides the fact that these models are based on plasmid partitioning system they are thought to work for other systems that include ParA-ATPases, as observed in chromosome segregation systems and for the general transport of large intracellular cargoes by ParA-ATPases.

3.4 The ParAB*S* system in chromosome segregation

As mentioned, a variety of chromosomes exhibit genes encoding for a ParAB system together with a centromeric *parS* sequence. These operons are generally found near the origin of replication (*ori*) (Livny *et al.*, 2007). Because several bacteria as well archaea lack a ParAB*S* system it raises the hypothesis that other segregation mechanisms will be discovered in the future.

Up until now all identified ParAB*S* systems found on bacterial genomes belong to the category of small ParA systems (Gerdes *et al.*, 2010). The best studied ParAB*S* systems studied so far are the chromosomal system of *C. crescentus* (Ptacin *et al.*, 2010, Mohl & Gober, 1997), the Par system of *V. cholerae* chromosome I and the Soj/Spo0J system of *B. subtilis* (Lin & Grossman, 1998, Fogel & Waldor, 2006). However, in the last years more and more system were analyzed in more detail like in *M. xanthus*, *S. coelicolor*, *C. glutamicum* and others (Jakimowicz *et al.*, 2005, Harms *et al.*, 2013, Donovan *et al.*, 2010). The ParAB*S* systems have been identified to be important transport systems of chromosomal origin regions (Mohl & Gober, 1997, Lewis *et al.*, 2002, Kim *et al.*, 2000, Harms *et al.*, 2013, Fogel & Waldor, 2006). They consist of a ParA ATPase with low intrinsic ATPase activity (Lim *et al.*, 2014) and a ParB protein that recognizes multiple *parS* sequences close to the *ori* (Murray *et al.*, 2006, Harms *et al.*, 2013, Breier & Grossman, 2007). While this system is dispensable for growth in *B. subtilis* and *C. glutamicum* and not essential on the *V. cholerae* chromosome I, it is essential in *C. crescentus*, *M. xanthus* and on the *V. cholerae* chromosome II (Murray *et al.*, 2006, Mohl & Gober, 1997, Harms *et al.*, 2013, Donovan *et al.*, 2010, Fogel & Waldor, 2006, Yamaichi *et al.*, 2007). Similar

to the observations made for plasmid ParAB*S* systems, ParA's of chromosome segregation systems form a cloud-like structure that extents from the polar chromosome edge over the nucleoid until they reach a duplicated ParB/*parS* complex during replication. Upon binding to that complex the ParA structure retracts and "pulls" on the ParB/*parS* complex on the nucleoid resulting in the complex following the retracting ParA structure (Ptacin *et al.*, 2010, Fogel & Waldor, 2006). This process is ATP-hydrolysis dependent, as mutations in the ATPase domain of ParA interfere with the localization of ParA and segregation (Ptacin *et al.*, 2010, Murray *et al.*, 2006, Fogel & Waldor, 2006). Similar to plasmid partitioning systems, the ability of ParA to bind to DNA is important for segregation (Ptacin *et al.*, 2010).

Lack of the ParAB homologs Soj and Spo0J in *B. subtilis* affects chromosome segregation but has a milder effect compared to those in other bacteria. A *spo0J* mutant was shown to produce anucleate minicells but only at low frequency (Lee & Grossman, 2006, Ireton *et al.*, 1994, Ireton & Grossman, 1994). Consistently, a deletion in *soj* showed an even milder defect in chromosome segregation (Lee & Grossman, 2006). Interestingly, Soj was shown to play a role in regulation of initiation of replication and sporulation in addition to its function in chromosome segregation (Murray & Errington, 2008, Ireton *et al.*, 1994, Ireton & Grossman, 1994). Cells lacking Soj initiate replication earlier suggesting that Soj, by an unknown mechanism, regulates initiation of replication. Indeed, monomeric Soj interacts with DnaA, the replication initiator protein and forms DnaA-dependent foci *in vivo*. A model was proposed by Murray and Errington in which monomeric Soj directly interacts with DnaA to inhibit or delay DnaA function, but dimeric Soj indirectly stimulates initiation of replication by releasing DnaA from the complex (Murray & Errington, 2008).

In *C. crescentus* the chromosome is arranged along the longitudinal axis and in newborn cells the origin of replication (*oriC*) is located at the old cell pole whereas the terminus region is located on the opposite cell site (Viollier *et al.*, 2004). The ParAB*S* system is essential and mediates the active transport of the *oriC* from the old pole to the new cell pole (Ptacin *et al.*, 2010, Mohl *et al.*, 2001). ParB binds the *oriC* proximal *parS* sequences and is tethered to the cell pole by PopZ (Ebersbach *et al.*, 2008a, Bowman *et al.*, 2008). Once replicated the ParB-bound *parS* sequences follow a retracting ParA cloud *in vivo* towards the new cell pole (Ptacin *et al.*, 2010). Upon arrival, the segregated ParB is tethered to the new cell pole by PopZ (Ebersbach *et al.*, 2008a, Bowman *et al.*, 2008). The transport is ParA ATP-hydrolysis-dependent and its directionality is affected by TipN, a new pole marker protein (Ptacin *et al.*, 2010). For chromosomal ParAB*S* systems, and similarly for plasmid partitioning systems, different molecular models have been proposed. Starting from a "filament-pulling mechanism" in which a structure similar to a eukaryotic spindle segregates the nucleoids, ranging to a biased-diffusion mechanism in which the ParB-*parS* complex diffuses along a ParA gradient (Schofield *et al.*, 2010, Ptacin *et al.*, 2010, Fogel & Waldor, 2006). Recently a novel mechanism was proposed based on the ParAB*S* system of *C. crescentus*. Based on *in silico* simulations and biochemical characterization of ParA and ParB the "DNA-relay" mechanism was proposed (Lim *et al.*, 2014). In this model the DNA-bound dimeric ParA transiently tethers ParB-bound *parS* to the nucleoid. On the basis of the elastic and dynamic properties of the DNA the ParB-*parS* complex is relayed from one ATP-bound ParA dimer to the next along the global ParA gradient in the *C. crescentus* cell. Directionality is given by the ParA gradient but force is generated by the elasticity of the DNA (Lim *et al.*, 2014). In

conclusion, while there is strong evidence that several bacteria make use of the dynamic function of ParAB*S* systems for actively moving chromosomal DNA during segregation process, specific mechanisms that allow such movements are diverse and have not been clearly understood.

3.5 ParA/MinD ATPases involved in positioning of chemosensory clusters and enzymes

In addition to their important function in the segregation of chromosomes and in stable inheritance of plasmids as well as their function in regulation of cell division ParA/MinD ATPases are also involved in regulation of other cellular processes. Because of their close structural and biochemical relationship to ParA they are often called ParA (-like) ATPases. In the last years several ParA-like ATPases were identified to have chromosome segregation independent cellular functions that are often related to positioning of cellular proteins to specific locations. Two of these are MinD and MipZ, which regulate cell division site placement in *E. coli*, *B. subtilis* and *C. crescentus* (Thanbichler & Shapiro, 2006, de Boer *et al.*, 1991).

In *R. sphaeroides* the ParA-like ATPase PpfA (**p**rotein **p**ositioning **f**actor **A**) was found which gene is encoded within one of the chemotaxis operons (Thompson *et al.*, 2006). Indeed it was shown that lack of PpfA results in a chemotaxis defect, which is caused by the mislocalization of cytoplasmic chemotaxis clusters observed by TlpT (**t**ransducer-**l**ike **p**rotein **T**), a soluble chemoreceptor encoded directly downstream of *ppfA* in the genome. PpfA, like Soj and other ParA ATPases, colocalizes with the nucleoid in a dimeric ATP-bound form. In addition, ATP-hydrolysis as well as DNA-binding are required for its function (Roberts *et al.*, 2012). PpfA positiones a cluster of soluble chemoreceptors, including TlpT, by direct interaction with its N-terminus, in the middle of the nucleoid. This chemotaxis cluster is duplicated and segregates PpfA-dependent to the ¼ and ¾ position before cell division. By this mechanism each daughter cell receives a chemotaxis cluster and is subsequently able to be chemotactically active (Roberts *et al.*, 2012). Because of the similarity to plasmid partitioning ParA systems and the lack of observable filaments of PpfA *in vivo*, a “diffusion-ratchet” mechanism was proposed for the mode of action of PpfA as it was proposed for the SopAB*S* system (Vecchiarelli *et al.*, 2010, Roberts *et al.*, 2012).

In *V. cholerae*, which uses the ParAB*S* system for segregation of the two chromosomes, another ParA-like ATPase, ParC, was identified to regulate the subcellular position of polar chemotaxis clusters in a cell cycle dependent manner (Ringgaard *et al.*, 2011). ParC efficiently localizes chemotaxis complexes to the cell pole by itself localizing dynamically to the pole, in a manner that depends on ATP-hydrolysis (Ringgaard *et al.*, 2011). The mediator between the chemotaxis clusters and ParC is ParP. ParP is recruitet to the cell pole by ParC and is in turn required for the recruitment of the chemotaxis complexes (Ringgaard *et al.*, 2014). Thus ParA ATPases encoded in chemotaxis clusters can be used to position these chemotaxis complexes over the nucleoid in the cell centre or at the cell pole(s).

The rod-shaped cyanobacterium *Synecococcus elongates* PCC7942 fixes carbon in proteinaceous microcompartments called carboxysomes. Production and inheritance of these carboxysomes is essential for efficient cell proliferation. Segregation of these compartments upon cell

division and its correct cellular distribution is regulated by a ParA ATPase called ParA (Savage *et al.*, 2010). ParA forms a cloud-like structure over the nucleoid that is dynamically localized and oscillates from pole to pole. Lack of ParA results in aberrant localization patterns and segregation defects of carboxysomes (Savage *et al.*, 2010).

Similarly to ParC, BcsQ, another ParA ATPase, was shown to position the cellulose biosynthesis machinery to the cell pole in *E. coli* but how it is regulated and if ATP-hydrolysis is important for function is not known (Le Quere & Ghigo, 2009).

These studies demonstrate that ParA ATPases not only position DNA in form of plasmids or chromosomes, but also chemotaxis proteins as well as enzymes and regulate the correct localization of FtsZ. Importantly, these cellular cargoes can be positioned at midcell, in the middle of the nucleoid, to the cell membrane or even at the cell poles.

3.6 Model organism *M. xanthus*

Myxococcus xanthus is a Gram-negative, rod-shaped, soil bacterium that belongs to the δ-proteobacteria. *M. xanthus* is a model organism to study social behaviour among bacteria, motility by means of Type IV pili and focal adhesions, gene regulation during starvation-induced fruiting body formation and sporulation as well as recently also the cell biology of chromosome metabolism and cell division.

3.6.1 Chromosome segregation in *M. xanthus*

M. xanthus has an approximately 9.1 million bp circular genome with an *ori* proximally located *parABS* operon (Koch *et al.*, 2011, Goldman *et al.*, 2006). As in other chromosomally located ParAB*S* systems, ParA shows all the important residues for ATP-binding, ATP-hydrolysis and non-specific DNA-binding (Treuner-Lange *et al.*, 2013, Harms *et al.*, 2013). ParB binds to a consensus of the 24 identified *parS* sequences *in vitro,* suggesting that it also does so *in vivo* (Harms *et al.*, 2013).

The ParAB*S* system is essential in *M. xanthus*, as *parA* and *parB* in-frame deletions could not be obtained and a depletion of ParB results in strong chromosome segregation defects and cell divisions over the nucleoid (Harms *et al.*, 2013). The *ori*, observed by the localization of ParB-YFP bound to *parS* sequences is located in a subpolar localization close to the old cell pole. Once duplicated, the ParB-*parS* complex is asymmetrically segregated to the opposite cell pole direction and arrives the final subpolar position within 30-50 min. Here, the ParB-*parS* complex is kept at a stationary position until cell division and the re-initiation of a new round of segregation (Harms *et al.*, 2013). ParA localizes in the nucleoid free subpolar regions and extends from the cell pole towards the ParB-*parS* complex. As in other bacteria, upon duplication of the ParB-*parS* complex, an elongating ParA structure extents from the other (new) cell pole until it reaches one ParB-*parS* complex. The complex follows a retracting ParA structure until it reaches the subpolar position, where it is kept over several hours, until cells divide in the middle between the two replicated and segregated nucleoids (Treuner-Lange *et al.*, 2013, Harms *et al.*, 2013). This process occurs concurrently with the replication of the chromosome by two independently moving replication forks. They start at the *ori* and ultimately

replicate the terminus region at midcell in a process that takes appropriately ¾ of the cell cycle (Harms *et al.*, 2013) (Figure 6).

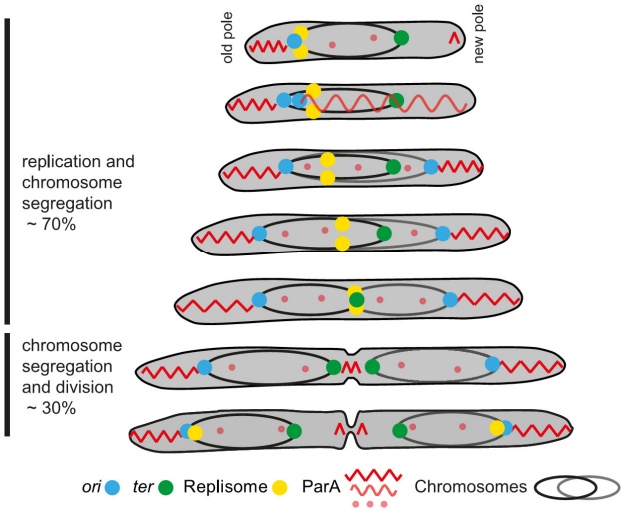

Figure 6: Model for chromosome arrangement in *M. xanthus*.
In newborn cells the *M. xanthus* chromosome is oriented with the *ori* (blue) pointing towards the old cell pole, while the terminus region (green) points towards the new cell pole. ParA (red) predominantly localizes in the subpolar nucleoid-free regions. Upon duplication of the *ori* ParB-*parS* duplicates and associates with an extending ParA structure coming from the new pole. Attached to the ParB-*parS* complex the ParA structure retracts and the complex follows. Concurrent with replication the terminus region is passively displaced towards midcell where it is finally replicated before cell division (Picture was obtained from Harms *et al.*, 2013).

3.6.2 Regulation of cell division in *M. xanthus*

Cell division and its positioning is also a highly regulated process in *M. xanthus* to generate progenies with the same genomic content and of same size. Rod-shaped bacteria generally divide with high precision at midcell. Similarly, *M. xanthus* cells divide precisely at midcell, however, how cells regulate the positioning with high accuracy is unknown, because *M. xanthus* and its close relatives lack known systems to regulate cell division and its positioning like the Min-system, MipZ, MapZ or the SsgAB system. Recently, we identified PomZ, a ParA ATPase, which is involved in correct positioning of cell division at midcell at normal frequency (Treuner-Lange *et al.*, 2013). A Δ*pomZ* mutant has a cell length phenotype, producing filamentous cells and anucleate minicells. This phenotype is caused by a reduction in formed Z-rings that are also incorrectly localized (Treuner-Lange *et al.*, 2013). ATP-hydrolysis by PomZ is essential for function but how it is regulated is still elusive. Consistently, purified PomZ has essentially no ATPase activity *in vitro* although it binds ATP. Compared to other systems that incorporate the function of a ParA ATPase, PomZ localizes in a novel pattern that correlates with cell length. Small cells display PomZ localization in a patchy pattern over the nucleoid. In longer cells an additional cluster is formed in the region between the cell pole and midcell on the nucleoid that ultimately localizes at midcell before cell division. Here it colocalizes with constrictions and FtsZ (Treuner-Lange *et al.*, 2013). Importantly, it forms clusters at midcell before Z-rings form and even in the absence of FtsZ, suggesting that PomZ localization is independent of FtsZ. Based on these findings, PomZ was suggested to be a positive regulator for cell division by finding midcell, recruiting FtsZ and stimulating Z-ring formation. Indeed FtsZ of *M. xanthus* was reported to not form filaments *in vitro* although it shows cooperative GTPase activity. However, GTPase activity

was not altered by PomZ *in vitro* (Treuner-Lange *et al.*, 2013). Therefore the question of how PomZ stimulates Z-ring formation and furthermore how PomZ localization and ATPase activity are regulated is unknown.

4 Scope of this study

PomZ belongs to the ParA/MinD superfamily of P-loop ATPases, containing a deviant Walker A motif and was identified as a protein involved in regulation of cell division site placement and cell division itself in *M. xanthus* (Treuner-Lange *et al.*, 2013). It was shown that lack of PomZ results in cell division defects caused by the reduction of observed Z-rings and their aberrant localization away from midcell, which is normally utilized as the site of cell division in *M. xanthus*. Despite the fact that a cluster of PomZ was shown to colocalize with Z-rings at midcell and its localization here ocurred temporally before and even in the absence of FtsZ, the role of PomZ in Z-ring placement and regulation was unknown. Furthermore, the question arose, if PomZ localization is independent of FtsZ, then how does PomZ recognize midcell and marks it for FtsZ to produce the Z-ring at correct time and place? In addition ATPase activity by PomZ was essential for function but could not be measured *in vitro,* because ParA ATPases generally show low intrinsic ATPase activity. However, this ATPase activity is often stimulated by interaction partners to regulate ParA function and localization.

Based on these findings it was proposed that PomZ does not work alone, but works together with unknown partners to regulate cell division site placement in *M. xanthus* that need to be identified (Treuner-Lange *et al.*, 2013). Therefore, the aim of this study is to identify interaction partners of PomZ that work together with PomZ in positioning of FtsZ at midcell. Furthermore, we want to understand (1) how PomZ identifies midcell as the site of cell division, (2) how midcell is marked for the recruitment of FtsZ and (3) how the ATPase cycle of PomZ is regulated.

5 Results

5.1 The *pomXYZ* gene cluster is involved in cell division site placement and Z-ring formation

5.1.1 Identification of the *pomXYZ* gene cluster

In order to identify proteins that could potentially work together with PomZ in cell division site positioning and regulation of cell division we performed BLASTp searches with PomZ against sequenced genomes of the myxobacteria, including *Myxococcus xanthus* DK1622, *Myxococcus stipitatus* DSM14675, *Myxococcus fulvus* HW-1, *Stigmatella aurantiaca* DW43-1, *Corallococcus coralloides* DSM2259, *Sorangium cellulosum* 0157-2, *Haliangium ochraceum* DSM14365, *Anaeromyxobacter dehalogenans* 2CP-C as well as against the unpublished genomes of *Cystobacter fuscus*, *Myxococcus macrosporus* and *Mellitangium boletus* to identify homologs of PomZ. PomZ was identified as a member of the ParA/MinD superfamily of P-loop ATPase (Treuner-Lange *et al.*, 2013) that is part of the SIMIBI (for **si**gnal recognition particle; **Mi**nD; **Bi**oD) superfamily of GTPases (Leipe *et al.*, 2002). This family of proteins contains a deviant Walker A motif with a xKGGhGK[ST] consensus and a Walker B motif with a conserved N-terminal aspartate. Additionally these proteins have a catalytic aspartate that is important for coordinating the Mg^{2+} ion, crucial for ATP hydrolysis. The BLASTp analysis resulted in 42 proteins with similar length that shared similarity with PomZ. Among these proteins we found the chromosomal ParA of the ParAB*S* system of *M. xanthus*, which is another member of the same superfamily of P-loop ATPases. To find the best homologs of PomZ in the family of ParA/MinD ATPases we used all 42 sequences and built an alignment with different other members of the same superfamily (Figure 7 A). For our analysis we used members of the families of MipZ, that regulate cell division site placement in a variety of α-proteobacteria (Thanbichler & Shapiro, 2006), ArsA, which is the catalytic part of arsenic efflux pumps (Rosen *et al.*, 1988b, Rosen *et al.*, 1988a), MotR, which is involved in flagella regulation (Schuhmacher *et al.*, 2015) and ParA that are crucial for chromosome segregation, or in the case of Soj for regulation of replication initiation in *B. subtilis* (Ptacin *et al.*, 2010, Murray & Errington, 2008, Harms *et al.*, 2013). Additionally, we used sequences of different NifH proteins which are involved in nitrogen fixation, ParC's that were shown to regulate and position chemotactic arrays in *Vibrio cholera* (Ringgaard *et al.*, 2011), Mrp, a family of multi resistance transporters, and MinD's, which regulate cell division site placement in a wide range of bacterial species (de Boer *et al.*, 1991). Also included was PpfA that positions soluble chemotaxis clusters in *R. sphaeroides,* and SopA as a member of the large ParA's that are important for plasmid stability (Roberts *et al.*, 2012, Hirano *et al.*, 1998). Using the MAFFT algorithm we aligned all these sequences and built a phylogenetic tree of the alignment with ClustalW2_phylogeny (Figure 7 A).

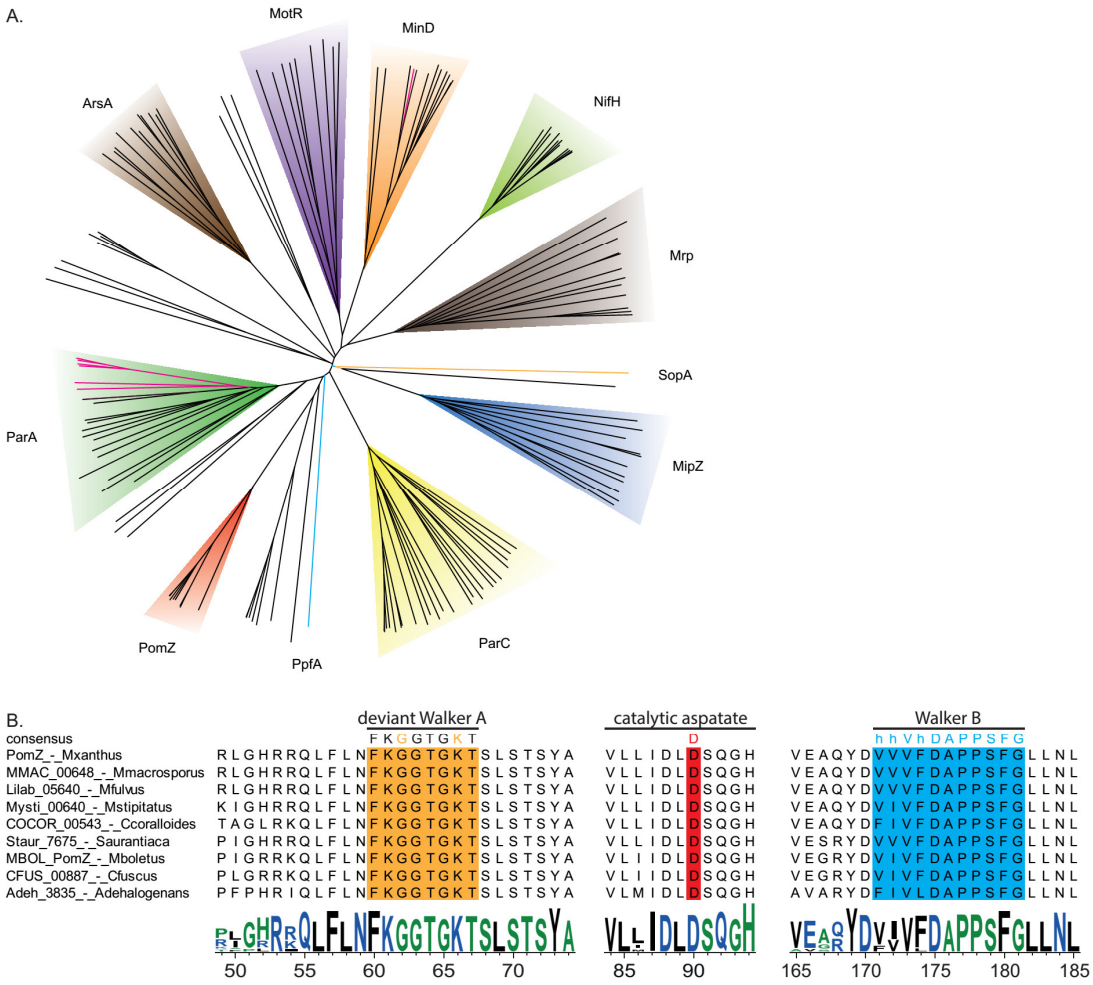

Figure 7: Phylogenetic classification of PomZ into the Mrp/MinD family of P-loop ATPases.
(A) 42 sequences of ParA/MinD-like ATPases found in myxobacteria were aligned with representive members of different indicated groups of the family of ParA/MinD ATPases using the MAFFT algorithm (Katoh & Toh, 2008). Phylogenetic analysis was performed using the Neighbour-joining clustering method. The tree was built with iTOL (Letunic & Bork, 2007, Letunic & Bork, 2011). Coloured triangles display sequences belonging to specific groups with their indicated names. Single sequences in case of PpfA and SopA are indicated as light blue and orange lines, respectively. Single black lines outside of specific groups correspond to myxobacterial ParA-like ATPases that cluster independent of other known groups. Pink lines correspond to myxobacterial ParA-like ATPases that cluster within other known groups. **(B)** Partial sequence alignment of members of the PomZ group of P-loop ATPases. Alignment was performed with the MAFFT algorithm on full length proteins sequences. Areas of interest are shown, corresponding to the deviant Walker A motif (orange) the catalytic Aspartate (red) and the Walker B motif (blue). Consensus sequences were generated with WebLogo3 using default parameters.

The analysis showed that members of the different families cluster as specific groups within the tree, whereas most of the myxobacterial ParA-like ATPases cluster independently of these groups with two exceptions (Figure 7 A). A set of nine protein sequences cluster together with proteins of the ParA/Soj subfamily of ATPases that together with their ParB partner are crucial for chromosome segregation, including ParA of *M. xanthus*. In addition eight sequences group close together with PomZ in a specific subfamily, suggesting that these nine proteins make up the PomZ group within the ParA/MinD superfamily of P-loop ATPases. This PomZ group clusters independently of the other protein families but close with ParA/Soj subfamily and PpfA, indicating that their mode of action might be similar and that they all work in correct positioning of cellular cargo. Interestingly, neither *H. ochraceum* nor *S. cellulosum* posses a PomZ homolog, suggesting that these two organisms do not

use PomZ for cell division site placement. In case of *S. cellulosum*, a MinD homolog (*Sce_20405*) was found that clusters within the MinD subfamily. Additionally, *S. cellulosum* possesses genes encoding for a MinE and a MinC homolog. While *minE* is encoded directly downstream of *minD*, the *minC* locus is more distant to *minD*. Therefore, we believe that *S. cellulosum* uses the Min-system for cell division site placement instead of the PomZ system.

All nine sequences from the PomZ subfamily were aligned with the MAFFT algorithm to see if they show the deviant Walker A motif, the catalytic aspartate and the Walker B motif with the conserved N-terminal aspartate found in PomZ of *M. xanthus* (Figure 7 B). Not surprisingly, they showed a high degree of similarity along the whole sequence. We found the deviant Walker A motif with the consensus FKGGTGKT, which is similar to the motif of many other members of the SIMIBI NTPase family, but differs in the motif preceding phenylalanine, that in many other families is a glycine (Leipe *et al.*, 2002). We identified the Walker B motif with the consensus hhVhDAPPSFG, where h corresponds to a hydrophobic residue. This Walker B motif varies in length from that of MinD or MipZ but still containes the hydrophobic patch of amino acids directly followed by the conserved aspartate and the C-terminal glycine. Furthermore, we found the catalytic aspartate (D^{90}) which coordinates the Mg^{2+} ion for ATP hydrolysis that is conserved in all members of the ParA/MinD superfamily (Leipe *et al.*, 2002). Members of the PomZ subfamily do not have a C-terminal NKxD motif, like other members of the SIMIBI superfamily, which is important for GTP specificity over ATP in GTPases. This fits with the notion that PomZ has higher affinity for ATP than for GTP *in vitro* (Treuner-Lange *et al.*, 2013, Leipe *et al.*, 2002).

By analyzing the genomic context of *pomZ* (*mxan_0635*) of *M. xanthus* we found that it is encoded in a gene cluster together with two genes *mxan_0634* and *mxan_0636* upstream and downstream, encoding for hypothetical proteins. These three genes are transcribed in the same direction as *pomZ* (Figure 8 A, B). Because the intergenic region is small upstream (40 bp) and downstream (6 bp) of *pomZ* we hypothesized that these three genes are transcribed as an operon. Aside of these gene cluster, *pomZ* is flanked by a gene for a fatty acid desaturase-like protein (*mxan_0632*) and a gene coding for a DNA-binding protein (*mxan_0633*) upstream of *mxan_0634*, a gene for a M48 family peptidase (*mxan_0637*) and another gene for a hypothetical protein (*mxan_0638*) downstream of *mxan_0636* (Figure 8 A). Interestingly, in the genomic region of all eight *pomZ* homologs, we found that they are all flanked by genes encoding for hypothetical proteins that, by reciprocal BLASTp analysis, are orthologs of MXAN_0634 and MXAN_0636. Using a global pairwise sequence alignment tool (EMBOSS_Needle) we made several observations. First, all nine PomZ homologs share a high degree of identity (61 % - 99 %) and secondly, the proteins encoded by genes upstream of *pomZ* homologs show high similarity to MXAN_0634.

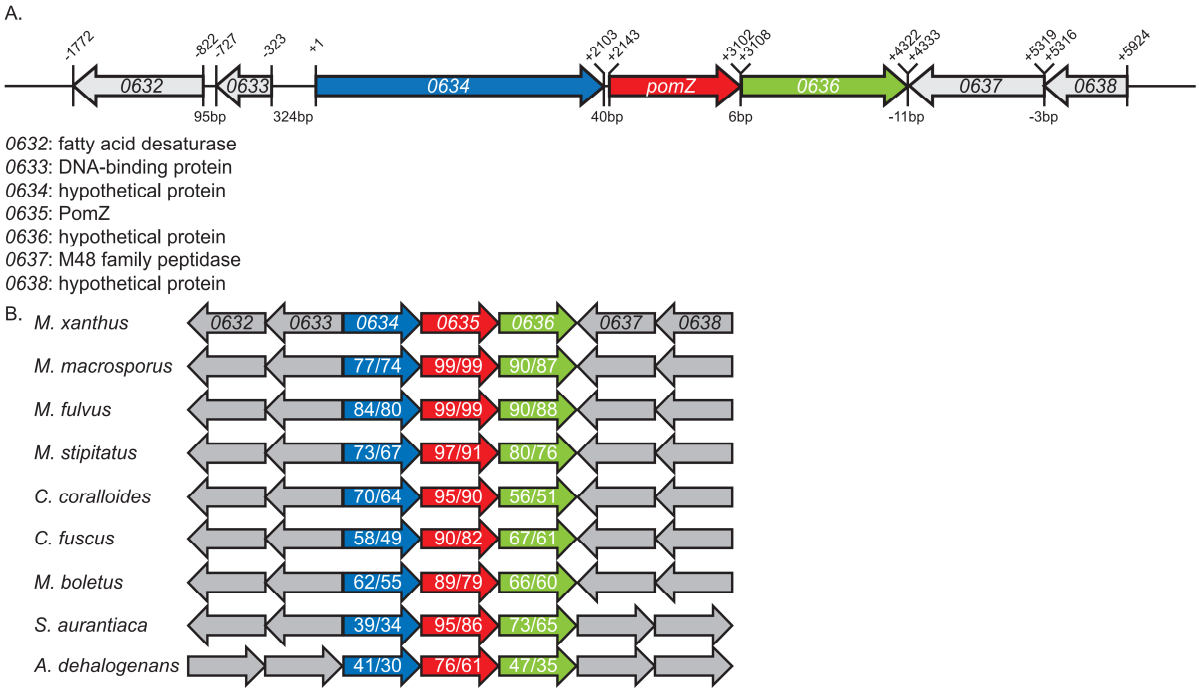

Figure 8: Schematic representation of the genomic region of *pom* gene cluster.
(A) Numbers on top display display start and stop base in correlation to the start base of mxan_0634. Numbers below display distances between genes. Genes are indicated as arrows. Arrow orientation reflects how genes are encoded on the genome. Grey arrows display genes outside the pom genecluster. Putative proteins encoded by the depicted genes were obtained from BLAST analysis (Altschul *et al.*, 1990). **(B)** Conservation of the pom genecluster in other sequenced members oft he myxobacteria. Genes are depicted as arrows. Arrow orientation displays coding direction of the genes. Homologous proteins are indicated in same colours. Grey arrows show that these genes and their encoded proteins are not conserved in genomic region. Numbers in arrows (outside of *M. xanthus*) display global identity and similarity of their encoded protein to their homolog in *M. xanthus*. Numbers were obtained from Pairwise Sequence Alignement of proteins using EMBOSS Needle (Li *et al.*, 2015). Figures were modified from Schumacher, 2011.

The same observations were made for MXAN_0636 (Figure 8 B). Outside of these three genes synteny is lost with the exception of *mxan_0633*, a gene encoding a DNA-binding protein. A homolog of this is found directly upstream of all *mxan_0634* homologs. However, the gene is not encoded directly upstream of *mxan_0634* homologs in more distantly related organisms to *M. xanthus*. Based on these findings *mxan_0634* and *mxan_0636* (from now on called *pomY* and *pomX*, respectively) are good candidates for interaction partners of PomZ that work together with PomZ in regulating cell division site placement in *M. xanthus* and close relatives.

5.1.2 Bioinformatics analysis of PomX and PomY

To characterize the hypothetical proteins PomY and PomX a bioinformatics analysis was performed, using the full length PomY and PomX protein sequence of *M. xanthus*. It is important to mention that *pomY* is likely to be wrongly annotated for two reasons. First, in alignments with the PomY homologs it was found that it has an N-terminal extension of 18 aa, which is not observed for any other homolog. Furthermore, while the longer version of *pomY* lacks a Shine-Dalgarno sequence, the shorter version has an upstream sequence with a GAGG motif, which could serve as a Shine-Dalgarno sequence in *M. xanthus*. This suggests that the *pomY* start codon is most likely 62 bp

downstream of its annotated start codon. For all further *in vivo* and *in vitro* analysis the shorter version of *pomY* and its gene product is used.

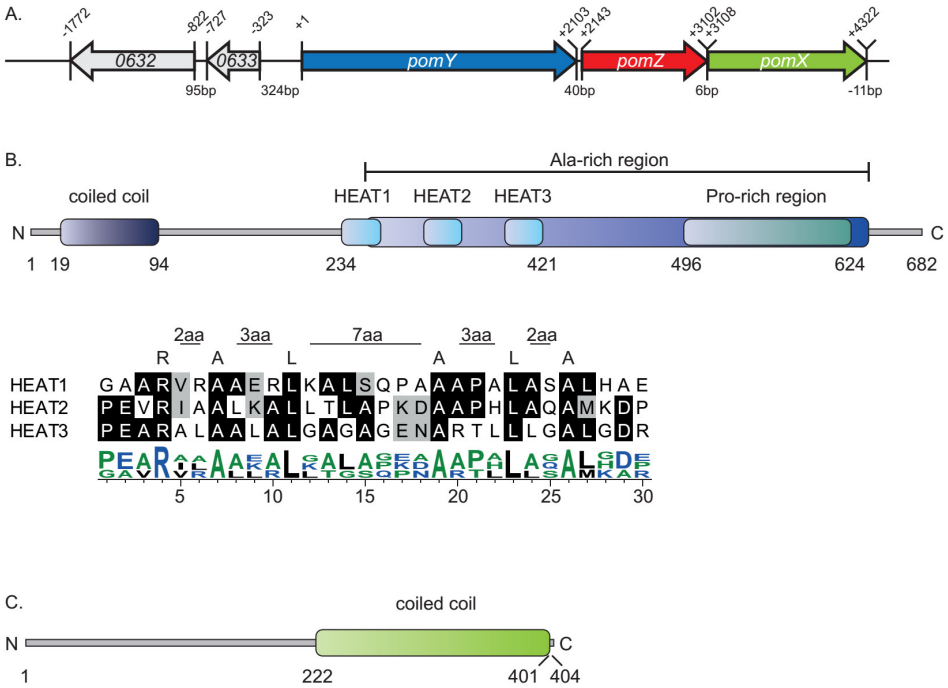

Figure 9: Bioinformatics analysis of PomY and PomX.
(A) Numbers on top display start and stop base in correlation to the start of *mxan_0634*. Numbers below display distances between genes. Genes are indicated as arrows. Arrow orientation reflects how genes are encoded on the genome. Grey arrows display genes outside the pom gene cluster. Putative proteins encoded by the depicted genes were obtained from BLAST analysis (Altschul *et al.*, 1990). Figure was modified from Schumacher, 2011. **(B)** Schematic domain structure of PomY was obtained from SMART analysis of the full length protein (Schultz *et al.*, 1998, Letunic *et al.*, 2015). Numbers below depict the start and the stop of domains in amino acid positions. Alignment and consensus of HEAT domains were performed with the MAFFT algorithm (Katoh & Toh, 2008) and WebLogo3, respectively (Crooks *et al.*, 2004). **(C)** Schematic domain structure of PomX was obtained from SMART analysis of the full length protein.

A combination of a SMART analysis together with a search for conserved domains using the MyHits database from the ExPASy bioinformatics resource portal revealed that PomY consists of several domains that are separated by regions of low complexity (Letunic *et al.*, 2015, Artimo *et al.*, 2012). PomY has an N-terminal coiled coil domain of 75 amino acids that is followed by a region in the centre of the protein, consisting of three HEAT repeats. A long alanine-rich region spans the protein from the middle to the C-terminus. A proline-rich region overlaps with the Ala-rich region in the C-terminal part (Figure 9 B). HEAT domains are named after four eukaryotic proteins, which possess these kind of domains. These proteins are the **H**untington protein, **e**longation factor III, the scaffolding subunit A of protein phosphatase II (PR65/**A**) and the **T**OR kinase and they are further identified in the nuclear pore transport protein importin β (Malik *et al.*, 1997, Andrade & Bork, 1995). It was shown that HEAT domains facilitate protein-protein interaction in case of the nuclear pore import complex, where importin β plays a key role in interaction with both importin α and Ran GTP (Enenkel *et al.*, 1996). Furthermore, HEAT repeats play a crucial role to mediate interaction of the catalytic subunit C of protein phosphatase 2A (PP2A C) with its multiple and diverse regulatory B subunits to regulate metabolism and cell cycle progression in eukaryotes (Groves *et al.*, 1999). Interestingly, in alignments of the three HEAT repeats, which all have a length of 30 amino acids, six conserved residues (R4, A7,

L11, A19, L23 and A26) were observed, which may play an important structural role in HEAT repeat formation (Figure 9 B). Presence of the HEAT domains, which are often arranged in repeated arrays suggests that PomY might function as an interaction partner for other proteins, or a mediator for multi protein complex formation. This hypothesis is strengthened by the finding of a coiled-coil domain in the N-terminal region of PomY that are often involved in protein self-interaction or protein-protein interaction. Moreover an Ala-Pro-rich region, which may also facilitate in protein-protein recognition (Williamson, 1994, Melby *et al.*, 1998, Berger *et al.*, 1996). While PomY appears to be composed of several domains, PomX shows a clear separation into only two regions. The N-terminus of PomX does not contain any annotated domain and when analyzed by SMART, it only shows regions of low complexity (data not shown), whereas the C-terminal part of PomX consists of a 179 aa coiled coil domain, which may function in protein-protein interaction (Figure 9 C). Notably ParA ATPases often work together with an interaction partner, which in the case of ParA and MipZ is ParB (Thanbichler & Shapiro, 2006, Ptacin *et al.*, 2010) and in the case of MinD is MinE (Hu & Lutkenhaus, 1999). However, interaction partners can be diverse based on the diverse parthways ParA ATPases work in (Lutkenhaus, 2012). This makes PomX and PomY perfect candidates to study for its function in regulation of cell division and moreover in correct localization of PomZ at midcell.

5.1.3 PomX is required for cell division positioning and divisions at correct frequency

It was shown that PomZ is required for cell division at correct frequency and correct place (Treuner-Lange *et al.*, 2013). Based on that, we predicted that deletion of *pomX* and *pomY* results in a similar phenotype to a Δ*pomZ* mutant, if they affect cell division and furthermore are required for correct localization of PomZ. To unravel if PomX is involved in regulation of cell division a *pomX* in-frame deletion mutation was created (SA4223) and analyzed by microscopy for cell length, positioning of cell division constrictions and the production of minicells (Figure 10). For this purpose exponentially growing cells were spotted on a 1 % TPM agarose patch and analyzed by microscopy at 32 °C.

A Δ*pomX* mutant has a cell length phenotype compared to wildtype (WT), producing filamentous cells and cells that are smaller than observed in WT (Figure 10 A). Cells of a WT population and cells of Δ*pomX* mutant differed significantly in length, while cell width was the same. On average WT cells were 7.7 ± 1.8 µm (n=301), whereas Δ*pomX* cells were 15.4 ± 9.5 µm in length (n=498) (Figure 10 C). The observed phenotype of the Δ*pomX* mutant was similar to that of the Δ*pomZ* mutant. Therefore constriction frequency and their positioning was measured (Figure 10 A, B). Consistently, cells lacking PomX displayed a reduced constriction frequency with only 3 % compared to WT with 7 %. Moreover the few constrictions formed were not exclusively observed at midcell (which was considered as 50 % ± 5 % of cell length), but were formed along the long axis of the cell with an average position at 24 ± 15 % (Figure 10 B). These data suggest that the cell length phenotype arises from aberrant cell division positioning in the Δ*pomX* mutant and that PomX also promotes the formation of cell division constrictions *in vivo*. Notably, the mean cell length at which cell division took place increased in Δ*pomX* cells to 18.7 ± 10.4 µm in comparison to WT that normally divides at a cell length of 11.2 ± 2.3 µm. This suggests a delay of cell division timing by the lack of

PomX. To confirm that the observed cell length phenotype was caused by the Δ*pomX* in-frame deletion, complementation strains were created.

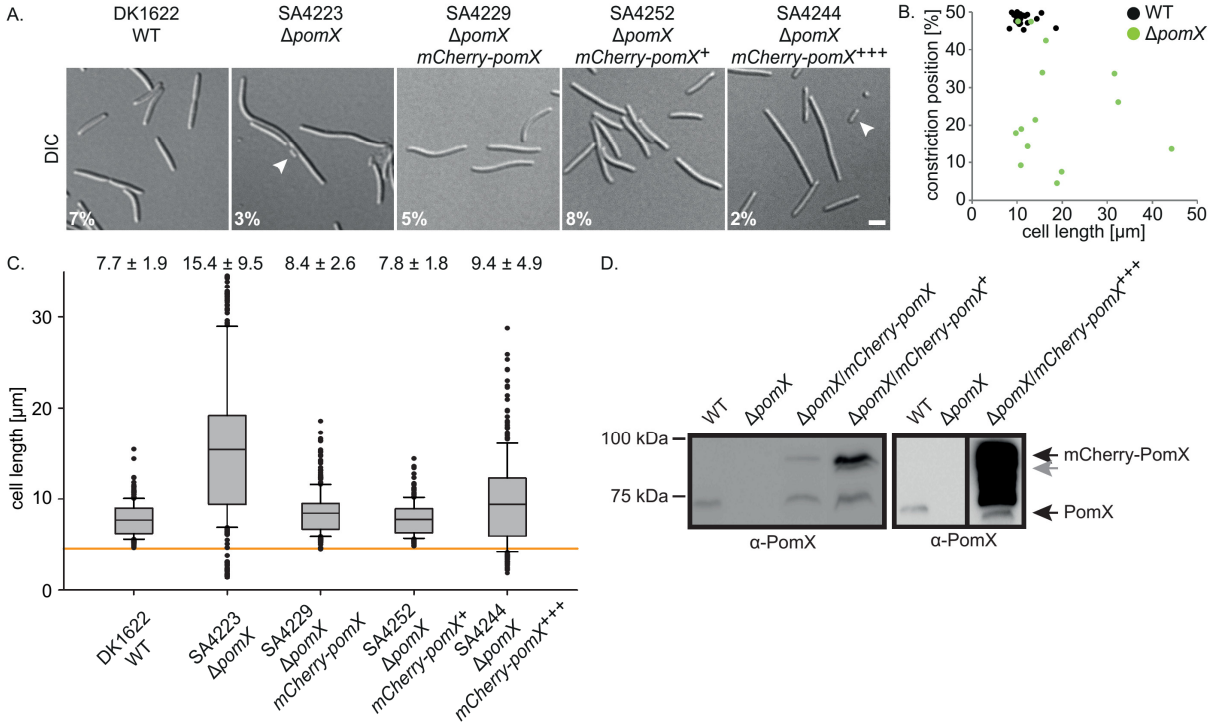

Figure 10: Lack of PomX causes a cell length phenotype that is complemented by expression of *mCherry-pomX*.
(A) DIC microscopy of strains with indicated genotypes. Cells were collected from exponentially growing cultures and analysed on 1% agarose buffered with TPM. White arrows display minicells. White numbers depict constriction frequency (n>200). Scale bar: 2 µm. **(B)** Positioning of cell division constrictions in WT (black) and a Δ*pomX* mutant (green). Constriction positioning was obtained from linescans on DIC pictures and calculated as % of total cell length (50 % is midcell). **(C)** Cell length distribution of indicated strains as box plots. Grey boxes enclose 25th and 75th percentile, with the black line showing the mean that is also given in numbers ± standard deviation (SD) on top. Whiskers display 10th and 90th percentile. Outliers smaller than 35 µm are depicted as black dots. Outliers bigger than 35 µm are not shown but are included for the calculation of the mean cell length. Dots below the orange line indicate minicells. **(D)** Immunoblot analysis of lysates of indicated straines for the presence of PomX and mCherry-PomX using specific α-PomX antibodies. Black arrows indicate PomX and mCherry-PomX, grey arrows indicate unspecific binding of the antibody and degradation products. Equal amount of total protein was loaded per lane.

The described Δ*pomX* phenotype was complemented by expression of *mCherry-pomX* under the control of the putative native *pomX* promoter from the *Mx8* attachment site in the genome in strain SA4229 (Δ*pomX*/*mCherry-pomX*). This expression resulted in an elevated constriction frequency of 5 % and an average cell length of 8.4 ± 2.6 µm (n=322). Expressed from this promoter, mCherry-PomX accumulates at WT levels (Figure 10 D), demonstrating that the phenotype was caused by the lack of PomX.

Expressing *mCherry-pomX* at higher levels from the native *pomZ* promoter from the *Mx8* attachment site (SA4252; approximately 10 x more) also restored the WT phenotype (n=207), while expression from the strong *pilA* promoter (SA4244) did not (n=268) (Figure 10 C, D). In this strain mCherry-PomX accumulated at very high levels, giving rise to the formation of filamentous cells and small cells, together with a reduction in constriction frequency to 2 %, as observed for a Δ*pomX* mutant (Figure 10 C, D). This indicates that correct levels of PomX, with small variations, are crucial

for its function. In summary, these data show that in addition to PomZ, PomX is involved in correct cell division site placement and cell division at the correct frequency.

5.1.4 A Δ*pomY* in-frame deletion mutant phenocopies the Δ*pomX* and the Δ*pomZ* mutant

To determine if PomY is also involved in cell division in *M. xanthus* an in-frame deletion mutant of *pomY* was created, resulting in strain SA4703 (Schumacher, 2011). Like the Δ*pomX* and the Δ*pomZ* mutant, an in-frame deletion in *pomY* resulted in the formation of filamentous cells and the production of minicells (Figure 11 A). Cell length quantification showed that cells of a Δ*pomY* mutant were on average 16.2 ± 11.2 µm (n=903) (Schumacher, 2011), which was more than two times longer than WT cells. A Δ*pomY* mutant showed a reduction in cell division constrictions, suggesting that like PomZ, PomY promotes cell divisions *in vivo* (Treuner-Lange *et al.*, 2013) (Figure 11 A). The few constrictions produced in a Δ*pomY* mutant were not exclusively found at midcell but could be found along the long cell axis (average position 31 ± 13 %). This is likely to cause the minicell phenotype together with cell filamentation, as observed for the Δ*pomX* and the Δ*pomZ* mutant (Figure 11 B). Similar to a Δ*pomX* mutant, in absence of PomY cell divisions occurred predominantly in longer cells (25.7 ± 17.1 µm), also indicating a deregulation in cell division timing for a Δ*pomY* mutant.

The WT phenotype could be restored by expression of *pomY-mCherry* from the *Mx8* attachment site under the regulation of the putative native *pomY* promoter (620 bp upstream up *pomY*) in a Δ*pomY* background (SA4713). PomY-mCherry accumulated under these conditions at WT levels and rescued both, the cell length and the constriction phenotype, producing cells of 8.0 ± 1.8 µm with cell divisions in 10 % of cells (n=218) (Figure 11 A, C, D). Importantly, overexpression of *pomY-mCherry* under control of the strong *pilA* promoter led to high accumulation of PomY-mCherry in cell lysates of strain SA4712 (Δ*pomY*/*pomY-mCherry*+++; approximately 50 x more), as detected by western blot analysis. This re-established the WT phenotype with an average cell length of 8.5 ± 2.2 µm and a constriction frequency of 7 % (n=541) (Figure 11 C, D)(Schumacher, 2011). These data show that in contrast to the observations made for PomX, accumulation of high levels of PomY supports normal cell division under the tested conditions. In total, the data demonstrate that the observed phenotype is caused by the Δ*pomY* in-frame deletion.

Based on our bioinformatics approach we were able to identify two new proteins, PomX and PomY, that work together with PomZ in regulation of cell division and positioning of the cell division site in *M. xanthus* and most probably in a variety of myxobacteria. Based on these findings we hypothesized that we had identified a novel regulation system for cell division and cell division site placement, which we from now on refer to as the Pom-system.

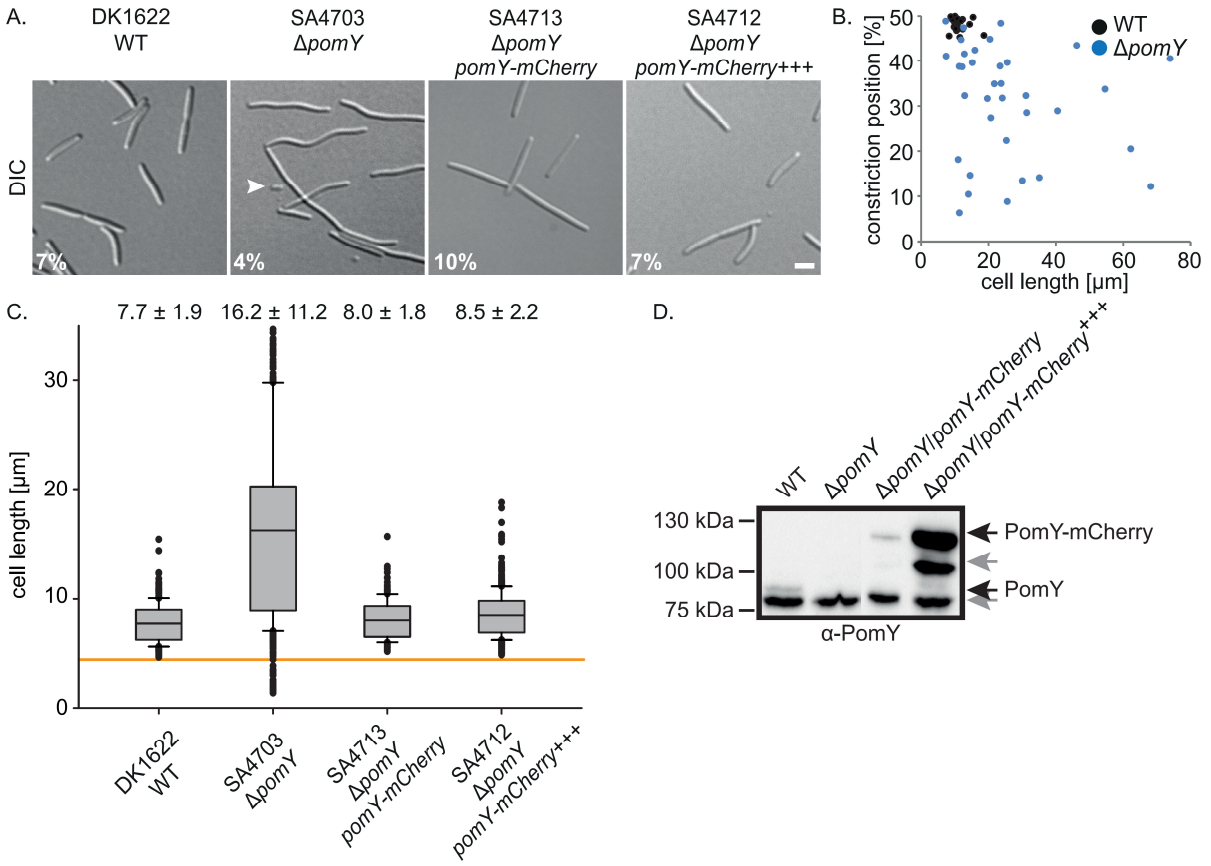

Figure 11: A Δ*pomY* mutant has a cell length phenotype and can be rescued by expression of *pomY-mCherry*.
(A) DIC microscopy of strains with indicated genotypes. Cells were collected from exponentially growing cultures and analysed on 1% agarose buffered with TPM. White arrows display minicells. White numbers depict constriction frequency (n>200). Scale bar: 2 µm. **(B)** Positioning of cell division constrictions in WT (black) and a Δ*pomY* mutant (blue). Constriction position was obtained from linescans on DIC pictures and calculated as % of total cell length (50 % is midcell). Adapted from Schumacher, 2011. **(C)** Cell length distribution of indicated strains as box plots. Grey boxes enclose 25th and 75th percentile, with the black line showing the mean that is also given in numbers + standard deviation (SD) on top. Whiskers display 10th and 90th percentile. Outliers smaller than 35 µm are depicted as black dots. Outliers bigger than 35 µm are not shown but are included for the calculation of the mean cell length. Dots below the orange line indicate minicells. Data adapted from Schumacher, 2011. **(D)** Immunoblot analysis of lysates of indicated straines for the presence of PomY and PomY-mCherry using specific α-PomY antibodies. Equal amount of total protein was loaded per lane. Black arrows indicate PomY and PomY-mCherry, grey arrows indicate unspecific binding of the antibody and protein degradation.

5.1.5 Lack of PomX, PomY and PomZ results in the formation of anucleate minicells

Minicell formation is a well described phenotype of mutations in the Min-system in *B. subtilis* and *E. coli* and was also described for a Δ*pomZ* mutant (Treuner-Lange *et al.*, 2013, de Boer *et al.*, 1989). These cells are substantially smaller than WT cells and do not possess any DNA. To characterize this phenotype in more detail the presence of these cells was quantified by DIC microscopy in mutants lacking PomX and PomY. As a control, minicell formation was analysed in a Δ*pomZ* mutant in parallel. In a WT population, the smallest cells were 4.6 µm, suggesting that cells smaller than that are produced by aberrant cell divisions away from midcell. 5.3 % of all cells of a Δ*pomX* population were smaller than 4.6 µm, indicating that these cells originated from asymmetric cell divisions. The number of these cells is similar in a Δ*pomY* mutant with 8.4 % but is significantly increased in absence of PomZ with 18.7 %. To answer the question if these cells are real minicells

lacking any chromosomal DNA, cells were stained with 1 µg/ml DAPI and analysed by fluorescence microscopy. In a Δ*pomX* mutant 5.9 % of all cells were anucleate, indicating that some anucleate cells are longer than 4.6 µm, whereas 8.4 % and 12.4 % of cells were anucleate in a Δ*pomY* and Δ*pomZ* mutant, respectively. Minicells observed in *M. xanthus* are not as small as observed in other bacteria. In fact they are as big as a *C. crescentus* cell (Campos *et al.*, 2014) and furthermore formation of these cells is strongly increased by lack of PomZ. Based on these findings we hypothesized that in absence of PomZ cell divisions occur predominantly at the poles or in subpolar regions of the cell, whereas in a Δ*pomX* or Δ*pomY* mutant cell division takes place everywhere in the cell.

A.

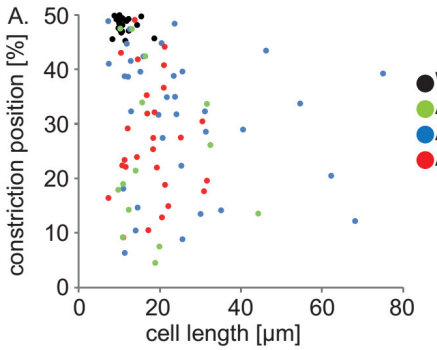

B.

strain	constriction position	constriction occurrence µm	<4.6µm	anuc. cells	anucleate cells µm
WT	50 ± 1%	11.2 ± 2.3	-	-	-
Δ*pomX*	24 ± 15%	18.7 ± 10.4	5.3%	5.9%	2.8 ± 1.5
Δ*pomY*	31 ± 13%	25.7 ± 17.1	8.4%	7.4%	3.2 ± 1.3
Δ*pomZ*	27 ± 11%	10.8 ± 8.0	18.7%	12.4%	3.2 ± 1.5

Figure 12: Minicells produced in the absence of PomXYZ are similar but their number is increased in absence of PomZ.
(A) Positioning of cell division constrictions in a Δ*pomX* (green) and Δ*pomY* (blue) mutant in comparison to constrictions in a Δ*pomZ* mutant (red) and WT (black). Constrictions were identified from DIC pictures and calculated in % of total cell length (50 % is midcell). Data partially adapted from Schumacher, 2011 **(B)** Summary of the analysis of constriction positioning and minicell formation in WT and Δ*pom* mutants. All values were obtained from DIC microscopy of exponentially grown cells on 1 % agarose buffered with TPM. Mean constriction position, constriction occurrence and length of anucleate cells is given ± SD

Unexpectedly, cell divisions in all three mutants occurred in the same area, between 24 % and 31 % of cell length, producing minicells with a mean length of 2.8 µm to 3.2 µm, contradicting the hypotheses made before (Figure 12 A, B). Therefore the question arises if the high amount of minicells produced by a Δ*pomZ* mutant is generated by multiple cell divisions at the poles which would disagree with the reduction of cell divisions in a Δ*pomZ* mutant, however, needs to be analysed further. At this point in time these observations can not be explained by the presented data.

5.1.6 PomX, PomY and PomZ work in the same genetic pathway but accumulate independently of each other

The effect of PomX and PomY is very similar to the effect of PomZ on cell division. Therefore we reasoned that PomX and/or PomY could have an effect on the accumulation of PomZ, either by regulating the expression levels of *pomZ*, or by increasing protein instability, which is regularly seen for protein in complexes (Friedrich *et al.*, 2014). Both mechanisms would in the end lead to decrease in the accumulation of PomZ, resulting in a Δ*pomZ* phenotype. To investigate this hypothesis, lysates of a Δ*pomX*, Δ*pomY* and Δ*pomZ* mutant were probed for the presence of PomZ and additionally for PomX and PomY using specific antibodies raised against purified His_6-tagged PomX, PomY and

PomZ protein. As control WT lysate was probed for the presence of all three proteins to detect differences in accumulation.

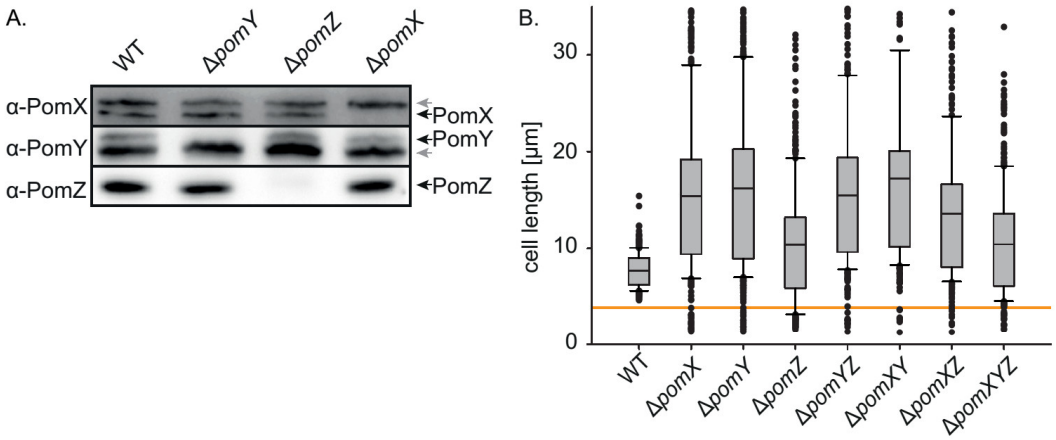

C.

strain		mean cell length	constrictions	n
DK1622	WT	7.7 ± 1.9	7%	301
SA4223	Δ*pomX*	15.4 ± 9.5	3%	498
SA4703	Δ*pomY*	16.2 ± 11.2	4%	903
SA3109	Δ*pomZ*	10.4 ± 7.1	3%	725
SA4743	Δ*pomYZ*	15.5 ± 8.5	4%	316
SA4254	Δ*pomXY*	17.2 ± 11.8	1%	328
SA6130	Δ*pomXZ*	13.6 ± 7.8	2%	307
SA4722	Δ*pomXYZ*	10.4 ± 5.6	<1%	336

Figure 13: PomXYZ work together in one system.
(A) Immunoblot analysis of lysates of indicated strains for the presence and the accumulation level of PomX, PomY and PomZ. Lysates were obtained from exponentially growing cultures. Equal amount of total protein content was loaded per lane to allow detection of differences in accumulation level. Specific α-PomX, α-PomY and α-PomZ antibodies were used to detect PomX (43.9 kDa), PomY (70.1 kDa) and PomZ (44.7 kDa), respectively. Grey arrows depict unspecific binding of α-PomX and α-PomY antibodies. **(B)** Cell length distribution of indicated strains as box plots. Grey boxes enclose 25th and 75th percentile, with the black line showing the mean. Whiskers display 10th and 90th percentile. Outliers smaller than 35 µm are depicted as black dots. Outliers bigger than 35 µm are not shown but are included for the calculation of the mean cell length. Dots below the orange line show depict minicells. **(C)** Summary of all Δ*pom*-mutants with their mean cell length ± SD in µm and constriction frequency in comparison to WT.

PomZ accumulated in WT cell lysate as well as in lysates of a Δ*pomX* and Δ*pomY* mutant at WT-like levels, excluding the possibility that Δ*pomX* and Δ*pomY* phenotypes solely arose from the lack of PomZ and demonstrating that PomX and PomY are important for cell division (Figure 13 A) (Schumacher, 2011). The other way around, both PomX and PomY accumulated at WT levels in a Δ*pomZ* mutant, which ruled out that PomZ affected the stability of PomX and PomY (Figure 13 A). Importantly, PomY accumulated at WT levels in absence of PomX, like PomX accumulated in the absence of PomY (Figure 13 A), showing that PomX, PomY and PomZ do not affect each other's stability *in vivo* but accumulate independently of each other (Schumacher, 2011).

Next, we asked if the three Pom proteins work in the same parthway. To this end a Δ*pomYZ* (SA4743), a Δ*pomXZ* (SA4254) and a Δ*pomXY* (SA6130) mutant were generated, together with a Δ*pomXYZ* triple mutant (SA4722) and analyzed for their cell division phenotype (Figure 13 B). All double mutants had a similar cell division phenotype, suggesting that the three Pom-proteins work in the same parthway (Figure 13 B, C). Even a deletion of the whole *pomXYZ* gene cluster was not lethal, suggesting that the Pom-system is not essential in *M. xanthus*. However, a Δ*pomXY* mutant as

well as a Δ*pomXYZ* mutant had the most dramatic effect on cell division with the production of 1 % or even less than 1 % constrictions, respectively. We conclude that deletion of *pomX* and *pomY* affects cell division, like it was observed for deletion of *pomZ*. Moreover all three proteins work in the same parthway, suggesting that these three proteins build up the PomXYZ system.

5.1.7 Lack of PomX and PomY does not perturb chromosome replication or segregation

Cell division defects with cell filamentation or minicell formation result from a variety of mutants that are affected in different cellular processes like sugar metabolism (Monahan *et al.*, 2014, Weart *et al.*, 2007), cellular polarity (Matroule *et al.*, 2004), chromosome replication, segregation or its condensation status (Donovan *et al.*, 2010, Harms *et al.*, 2013, Niki *et al.*, 1991, Ptacin *et al.*, 2010) and finally mutations that directly affect assembly and/or positioning of the divisome (de Boer *et al.*, 1989, Hirota *et al.*, 1968, Pichoff & Lutkenhaus, 2002, Thanbichler & Shapiro, 2006, Treuner-Lange *et al.*, 2013).

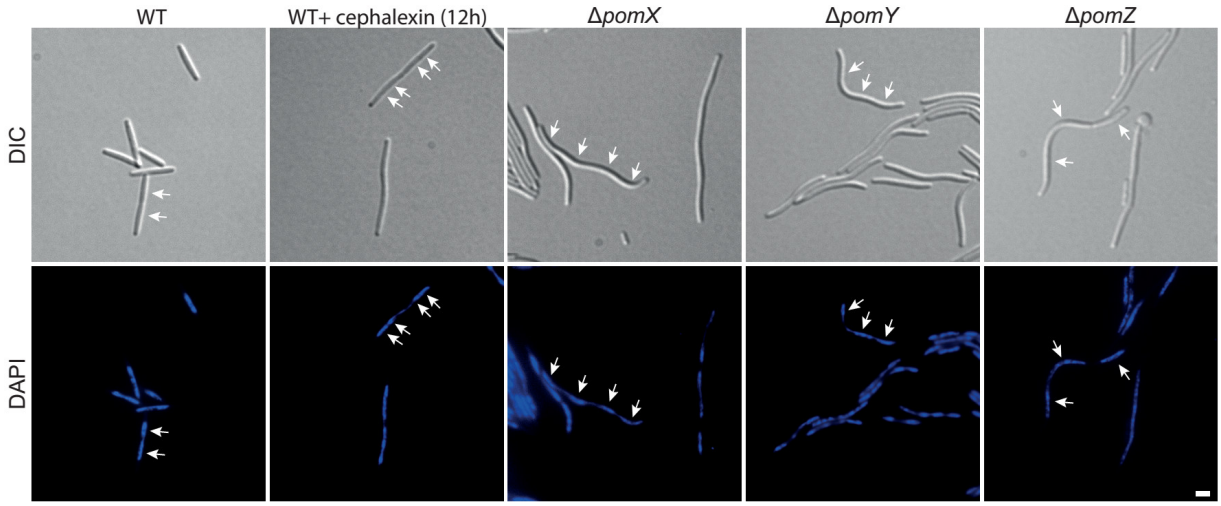

Figure 14: A Δ*pomX* and a Δ*pomY* mutant produce cells with multiple nucleoids and minicells.
Microscopic analysis of cells of indicated strains. Exponentially grown cells were imaged on 1 % agarose buffered with TPM. Nucleoids were stained with 1 µg/ml DAPI prior to picture acquisition. White arrows indicate single nucleoids in cells that are representative for indicated strains. Scale bar: 2 µm.

Lack of PomZ neither affects chromosome replication nor its segregation, but is likely to be directly involved in positioning of the cell division site by affecting FtsZ localization and Z-ring formation (Treuner-Lange *et al.*, 2013). To rule out that PomX and PomY affect these cellular processes, chromosome content, together with the intracellular positioning of the nucleoids was quantified. For quantification, WT cells along with cells of a Δ*pomX* and Δ*pomY* mutant were stained with DAPI and analyzed by microscopy. Cells lacking PomX and PomY showed multiple nucleoids at high frequency in addition to cells that did not contain any DAPI signal. Latter cells were predominantly small and as described are anucleate minicells. Cells of WT in contrast contained either one or two nucleoids (Figure 14). This is consistent with the recent finding that *M. xanthus* has one replication cycle per cell division cycle, giving rise to two chromosomes directly before cell division (Harms *et al.*, 2013).

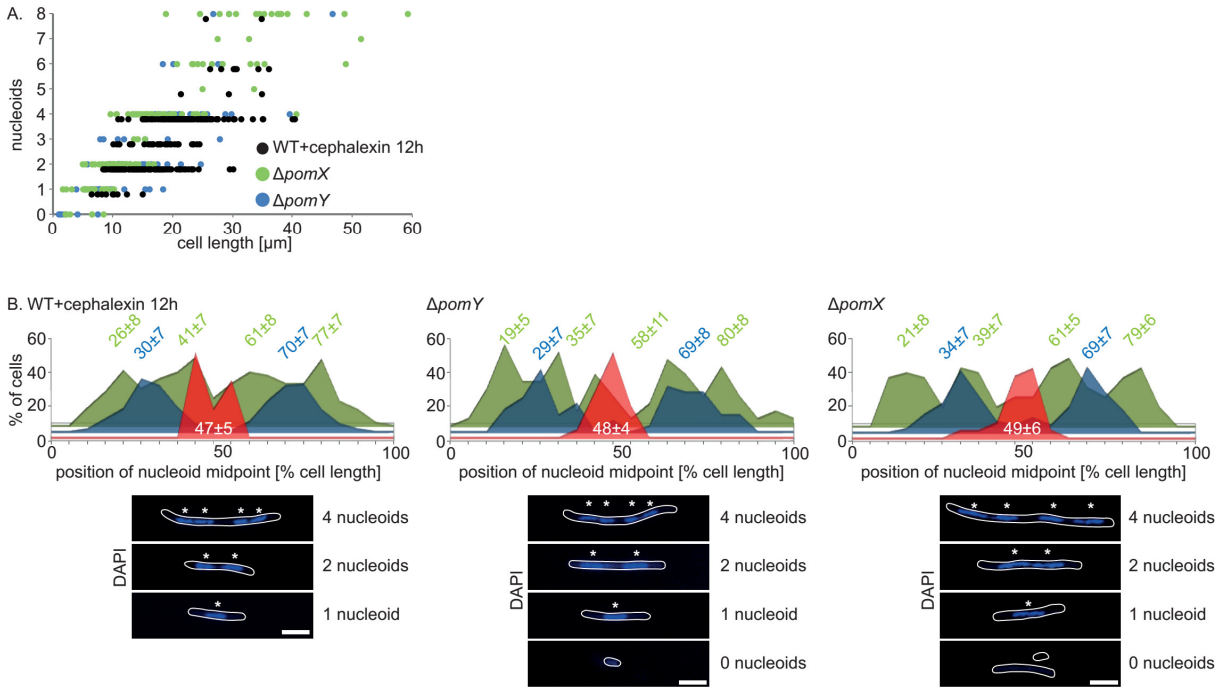

Figure 15: PomX and PomY do not affect chromosome replication or its segregation.
(A) Analysis of nucleoid number in WT, Δ*pomX* and Δ*pomY* mutant per cell length. Exponentially grown WT, Δ*pomX* and Δ*pomY* cells were stained with DAPI and visualized by DIC and fluorescence microscopy. In case of WT cells were treated with cephalexin for 12 h before analysis. n>200 cells per strain. **(B)** Histograms, showing the position of nucleoid midpoints along the long cell axis in cephalexin treated WT, Δ*pomX* and Δ*pomY* mutant in cells with one (red), two (blue) and four (green) nucleoids. Numbers display mean position ± SD for nucleoid midpoints in % of cell length. n>200 cells per strain. Representative pictures of analyzed, DAPI-stained cells are shown below. White stars indicate nucleoid midpoints. Cell outlines were obtained from DIC pictures. Scale bar: 2 µm.

We considered that multiple nucleoids observed in cells lacking PomX or PomY can occur for different reasons. First, polyploidy could originate from replication defects that result in over-initiation of replication. Secondly, multiple nucleoids were primarily found in longer cells, suggesting that growing cells, which have defects in cell division, have ongoing replication cycles. To differentiate between these two hypotheses DAPI-stained nucleoids were counted and their number was plotted as function of cells length (Figure 15 A). If PomX and PomY do not affect chromosome replication but multiple nucleoids originated from ongoing replication cycles in growing cells, the number of nucleoids would correlate with cell length. In the other case, the number of nucleoids would be more or less independent of cell length because of the de-regulation of initiation of replication. To have a direct comparison, we treated WT cells with cephalexin for 12 h before analysis to artificially elongate cells. Cephalexin inhibits cell division at the level of cell constriction by interference with FtsI and the consecutive peptidoglycan synthesis at the cell division site. Importantly, cephalexin does not affect DNA replication, its segregation and furthermore does not perturb cell growth in general in *E. coli* (Pogliano *et al.*, 1997).

Cells of WT contained either one or two nucleoids, whereas the number of nucleoids ranged from one to eight in WT cells treated with cephalexin for 12 h (n>200). The number of nucleoids, if plotted as a function of cell length, increased with increasing cell length, showing that nucleoid number correlates with cell length in treated WT cells (Figure 15 A). In this analysis, number of nucleoids in a Δ*pomX* (n=210) and a Δ*pomY* (n=212) mutant also correlated with increasing cell length, making both

mutants indistinguishable from WT in terms of chromosome content. This led to the conclusion that the multiple chromosome phenotype in cells lacking PomX or PomY originates from cell division defects rather than from over-initiation of replication (Schumacher, 2011).

To determine if PomX and PomY are involved in chromosome segregation, the midpoints of the DAPI stained nucleoids in cells with one, two or four nucleoids were plotted as function of cell length (Figure 15 B). In treated WT cells with one nucleoid the midpoint was arranged around midcell with 47 ± 5 %, while cells with two nucleoids arranged these at 30 ± 7 % and 70 ± 7 %, which was consistent with the previously described chromosome arrangement in *M. xanthus* (Harms *et al.*, 2013).

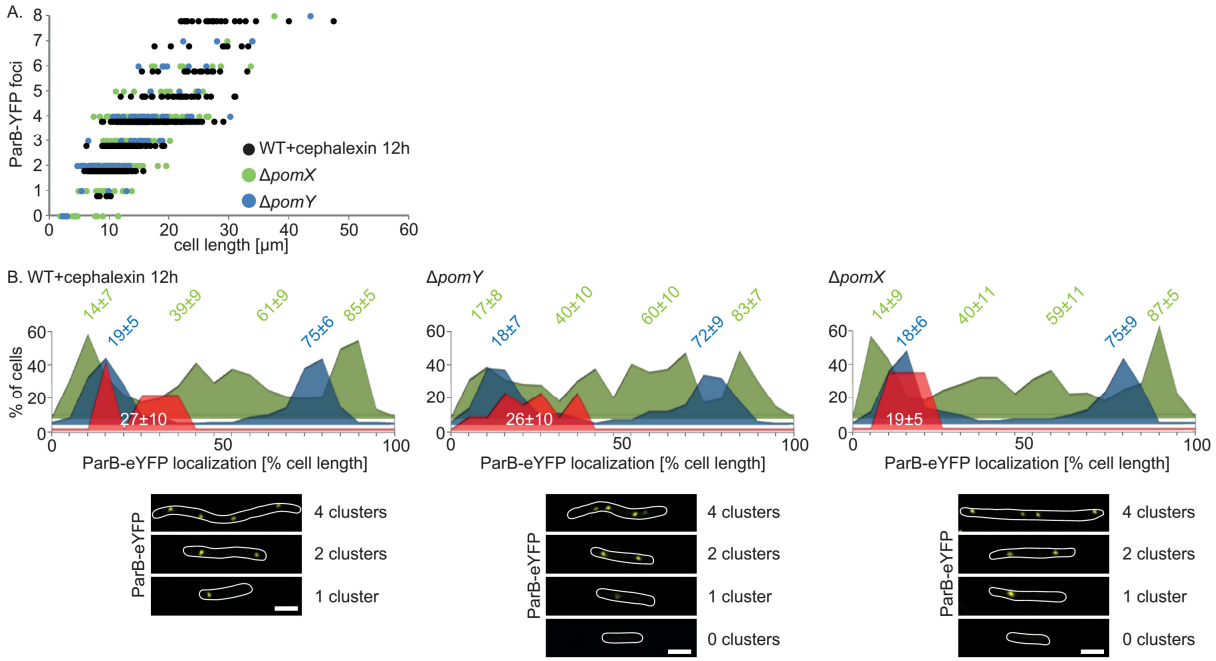

Figure 16: ParB-eYFP cluster number and localization is unaffected by lack of PomX and PomY.
(A) WT, Δ*pomX* and Δ*pomY* mutant display the same ParB-eYFP foci number per cell length. Exponentially grown WT, Δ*pomX* and Δ*pomY* cells expressing *parB-eyfp* in addition to native *parB* were visualized by DIC and fluorescence microscopy (n>200). In case of WT, cells were treated with cephalexin for 12 h before analysis. **(B)** Histograms, showing the position of ParB-eYFP along the long cell axes in cephalexin treated WT, Δ*pomX* and Δ*pomY* mutant in cells with one (red), two (blue) and four (green) ParB-eYFP foci. Numbers display mean position ± SD for ParB-eYFP foci in % of cell length. Representative pictures of analyzed cells are shown below. Cell outlines were obtained from DIC pictures. Scale bar: 2 µm.

If cells contained 4 nucleoids, their midpoints were segregated within the cell with nucleoid 1 at 26 ± 8 %, nucleoid 2 at 41 ± 7 %, nucleoid 3 at 61 ± 8 % and the fourth nucleoid at 77 ± 7 %. This demonstrates that long cells, which are treated with cephalexin, are still able to segregate their nucleoids. Like observed in treated WT cells, in Δ*pomX* and Δ*pomY* cells, nucleoids were arranged in the same way, with a single chromosome mass at midcell (49 ± 6 % and 48 ± 4 %, respectively) and two chromosomes at approximately 20 % and 75 % positions. Even cells with four nucleoids positioned these similar to treated WT cells, strongly suggesting that both, PomX and PomY are not involved in chromosome segregation (Figure 15 B).

Because midpoints of DAPI-stained nucleoids are not a precise marker, the same experiment was repeated by using ParB-eYFP localization as a reference point for the number and localization of the origin of replication (Figure 16). ParB binds specifically to *parS* sequences that are found proximal

to the *ori* on the *M. xanthus* genome and was therefore shown to be an excellent tool to follow the origin of replication (Harms *et al.*, 2013). In cephalexin-treated cells of SA4202 (*parB*$^{+}$/*parB-eyfp*) ParB-eYFP was expressed from its native promoter at the *Mx8* attachment site and localized in one to eight separated clusters. This suggests that these cells contained one to eight *parS* regions and therefore up to eight origins of replication. Consistent with previous findings, the number of ParB-eYFP clusters increased with increasing cell length. Similarly, up to eight clusters were observed in cells of a Δ*pomX* (SA4219 Δ*pomX*; *parB*$^{+}$/*parB-eyfp*) or Δ*pomY* mutant (SA4709 Δ*pomY*;*parB*$^{+}$/*parB-eyfp*). However, small cells were observed that lacked a ParB-eYFP signal, which belonged to the anucleate minicells. Importantly, if the number of ParB-eYFP clusters is plotted as function of cell length, the number of clusters correlates with increasing cell length (Figure 16 A), reflecting the results obtained by nucleoid counting before. Again the same cells were used to plot the position of ParB-eYFP clusters as function of cell length to determine if ParB-eYFP clusters are misplaced in cells lacking PomX or PomY. Cells with one, two and four ParB-eYFP clusters were used for this analysis. Similar to the observations made in WT background ParB-eYFP localization showed the same overall positioning pattern in a Δ*pomX* and Δ*pomY* mutant (Figure 16 B). This is in agreement with the described nucleoid positioning results and demonstrates that PomX and PomY, like PomZ, are neither involved in chromosome replication nor its segregation (Schumacher, 2011).

5.1.8 PomX and PomY directly affect Z-ring formation and localization

Because accumulation of FtsZ is important for correct cell division, we hypothesized that the phenotypes observed in a Δ*pom* mutant may arise from inappropriate FtsZ levels in the cells. By testing lysates of WT and the three Δ*pom* mutants for FtsZ accumulation it was shown that FtsZ is produced in all three mutant strains and the accumulation levels are similar to that of WT (Figure 17 A), thereby disproving this hypothesis.

In 50 % of WT cells FtsZ-mCherry showed one defined Z-ring at midcell, whereas in the other half of the cells FtsZ-mCherry displayed a diffuse localization throughout the cell. These patterns were changed in absence of PomZ, where most cells displayed a diffuse FtsZ-mCherry localization with only few Z-rings formed (Treuner-Lange *et al.*, 2013) (Figure 17 B). To investigate the function of PomX and PomY in correct Z-ring localization and formation, strains SA4228 (Δ*pomX*; *ftsZ*$^{+}$/*ftsZ-mCherry*) and SA4707 (Δ*pomY; ftsZ*$^{+}$/*ftsZ-mCherry*) (Schumacher, 2011) were created. These strains express *ftsZ-mCherry* under the control of the native *ftsZ* promoter in presence of unlabeled *ftsZ* from the *Mx8* attachment site, because FtsZ-mCherry alone does not support growth (Treuner-Lange *et al.*, 2013). In both cases cells predominantly showed a diffuse localization of FtsZ-mCherry with small clusters that did not span the cell width (Figure 17 B). Only rarely defined Z-rings were formed in 2 % - 5 % of cells, indicating that either production of Z-rings or their stability was affected by the lack of PomX and PomY. Notably, the few Z-rings formed were distributed along the long cell axis. This phenotype was similar to the phenotype observed for a Δ*pomZ* mutant. In total, we conclude that PomX and PomY are required for correct Z-ring localization and stimulate its formation or its stability at midcell. Additionally, the data provides strong evidence that PomX and PomY work together with PomZ in the same parthway, in regulating cell division and cell division site placement in *M. xanthus.*

Finally, these data also show that FtsZ forms Z-rings that are able to perform cell division even in the absence of PomXYZ.

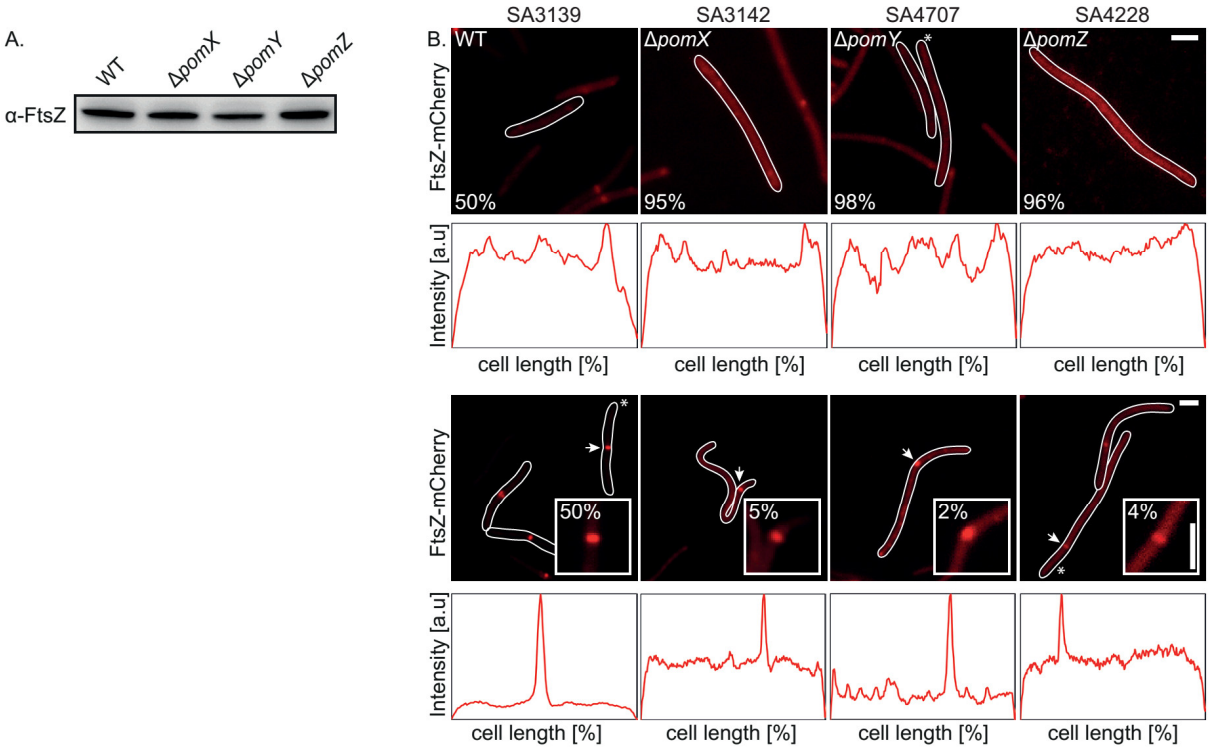

Figure 17: PomX and PomY are required for correct formation and localization of Z-rings.
(A) Immunoblot analysis of indicated strains for the presence and accumulation of FtsZ (44.7 kDa). Lysates were obtained from exponentially grown cultures. Equal amount of total protein content was loaded per lane to allow for detection of differences in accumulation level. Specific α-FstZ antibodies were used to detect FtsZ. **(B)** Localization and production of Z-rings is affected by lack of PomX and PomY. Exponentially grown cells were imaged on 1 % agarose buffered with TPM at 32 °C. Outline of cells was obtained from DIC pictures. Linescans display mCherry signal intensity along long cell axis and were created from fluorescence pictures using Metamorph. White numbers indicate the occurrence of the given localization patterns (n>150 cells). White arrows indicate Z-rings. Scale bar: 2 µm.

5.2 PomX, PomY and PomZ form a complex that is positioned at midcell by PomZ

While the divisome components are conserved in bacteria, they have evolved different systems to ensure proper spatial and temporal regulation of Z-ring formation. Generally, these systems can be classified into two groups. In *B. subtilis*, *E. coli* and *C. crescentus* negative regulation systems guarantee correct Z-ring localization at midcell, directly acting on the Z-ring, by inhibiting its formation all over the cell (de Boer *et al.*, 1992, Kiekebusch *et al.*, 2012, Marston *et al.*, 1998). In order to do so the negative regulators are sequestered to the cell poles away from the site of cell division, either by direct targeting or by a dynamic oscillatory movement over time in the case of the *E. coli* Min system (Hu & Lutkenhaus, 1999, Marston *et al.*, 1998). On the other hand regulators in *S. pneumoniae* and *S. coelicolor* localize at the incipient site of cell division to guide Z-ring formation. Here they function as a marker for FtsZ recruitment and may stabilize Z-ring formation (Fleurie *et al.*, 2014, Holeckova *et al.*, 2015, Willemse *et al.*, 2011). PomZ was shown to localize at the site of cell division, which in *M. xanthus* is midcell, before the Z-ring forms and furthermore colocalizes with FtsZ and cell division constrictions. This suggested that PomZ might recruit FtsZ to midcell, directly or indirectly, to stimulate

Z-ring formation and cell division (Treuner-Lange *et al.*, 2013). The mechanism of how PomZ identifies midcell and stimulates Z-ring formation is still uncovered. To understand how PomX and PomY work in this system the spatial and temporal localization of both proteins was studied in detail.

5.2.1 PomX and PomY form clusters at the incipient cell division site before cell division

To reveal the spatial localization of PomX and PomY, *mCherry-pomX* and *pomY-mCherry* fusions were generated and expressed from the *Mx8* attachment site under the control of their putative native promoters. Strains SA4229 (Δ*pomX*/*mCherry-pomX*) and SA4713 (Δ*pomY*/*pomY-mCherry*; Schumacher, 2011) were created to study mCherry-PomX and PomY-mCherry localization. Expressed under these conditions, the full length proteins of mCherry-PomX and PomY-mCherry accumulated at WT levels, nevertheless mCherry-PomX was partial degraded as detected by immunoblot analysis with α-PomX antibodies (Figure 10 D; Figure 11 D). These strains displayed a WT phenotype, indicating that the generated fusion proteins are functional under the tested conditions (Figure 10 A; Figure 11 A). mCherry-PomX and PomY-mCherry generally showed the same localization patterns. In 24 % of cells mCherry-PomX showed no signal, or a signal with very low signal to noise ratio compared to the background, while PomY-mCherry displayed a diffuse signal throughout the entire cell. 25 % of cells displayed a single cluster between the pole and 45% of cell length which was named the off-centre cluster, with an average position at 36 ± 9 % and 39 ± 6 % of cell length for mCherry-PomX and PomY-mCherry, respectively. Both fusion proteins localized precisely at midcell (50 % ± 5 % for all further analysis) in the majority of all cells (51 % in both cases; SA4229 n=213; SA4713 n=220) (Figure 18 A).

Although clusters of mCherry-PomX and PomY-mCherry displayed similar patterns, localization of the fluorophores differed in the diffuse background fluorescence of PomY-mCherry that was not observed in case of the strong mCherry-PomX cluster. To determine the difference between the localization of PomY-mCherry and mCherry-PomX cluster intensity was quantified as a marker of how much fluorescently labeled protein is captured in the cluster. While PomY-mCherry clusters contained 14 ± 4 % (n=91) of the total cellular fluorescence nearly half of it was enclosed in the mCherry-PomX cluster with 41 ± 3 % (n=75).

These localization patterns were strikingly similar to the PomZ-mCherry localization with the exception that PomZ-mCherry was not observed in a diffuse localization in the cell. It is found to localize in a patchy pattern in 25 % of cells and formed an additional off-centre cluster in another 25 % of cells. In the remaining 50 % PomZ-mCherry formed a midcell cluster with the additional patchy localization on either side of that cluster (Treuner-Lange *et al.*, 2013) (Figure 18 A). Like for PomY-mCherry, only little PomZ-mCherry signal is observed within the cluster (9 ± 3 %; n=75).

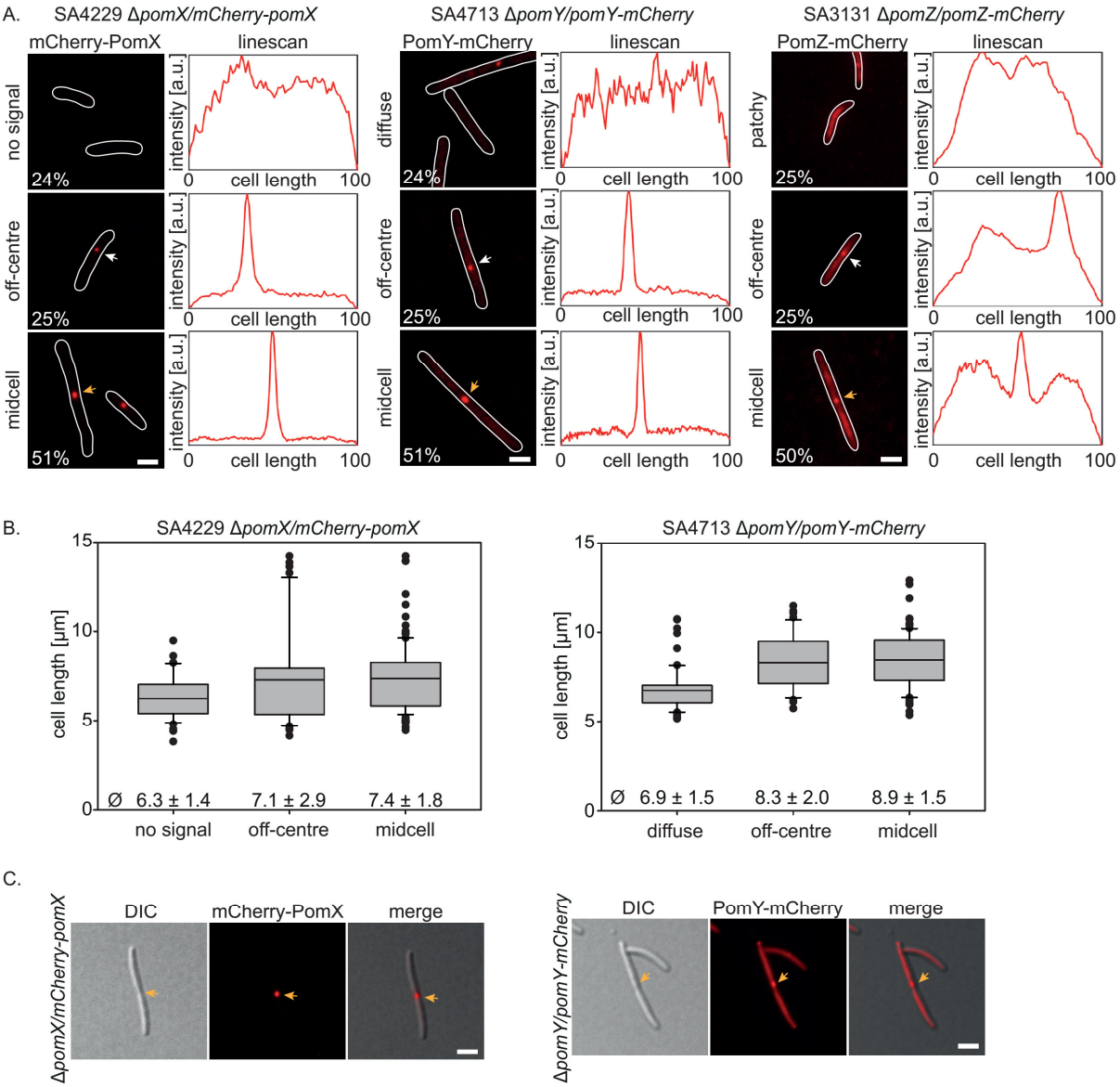

Figure 18: mCherry-PomX and PomY-mCherry localize similar to PomZ-mCherry in three patterns.
(A) Localization of mCherry-PomX, PomY-mCherry and PomZ-mCherry by fluorescence microscopy. Pictures of indicated strains were acquired on 1 % agarose buffered with TPM at 32 °C. White numbers represent pattern quantifications (n>200 per strain). Cell outlines were obtained from DIC pictures. White arrows depict off-centre clusters while orange arrows depict midcell clusters. Linescans show mCherry signal along long cell axis and were obtained from fluorescence pictures using Metamorph. Scale bar: 2 µm. **(B)** Localization patterns of mCherry-PomX and PomY-mCherry correlate with increasing cell length. Grey boxes enclose 25th and 75th percentile, with the black line showing the mean, which is also indicated below boxes ± SD. Whiskers display 10th and 90th percentile. All outliers are depicted as black dots. **(C)** mCherry-PomX and PomY-mCherry colocalize with cell division constrictions. Representative cells of indicated strains were imaged as described in (A). Orange arrows indicate midcell clusters. Merged pictures were produced with Metamorph. Scale bar: 2 µm.

By eye the localization patterns of mCherry-PomX and PomY-mCherry correlated with cell length (Figure 18 B). To this end, the total cell population was divided based on the localization patterns and for each group mean cell length was determined. No signal of mCherry-PomX and a diffuse signal for PomY-mCherry were observed in small cells (Ø 6.3 ± 1.4 µm and 6.9 ± 1.5 µm, respectively). Off-centre clusters of mCherry-PomX and PomY-mCherry were detected in longer cells with 7.1 ± 2.9 µm and 8.3 ± 2.0 µm. The longest cells showed mCherry-PomX (7.4 ± 1.8 µm) and PomY-mCherry (8.9 ± 1.5 µm) clusters at midcell. Notably, these clusters colocalized with cell division

constrictions at midcell (Figure 18 C), indicating that they are part of the divisome at the onset and during cell division.

It is important to mention that similar results were obtained, if mCherry-PomX (SA4252 Δ*pomX/mCherry-pomX*+) and PomY-mCherry (SA4712 Δ*pomY/pomY-mCherry*+++; Schumacher, 2011) were under the control of stronger promoters, accumulating at higher levels in the cells (Figure S 1 A). Under these conditions mCherry-PomX displayed clusters at higher frequency, giving rise to less cells with no signal. Nevertheless, the localization patterns still correlated with increasing cell length (Figure S 1 B). In addition, expression of mCherry-PomX at even higher levels in strain SA4244 (Δ*pomX*/*mCherry-pomX*+++) resulted in the loss of cluster formation, but the production of mCherry-PomX filaments that spanned the whole cell length (Figure S 1 C). These mCherry-PomX clusters/filaments did not colocalize with constrictions, but cell division took place away from the filament in a PomX-free area (Figure S 1 D).

Assuming a cell cycle of approximately 5 h under laboratory conditions the presented data provides evidence that PomX and PomY localize at midcell on average 2.5 h before cell division takes place. This coincides with the notion that both PomZ and FtsZ localize at midcell during 50 % of the cell cycle (Treuner-Lange *et al.*, 2013), suggesting that all four proteins arrive at midcell around the same time based on snap-shots. Because PomX and PomY similarly to PomZ localize at midcell as a cluster in the majority of cells and colocalize with cell division constrictions during cell division, we hypothesize that PomX and PomY together with PomZ are positive regulators for Z-ring formation at midcell and may work as an anchor or platform for Z-ring formation.

5.2.2 PomX, PomY and PomZ colocalize *in vivo*

PomX, PomY and PomZ show a similar localization pattern with defined off-centre clusters in small cells, which ultimately localize at midcell before cell division. This finding let us to predict that PomX, PomY and PomZ colocalize *in vivo*. To investigate this idea a PomY-eYFP fusion was constructed to analyze PomY localization in cells that express mCherry-PomX and PomZ-mCherry. For this, we created strains SA7020 (Δ*pomZ*/*pomZ-mCherry*; *pomY*$^{+}$/P$_{cuoA}$*pomY-eyfp*) and SA7041 (Δ*pomY*/P$_{cuoA}$*pomY-eyfp*; *pomX*$^{+}$/*mCherry-pomX*+). In these strains *pomY-eyfp* was expressed under copper-dependent regulation in presence of 150 µM $CuSO_4$. Expression of *pomY-eyfp* under these conditions in a Δ*pomY* mutant (SA7024; Δ*pomY*/P$_{cuoA}$*pomY-eyfp*) resulted in a WT cell length phenotype and constriction frequency (Figure S 3). In a similar experiment PomY-mCherry accumulated slightly above WT levels as detected by immunoblot analysis with specific α-PomY antibodies (Figure S 2). These data indicate that the PomY-eYFP fusion protein is active *in vivo*.

Both strains produced clusters of PomY-eYFP together with either mCherry-PomX or PomZ-mCherry. As expected, from the snap shot analysis of the single-labeled strains, clusters of PomY-eYFP colocalized with cluster of mCherry-PomX and PomZ-mCherry in the off-centre position and at midcell (Figure 19). This demonstrates that PomX, PomY and PomZ all colocalize in a cluster. These observations suggest that a complex, consisting of all three Pom proteins, localizes at midcell and that this complex forms before it reaches midcell.

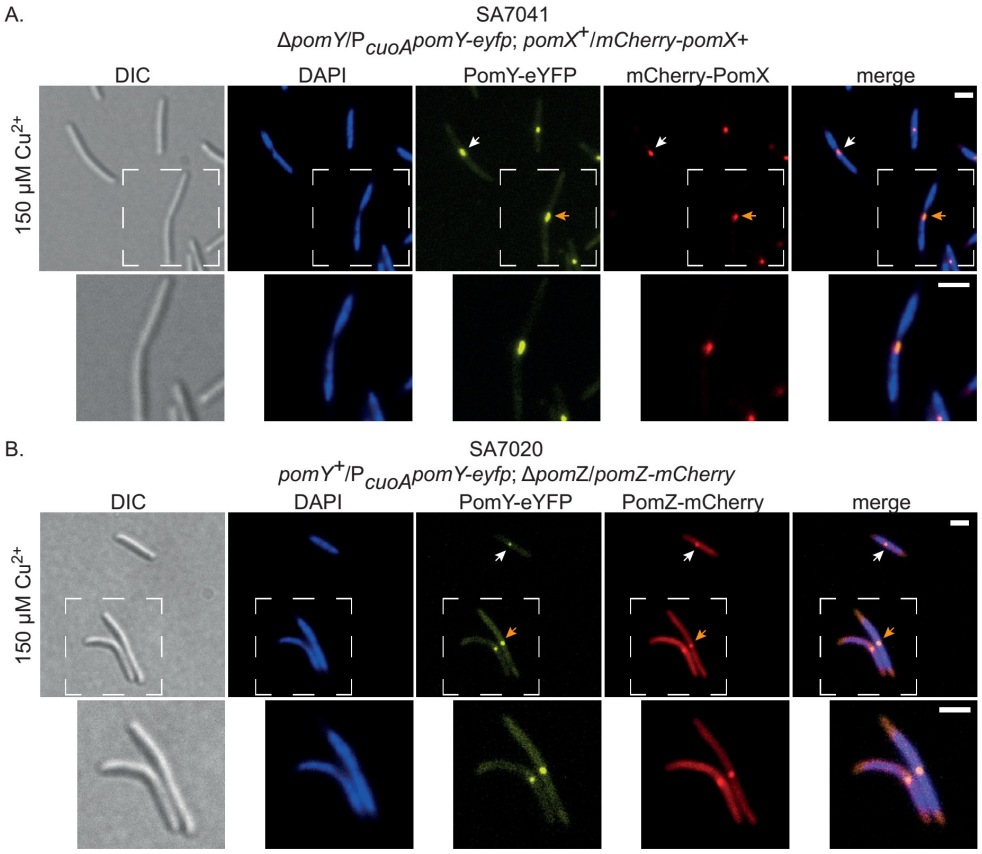

Figure 19: PomX, PomY and PomZ colocalize in the cluster.
(A) PomY-eYFP and mCherry-PomX clusters colocalize. Pictures show representative cells of each strain and were acquired from exponentially grown cells on 1 % TPM buffered agarose at 32 °C. Cells were grown in presence of 150 µM $CuSO_4$ for 24 h and stained with DAPI prior to imaging. White arrows indicate off-centre clusters while orange arrows indicate midcell clusters. Areas in stippled lines are magnified below pictures. Scale bar: 2µm. **(B)** Clusters of PomY-eYFP and PomZ-mCherry colocalize. Pictures show representative cells and were acquired as in (A). Images were acquired as in (A).

5.2.3 PomX and PomY form clusters over the nucleoid and localize at midcell before the end of replication

PomX and PomY localization correlates with cell length, i.e. small cells have no, or a diffuse signal and longer cells show an off-centre cluster. Ultimately, in long cells both mCherry-PomX and PomY-mCherry localize at midcell where they colocalize with cell division constrictions at the onset of cell division. This implies that PomX and PomY localization not only correlates with cell length but may also correlate with, or depend on cell cycle progression.

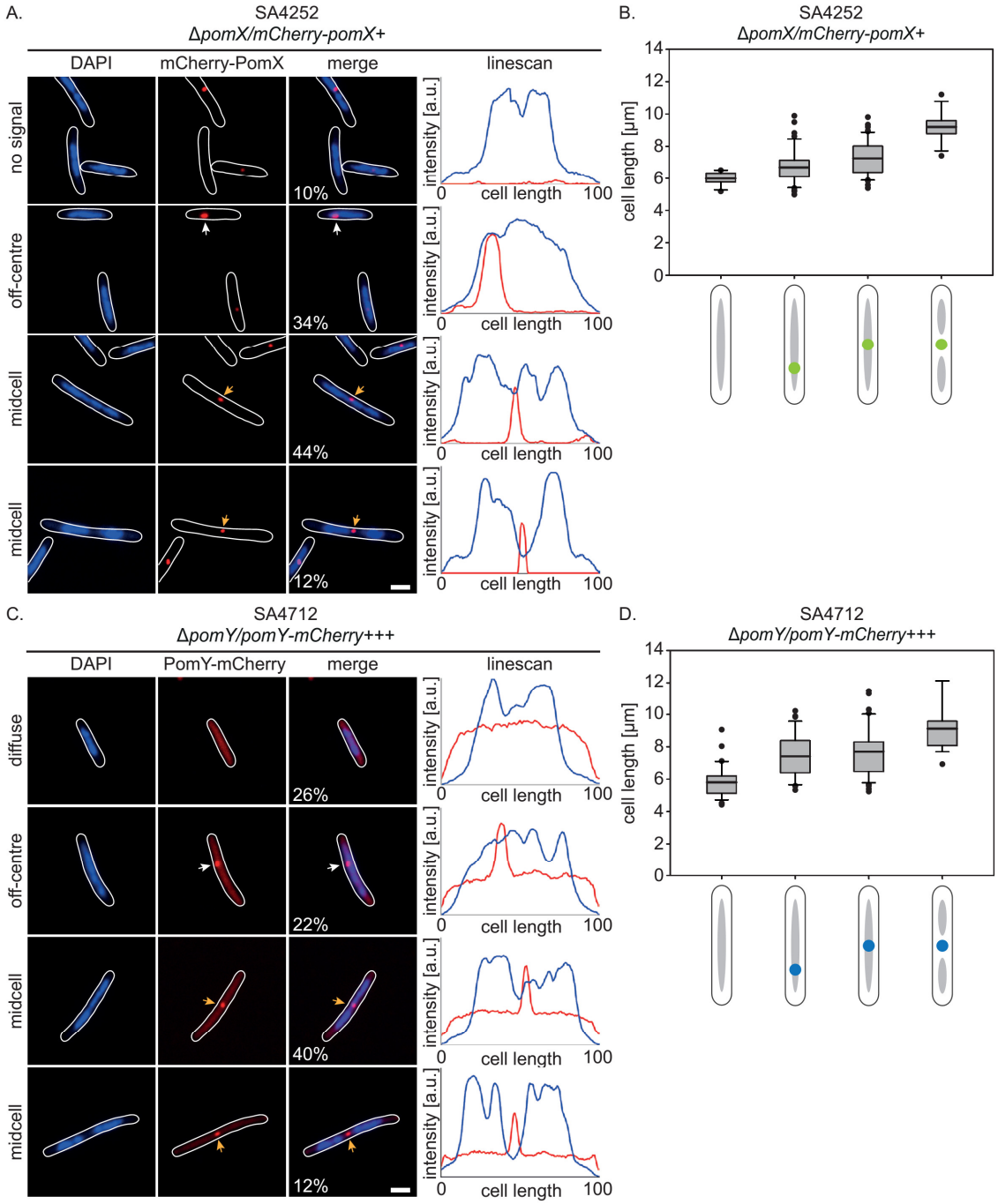

Figure 20: PomX and PomY localization correlate with cell cycle progression.
(A) Fluorescence microscopy of mCherry-PomX in correlation to the nucleoid status. Cells of exponentially grown cultures were stained with DAPI prior to picture acquisition on a TPM buffered 1 % agarose at 32 °C patch. Pictures show representative cells. Cell outlines were obtained from DIC pictures. White arrows indicate off-centre clusters, while orange arrows indicate midcell clusters. Numbers display quantification of localization pattern abundance (n>150 cells). Linescans show fluorescence intensity signal of mCherry and DAPI signal along long cell axis and were produced from fluorescent pictures using Metamorph. Scale bar: 2 µm. **(B)** mCherry-PomX localization patterns corellate with cell length. Grey boxes enclose 25th and 75th percentile, with the black line showing the mean. Whiskers display 10th and 90th percentile. All outliers are depicted as black dots. **(C)** Fluorescence microscopy of PomY-mCherry in correlation to the nucleoid status. Cells were treated as described in (A). **(D)** PomY-mCherry localization patterns correlate with cell length. Box plots were created as in (B).

To investigate this idea, the localization of mCherry-PomX and PomY-mCherry was analyzed and quantified in DAPI-stained cells of strain SA4712 (Δ*pomY*/*pomY-mCherry*+++) and SA4252

(Δ*pomX*/*mCherry-pomX*+). Here the nucleoid status was used as a marker for cell cycle progression, knowing that newborn *M. xanthus* cells contain one centrally positioned, replicating chromosome, while cells before cell division exhibit two fully replicated and segregated chromosomes (Harms *et al.*, 2013). Small cells with no mCherry-PomX or a diffuse PomY-mCherry signal contained a single nucleoid in the cell centre and off-centre clusters were exclusively found over the DAPI-stained nucleoid in 22 % to 34 % of cells, respectively. In half of the cells the fusion proteins were observed at at midcell. Importantly, nearly 80 % of the latter colocalized with the nucleoid midpoint at midcell, while 20 % localized precisely in between two fully segregated nucleoids (Figure 20 A, B).

Equally, PomZ-mCherry localized in a patchy pattern over a central nucleoid mass and formed an additional off-centre cluster over the DAPI signal. Moreover, we observed that the patchy localization of PomZ-mCherry exactly matched the localization of the nucleoid mass, with only little fluorescence outside in the polar and subpolar regions of the cell, which are devoid of DNA (Figure 21).

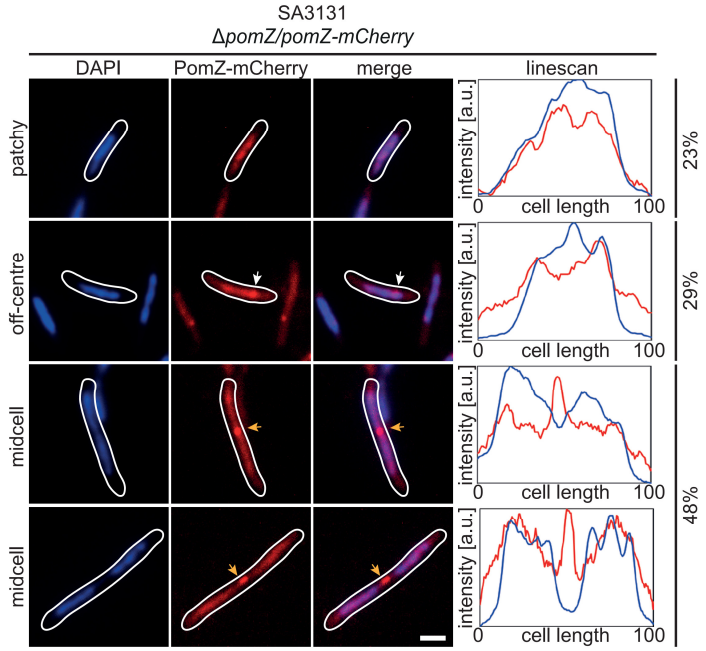

Figure 21: PomZ localization correlates with the nucleoid status.
Cells of exponentially grown cultures were stained with DAPI prior to picture acquisition on TPM buffered 1 % agarose at 32 °C. Pictures show representative cells. Cell outlines were obtained from DIC pictures. White arrows indicate off-centre clusters, while orange arrows indicate midcell clusters. Linescans show fluorescence intensity signal of mCherry and DAPI signal along long cell axis and were produced from fluorescence pictures using Metamorph. Numbers were obtained from Treuner-Lange *et al.*, 2013. Scale bar: 2 µm.

These observations are consistent with published data (Treuner-Lange *et al.*, 2013) and raised the hypothesis that PomZ does not only colocalize with PomXY in the cluster but also interacts with the chromosomal DNA in *M. xanthus*.

First, these analyses show that PomX and PomY, as well as PomZ localization correlates with cell cycle progression and furthermore that both proteins spend around ¾ of the cell cycle over the nucleoid (62 % - 78 %).

Because the PomXYZ cluster localized at midcell over the midpoint of the nucleoid in around 40 % to 50 % of cells, we asked if they localize here before completion of replication, or if termination of replication is a signal for PomXYZ to locate to midcell.

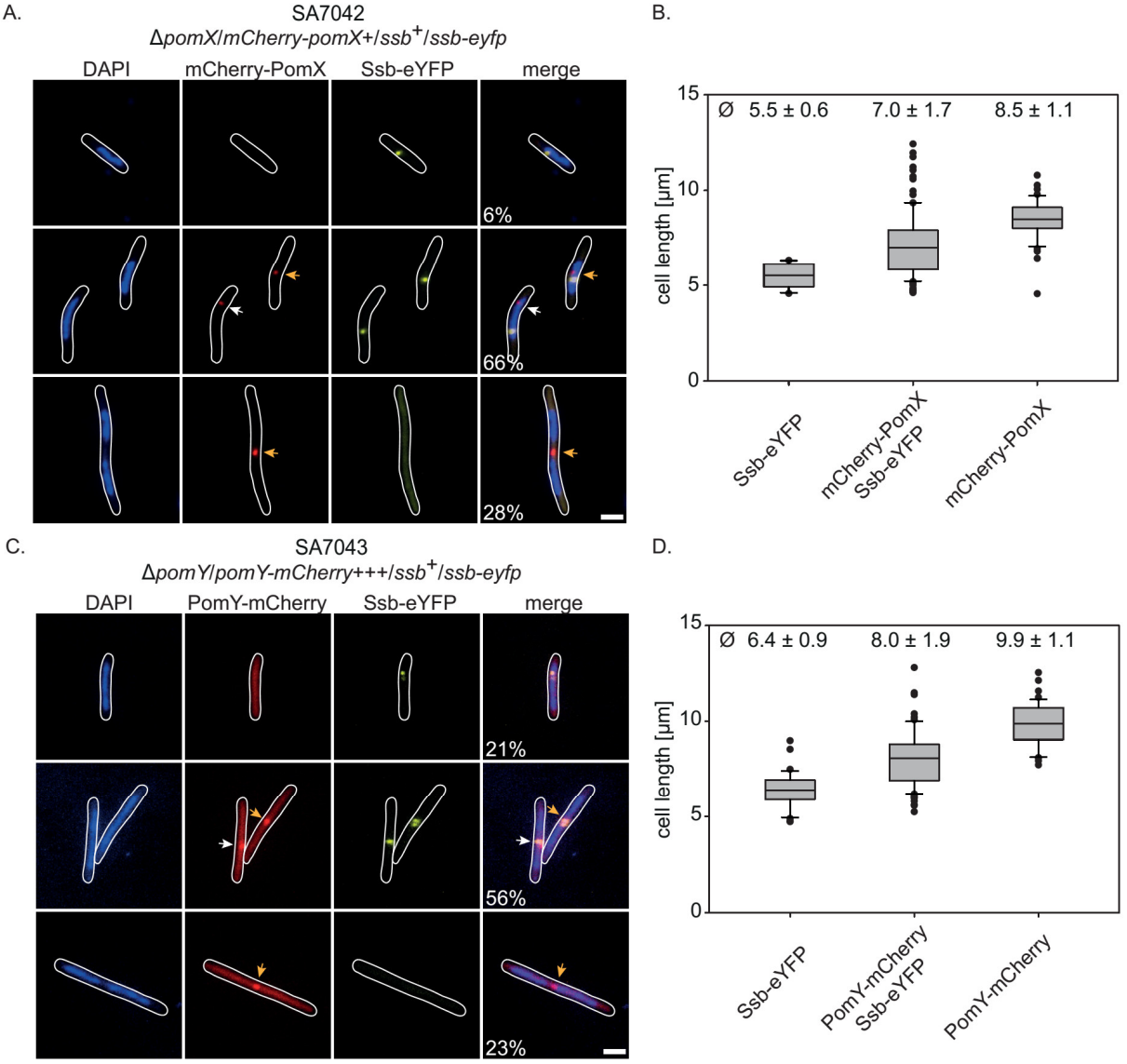

Figure 22: PomXY clusters localize at midcell before the end of chromosome replication.
(A) Colocalization of mCherry-PomX with Ssb-eYFP as a marker for the replication forks. Exponentially grown cells were imaged on 1 % agarose buffered with TPM and labelled proteins were visualized by fluorescence microscopy. Cells were treated with DAPI prior to picture acquisition. White numbers indicate abundance of localization patterns. Cell outlines were obtained from DIC pictures. **(B)** Localization patterns of mCherry-PomX and Ssb-eYFP correlate to cell length. Box plots enclose 25th and 75th percentile, with the black line showing the mean, which are also indicated in numbers ± SD above the plots. Whiskers display 10th and 90th percentile. All outliers are depicted as black dots. **(C)** Colocalization of PomY-mCherry with Ssb-eYFP. Cells were treated and imaged as described in (A). **(D)** Localization pattern of PomY-mCherry and Ssb-eYFP correlate to cell length. Box plots were created as explained in (B).

To study replication, an Ssb-eYFP fusion was used as a proxy for the replication forks, as Ssb binds to single stranded DNA, which occurs during replication behind the proceeding replication machinery (Harms *et al.*, 2013). Expressed from its native promoter in presence of WT Ssb it produces one or two clusters. These clusters occurred predominantly in smaller cells, while longer cells showed

a diffuse localization of Ssb-eYFP. In time-lapse recordings Ssb-eYFP formed foci in a sub-polar region in small cells and moved to midcell within 3-4 h where clusters disappeared before cell division. Based on these findings the replication time was calculated to be around ¾ of the cell cycle (Harms *et al.*, 2013).

For colocalization analysis strains SA7042 (Δ*pomX*/*mCherry-pomX+;ssb*$^{+}$/*ssb-eyfp*) and SA7043 (Δ*pomY*/*pomY-mCherry+++;ssb*$^{+}$/*ssb-eyfp*) were created. In these straines *mCherry-pomX* and *pomY-mCherry* were expressed from the *Mx8* attachment site, while *ssb-yfp* was expressed from the endogenous promoter. Three localization patterns were detected. As expected, small cells of both strains showed only clusters for Ssb-eYFP, while mCherry-PomX and PomY-mCherry showed no signal or were diffuse (6 % and 21 %, respectively). By contrast, in a quarter of cells, which were long cells, Ssb-eYFP displayed a diffuse localization, while mCherry-PomX and PomY-mCherry localized at midcell. In the majority of cells mCherry-PomX (66 %) and PomY-mCherry (56 %) cooccurred with Ssb-eYFP clusters (Figure 22 B, D). Importantly, mCherry-PomX and PomY-mCherry clusters were found at midcell in high frequency in these cells, demonstrating that cluster localization at midcell over the middle of the nucleoid takes place before the end of replication.

In conclusion, PomX, PomY and PomZ form clusters over the nucleoid in the off-centre and at midcell, which coincides with the middle of the replicating nucleoid mass early during the cell cycle, before replication is terminated. This demonstrates that completion of replication is not the signal for midcell localization of PomXYZ clusters.

5.2.4 Cluster formation depends on PomX, while cluster positioning at midcell depends on PomZ

Based on the colocalization analysis, we hypothesized that the three Pom proteins may have different functions and that lack of one of the components would perturb cluster formation or its correct localization. To explore this idea, localization of each Pom protein in the absence of one or the other was systematically analyzed.

In a Δ*pomX* mutant mCherry-PomX formed clusters in nearly all cells when expressed in strain SA4252 (Δ*pomX*/*mCherry-pomX*+). Of these 1/3 localized in the off-centre position and nearly 2/3 formed a midcell cluster, while only 2% of cells showed no signal for mCherry-PomX (Figure 23 A). These localization patterns correlated with cell length, as small cells showed no signal of mCherry-PomX (mean 5.9 ± 0.6 µm), longer cells displayed an off-centre cluster (mean 7.2 ± 1.5 µm) and the longest cells had a midcell localization of mCherry-PomX (mean 8.4 ± 1.8 µm) (Figure 23 B).

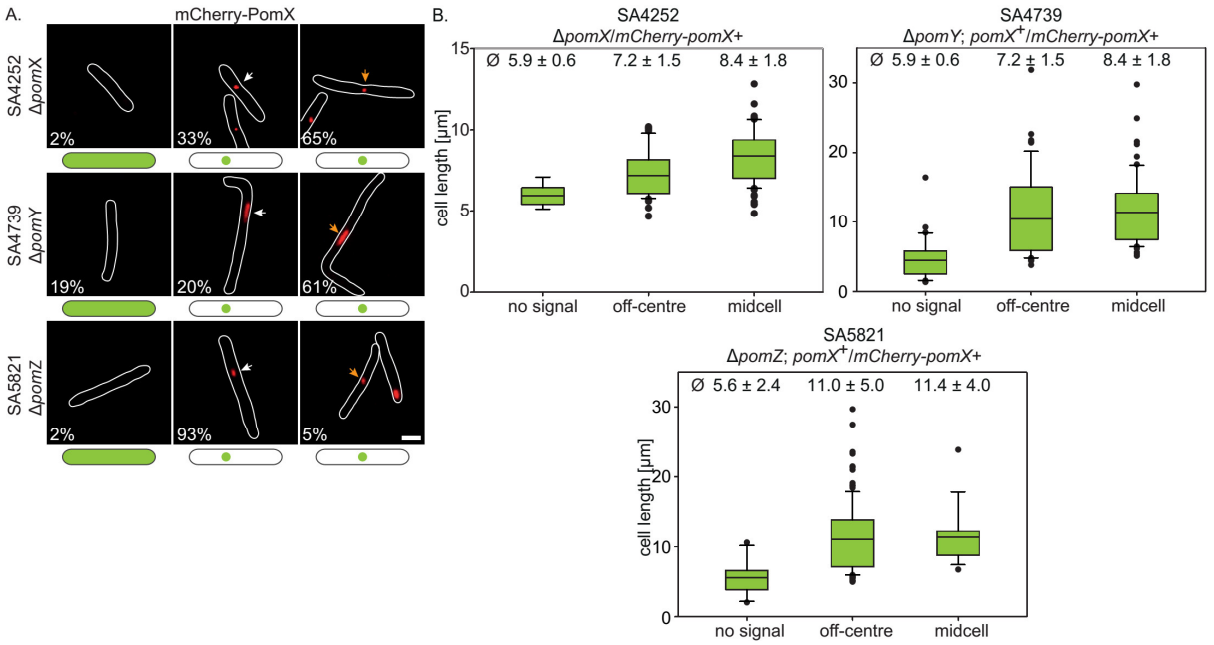

Figure 23: PomX forms clusters independently of PomY and PomZ, but depends on PomZ for midcell localization.
(A) Localization of mCherry-PomX in the three different Δ*pom* mutants. Cells were imaged from exponentially grown cultures on TPM-buffered agarose at 32 °C by fluorescence microscopy. Cell outlines were obtained from DIC pictures. White numbers monitor localization pattern abundance of mCherry-PomX. White arrows indicate off-centre clusters, while orange arrows depict midcell clusters. Scale bar: 2 µm. For each strain more than 140 cells were analyzed **(B)** Correlation of mCherry-PomX localization with cell length in indicated strains. Box plots enclose 25th and 75th percentile, with the black line showing the mean, which are also indicated in numbers ± SD above the plots in µm. Whiskers display 10th and 90th percentile. All outliers are depicted as black dots.

This pattern distribution was largely unaffected when mCherry-PomX was expressed in absence of PomY (SA4739; Δ*pomY*,*pomX*$^{+}$/*mCherry-pomX*+), only a few more cells showed no signal (20%). mCherry-PomX localization still correlated with cell length in the absence of PomY, although cells had a cell length phenotype, with a mean cell length of 9.6 ± 6.8 and a low constriction frequency with 1 % (n=146) (Figure 23 A B). However, while clusters in presence of PomY were round-shaped or sometimes elliptic with an aspect ratio (length/width) of 1.21 ± 0.19 (n=158), clusters were elongated along the long cell axis in absence of PomY (aspect ratio of 3.62 ± 2.87; n=140).This indicated that PomY has a structural “condensation” effect on PomX *in vivo*. Of importance, although PomX clusters were misshaped they were still able to correctly localize at midcell at the normal frequency. By contrast, in cells lacking PomZ (SA5821; Δ*pomZ*; *pomX*$^{+}$/*mCherry-pomX*+), mCherry-PomX cluster formation was unaffected (98 % of cells, n=142) but clusters formed, were only found at midcell in 5 % of cells (Figure 23 A). Consistently, cluster localization in absence of PomZ showed less correlation to cell length (Figure 23 B). By addition, this strain also had a cell length phenotype with an average cell length of 10.6 ± 4.9 µm.

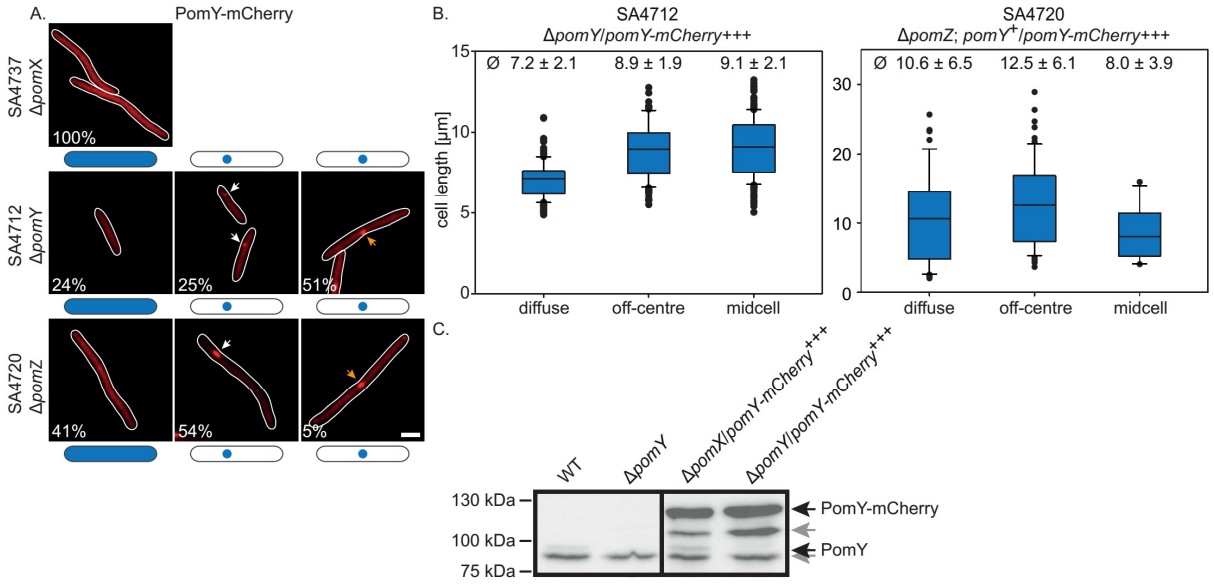

Figure 24: PomY cluster formation requires PomX and clusters are misplaced by the lack of PomZ.
(A) Localization of PomY-mCherry in indicated strains. Cells were imaged from exponentially grown cultures on TPM-buffered agarose at 32 °C by fluorescence microscopy. Cell outlines were obtained from DIC pictures. White numbers monitor localization pattern abundance of PomY-mCherry. White arrows indicate off-centre clusters, while orange arrows depict midcell clusters. Scale bar: 2 µm. For each analysis more than 120 cells were analyzed. **(B)** Correlation of PomY-mCherry localization with cell length in indicated strains. Box plots enclose 25th and 75th percentile, with the black line showing the mean which are also indicated in numbers ± SD above the plots in µm. Whiskers display 10th and 90th percentile. All outliers are depicted as black dots. **(C)** Immunoblot analysis of indicated strains, probed with specific α-PomY antibodies for the presence of PomY and PomY-mCherry. Grey arrows indicate unspecific binding of the antibodies and protein degradation. Black arrows indicate full-length PomY and PomY-mCherry proteins. Note that PomY is always observed as a faint band above an unspecific band.

In the next step PomY-mCherry localization was analyzed in cells lacking PomX (SA4737, Δ*pomX*, *pomY*$^{+}$/*pomY-mCherry*+++) or PomZ (SA4720; Δ*pomZ*, *pomY*$^{+}$/*pomY-mCherry*+++). Both strains showed a cell length phenotype with an average cell length of 16.7 ± 10.8 µm (n=130) and 11.4 ± 6.2 µm (n=127), respectively. PomY-mCherry cluster formation was absolutely dependent on PomX, as PomY-mCherry was diffuse in a Δ*pomX* mutant (Figure 24 A). To test if the defect of PomY-mCherry in cluster formation arose from degradation of the fusion protein or the lack of PomX we tested accumulation of PomY-mCherry by immunoblot analysis, using specific α-PomY antibodies. PomY-mCherry accumulated in cells lacking PomX to the same extent as in cells lacking PomY (Figure 24 C). This matched the previous finding that PomXYZ accumulate independently of each other (5.1.6).

By contrast, in a Δ*pomZ* mutant PomY-mCherry formed clusters in 59 % of cells. In these cells cluster localization did not correlate with cell length and over 90 % of these clusters localized in the off-centre position, arguing that PomZ is required for PomY and PomX clusters to localize at midcell (Figure 24 A, B).

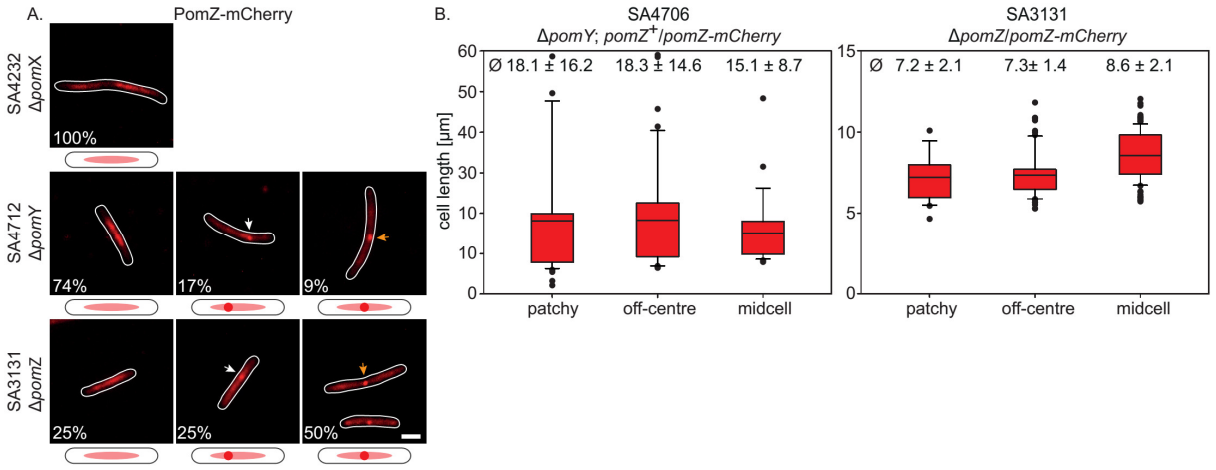

Figure 25: PomZ-mCherry colocalizes with the nucleoid and cluster formation depends on PomX and PomY.
(A) Localization of PomZ-mCherry in indicated strains. Cells were imaged from exponentially grown cultures on TPM-buffered agarose at 32 °C by fluorescence microscopy. Cell outlines were obtained from DIC pictures. White numbers depict localization pattern abundance of PomZ-mCherry signals. White arrows indicate off-centre clusters, while orange arrows mark midcell clusters. Scale bar: 2 µm. For each analysis more than 120 cells were analyzed. **(B)** Correlation of PomY-mCherry localization with cell length in indicated strains. Box plots enclose 25th and 75th percentile, with the black line showing the mean which are also indicated in numbers ± SD above the plots in µm. Whiskers display 10th and 90th percentile. All outliers are depicted as black dots.

Finally, PomZ-mCherry localization was analyzed in cells lacking either PomX (SA4232; Δ*pomX*,*pomZ*$^+$/*pomZ-mCherry*) or PomY (SA4706; Δ*pomY*,*pomZ*$^+$/*pomZ-mCherry*) and compared to its localization in the complementation strain (SA3131). Cell lacking either PomX, or PomY displayed a cell length defect with an average cell length of 15.9 ± 7.8 µm and 17.5 ± 14.2 µm, respectively. Additionally, PomZ-mCherry had a strong defect in cluster formation. In 100% of cells that lacked PomX, PomZ-mCherry showed a patchy localization (n=120). Moreover, a patchy localization of PomZ-mCherry was detected in ¾ of cells in the absence of PomY, too (n=128). In 26% of cells clusters were formed in the absence of PomY, but their localization did not correlate with length (Figure 25 A, B).

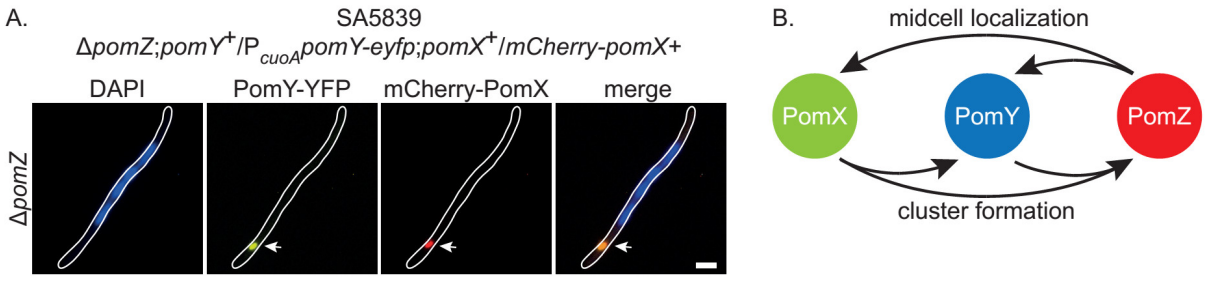

Figure 26: PomY-eYFP and mCherry-PomX colocalize in the absence of PomZ.
(A) Fluorescence microscopy of the indicated strain was performed on 1 % agarose buffered with TPM. Nucleoids were stained with DAPI prior to picture acquisition. Outline of cells was obtained from DIC pictures. White arrows indicate off-centre clusters of PomY-eYFP and mCherry-PomX. Merge picture was generated with Metamorph. Scale bar: 2 µm. **(B)** Schematic dependency map of PomX, PomY and PomZ. Interaction map was generated based on results explained in 5.2.4.

Next, we asked if lack of PomZ not only affects the localization of PomX and PomY clusters at midcell but perturbs the colocalization of PomX and PomY. Therefore, *pomY-eyfp* and *mCherry-pomX*

were expressed in cells lacking PomZ. In the absence of PomZ, PomY-eYFP and mCherry-PomX still colocalized, suggesting that they form a complex *in vivo* independent of PomZ (Figure 26 A).

Based on these findings we made several conclusions. First, clusters of PomX, PomY and PomZ form in a hierarchical order with PomX at the top and PomZ at the bottom, i.e. PomX has to be present for both PomY and PomZ to produce clusters, while PomY presence is only important for PomZ. This gives PomX a function as a scaffold at nucleation for the PomXYZ cluster (Figure 26 B). Nevertheless, PomZ-mCherry formed clusters in absence of PomY, indicating that PomZ does not solely depend on PomY but may interact directly with PomX. On the other hand, PomZ only had little effect on cluster formation by PomY and did not affect PomX cluster formation. However, in the absence of PomZ the PomX and PomY clusters were rarely at midcell. Based on this analysis one central function of PomZ is the correct positioning of the PomXYZ cluster over the mid-nucleoid at midcell. The fact that PomZ in the absence of PomX and PomY showed a patchy colocalization with the nucleoid, strengthened the idea that PomZ is associated with the nucleoid and together with the interaction to PomX and PomY results in the mid-nucleoid localization of the PomXYZ cluster.

5.2.5 PomX and PomY form clusters at midcell before Z-ring occurs

FtsZ serves as a scaffold to recruit components of the divisome (Gamba *et al.*, 2009, Goehring *et al.*, 2006). As in other bacteria FtsZ is a key cell division protein in *M. xanthus* and its depletion is deleterious to cells (Addinall & Lutkenhaus, 1996, Treuner-Lange *et al.*, 2013). Because clusters of PomX and PomY as well as PomZ localize at midcell before cells start constricting we wondered if FtsZ is required for their localization at midcell. Recently we showed that PomZ cluster localization at midcell does not require FtsZ presence (Treuner-Lange *et al.*, 2013), presenting the first hint that also PomX and PomY find midcell independently of FtsZ. To investigate the relationship between PomX, PomY and FtsZ and to clarify if FtsZ is needed for midcell localization of PomX and PomY dual labeled strains were created to follow PomX (SA4295; Δ*pomX*/P$_{cuoA}$*mCherry-pomX; ftsZ*$^{+}$/*ftsZ-gfp*) and PomY (SA4747; Δ*pomY*/P$_{cuoA}$*pomY-mCherry; ftsZ*$^{+}$/*ftsZ-gfp*) together with FtsZ in the same cells.

For the colocalization an *ftsZ-gfp* fusion was expressed from its native promoter in the presence of native *ftsZ* as previously described (Treuner-Lange *et al.*, 2013). Additionally, mCherry-PomX and PomY-mCherry were expressed under the control of a Cu^{2+} inducible promoter in presence of 150 µM $CuSO_4$ to complement the deletion mutant phenotypes (5.5.2; personal communication A. Harms). Both strains displayed an average cell length with a WT phenotype, with 7.7 ± 1.9 µm for strain SA4295 (n=101) and 7.1 ± 1.5 µm for strain SA4747 (n=210). Similarly, they showed a normal constriction frequency with 5 % to 7 %.

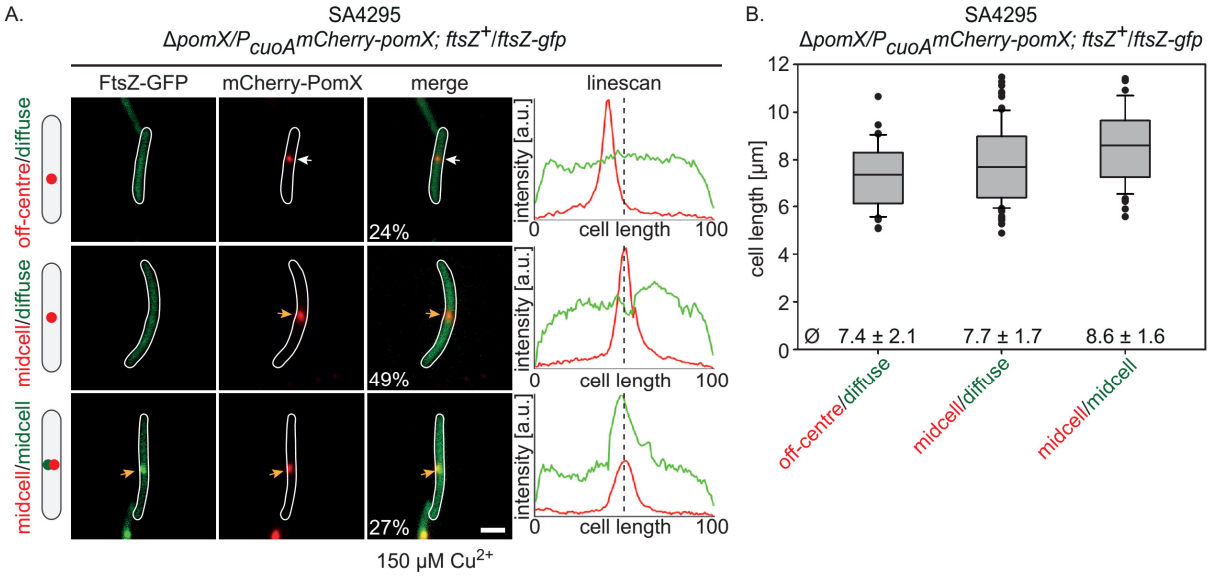

Figure 27: PomX clusters localize at midcell before Z-rings are formed.
(A) Colocalization of mCherry-PomX and FtsZ-GFP. Cells of strain SA4295 were exponentially grown in presence of 150 µM $CuSO_4$ and imaged on a 1 % agarose patch buffered with TPM at 32 °C. Outlines of cells were generated from DIC pictures. White numbers indicate abundance of localization patterns. White arrows indicate off-centre clusters, while orange arrows mark midcell clusters of mCherry-PomX. Scale bar: 2 µm. Linescans show fluorescence intensity of mCherry-PomX (red) and FtsZ-GFP (green) signal along long cell axis as function of cell length in %. **(B)** Localization patterns of mCherry-PomX and FtsZ-GFP correlate with cell length. Box plots enclose the 25th and the 75th percentile with the black line indicating the mean, which is also displayed in number ± SD below the plots in µm. Whiskers depict the 10th and 90th percentile and outliers are shown as black dots.

For mCherry-PomX and FtsZ-GFP localization, three patterns were observed that correlated with cell length (Figure 27). In more than 2/3 of all cells (76 %) mCherry-PomX formed a cluster precisely at midcell, whereas it formed an off-centre cluster in the remaining 24 %. The latter exclusively coexisted with a diffusely localized FtsZ-GFP protein and were on average the shortest cells (7.4 ± 2.1 µm). Interestingly, in the longest cells (8.6 ± 1.6 µm) mCherry-PomX colocalized with FtsZ-GFP at midcell in 27 % of observed cases, while it formed a midcell cluster in 49 % of cells in the absence of a Z-ring (Figure 27 A, B).

Similarly, four patterns were observed for the colocalization of PomY-mCherry and FtsZ-GFP (Figure 28 A). In 10 % of cells, which were on average the shortest (5.4 ± 0.5 µm), both proteins displayed a diffuse localization. Longer cells with an average length of 6.6 ± 1.2 µm showed PomY-mCherry in an off-centre cluster and FtsZ-GFP in a diffuse localization. In 62 % of cells PomY-mCherry formed a cluster a midcell, which in 55% of cases colocalized precisely with a Z-ring (Figure 28 A, B). Importantly, we did not observe cells with a Z-ring at midcell without a cluster of PomX or PomY. Thus PomX and PomY clusters localize at midcell before Z-rings are produced, suggesting that PomX and PomY find midcell independent of the production of Z-rings. This fits to the previously described data that PomZ cluster localization at midcell occurs prior to Z-ring formation (Treuner-Lange *et al.*, 2013). These data strongly suggest that PomX and PomY do not only colocalize with cell division constrictions, as described earlier, but they colocalize with FtsZ before constrictions occur.

Of importance, PomX and PomY clusters arrive at midcell before Z-rings are produced. We propose that PomX, PomY and PomZ mark midcell and recruit FtsZ to midcell by acting as positive regulators for cell division placement and by stabilizing Z-ring formation.

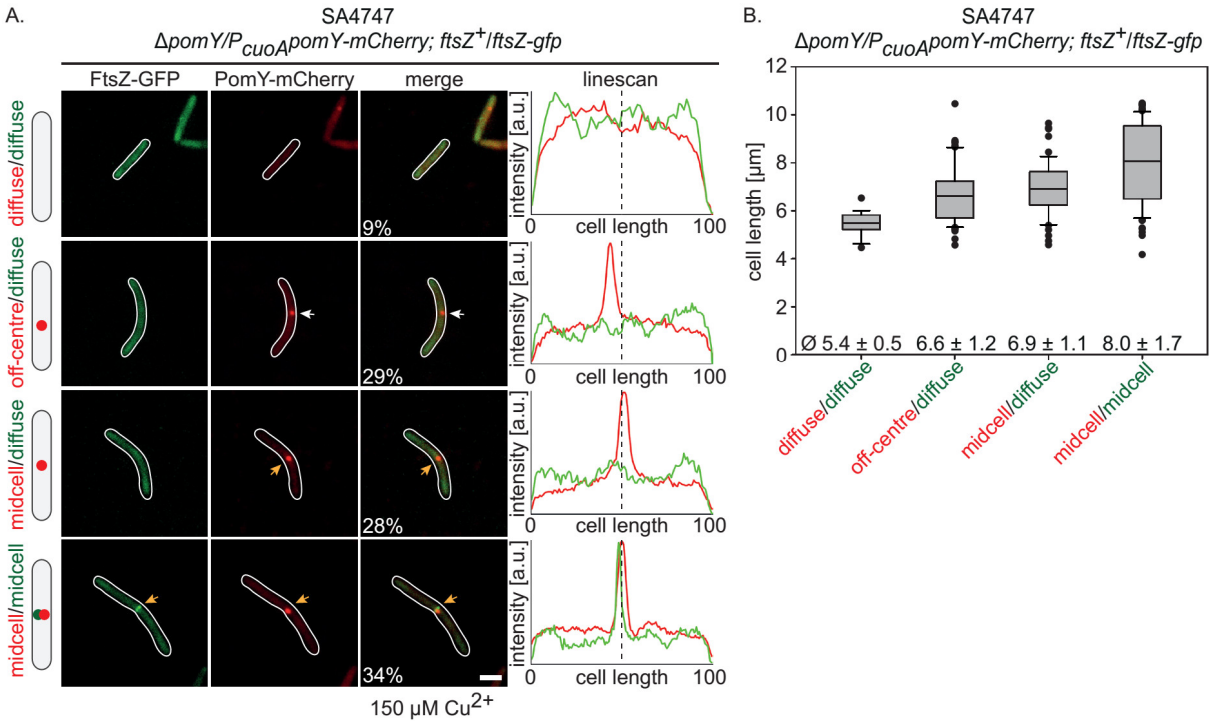

Figure 28: PomY-mCherry clusters localize at midcell before Z-rings are formed.
(A) Colocalization of PomY-mCherry and FtsZ-GFP. Cells of strain SA4747 were exponentially grown in presence of 150 µM CuSO4 and imaged on a 1 % agarose patch buffered with TPM at 32 °C. Outlines of cells were obtained from DIC pictures. White numbers indicate abundance of localization patterns. White arrows indicate off-centre clusters, while orange arrows mark midcell clusters of PomY-mCherry. Scale bar: 2 µm. Linescans show fluorescence intensity of PomY-mCherry (red) and FtsZ-GFP (green) signals along long cell axis plotted as function of cell length in %. **(B)** Localization patterns of PomY-mCherry and FtsZ-GFP correlate with cell length. Box plots enclose the 25th and the 75th percentile with the black line indicating the mean which is also displayed in number ± SD below the plots in µm. Whiskers depict the 10th and 90th percentile and outliers are shown as black dots.

5.2.6 PomX and PomY form clusters in the absence of FtsZ that localize at midcell

If PomXYZ serve as positive regulators for FtsZ at midcell, we hypothesized that their ability to form clusters and their localization should be independent of FtsZ. In order to test this hypothesis, the localization of PomX and PomY was analyzed in *ftsZ*-depleted cells, by expressing the only copy of *ftsZ* under control of a Cu^{2+} regulated promoter from the *cuoA* locus in a Δ*ftsZ* mutant. This resulted in strains SA5809 (*pilQ1*, Δ*ftsZ*/P$_{cuoA}$*ftsZ*, *pomX*$^{+}$/*mCherry-pomX*+) and SA4718 (*pilQ1*, Δ*ftsZ*/P$_{cuoA}$*ftsZ*, *pomY*$^{+}$/*pomY-mCherry*+++). In presence of 300 µM $CuSO_4$ FtsZ was produced and accumulated at WT levels (Treuner-Lange *et al.*, 2013). Cells displayed an average cell length of 7.2 ± 1.4 µm and 7.0 ± 1.8, which is comparable to WT. In addition, cells showed 7 % - 11 % of constrictions, indicating that they divide with a normal frequency. Under these conditions mCherry-PomX clusters were observed in 98 % of cells, of which ¾ localized at midcell. Similarly, PomY-mCherry formed cluster in 78 % of cells, which could be divided into 47 % of cells that display a midcell cluster and 31 % with an off-centre cluster (Figure 29 A, C). After washing cells twice with copper-free medium, cells were

grown in the absence of copper and monitored in a time course experiment every 3 h for 12 h by fluorescence microscopy (Figure 29 B, D). During the depletion experiment the average cell length of both strains increased over time, concurrent with the depleting FtsZ levels, as shown by immunoblot analysis (Figure 29 A, C). Consistently, the constriction frequency dropped during FtsZ depletion and constrictions disappeared when FtsZ was not longer detectable by immunoblot analysis after 6 h – 9 h of depletion (Figure 29 A, C). As a loading control, we probed cell lysates of depleted cells for the presence of PilC using α-PilC antibodies. PilC is integral part of the type IV pilus complex that is required for cell motility and adhesion. Its accumulation is independent of FtsZ presence as shown by immunoblot analysis (Figure 29 A, C). After 12 h of depletion, which corresponds to a timepoint when FtsZ was not observable by immunoblots for 6 h – 9 h, all cells of both strains displayed clusters of mCherry-PomX and PomY-mCherry. Of these clusters 20 % in the case of mCherry-PomX and 60 % in the case of PomY-mCherry were found to localize in the off-centre. Importantly, clusters of both proteins were observed at midcell at high frequency (63 % of mCherry-PomX clusters and 29 % of PomY-mCherry clusters) (Figure 29 A, C). In the remaining cells both proteins formed two clusters at approximately 25 % and 75 % of cell length. These data show that PomX and PomY form clusters at midcell in absence of FtsZ.

Although PomX and PomY clusters colocalize *in vivo,* the frequency of midcell clusters is different for the two strains in *ftsZ*-depleted cells. This difference can not be explained by the provided data but may result from doing the experiments at different days. Because clusters of mCherry-PomX and PomY-mCherry were found to colocalize with the nucleoid during most of the cell cycle in WT we analyzed the localization of PomY-mCherry as a reference for the PomXY cluster in comparison to the DAPI-nucleoid. Interestingly, in *ftsZ*-depleted cells PomY-mCherry clusters were exclusively found to colocalize with the nucleoid or localized at the edge of the nucleoid, irrespective of their localization in the off-centre, or at midcell (Figure 29 D).

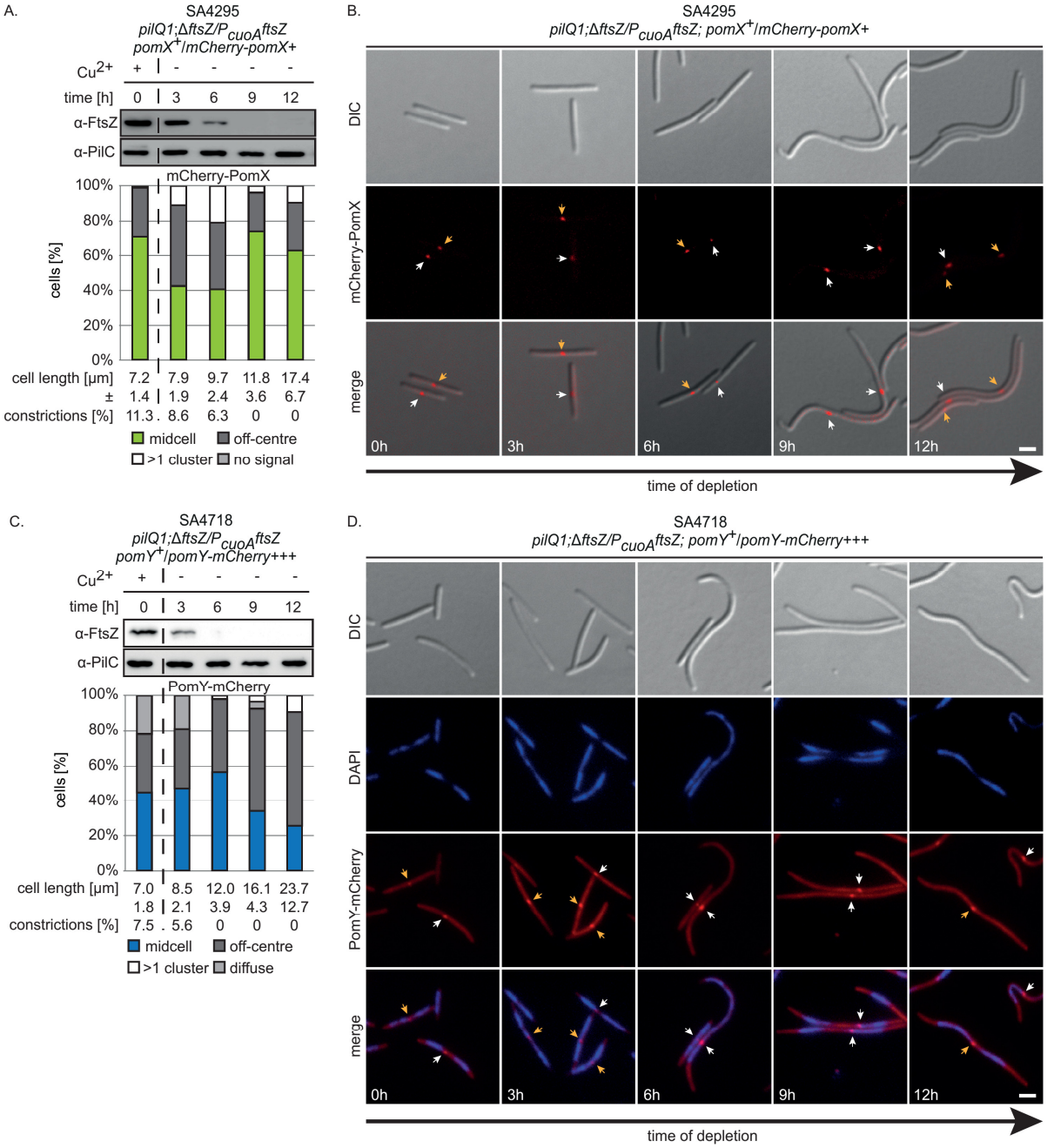

Figure 29 PomX and PomY form clusters independent of FtsZ that localize at midcell.
(A) PomX localizes at midcell in FtsZ-depleted cells. Cells were shifted to copper-free medium at 0 h and further cultured at 32 °C. Cells were analyzed in intervals of 3 h for 12 h. Upper part, levels of FtsZ and PilC during FtsZ-depletion in strain SA4295. FtsZ and PilC were detected, using specific α-FtsZ and α-PilC antibodies, respectively. PilC is part of the type IV pili machinery and was used as a loading control (Bulyha *et al.*, 2009). Lower part, localization patterns of mCherry-PomX during the depletion experiment. More than 150 cells were analyzed per timepoint. **(B)** Fluorescence microscopy of strain SA4295 during the depletion experiment. Cells were imaged on 1 % agarose patches buffered with TPM at 32 °C. White arrows indicate off-centre clusters, while orange arrows mark midcell clusters. Merge pictures were generated with Metamorph. Scale bar: 2 µm. **(C)** PomY localizes at midcell in FtsZ-depleted cells. Cells were treated as described in (A). Upper part, levels of FtsZ and PilC during FtsZ-depletion in strain SA4718. Lower part, localization patterns of PomY-mCherry during the depletion experiment. More than 150 cells were analyzed per timepoint. **(D)** Fluorescence microscopy of strain SA4718 during the depletion experiment. Cells were imaged as in (B), but nucleoids were stained with DAPI prior to picture acquisition. White arrows indicate off-centre clusters, while orange arrows mark midcell clusters. Scale bar: 2 µm.

As a control that FtsZ has a central role in divisome formation in *M. xanthus*, FtsK-mCherry localization was analyzed in *ftsZ*-expressing and *ftsZ*-depleted cells. FtsK is a component of the cell division machinery with a function during late cell division and FtsK localization at the cell division site depends on FtsZ in *E. coli* (Yu *et al.*, 1998a). In presence of 300 µM $CuSO_4$ cells of strain SA4169 (*pilQ1*, Δ*ftsZ*/P_{cuoA}*ftsZ*, *ftsK*$^+$/*ftsK-mCherry+++)* had an average cell length and a constriction frequency similar to WT (Figure 30 A). In this strain, FtsK-mCherry clusters were found at midcell in 15 % of cells and in 8 % of cells in the off-centre position (Figure 30 A, B). During the depletion experiment FtsZ levels decreased and were undetectable by immunoblot analysis after 6 h. As described earlier, this resulted in cell elongation and a reduction in the constriction frequency (Figure 30 A). Concurrent with *ftsZ*-depletion, FtsK-mCherry cluster formation reduced and was lost after 12 h of depletion. Importantly, depletion of *ftsZ* did not affect the accumulation of FtsK-mCherry as shown by western blot analysis (Figure 30 A).

In conclusion, these data show that PomX and PomY similarly to PomZ (Treuner-Lange *et al.*, 2013) form clusters independently of FtsZ that are able to localize at midcell in absence of FtsZ. This information strongly suggests that they function as midcell landmarks to guide Z-ring formation at midcell and promote Z-ring formation. In addition, FtsZ is still required for the correct localization of FtsK to the cell division site.

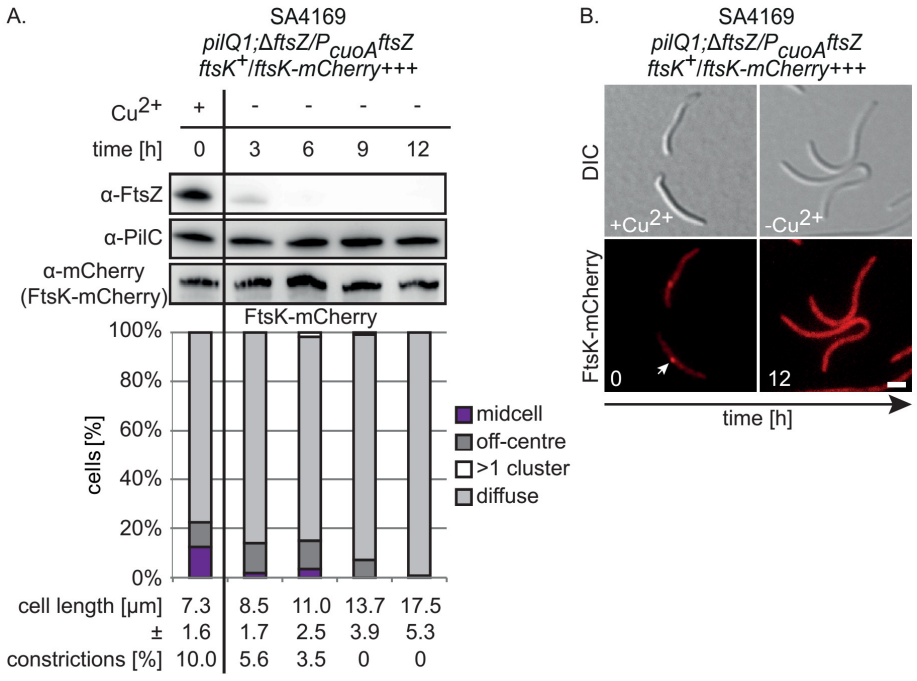

Figure 30: FtsK-mCherry localization depends on FtsZ presence.
(A) FtsK cluster formation at midcell depends on FtsZ. Cells were shifted to copper-free medium at 0 h and further cultured at 32 °C. Cells were analyzed in intervals of 3 h for 12 h. Upper part, levels of FtsZ and PilC and FtsK-mCherry during FtsZ-depletion in strain SA4169. FtsZ and PilC were detected, using specific α-FtsZ and α-PilC antibodies, respectively. PilC is spart of the type IV pili machinery and was used as a loading control (Bulyha *et al.*, 2009). FtsK-mCherry was detected using specific α-mCherry antibodies. Lower part, localization patterns of FtsK-mCherry during the depletion experiment. More than 100 cells were analyzed per timepoint. **(B)** Fluorescence microscopy of strain SA4169 during the depletion experiment. Cells were imaged on 1 % agarose patches buffered with TPM at 32 °C. White arrows indicate clusters of FtsK-mCherry. Scale bar: 2 µm.

5.2.7 A block in cell division stalls PomXY clusters in division constrictions

FtsZ-depleted cells grow in length and elongate, but mainly show one PomXYZ cluster that colocalizes with the nucleoid at midcell, which is the site of cell division in *ftsZ*-expressing cells. We hypothesized that release of PomXYZ from the site of cell division depends on completion of cell division and therefore multiple cluster are rarely observed in *ftsZ*-depleted cells. To test this hypothesis cell division was blocked using cephalexin.

Strains SA4252 and SA4712, accumulating mCherry-PomX and PomY-mCherry as only source of PomX and PomY, were analyzed by microscopy in a time course experiment of 3 h intervals for 12 h in the presence of cephalexin. Cells expressing *pomY-mCherry* were stained with 1 µg/ml DAPI for 10 min directly before microscopy to be able to correlate PomY-mCherry localization to nucleoid position.

At the start of cephalexin treatment both strains showed a cell length distribution that was comparable to WT cells, with 7.9 ± 1.9 µm in case of SA4252 and 8.3 ± 2.0 µm in case of SA4712 (Figure 31 A, C). As described earlier cell division constrictions colocalized with the mCherry-PomX and PomY-mCherry cluster. Over time, the average cell length increased and reached 21 µm - 25 µm after 12 h of cephalexin treatment. Concurrent with cell elongation the constriction frequency increased from 3 % - 8 % at the start of the experiment to 35 % and 60 % in cells with PomY-mCherry and mCherry-PomX, respectively (Figure 31 A, C). Notably, multiple constrictions were not detected even in long cells, indicating that constrictions were stalled by cephalexin treatment and cells were not able to form a second constriction. The increased constriction frequency further indicated that divisions did not disassemble if they were formed, but persisted at least for the time period of the experiment.

At 0 h mCherry-PomX produced clusters in 92 % of cells of which 1/3 localized in the off-centre position, while the remaining clusters were found at midcell. Similarly, PomY-mCherry formed clusters in the off-centre position in 25 % of cells and localized at midcell in 53 % of cells. After 12 h of treatment no cells without a mCherry-PomX cluster or a diffuse PomY-mCherry localization were observed and 40 % of mCherry-PomX clusters and 52 % of PomY-mCherry clusters were at midcell similar to the untreated cells. Rarely, two clusters of mCherry-PomX and PomY-mCherry were visible. As discussed before, constrictions at midcell in the cephalexin treated cells colocalized with mCherry-PomX and PomY-mCherry clusters as in the untreated cells (Figure 31 B, D).

Because multiple clusters were observed in rare cases and all constrictions colocalized with PomX and PomY clusters, we conclude that clusters are stalled at the constriction if cell division is blocked by inhibition with cephalexin and that release from the constriction depends on cell division completion.

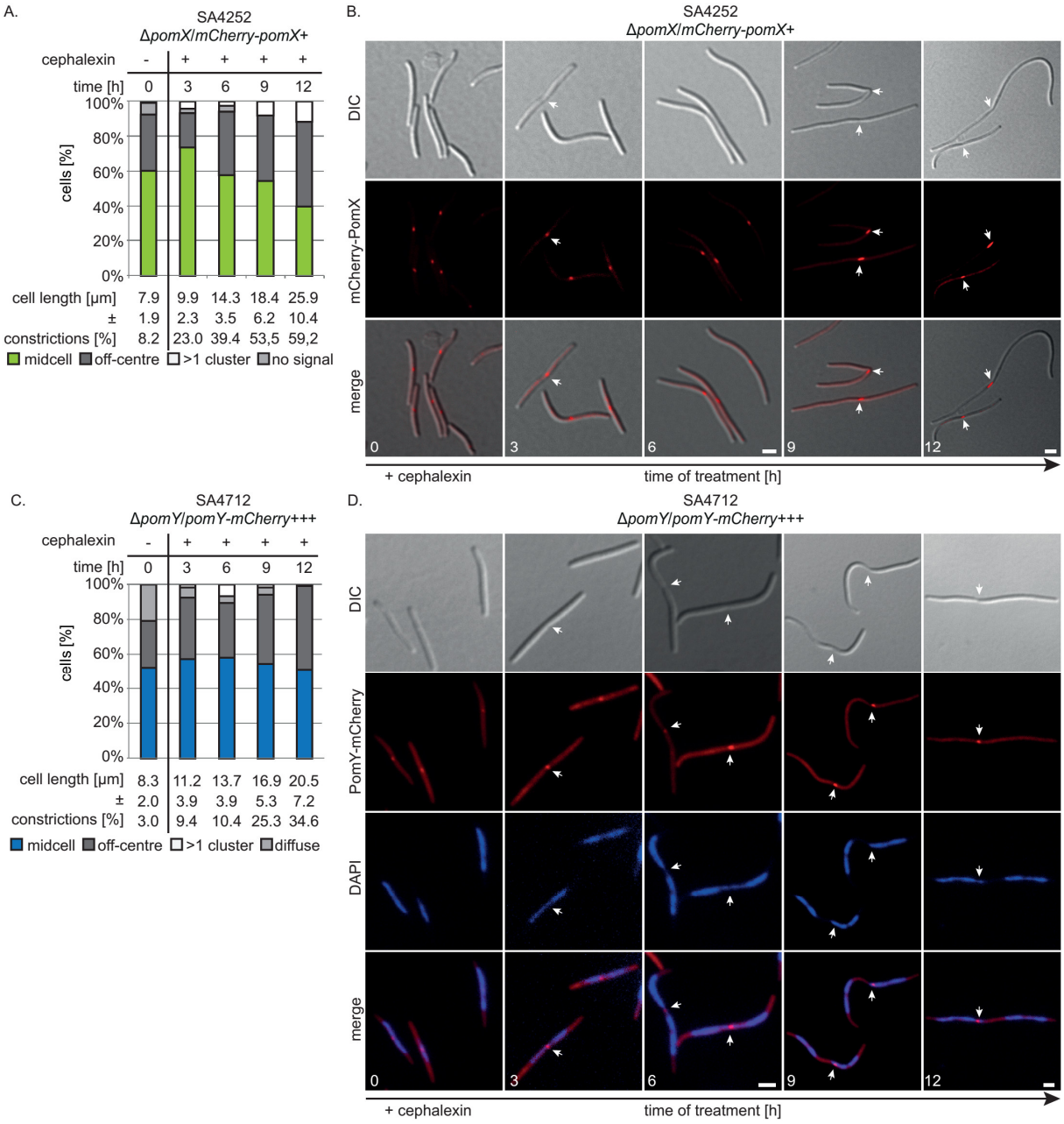

Figure 31 PomX and PomY colocalize with constrictions in cells that are inhibited in cell division.
(A) mCherry-PomX localization after cephalexin treatment in SA4252. Cells were shifted to cephalexin containing medium at 0 h and further cultured at 32 °C. Cells were analyzed in intervals of 3 h for 12 h. Upper part, localization pattern abundance of mCherry-PomX in % of total cells. Lower part, average cell length and constriction frequency of cells during cephalexin treatment. For each timepoint >100 cells were analyzed. **(B)** Fluorescence microscopy of strain SA4252 during the time course experiment. Representative cells are shown for each timepoint. White arrows indicate mCherry-PomX clusters that colocalize with cell division constrictions. Numbers indicate hours of cephalexin treatment. Scale bar: 2 µm. **(C)** PomY-mCherry localization after cephalexin treatment of SA4712. Cells were treated as described in (A). Cells were analyzed as in (A). **(D)** Fluorescence microscopy of strain SA4712 during cephalexin treatment. Cells were additionally treated with DAPI prior to picture acquisition. White arrows indicate PomY-mCherry clusters that colocalize with cell division constrictions. Numbers show time of treatment in hours. Scale bar: 2 µm. Merge pictures were generated with Metamorph.

5.2.8 PomZ recruits PomX and PomY to the nucleoid and positions them at midcell

The finding, that PomX and PomY colocalized in the presence as well as in the absence of PomZ led us conclude that PomXY associate into a cluster independently of PomZ. However, in cells lacking

PomZ these clusters were not correctly found at midcell, but very often in an off-centre position. Based on these observations we suspected that PomZ guides the PomXY cluster to midcell by some unknown mechanism. Because clusters spend most of the cell cycle colocalizing with the nucleoid, their localization was analyzed in the presence and absence of PomZ in correlation to the nucleoids. For this purpose cells of strain SA4252 and SA4712 that express *mCherry-pomX* and *pomY-mCherry* in presence of PomZ, respectively, were compared with cells of strain SA5821 and SA4720 that express the same fusion proteins in its absence. As previously described (5.2.3), mCherry-PomX and PomY-mCherry formed clusters that colocalized with the DAPI-stained nucleoids in the majority of all cells in presence of PomZ (73 % of PomY-mCherry clusters and 85 % of mCherry-PomX clusters). These cells included cells with off-centre and midcell clusters of the two fusion proteins. Moreover, both fluorescent proteins formed clusters at midcell in between segregated nucleoid masses in 8 % - 9 % of cells, which were the only cells displaying a cluster of mCherry-PomX and PomY-mCherry that did not colocalize with the nucleoid. In these cells clusters appeared to be closer to one of the nucleoids than to the other, based on linescans (Figure 32 A, B). Additionally, 6 % of cells showed no mCherry-PomX signal and a diffuse localization of PomY-mCherry was observed in 18 % of cells (Figure 32 C).

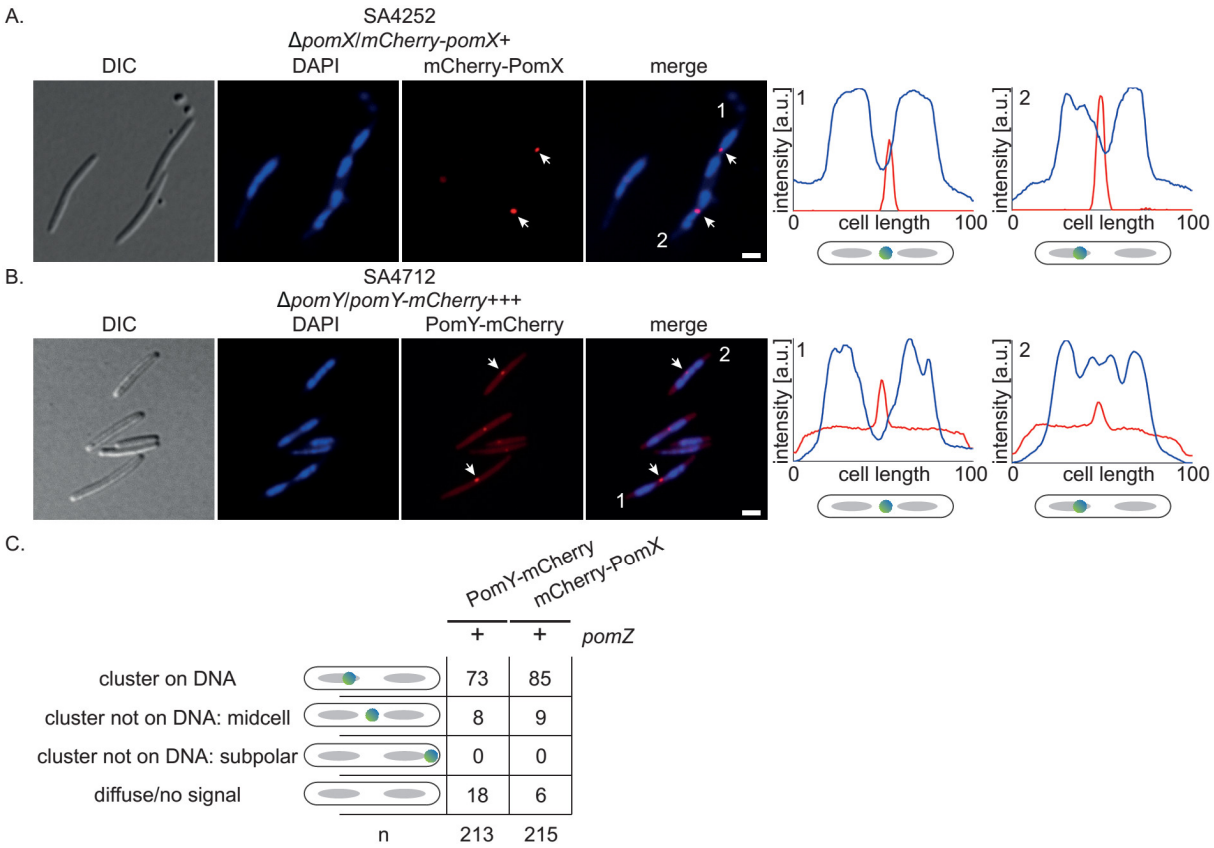

Figure 32: PomX and PomY colocalize with the nucleoid or at midcell in between nucleoids in presence of PomZ.
(A) Fluorescence microscopy of strain SA4252. Cells were imaged on a 1% agarose pad buffered with TPM. Cells were treated with DAPI for 10 min prior to microscopy to stain nucleoids. White arrows depict clusters in cells that were used for linescans. White numbers mark linescan number. Merge pictures and linescans were created using Metamorph. Linescans show fluorescence signal of mCherry-PomX and DAPI signal along the long cell axis plotted as function of cell length in %. Scale bar: 2 µm. **(B)** Fluorescence microscopy of strain SA4712. Cells were imaged as described in (A). **(C)** Schematic analysis of cluster localization in presence of PomZ. Clusters patterns were divided into 4 categories as depicted. „Cluster on DNA"-category includes all clusters on DNA irrespective of their localization and nucleoid number. Numbers are given in % of total cells.

In the absence of PomZ, mCherry-PomX and PomY-mCherry formed a cluster in 91 % and 65 % of cells, respectively. This demonstrates that overall PomZ has no effect on the PomX cluster formation, while PomY-mCherry cluster formation is slightly impaired (Figure 33 C). Importantly, we found that clusters colocalized with the DAPI-stained nucleoid to a lesser extent than in cells expressing *pomZ*. Moreover, these cluster were not exclusively found at midcell in between segregated nucleoids (3 % - 4 % in a Δ*pomZ* mutant) but 8 % of PomY-mCherry cluster and 35 % of mCherry-PomX clusters were found in the polar/subpolar regions which were devoid of DNA or at the distant edge of the nucleoid pointing towards the pole (Figure 33 A, B). However, in 50 % - 54 % of cells mCherry-PomX and PomY-mCherry clusters colocalized with the nucleoid (Figure 33 C).

We conclude that PomZ brings PomX and PomY clusters to the nucleoid and furthermore by some mechanism positions them at midcell. Based on the finding that PomZ localizes in a patchy pattern on the nucleoid, we propose a model in which PomZ recruits PomXY clusters to the nucleoid and positions them over the middle of the nucleoid mass.

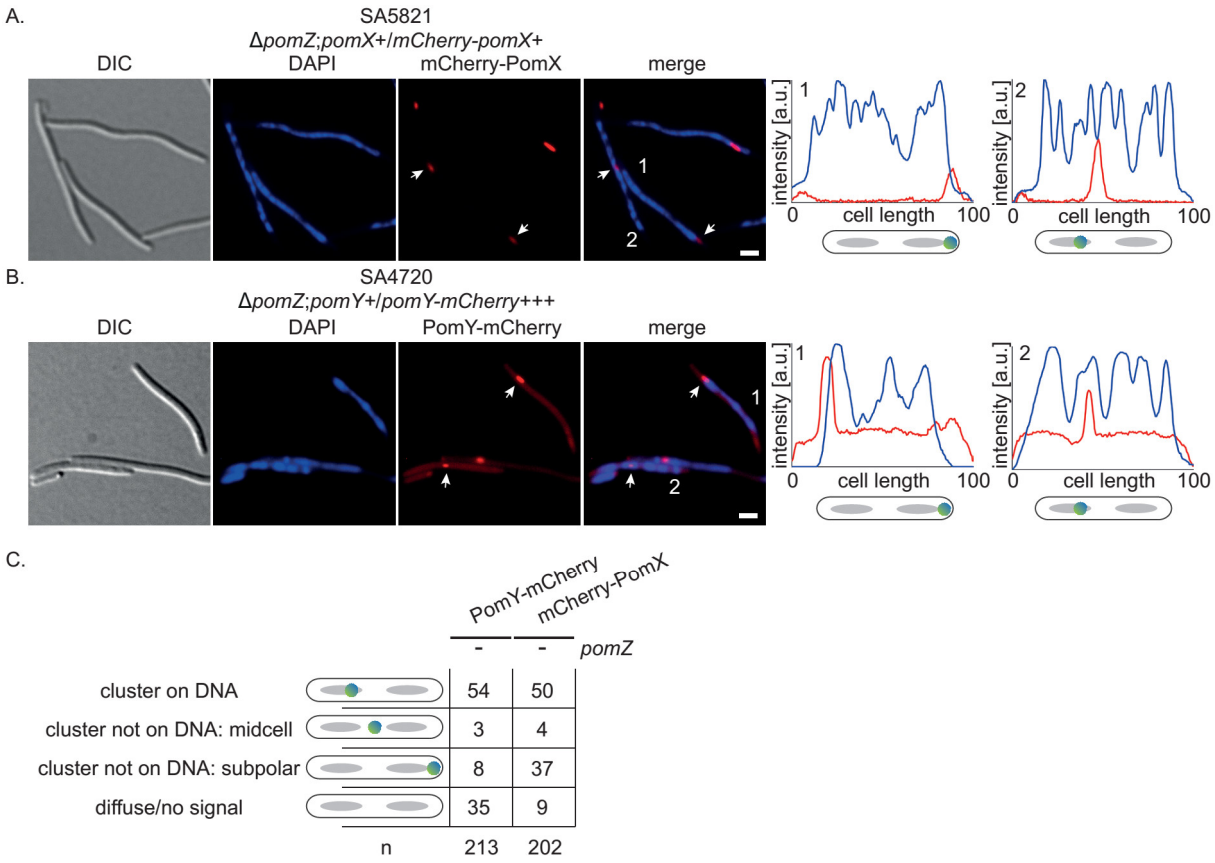

Figure 33: PomX and PomY localize randomly in absence of PomZ.
(A) Fluorescence microscopy of strain SA5821. Cells were imaged on a 1% agarose pad buffered with TPM. Cells were treated with DAPI for 10 min prior to microscopy to stain nucleoids. White arrows depict clusters in cells, which were used for linescans. White numbers mark linescan number. Merge pictures and linescans were created using Metamorph. Scale bar: 2 µm. **(B)** Fluorescence microscopy of strain SA4720. Cells were imaged as described in (A). **(C)** Schematic analysis of cluster localization in absence of PomZ. Cluster patterns were divided into 4 categories as depicted. „Cluster on DNA"-category includes all clusters on DNA irrespective of their localization and nucleoid number. Numbers are given in % of total cells.

5.2.9 PomX and PomY cluster move towards midcell and split during cell division

To understand how PomXYZ clusters localize to the mid-nucleoid in a PomZ-dependent manner, we performed time-lapse microscopy on cells expressing *mCherry-pomX* or *pomY-mCherry*. Because *M. xanthus* cells are able to move by means of type IV pili-dependent motility and gliding motility, we were not able to monitor WT cells during cell division over a time period of several hours. To improve time-lapse microscopy, non-motile Δ*pomX* and Δ*pomY* strains were created that expressed *mCherry-pomX* or *pomY-mCherry* as the only source of *pomX* and *pomY*. To create non-motile strains the *mglA* gene was deleted in Δ*pomX* or Δ*pomY* mutant background. Deletion of *mglA* results in a complete loss of motility (Miertzschke *et al.*, 2011, Hodgkin & Kaiser, 1977). Concordantly, a double in-frame deletion mutant of *pomX* or *pomY* with *mglA* also showed no motility, based on single cell analysis. The resulting strains SA4796 (Δ*mglA*; Δ*pomX*/*mCherry-pomX*+) and SA7000 (Δ*mglA*; Δ*pomY*/*pomY-mCherry*+++) displayed no cell length phenotype, suggesting that MglA is not involved in cell division in *M. xanthus*. In order to follow at least one complete cell cycle, from a newborn cell, to cell division, cells were imaged on a TPM-buffered agarose containing 0.25 % CTT medium at 32°C. Under these conditions cells had a doubling time of around 4 h - 5 h based on single cell analysis.

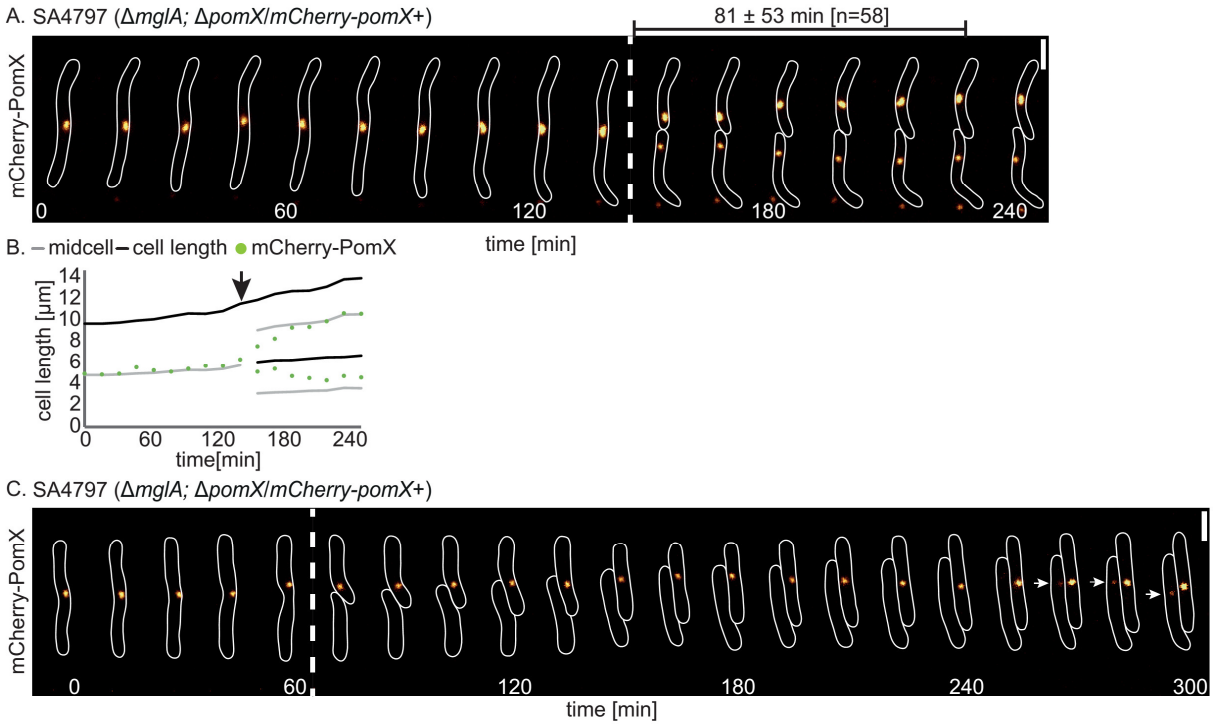

Figure 34: PomX clusters display a dynamic localization towards midcell and are split during division. **(A)** Time-lapse microscopy of mCherry-PomX clusters in non-motile cells of strain SA4797. Cells were imaged on 1 % agarose buffered with TPM and 0.25 % CTT medium at 32 °C. Cell outlines were obtained from DIC pictures. White stippled line indicates a cell division event. Numbers on top indicate the re-localization time ± SD in minutes from the old midcell to the new midcell after cell division. Movies were aligned using Metamorph. Scale bar: 2 µm. **(B)** Cartoon of the cluster motion observed in (A). Cluster position was obtained from linescans of fluorescence pictures along long cell axis. Black arrow indicates a cell division event. **(C)** Time-lapse microscopy of strain SA4749 as in (A), showing an asymmetric clusters distribution during cell division.

Starting from a midcell cluster of mCherry-PomX, cells were imaged during cell division (Figure 34 A). In these recordings, clusters showed little dynamics in the midcell area, with motion along the long or the short cell axis. If clusters were not completely round-shaped but elliptic, some clusters occasionally displayed a behavior in which the long cluster axis tilted towards one or the other direction (Figure 34 A, B). In all observed cases (n=29) constrictions occurred over the mCherry-PomX cluster at midcell and colocalization of cluster and constriction was observed for one to three time points, which corresponds to 15 - 45 minutes. During cell division several observations were made. In the majority of cases the cluster was split into two smaller clusters during cell division (Figure 34 A, B). These clusters were redistributed into the two daughter cells, where they formed small clusters in the off-centre position close to the new pole. Cluster separation was rarely symmetric. Some cell divisions produced daughter cells of which only one cell showed a mCherry-PomX cluster, while the other daughter displayed no signal (Figure 34 C). If cluster split events were strongly asymmetric and one daughter cell did not show a PomX cluster, a cluster reappeared either in the off-centre position or directly at midcell. We speculate that this finding explains why, based on snap-shot analysis, small cells show no signal of mCherry-PomX.

Directly after division PomX clusters showed dynamic motion towards the new midcell and reached this position on average after 81 ± 53 min. Notably, clusters did not leave the midcell area once they reached it.

In a similar experiment PomY-mCherry was followed in the background of a non-motile Δ*pomY* mutant. Like PomX, clusters of PomY-mCherry displayed a midcell localization for several hours until cell division took place (Figure 35 A). Cell division constrictions were exclusively observed over the PomY-mCherry cluster at midcell. As reported for PomX, PomY-mCherry clusters split asymmetrically during cell division. Concordantly with the observations made for PomX, clusters moved towards the new midcell and arrived here in 82 ± 51 min (n=72) (Figure 35 A, B). If clusters split asymmetrically during cell division and daughter cells did not receive part of the cluster, they produced a new cluster within 1 h - 2 h, which occurred in the off-centre position or at midcell (Figure 35 C).

A relocalization time of 80 minutes is around ¼ of the *M. xanthus* cell cycle and suggests that PomX and PomY clusters reach midcell, which at this point in time coincides with the middle of the nucleoid, early and stay here for several hours, until cell division takes place. Based on these findings we predicted that PomX and PomY clusters colocalize during the relocalization from off-centre to midcell and during cell division.

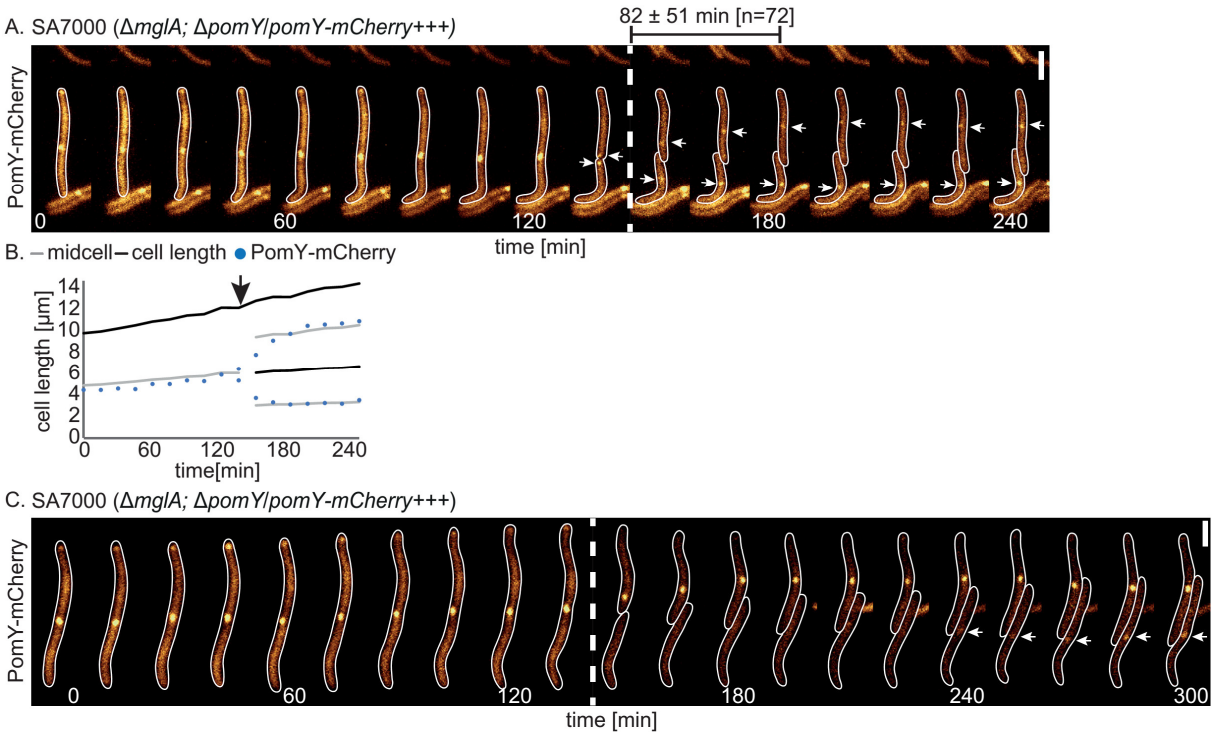

Figure 35: PomY clusters display a dynamic localization towards midcell and are split during division like PomX.
(A) Time-lapse microscopy of PomY-mCherry clusters in non-motile cells of strain SA7000. Cells were imaged on 1 % agarose buffered with TPM and 0.25 % CTT medium at 32°C. Cell outlines were obtained from DIC pictures. White stippled line indicates a cell division event. Numbers on top indicate the relocalization time ± SD in minutes from the old midcell to the new midcell after cell division. Movies were aligned using Metamorph. Scale bar: 2 µm. **(B)** Cartoon of the cluster motion observed in (A). Cluster position was obtained from linescans of fluorescence pictures along long cell axis. Black arrow indicates a cell division event. **(C)** Time-lapse microscopy of strain SA7000 as in (A), showing an asymmetric clusters distribution during cell division.

To test this, time-lapse microscopy was performed on dual-labeled cells that express *mCherry-pomX* and *pomY-eyfp* (SA7041; Δ*pomX*/*mCherry-pomX*+; *pomY*$^{+}$/P$_{couA}$*pomY-eyfp*). In these movies, cells were imaged in presence of 150 µM $CuSO_4$ to express *pomY-eyfp* in presence of native *pomY*, while mCherry-PomX served as the only source of PomX. Consistently with the hypothesis, clusters of mCherry-PomX and PomY-mCherry colocalized during the whole cell cycle and split similarly during cell division (Figure 36 A, B).

In summary, these data show that PomX and PomY undergo a dynamic localization cycle. Starting from a cell without a cluster, a cluster is formed in the off-centre or at midcell. Ultimately clusters translocate towards midcell early and spend ¾ of the cell cycle at midcell where they dictate the position of Z-ring formation and cell division. However, even at midcell clusters are not completely stationary but display a dynamic motion around the midcell area. Furthermore, the data provide evidence that cell division is a signal for PomXY clusters to split and relocate and is in agreement with the finding that clusters accumulate in constrictions and do not split, if cell division is inhibited by cephalexin as reported earlier (5.2.7).

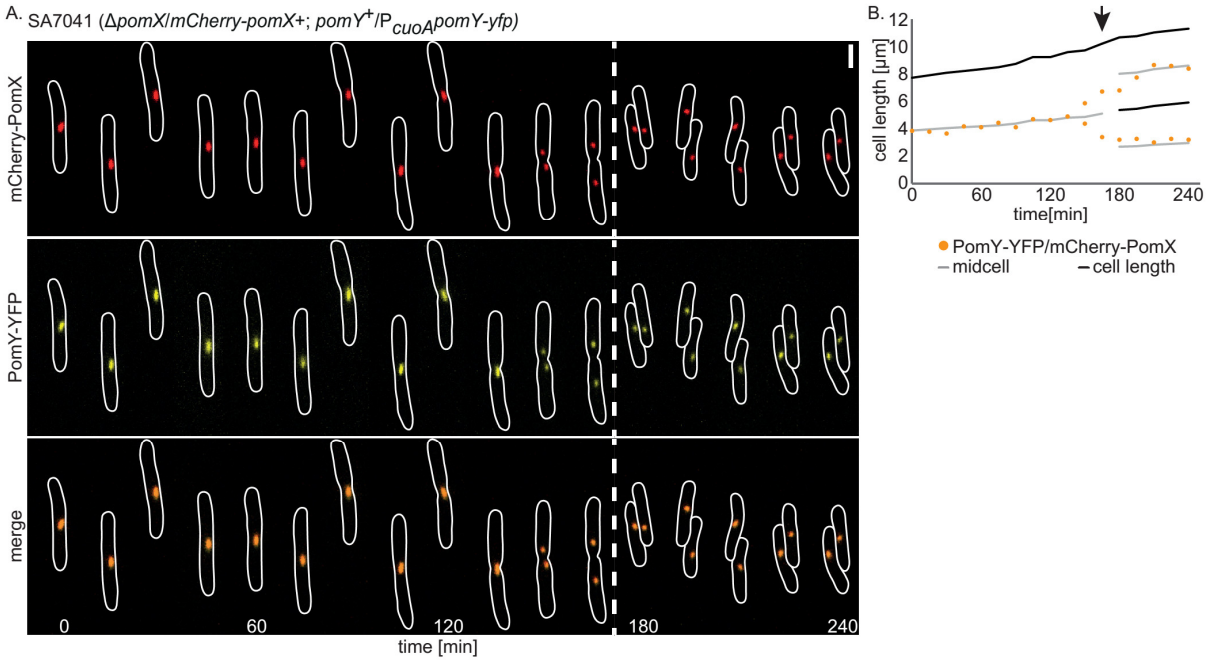

Figure 36: PomX and PomY clusters colocalize during the whole cell cycle and are similarly split during cell division.
(A) Time-lapse microscopy of PomY-eYFP and mCherry-PomX clusters in motile cells of strain SA7041. Cells were grown exponentially prior to time-lapse microscopy in presence of 150 µM $CuSO_4$ and imaged on 1 % agarose buffered with TPM and 0.25 % CTT medium, containing 150 µM $CuSO_4$, at 32 C. Cell outlines were obtained from DIC pictures. White stippled line indicates a cell division event. Merge pictures and movie alignement was performed with Metamorph. Scale bar: 2 µm. **(B)** Cartoon of the cluster motion observed in (A). Cluster position was obtained from linescans of fluorescence pictures along long cell axis. The black arrow indicates a cell division event.

5.2.10 PomXYZ clusters display biased-random motion towards midcell and constrained motion at midcell

To obtain further insights into the translocation mechanism, PomY-mCherry cluster motion was monitored as a marker for the PomXYZ cluster in strain SA4746 (Δ*mglA*; *pomY*$^+$/*pomY-mCherry*+++), at higher temporal resolution. To analyze cluster motion, SA4746 carried a Δ*mglA* deletion, causing a non-motile phenotype. Images were acquired at 30 second intervals for 20 min on TPM agarose containing 0.25 % CTT. When imaged at this high frequency essentially all clusters showed dynamic localization. PomY-mCherry clusters moved in the direction of both, the long and short cell axes. Motion along the Z-axis was not taken into account in this analysis. Additionally, if clusters had an elliptic appearance they also showed tilting motion with a clockwise or counterclockwise rotation.

Off-centre clusters moved towards midcell, but did not follow a straight path (Figure 37 A). Clusters showed small forwards and backwards movements with an overall direction towards midcell. This was strikingly visible in kymographs of off-centre clusters (Figure 37 B), suggesting that off-centre cluster follow a random motion with an overall directional bias towards midcell. Midcell clusters were also generally dynamic but had no overall bias (Figure 37 A, C). In around 10 % of cells, which were generally long cells, midcell clusters showed essentially no motion (Figure 37 C).

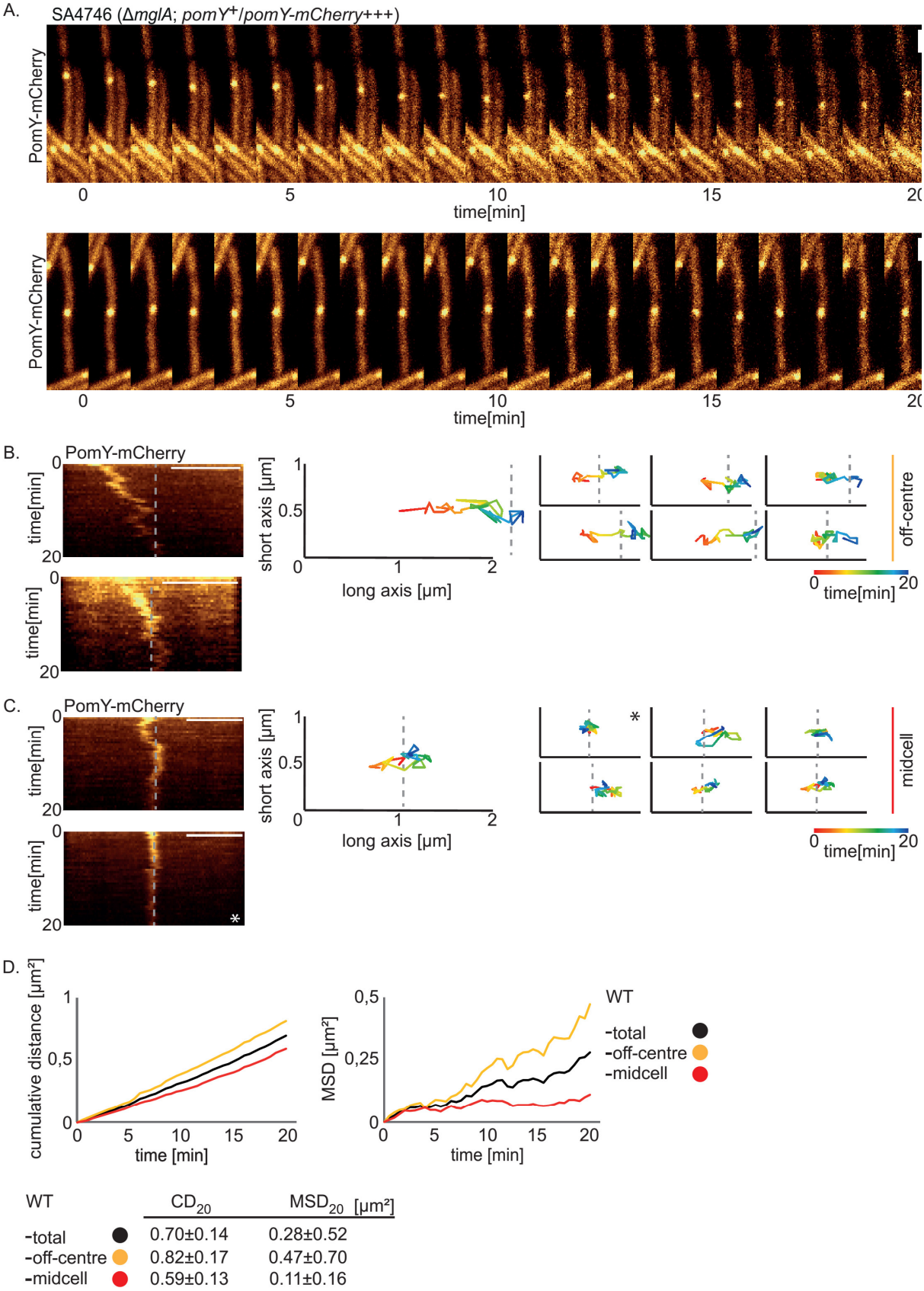

WT	CD_{20}	MSD_{20} [µm²]
-total	0.70±0.14	0.28±0.52
-off-centre	0.82±0.17	0.47±0.70
-midcell	0.59±0.13	0.11±0.16

Figure 37: PomY-mCherry clusters display a random biased motion towards midcell and a constrained motion at midcell.

(A) Fluorescence microscopy of PomY-mCherry in strain SA4746 (Δ*mglA*; *pomY*$^{+}$/*pomY-mCherry*+++). Cells were divided into two groups: Midcell and off-centre. Cells were mixed with a 1:200 dilution TetraSpeck microspheres and imaged on 1 % agarose buffered with TPM supplemented with 0.25 % CTT at 32 °C in 30 seconds intervals for 20 minutes. Movies were aligned with Metamorph using the autoalignment function. Every

2nd picture is shown. Scale bar: 2 µm. **(B)** Kymographs of PomY-mCherry off-centre clusters were generated with Metamorph from linescans of cells along the long cell axis with a thickness of 10 pixels. Grey stippled line indicates midcell. Scale bar 2 µm. Representative XY-tracks were generated from the position of the centroid of the PomY-mCherry cluster at every timepoint during the time-lapse movies, as measured by Metamorph with the particle tracking plugin (8.6.6). X-axis corresponds to 2 µm distance along the long cell axis, Y-axis corresponds to 1 µm along the short cell axis. Grey stippled line indicates midcell. **(C)** Kymographs and XY-tracks of PomY-mCherry midcell clusters were generated as described in (B). Grey star indicates the same cells with very little cluster motion at midcell **(D)** Quantification of cluster motion, measured by cumulative distance and mean squared displacement. CD_{20} and MSD_{20} were calculated as described in 8.6.6 (n=71).

To quantify cluster motion, cluster midpoints were used to track their motion along the long and short cell axis, creating two-dimensional trajectories (8.6.6) (Figure 37 B, C). From that, the cumulative distance (CD_{20}) and mean squared displacement (MSD_{20}) for off-centre and midcell clusters was calculated (Figure 37 D). While cumulative distance gave information about total distance a cluster travelled over time, the mean squared displacement gave information about the distance a cluster had moved away from its original position at a given timepoint. Off-centre and midcell clusters displayed a CD_{20} of 0.82 ± 0.17 µm² and 0.59 ± 0.13 µm² (total CD_{20} 0.70 ± 0.14 µm²; n=71), respectively. This demonstrates that both types of clusters are dynamic and travel similar distances in the same period of time. Interestingly, off-centre clusters showed a MDS_{20} of 0.47 ± 0.70 µm² and therefore a strong displacement from their original localization, whereas the MSD_{20} of midcell clusters was four times lower, with a MDS_{20} of 0.11 ± 0.16 µm² (total MSD_{20} 0.28 ± 0.52 µm²) and reached a plateau. The linear/slightly increasing slope of the resulting MSD curve (Figure 37 D) confirmed that off-centre clusters displayed a directed motion away from their starting point, whereas midcell cluster reached a plateau, showing that they displayed constrained motion in the midcell area. This verifies the observations made earlier in longer time-lapse movies that clusters move towards midcell but do not leave midcell. These data strongly suggests that cluster motion towards midcell relies on a biased-random motion by a mechanism that guarantees an overall bias towards midcell. This bias, however, diminishes when clusters reach midcell, indicating that the translocation mechanism is sensitive to cluster position in the cellular space and translates distance to midcell into a directional bias.

5.2.11 PomZ induces the biased random motion of PomXY clusters *in vivo*

To investigate the role of PomZ in positioning the PomXYZ complex at the mid-nucleoid at midcell, PomY-mCherry clusters were analyzed in a non-motile Δ*pomZ* mutant (SA4796; Δ*mglA*; Δ*pomZ*; *pomY*$^{+}$/*pomY-mCherry*+++) and compared with their dynamic localization in a *pomZ*$^{+}$ background. For this purpose cells were imaged as described (5.2.10) and analyzed in the same way by tracking the centroid of the PomY-mCherry cluster. In these time-lapse recordings PomY-mCherry clusters showed dramatically less motion than in presence of PomZ. PomY-mCherry clusters mostly localized in the off-centre position and rarely at midcell in the absence of PomZ (5.2.4). Independent of cluster position, clusters displayed no directional motion within a period of 20 min (Figure 38 A). Consistently, in trajectories of single clusters they displayed a strong reduction in mobility along both, the long and short cell axes. Of note, this reduced cluster motion was observed for both off-centre and midcell clusters, independent of their distance to midcell (Figure 38 B). Therefore clusters were not separated into these groups in a Δ*pomZ* mutant. PomY-mCherry clusters had a CD_{20} of 0.19 ± 0.04 µm²,

showing that total dynamics were reduced and clusters only moved very little (n=42). Moreover, MSD_{20} was strongly reduced and overall clusters displaced less than midcell clusters in the presence of PomZ (MSD_{20} 0.07 ± 0.2 µm²). These observations demonstrate that PomZ is important for the dynamic localization of PomXYZ clusters and is also required for the directional bias of off-centre clusters. Based on the fact that PomZ recruits PomXY clusters to the nucleoid in *M. xanthus,* we hypothesize that PomZ positions the PomXYZ cluster at mid-nucleoid, at midcell, using the nucleoid as a surface for its function.

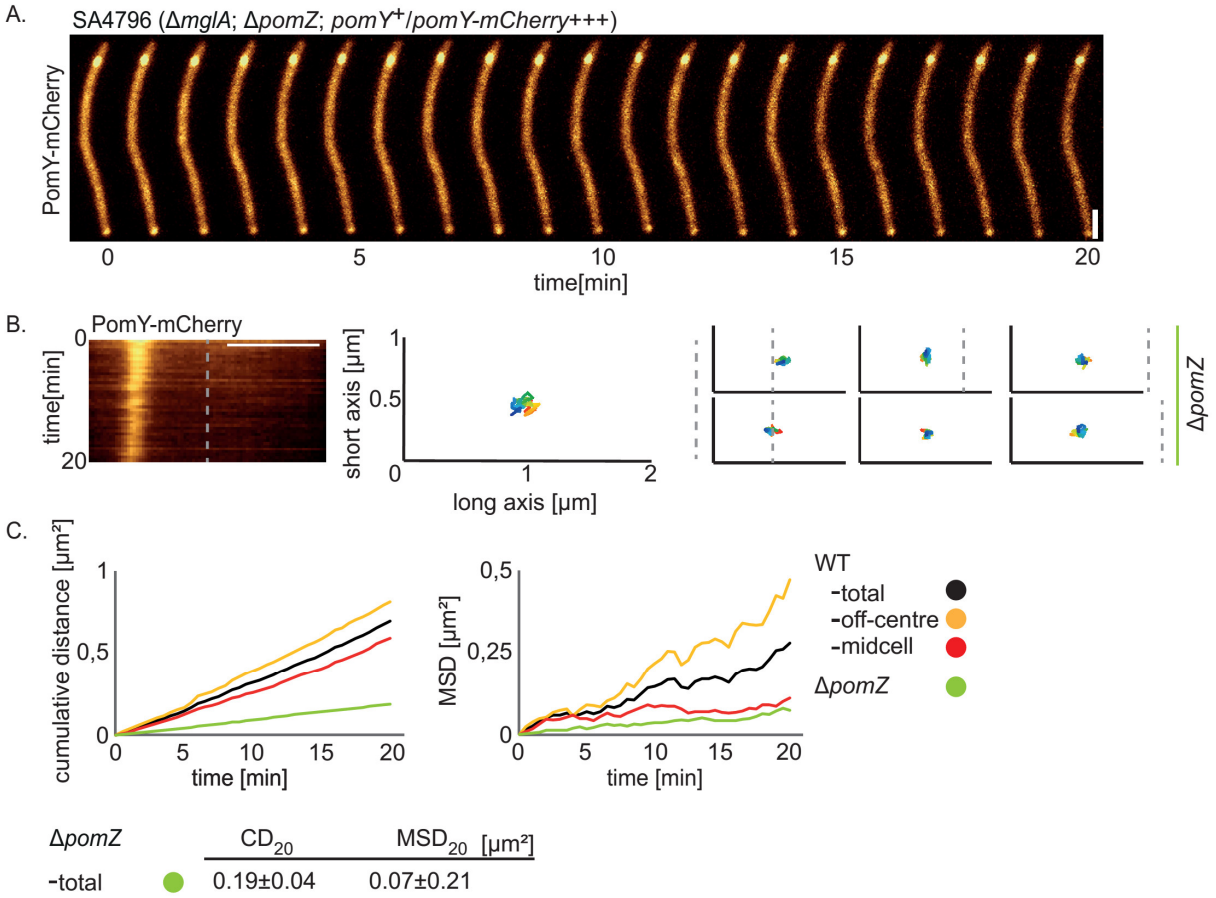

Figure 38: Biased random motion of PomY-mCherry clusters towards midcell is induced by PomZ.
(A) Fluorescence microscopy of PomY-mCherry in strain SA4796 (Δ*mglA*; Δ*pomZ*; *pomY*⁺/*pomY-mCherry*+++). Cells were mixed with a 1:200 dilution TetraSpeck microspheres and imaged on 1 % agarose buffered with TPM supplemented with 0.25 % CTT at 32 °C in 30 seconds intervals for 20 minutes. Movies were aligned with Metamorph using the autoalignment function. Every 2nd picture is shown. Scale bar: 2 µm. **(B)** Representative kymographs of PomY-mCherry clusters were generated with Metamorph from linescans of cells along the long cell axis with a thickness of 10 pixels. Grey stippled line indicates midcell. Scale bar 2 µm. Representative XY-tracks were generated from the position of the centroid of the PomY-mCherry cluster at every timepoint during the time-lapse movies, as measured by Metamorph with the particle tracking plugin (8.6.6). X-axis corresponds to 2 µm distance along the long cell axis, Y-axis corresponds to 1 µm along the short cell axis. Grey stippled line indicates midcell. (C) Quantification of cluster motion, measured by cumulative distance and mean squared displacement. CD_{20} and MSD_{20} were calculated as described in 8.6.6 (n=42).

To determine the resolution limit for the method used. Fluorescently labeled microspheres of 1 µm size were used as a marker for particles that would not undergo motion. Thus any motion of these particles would show the limits of the method. Microspheres were immobilized on a 1 % agarose patch and imaged under the same conditions as cells were imaged. Movies were automatically aligned

using Metamorph and the same particle tracking method was applied, that was used for PomY-mCherry clusters. Under these conditions, immobile microspheres had a CD_{20} of 0.05 ± 0.01 µm² but on average did not show any displacement as depicted by the MSD_{20} of 0 µm². In conclusion, this suggests that PomY-mCherry clusters are not completely immobilized in absence of PomZ, but they display little motion which is likely to be random diffusion.

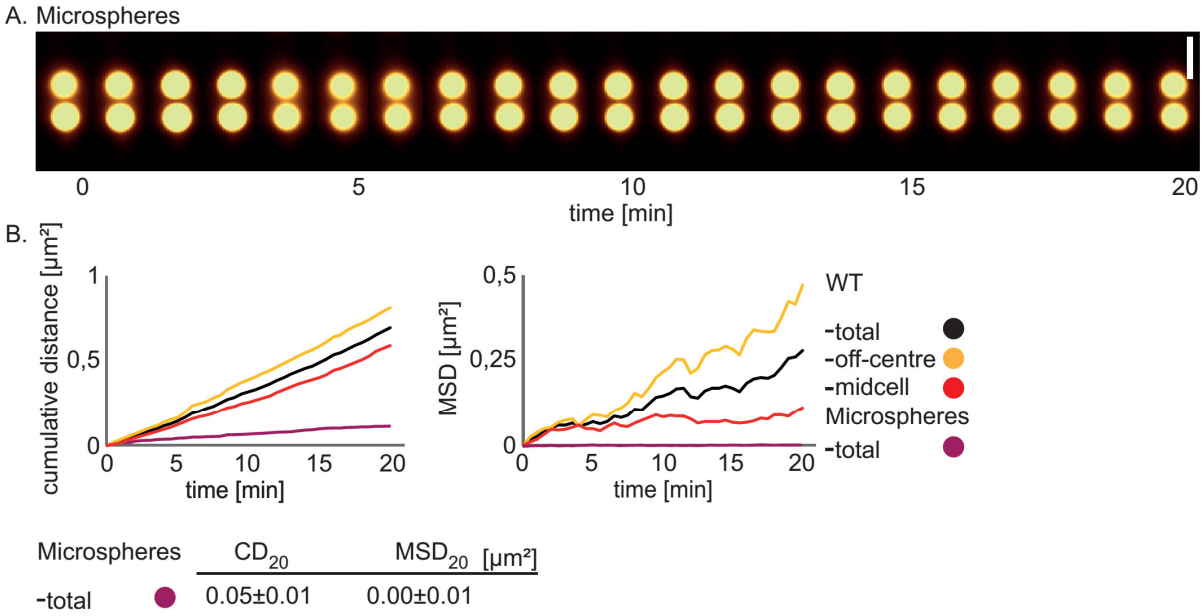

Figure 39: Analysis of dynamics of immobilized fluorescently labeled microspheres.
(A) Fluorescence microscopy of 1 µm TetraSpeck microspheres (Invitrogen). A 1:200 dilution of microspheres was imaged on 1 % agarose buffered with TPM supplemented with 0.25 % CTT at 32 °C in 30 seconds intervals for 20 minutes. Movies were aligned with Metamorph using the autoalignment function. Every 2nd picture is shown. Scale bar: 2 µm. **(B)** Quantification of microsphere motion, measured by cumulative distance and mean squared displacement. CD_{20} and MSD_{20} were calculated as described in 8.6.6 (n=65).

5.2.12 The PomXYZ cluster does not move to midcell bound to a specific chromosomal locus

After cell division the PomXYZ cluster moves from an off-centre position close to the new cell pole towards midcell by biased random motion. This dynamic translocation is reminiscent of the dynamic localization of the terminus region, which in *M. xanthus* is also placed close to the new cell pole in newborn cells and then passively displaces towards midcell, where it is replicated (Harms *et al.*, 2013). We wondered if PomZ connects the PomXY complex to a specific locus close to the terminus region and thereby passively displaces the PomXYZ cluster to the mid-nucleoid at midcell before cell division. In this situation we would expect that the terminus region, would show similar dynamics as the PomXY complex in presence of PomZ. In order to test our hypothesis, FROS (**f**luorescence **r**epressor **o**perator **s**ystem) was used to study the localization of a specific chromosomal locus. In this system an array of *tetO* sequences is inserted into the genome at a specific site. In parallel *tetR* fused to *eyfp* is expressed from a vanillate inducible promoter. After expression, TetR-eYFP binds to the *tetO*-array, allowing to follow the genomic locus by fluorescence microscopy. To analyze the localization of the terminus region the dynamic localization of TetR-eYFP was followed in non-motile cells under the same conditions that PomY-mCherry was followed. In this strain (SA6757; Δ*mglA, mxan_4000::tetO-array, mxan18-19*::P_{van} *tetR-eyfp*), a *tetO*-array was inserted

into *mxan_4000* at 192° of the *M. xanthus* chromosome (personal communication A. Treuner-Lange). To follow the terminus region over time *tetR-eyfp* was expressed in presence of 150 µM vanillate in the medium.

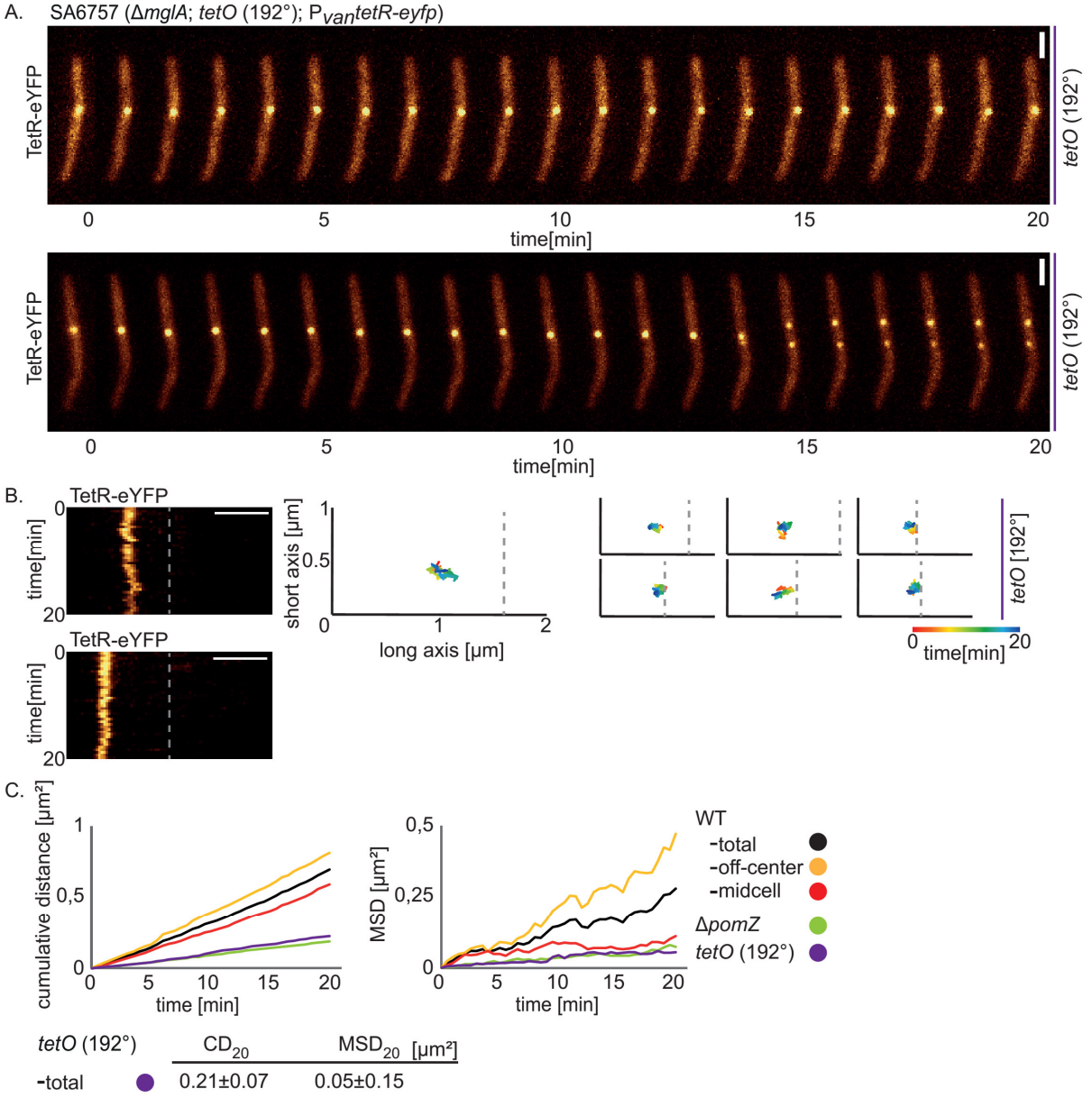

Figure 40: A chromosomal locus in the terminus region displays a random but constrained motion.
(A) Fluorescence microscopy of TetR-eYFP in strain SA6757 (Δ*mglA, mxan4000::tetO-array, mxan18-19*::P_{van} *tetR-eyfp*). Cells were mixed with a 1:200 dilution TetraSpeck microspheres and imaged on 1 % agarose, buffered with TPM, supplemented with 0.25 % CTT at 32 °C in 30 seconds intervals for 20 minutes. Movies were aligned with Metamorph using the autoalignment function. Every 2nd picture is shown. Scale bar: 2 µm. **(B)** Kymographs of TetR-eYFP clusters were generated with Metamorph from linescans of cells along the long cell axis with a thickness of 10 pixels. Grey stippled line indicates midcell. Scale bar 2 µm. Representative XY-tracks were generated from the position of the centroid of the TetR-eYFP cluster at every timepoint during the time-lapse movies, as measured by Metamorph with the particle tracking plugin (8.6.6). X-axis corresponds to 2 µm distance along the long cell axis, Y-axis corresponds to 1 µm along the short cell axis. Grey stippled line indicates midcell. **(C)** Quantification of TetR-eYFP cluster motion, measured by cumulative distance and mean squared displacement. CD_{20} and MSD_{20} were calculated as described in 8.6.6 (n=26).

As reported previously, in the majority of cells TetR-eYFP formed one single cluster, positioned in the off-centre localization or at midcell. Rarely, two signals were found, which both localized close to midcell (Harms *et al.*, 2013) (Figure 40 A). In time-lapse recordings (every 30 seconds for 20 min), TetR-eYFP clusters did not show strong motion. Moreover, off-centre clusters of TetR-eYFP did not displace towards midcell as it was reported for PomY-mCherry clusters (Figure 40 A, B). In some cases one cluster close to midcell split into two, that moved apart from each other and formed a more or less stationary cluster within minutes (Figure 40 A). From these cluster motions trajectories were built, which showed that TetR-eYFP displayed little motion independent of its distance to midcell (n=25). In agreement with this CD_{20} was low with 0.21 ± 0.07 µm². Similarly, TetR-eYFP bound to the terminus region at 192° also showed nearly no displacement (MSD_{20} 0.05 ± 0.15 µm²), which was indistinguishable from PomY-mCherry clusters in the absence of PomZ (Figure 40 C). Based on these findings, we conclude that PomXYZ complexes in the presence of PomZ are recruited to the chromosome but are not moving towards midcell passively by direct attachment to a specific locus in the terminus region.

5.3 PomX and PomY stimulated ATPase activity of PomZ is required for cluster translocation towards midcell

PomZ belongs to the ParA/MinD superfamily P-loop ATPases that generally shows low ATPase activity (Lim *et al.*, 2014). Accordingly, PomZ was shown to exhibit essentially no ATPase activity *in vitro*. However, mutational analysis showed that ATP-hydrolysis is required for PomZ function and its localization at midcell *in vivo* (Treuner-Lange *et al.*, 2013). To gain further insights into the importance and regulation of ATP-hydrolysis by PomZ, the interaction network between PomX, PomY and PomZ was analyzed

5.3.1 PomX and PomY form a complex that interacts with PomZ *in vivo* and *in vitro*

Based on previous findings we hypothesized that PomXYZ interact and recruit FtsZ to midcell. To clarify if the three Pom-proteins interact and furthermore interact with FtsZ a Bacterial Adenylate Cyclase based Two Hybrid (BACTH) screen was performed for potential interactions *in vivo* in *E. coli* (Karimova *et al.*, 2005). In this assay PomX, PomY and PomZ were able to self-interact, indicating that all three proteins have the capability to form at least dimers. As exprected, PomXYZ interacted in all pairwise combinations (Figure 41 A).These data suggest that PomXYZ can interact in pairwise combinations without the help of the third protein. This observation is consistent with the finding that PomX and PomY colocalize in the absence of PomZ (5.2.4). Of note, FtsZ was included in the BACTH interaction study and showed the ability to self-interact. By contrast it did not show interactions with PomX, PomY or PomZ in this assay. This indicates that either FtsZ interacts with PomXYZ via an additional linker protein which was not included in our screen, or that interaction of PomXYZ with FtsZ is only functional when all four components are present at the same time. This is in agreement with the idea that PomXYZ clusters colocalize with FtsZ at midcell.

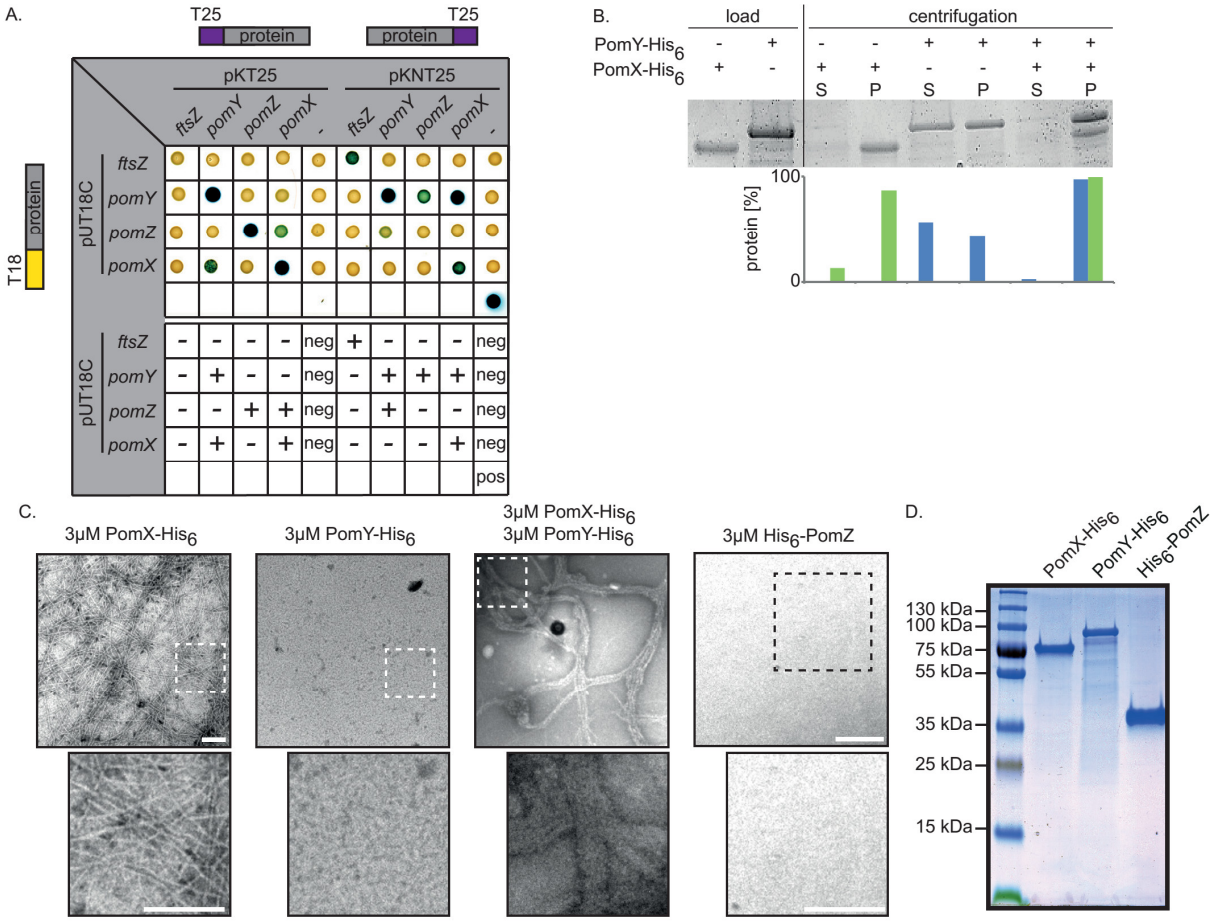

Figure 41: PomX and PomY associate *in vivo* and *in vitro* and interact with PomZ in a BACTH assay.
(A) Bacterial Two Hybrid assay to test for interaction between PomX, PomY, PomZ and FtsZ in *E. coli* BTH101. Assay was performed as described in 8.3.5. „+“ indicates interaction of two interaction partners as observed by the blue colony color on indicator agar plates, „-“ indicates no interaction. „pos“ marks the positive control and „neg“ indicates the negative controls. Picture shows one representative assay and all colonies were grown on the same plate at 30 °C. **(B)** PomX-His$_6$ and PomY-His$_6$ interact in a sedimentation assay. Proteins were applied to high-speed centrifugation at 160.000 x g alone or in combination and divided into soluble (S) and pellet (P) fraction and separated via SDS-PAGE. Bar graphs indicate the amount of PomX-His$_6$ (green) and PomY-His$_6$ (blue) in each fraction in %. **(C)** Transmission electron microscopy of indicated proteins. Proteins were visualized with 1% uranyl acetate. Scale bar: 100 nm. **(D)** Purification of PomX, PomY and PomZ. SDS-PAGE analysis of His$_6$-tagged PomX, PomY and PomZ after purification. Proteins were stained with Instant Blue.

To confirm the BACTH screen *in vitro* interaction studies were performed. For this purpose soluble full length PomX-His$_6$ (45.4 kDa), PomY-His$_6$ (73.9 kDa) and His$_6$-PomZ (37.7 kDa) were purified by Andrea Harms (Figure 41 D) and tested in *in vitro* assays together with Andrea Harms. In a first step, interaction among PomX-His$_6$ and PomY-His$_6$ was tested via sedimentation assay. We found that 90 % of 2 µM PomX-His$_6$ was recovered from the pellet fraction after high speed centrifugation at 160000 x g, while only 45 % of 2 µM PomY-His$_6$ sedimented into the pellet fraction under the same conditions. In contrast, if both proteins were mixed in equimolar ratio, they were found in the pellet fraction after high speed centrifugation (Figure 41 B).

We wondered if PomX-His$_6$ would form higher ordered structures that are visible by transmission electron microscopy and further if PomY-His$_6$ would have an impact on such structures. To gain further insights into the structure of the PomXY interaction *in vitro* we performed negative stain transmission electron microscopy together with Janet Vonck (MPI for Biophysics, Frankfurt). 3 µM

PomX-His$_6$ and 3 µM PomY-His$_6$ alone or in combination were applied to a microscopy grid and negatively stained by uranyl-acetate as described in 8.6.7. PomX-His$_6$ formed long thin filaments with a thickness of 19 ± 3 nm (n=150) and a length of several micrometers. By eye, merging or splitting of filaments was not observed, indicating that filaments grew at the ends. PomY-His$_6$ by contrast did not form any higher ordered structure. Importantly, when mixed in a 1:1 molar ratio and preincubated for 10 minutes, PomX-His$_6$ and PomY-His$_6$ formed bundles with a width in the rage of 60 nm - 160 nm. Occasionally, single small filaments emerged from these bundles, which had the appearance of PomX-His$_6$ filaments. PomZ on its own did not form any higher ordered structure in presence or absence of ATP that could be observed by electron microscopy. However, PomZ was not mixed with PomX or PomY in this assay (Figure 41 C). Finally, this demonstrates that first, PomX is able to form higher-ordered, polymeric structures on its own. Secondly, PomY bundles PomX filaments *in vitro,* as filament bundles of PomX are only observed in presence of PomY.

5.3.2 PomZ ATPase activity is stimulated in presence of the PomXY complex and DNA

Purified His$_6$-PomZ showed no ATPase activity *in vitro* but ATPase activity was important for function of PomZ *in vivo* (Treuner-Lange *et al.*, 2013). ParA/MinD ATPases generally show little ATPase activity on their own, but need an ATP-hydrolysis activating partner (Leonard *et al.*, 2005). To investigate if PomX and PomY stimulate ATPase activity by PomZ, phosphate release by ATP-hydrolysis was measured in a malachite green assay as described in 8.5.13. Consistently with previous findings (Treuner-Lange *et al.*, 2013), 2 µM His$_6$-PomZ displayed no observable ATPase actitivity. Similarly, 2 µM PomX-His$_6$ or PomY-His$_6$ did not show any ATP-hydrolysis activity. Additionally, ATPase activity of His$_6$-PomZ was not significantly altered by addition of PomY-His$_6$ or PomX-His$_6$. However, PomX-His$_6$ and PomY-His$_6$ in equimolar ratio of 2 µM stimulated His$_6$-PomZ ATPase activity *in vitro* to a turnover rate of 18.5 ATP h^{-1} (Figure 42 A).

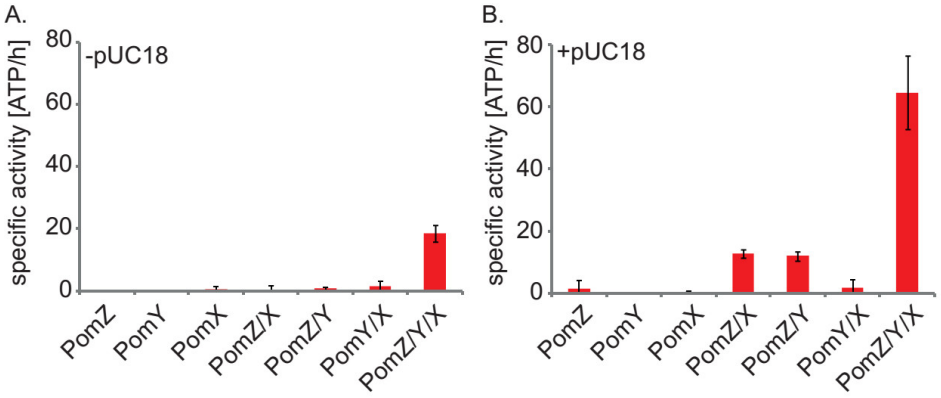

Figure 42: PomZ ATPase activity is stimulated by PomX and PomY in presence of DNA.
(A) Specific ATPase activity of 2 µM His$_6$-PomZ, PomY-His$_6$ and PomX-His$_6$ or combinations of the proteins was determined by a colorimetric malachite green assay in presence of 1 mM ATP. Proteins were mixed in equimolar ratios. **(B)** Specific ATPase activity of 2 µM His$_6$-PomZ, PomY-His$_6$ and PomX-His$_6$ or combinations of the proteins in presence of 5 nM DNA. Bars represent the mean specific activity of 6 assays.

Because addition of DNA was reportet to stimulate ATP hydrolysis by ParA ATPases involved in plasmid or chromosome segregation (Ah-Seng *et al.*, 2009, Castaing *et al.*, 2008, Lim *et al.*, 2014,

Schofield *et al.*, 2010) and PomZ *in vivo* colocalizes with the nucleoid we tested if ATPase activity is stimulated upon addition of 5 nM pUC18 plasmid DNA. Addition of plasmid DNA to His_6-PomZ resulted in a minor stimulation of ATP hydrolysis (1.6 ATP h^{-1}). By contrast, PomX-His_6 or PomY-His_6 alone stimulated ATPase activity by His_6-PomZ to 12.9 ATP h^{-1} and 12.1 ATP h^{-1} in the presence of DNA. This stimulatory effect was synergistic in presence of 2 µM PomX-His_6 and PomY-His_6 and plasmid DNA, leading to an ATPase activity of 64.7 ATP h^{-1} (Figure 42 B). We conclude that PomZ has ATPase activity that is not active when alone. However, ATP hydrolysis by PomZ is stimulated when interacting with PomX, PomY and DNA *in vitro*. Because PomX and PomY did not catalyse ATP-hydrolysis or showed any affinity for DNA *in vivo* this strongly suggests that PomZ has two ATPase activating proteins, PomX and PomY and furthermore that PomZ is capable to interact with DNA *in vitro*.

5.3.3 PomZ ATPase activity and DNA binding are required for its function

Knowing that PomZ shows ATP-hydrolysis activity *in vitro* which was stimulated by PomXY in presence of DNA, we asked why ATPase activity is essential for PomZ function *in vivo*. As reported, PomZ belongs to the ParA/MinD superfamily of P-loop ATPases and has homologs that work in chromosome or plasmid segregation like ParA (Ebersbach & Gerdes, 2001, Lim *et al.*, 2014), regulation of replication initiation like Soj (Murray & Errington, 2008), or cell disivion like MinD and MipZ (de Boer *et al.*, 1991, Kiekebusch *et al.*, 2012). All these proteins have in common that they share a Walker A motif, a catalytic aspartate and, in case of DNA-binding ParA's, conserved positively charged amino acids in their C-terminal part (Hester & Lutkenhaus, 2007, Roberts *et al.*, 2012) with the exception of MipZ (Kiekebusch *et al.*, 2012). By aligning PomZ and its homologs from other myxobacteria with different members of the ParA/MinD superfamily we found that PomZ harbors all these features (Figure 43 A).

The ATPase cycle of these ATPases can be blocked at specific steps by single substitutions. To generate mutants that were blocked in different steps of the ATPase cycle several substitutions were introduced into PomZ. Lysine at position 66 in PomZ was substituted by a glutamine, which corresponds to a K18Q and K20Q substitution in MipZ and Soj, respectively (Kiekebusch *et al.*, 2012, Leonard *et al.*, 2005). This residue is part of the ATP binding site and interacts with ATP and its substitution results in ATP-binding defects and a loss in dimerization.

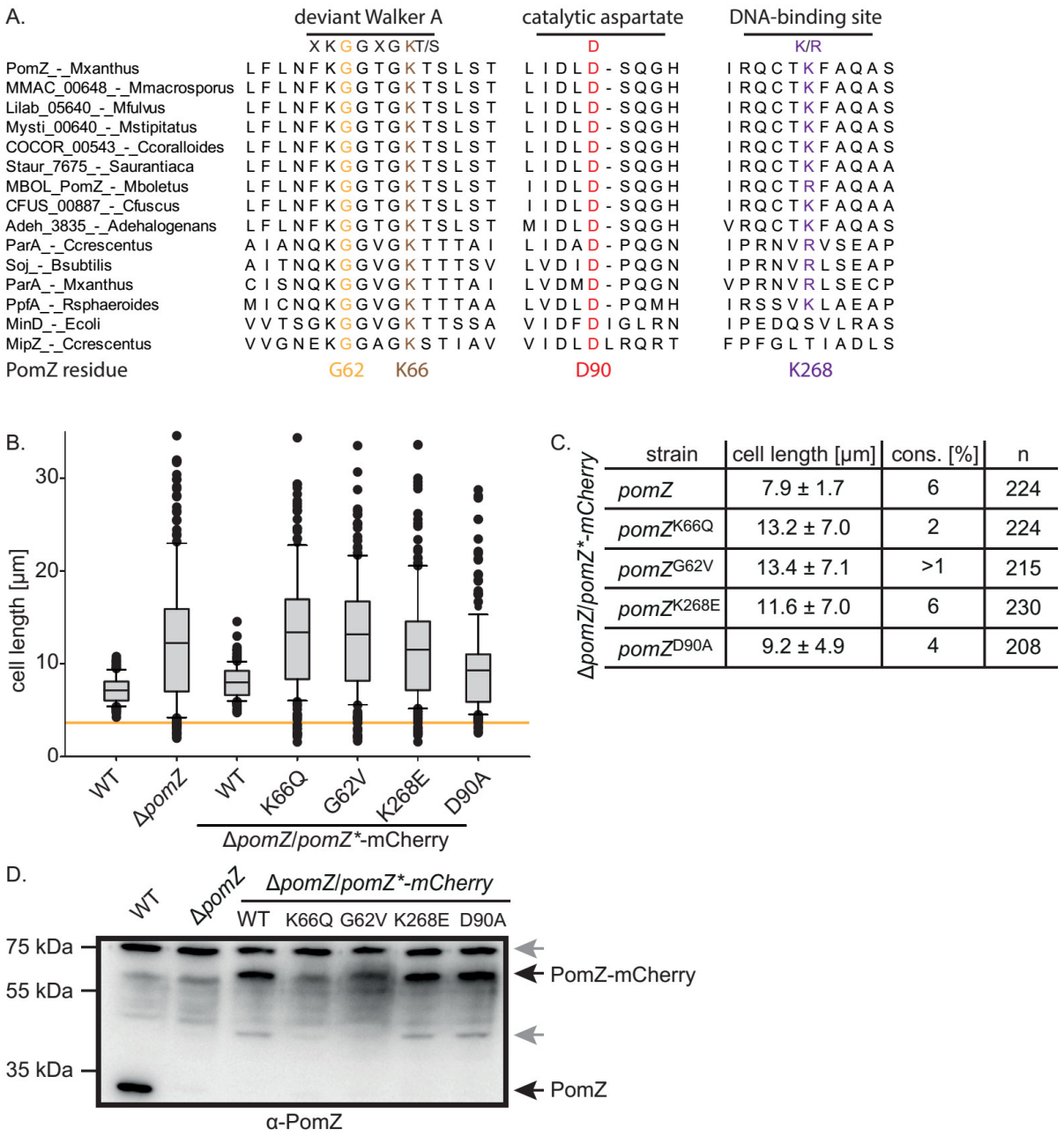

Figure 43: Inhibition of different steps of the ATPase cycle and DNA-binding interferes with PomZ function.
(A) Partial alignment of PomZ with other members of the PomZ group and Mrp/MinD family of P-loop ATPases. Alignment was performed with full length proteins, using the MAFFT algorithm (Katoh & Toh, 2008). Specific amino acids that were used for substitution are marked coloured. **(B)** PomZ-mCherry variants can not complement the Δ*pomZ* phenotype. Grey box plots enclose 25th and 75th percentile, with the mean indicated by the black line. Whiskers display 10th and 90th percentile. Outliers are shown as black dots. Cells below orange line count as minicells. **(C)** Summary of the cell length phenotypes of strains expressing PomZ-mCherry and the variants at native levels. Mean cell length is indicated ± SD. **(D)** Immunoblot analysis of cell lysates of indicated strains to test for accumulation of PomZ, PomZ-mCherry and the PomZ-mCherry variants using specific α-PomZ antibodies. Grey arrows indicate unspecific binding of the antibody and degradation products.

PomZ^{G62V} is suggested to interfere with ATP-binding-dependent dimerization of PomZ as it resembles the G14V and G16V substitution in MipZ and Soj (Kiekebusch *et al.*, 2012, Leonard *et al.*, 2005). Replacement of asparatate D90 with alanine is suggested to interfere with ATP-hydrolysis by PomZ and was shown to affect PomZ function *in vivo* (Treuner-Lange *et al.*, 2013). These three corresponding substitutions in Soj were shown to keep the protein monomeric and affect DNA-binding

(G16V and K20Q), or lock the protein in a dimeric form and enable it to bind to DNA (D44A) (Leonard *et al.*, 2005). In addition, we created a PomZ^{K268E} substitution, which is equivalent to an R218E substitution in Soj and the K196E substitution in PpfA. In these two proteins replacement of a positively charged amino acid at this position by a negatively charged interferes with non-specific DNA binding and function of the proteins (Hester & Lutkenhaus, 2007, Roberts *et al.*, 2012).

To test if the PomZ substitutions are functional *in vivo* and to analyse their cellular localization *pomZ-mCherry* was mutated to *pomZ*^{G62V}*-mCherry*, *pomZ*^{K66Q}*-mCherry*, *pomZ*^{D90A}*-mCherry* and *pomZ*^{K268E}*-mCherry* and introduced into the Δ*pomZ* mutant under the control of its native promoter at the *Mx8* attachment site.

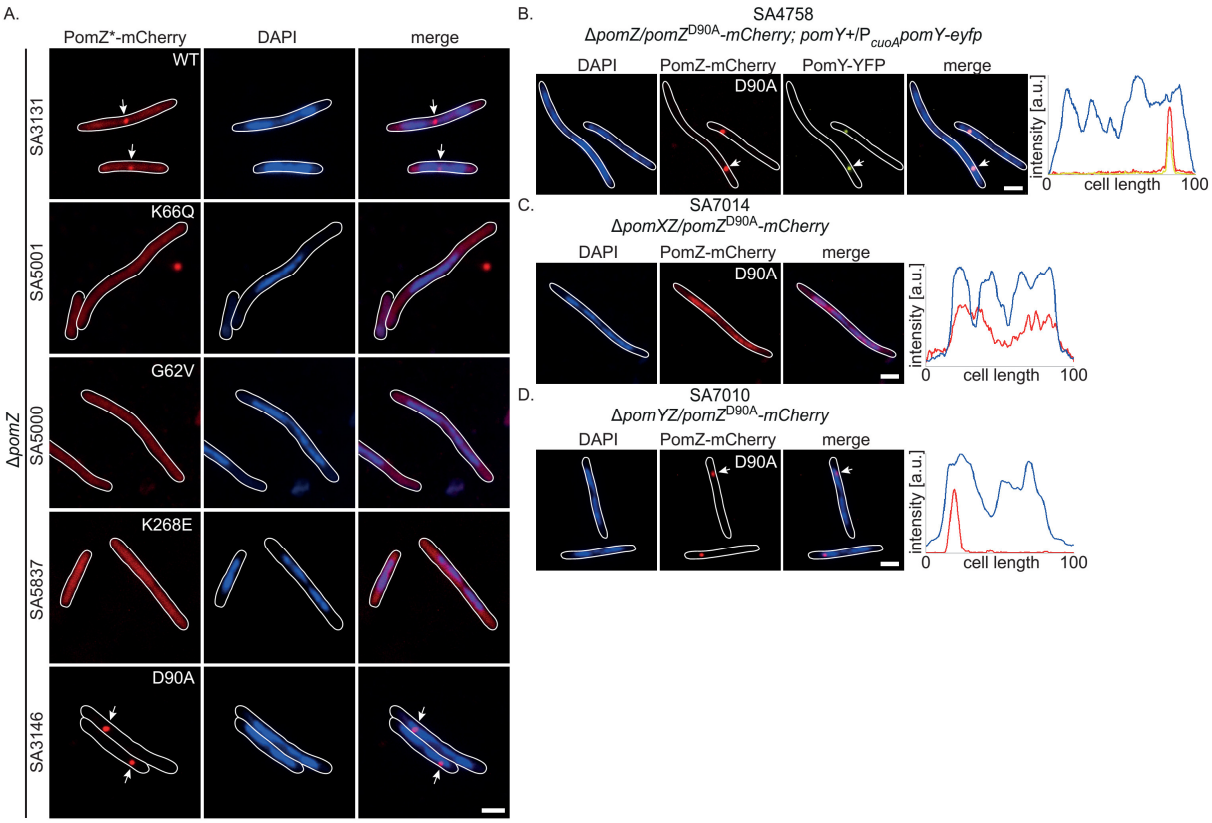

Figure 44: Localization of the PomZ-mCherry variants in *M. xanthus*.
(A) Fluorescence microscopy of indicated strains. Cells were imaged on 1 % agarose pads buffered with TPM at 32°C. Cells were collected from exponentially grown cultures and nucleoids were stained with DAPI before acquisition. Cell outlines were obtained from DIC pictures. Merge pictures were created using Metamorph. Scale bar: 2 µm. **(B)** Fluorescence microscopy of SA4758. Cells were grown in presence of 150 µM $CuSO_4$ and treated with DAPI as in (A). Images were acquired as in (A). Linescans show fluorescence intensity of PomZ^{D90A}-mCherry (red), PomY-eYFP (yellow) and DAPI signal (blue) along the long cell axis given in %. Linescans were created with Metamorph. **(C)** Fluorescence microscopy of SA7014. Images were acquired as in (A) and linescans produced as in (B). **(D)** Fluorescence microscopy of SA7010. Images were acquired as in (A) and linescans produced as in (B).

As reported earlier PomZ-mCherry is functional and complements a Δ*pomZ* phenotype when expressed at native levels. By contrast PomZ^{D90A}-mCherry was unable to complement a Δ*pomZ* mutant (Treuner-Lange *et al.*, 2013). Similarly to the PomZ^{D90A} fusion, neither PomZ^{K66Q}, PomZ^{G62V} nor PomZ^{K268E} fused to mCherry complemented the cell division defect of the Δ*pomZ* mutant (Figure 43 B, C). Of note, PomZ^{K66Q}- and PomZ^{G62V}-mCherry accumulated at lower levels than the WT protein,

PomZ^{D90A}- and PomZ^{K268E}-mCherry in immunoblot analysis, which could also lead to the observed cell division defects (Figure 43 D). To investigate the localization of the PomZ variants and PomZ^{WT}, nucleoids of the five strains were stained with DAPI and cells were analyzed by fluorescence microscopy. As expected PomZ-mCherry formed a cluster in the majority of cells that was either found at midcell or in the off-centre position. Additionally, it formed the patchy localization, which colocalizes with DAPI-stained nucleoids (Figure 44 A). Similarly, PomZ^{D90A}-mCherry formed one cluster, over the nucleoid, but lacked the patchy localization over the stained nucleoids as previously reported (Treuner-Lange *et al.*, 2013). These clusters were predominantly found in the off-centre position (Figure 44 A). Furthermore, PomZ^{D90A}-mCherry colocalized with the PomY-eYFP cluster as a marker for the PomXY complex, suggesting that PomZ^{D90A} interacts with PomXY (Figure 44 B). Its localization in the complex was only dependent on PomX but not on PomY, as cluster formation was abolished in the absence of PomX. Interestingly, in the absence of PomX the PomZ^{D90A}-mCherry signal was spread out and colocalized with the DAPI-stained nucleoids, demonstrating that it binds to the nucleoids as the WT protein (Figure 44 C, D). Importantly, the fact that PomZ^{D90A}-mCherry only forms a cluster but no patchy signal in presence of PomXY suggests that dimeric, ATP-bound PomZ can not leave the PomXYZ complex without ATP-hydrolysis and therefore PomZ^{D90A} is stuck to the cluster. In other words, detachment of dimeric, ATP-bound PomZ from the PomXYZ complex is ATP-hydrolysis-dependent. By contrast, PomZ^{K66Q}-, PomZ^{G62V}- and PomZ^{K268E}-mCherry were unable to colocalize with the nucleoid and to form a cluster and displayed a diffuse localization thoughout the cell (Figure 44 A). This suggests that the monomeric forms of PomZ are unable to interact with the nucleoid, like the DNA-binding mutant and furthermore that they are affected in interaction with the PomXY complex to form a PomZ-mCherry cluster.

In addition, PomZ-, PomZ^{K66Q}-, PomZ^{G62V}-, PomZ^{K268E}- and PomZ^{D90A}-mCherry were expressed from a stronger promoter (P_{pilA}) in a Δ*pomZ* mutant to determine the effect of overexpression of PomZ and its variants on cell division and to study their localization. When overproduced neither PomZ-mCherry nor one of its variants were able to complement a Δ*pomZ* phenotype (Figure 45 A, B). PomZ-mCherry and its variants accumulated as full length proteins at the same level (Figure 45 B). They accumulated at 50 – 100 x higher levels than when expressed from the native promoter, but strong degradation of the full length proteins was observed by immunoblot analysis (Figure 45 C). Of note, no free mCherry (27 kDa) was detectable by specific α-mCherry antibodies (Figure 45 D). Similarly to the expression of PomZ and its variants at native levels, PomZ-mCherry formed a cluster which was weakly detectable within the strong patchy signal on the nucleoids, but these clusters were rarely found at midcell (Figure 45 E). We conclude that PomZ-mCherry localization is similar under overexpression and native expression conditions, with the difference that signals are much stronger when PomZ-mCherry accumulates at higher levels.

As expected, PomZ^{K66Q}, PomZ^{G62V} and PomZ^{K268E}-mCherry displayed a diffuse localization throughout the cell, filling the nucleoid free spaces with signal and furthermore they did not form any PomZ clusters (Figure 45 E). In contrast PomZ^{D90A}-mCherry formed a PomZ cluster and a patchy localization that colocalized with the nucleoid (Figure 45 E). We conclude that the level of PomZ has to be tightly regulated in order for the protein to fulfill its function.

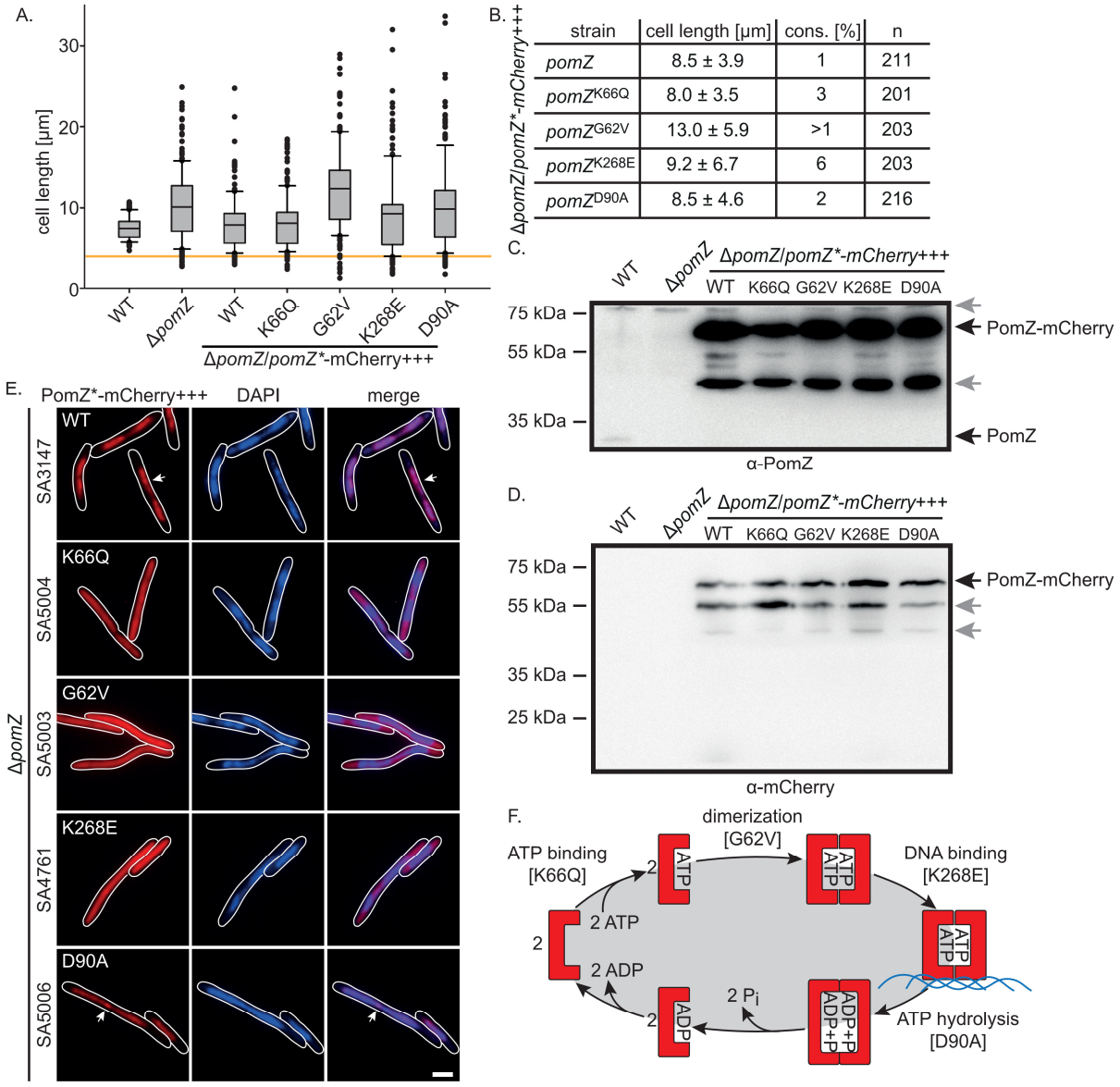

strain	cell length [µm]	cons. [%]	n
pomZ	8.5 ± 3.9	1	211
pomZ^{K66Q}	8.0 ± 3.5	3	201
pomZ^{G62V}	13.0 ± 5.9	>1	203
pomZ^{K268E}	9.2 ± 6.7	6	203
pomZ^{D90A}	8.5 ± 4.6	2	216

Figure 45: Overexpression of PomZ-mCherry *in vivo* compromises its function.
(A) Cell length phenotype of strains overexpressing PomZ-mCherry and its variants. Grey box plots enclose 25th and 75th percentile, with the mean indicated by the black line. Whiskers display 10th and 90th percentile. Outliers are shown as black dots. Dots below the orange line indicate minicells. **(B)** Summary of the cell length phenotypes of strains expressing PomZ-mCherry and the variants at high levels. Mean cell length is indicated ± SD. **(C) and (D)** Immunoblot analysis of cell lysates of indicated strains to test for accumulation of PomZ, PomZ-mCherry and the PomZ-mCherry variants using specific α-PomZ antibodies (C) as well as for the accumulation of PomZ-mCherry using specific α-mCherry antibodies (D). Grey arrows indicate unspecific binding of the antibody and degradation products. **(E)** Fluorescence microscopy of indicated strains. Cells were imaged on 1 % agarose pads, buffered with TPM at 32°C. Cells were collected from exponentially grown cultures and nucleoids were stained with DAPI before acquisition. Cell outlines were obtained from DIC pictures. Merge pictures were created using Metamorph. Scale bar: 2 µm. **(F)** Schematic of the PomZ ATPase cycle on the basis of the provided data. PomZ is shown in red and DNA is indicated as blue lines.

In summary we predict that the PomZ ATPase cycle consists of several steps (Figure 45 F). First monomeric PomZ binds ATP and dimerizes. Upon dimerization, dimeric ATP-bound PomZ is able to associate with nucleoid. If bound to DNA, PomZ dimers recruit the PomXY complex which results in PomZ cluster formation and ATP-hydrolysis by PomZ and its subsequent release from the DNA into the cytoplasm (Figure 45 F). In conclusion, these data demonstrate that PomZ has to cycle between an ADP-bound, monomeric and an ATP-bound, dimeric phase in order to function normally, similarly

to standard ParA's. Block of this cycle at any step results in an unfunctional protein. Additionally, DNA-binding is essential for function of the protein and its binding to the nucleoid is a prerequisite for PomZ to interact with PomXY to generate the PomZ cluster.

5.3.4 PomZ associates with the *E. coli* nucleoid and DNA in a non-specific manner

We demonstrated that PomZ can associate with the nucleoid in an ATP-dependent manner. While monomeric PomZ is diffuse in the cells, ATP-bound, dimeric PomZ interacts with the nucleoid and the PomXY cluster. Because PomZ-mCherry evenly colocalizes with the nucleoid in *M. xanthus* and several ParA-like ATPases were shown to non-specifically bind to DNA, we asked whether PomZ-mCherry would bind to the *E. coli* nucleoid. To address this question *pomZ-mCherry* and the four *pomZ-mCherry* variants were expressed in *E. coli* BL21(DE3). For this purpose, gene expression was induced by addition of 0.05 mM IPTG for 2 h in LB medium at 37 °C. To condense the *E. coli* nucleoid, cells were treated with chloramphenicol for 30 min prior to DAPI stain and subsequent microscopy. Expression of *pomZ-mCherry* and its variants did not interfere with cell division in *E. coli* (Figure 46 A). Under these conditions, all five proteins accumulated at similar levels as shown by immunoblot analysis (Figure 46 B). As expected from their localization in *M. xanthus* PomZ- and $PomZ^{D90A}$-mCherry colocalized with the nucleoid in *E. coli,* while $PomZ^{K66Q}$- $PomZ^{G62V}$ and $PomZ^{K268E}$-mCherry displayed a diffuse localization also filling the nucleoid free gaps (Figure 46 A). This confirmed our hypothesis that PomZ cannot only interact with the *M. xanthus* nucleoid. Of note, neither PomZ- nor $PomZ^{D90A}$-mCherry formed a cluster in *E. coli*, but colocalized evenly with the nucleoid.

Next, we asked if purified His_6-PomZ is able to bind to DNA *in vitro*. To examine the interaction of PomZ and DNA *in vitro* an electrophoretic mobility shift assay (EMSA) was performed together with Andrea Harms. In this assay increasing concentrations of His_6-PomZ from 0 - 10 µM, were incubated with 200 fmol pUC18 plasmid DNA in presence and absence of ATP. Even low concentrations of His_6-PomZ were able to shift plasmid DNA and increasing concentrations resulted in a complete shift of the pUC18 DNA in presence of ATP. Similarly, His_6-PomZ was able to shift plasmid DNA in the absence of ATP, however plasmid DNA was not comepletely shifted even at the highest concentration (Figure 46 C). As a control His_6-FrzZ (Trudeau *et al.*, 1996) was used in the same concentrations as His_6-PomZ, and did not shift DNA in presence or absence of ATP (Figure 46 C). Under these conditions, His_6-PomZ shifted the band corresponding to supercoiled plasmid DNA, whereas a slower band, which most likely correspondes to relaxed plasmid DNA, was unshifted. To investigate if PomZ binds with higher affinity to supercoiled DNA or to relaxed DNA, pUC18 DNA was linearized and purified.

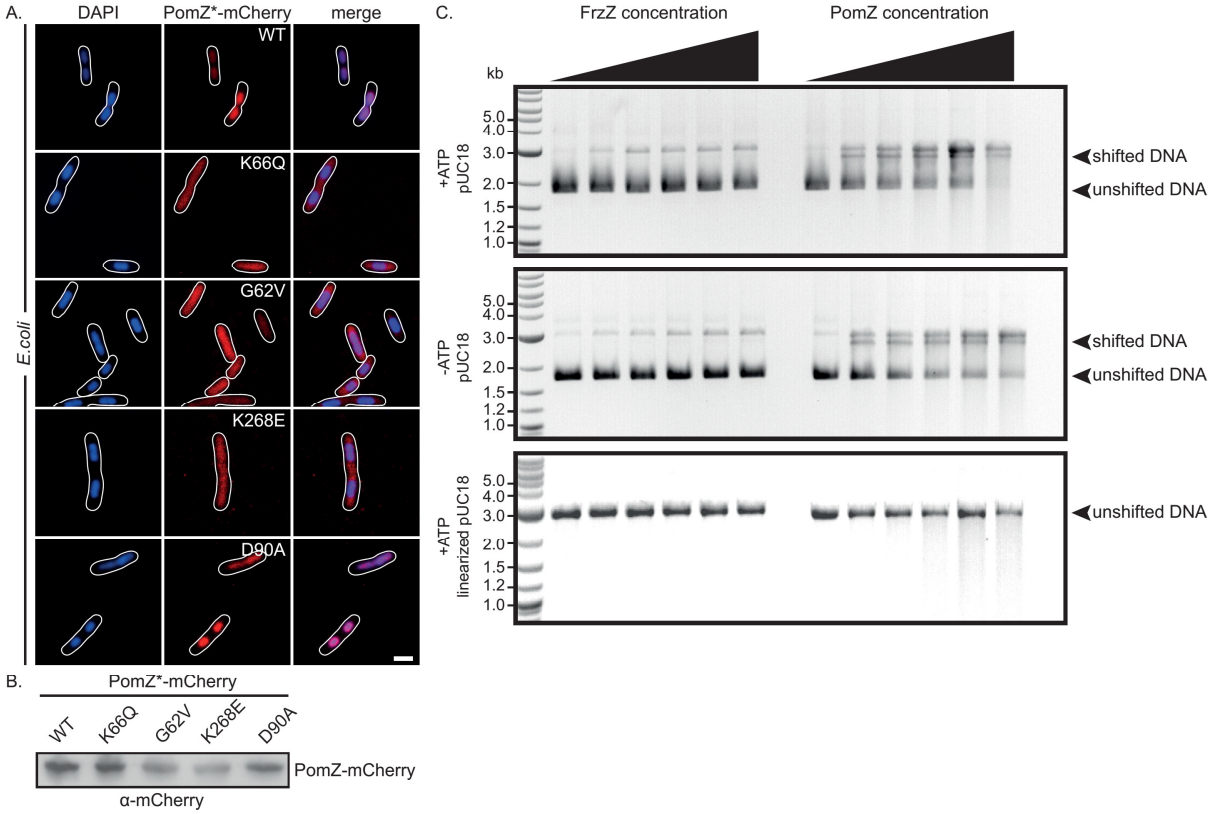

Figure 46: PomZ binds non-specifically to DNA *in vivo* and *in vitro*.
(A) Fluorescence microscopy of *E.coli* BL21(DE3) cells expressing PomZ-mCherry and its variants. Expression was induced with 0.05 mM IPTG for 2 h at 37 °C. Cells were treated with 30 µg/ml chloramphenicol for 30 min and with DAPI for 10 min at room temperature and were subsequently imaged on a 1 % agarose pad, buffered with TPM. Cellular outline was obtained from DIC pictures. Merged picures were created with Metamorph. Scale bar: 2 µm. **(B)** Immunoblot analysis of BL21(DE3) lysates for the expression of PomZ-mCherry and its variants after 2 h induction. PomZ-mCherry was detected using specific α-mCherry antibodies. **(C)** Electrophoretic mobility shift assay (EMSA) with His_6-PomZ and 200 fmol pUC18 plasmid DNA. EMSA's were performed as described in 8.5.12. Triangles indicate increasing protein concentrations from 0-10 µM His_6-PomZ.

Linearized plasmid DNA was unshifted even at high concentrations of His_6-PomZ in presence of ATP as was observed for high concentrations of His_6-FrzZ (Figure 46 C). In conclusion these data showed that PomZ *in vivo* and *in vitro* has affinity to DNA and binds DNA in a non-specific manner. Because monomeric PomZ-mCherry *in vivo* does not bind to the nucleoid we reason that purified His_6-PomZ contains ATP and predominantly exists as a dimer in solution because it binds DNA in absence of ATP *in vitro*. Interestingly, PomZ has higher affinity for supercoiled, than for relaxed DNA *in vitro*, indicating that the geometry and curvature of the DNA, and of the nucleoid *in vivo*, is important for binding of PomZ.

5.3.5 PomXYZ form DNA associated clusters in *E. coli*

In a next attempt, we analyzed if PomXYZ interact in an unrelated organism like *E. coli* as they do in *M. xanthus* to form clusters. First, individual Pom-proteins were expressed in *E. coli* BL21(DE3). For this purpose *mCherry-pomX*, *pomY-eyfp* and *pomZ-mCherry* expression was induced by addition of 0.05 mM IPTG to an exponentially growing culture. Induction was performed for 2 h and cells were treated with 30 µg/ml chloramphenicol for 30 min followed by DAPI-stain and microscopy. In case of *mCherry-pomX,* expression was induced only for 1 h.

As described earlier, PomZ-mCherry precisely colocalized with the *E. coli* nucleoid, without forming a cluster. In comparison PomY-eYFP displayed a weak diffuse localization and occasionally accumulated at the cell poles in areas that were devoid of DNA. Similarly to the observations made *in vitro*, mCherry-PomX formed clusters and longer filamentous structures (Figure 47 A). Knowing that PomX, PomY and PomZ pairwise interact *in vivo* and *in vitro* we asked if they have an effect on each other in *E. coli*. For this experiment *mCherry-pomX* and *pomZ-mCherry* were expressed under control of an IPTG inducible promoter, while *pomY-eyfp* was expressed under an arabinose inducible promoter. Cells were co-transformed with two plasmids and gene expression was induced simultaneously with 0.05 mM IPTG and 0.015 % arabinose for 2 h. As observed in *M. xanthus,* mCherry-PomX and PomY-eYFP colocalized in clusters and short filaments when co-expressed. Strikingly, when co-expressed with PomZ-mCherry, PomY-eYFP colocalized with the nucleoid similarly to PomZ-mCherry (Figure 47 A). Once more these experiments demonstrated, that PomX and PomY, as well as PomZ and PomY interact. Furthermore this observations showed directly that PomZ is able to recruit PomY to the nucleoid irrespective of the presence of PomX. We wondered whether recruitment to the DNA is dependent on specific states in the ATPase cycle and co-expressed *pomY-eyfp* with the PomZ variants. Expectedly, PomY was only recruited to the DNA if PomZ-mCherry was able to bind to the nucleoid itself i. e. only PomZ- and PomZ^{D90A}-mCherry were able to recruit PomY-eYFP to the nucleoid. In case, a monomeric PomZ variant, or the DNA-binding mutant were coexpressed with *pomY-eyfp*, PomY-eYFP occasionally colocalized with an otherwise diffusely localized PomZ-mCherry signal in a polar cluster.

Next, we reasoned that expression of *pomZ-mCherry*, *pomY-eyfp* and an unlabelled version of *pomX* would lead to reconstruction of the PomXYZ system in *E. coli*. To test this idea, *pomY-eyfp* and *pomZ-mCherry* were co-expressed by addition of 0.05 mM IPTG for 2 h, followed by expression of *pomX,* by addition of 0.015 % arabinose for 30 min. Strikingly PomY-eYFP and PomZ-mCherry formed clusters that colocalized. Furthermore, PomZ-mCherry also displayed a patchy localization on the nucleoid similar to the patchy pattern in *M. xanthus.* At high frequency (91% of cells) clusters of PomY-eYFP and PomZ-mCherry colocalized with a nucleoid and interestingly, the number of clusters corresponded in 65 % of cell to the number of observed nucleoid masses (Figure 47 A). In total these data demonstrate that PomXYZ interact *in vivo* in an unrelated organism to form a complex. It further shows that all three Pom-proteins are required and also sufficient to form nucleoid associated complexes. Notably, in contrast to *M. xanthus,* in *E. coli* PomXYZ form multiple clusters with each nucleoid containing one of them. This observation may arise from the induction event and subsequent production of clusters *in vivo,* which so far has not been done in *M. xanthus*. Furthermore, in *M. xanthus*, which in contrast to *E. coli* performs only one round of replication per round of cell division (Harms *et al.*, 2013), we only find one nucleoid mass during the midcell positioning event of PomXYZ. Finally, PomXYZ do not interfere with cell division in *E. coli,* suggesting that they do not interact with *E. coli* FtsZ, indicating that FtsZ of *M. xanthus* is slightly different from *E. coli* FtsZ.

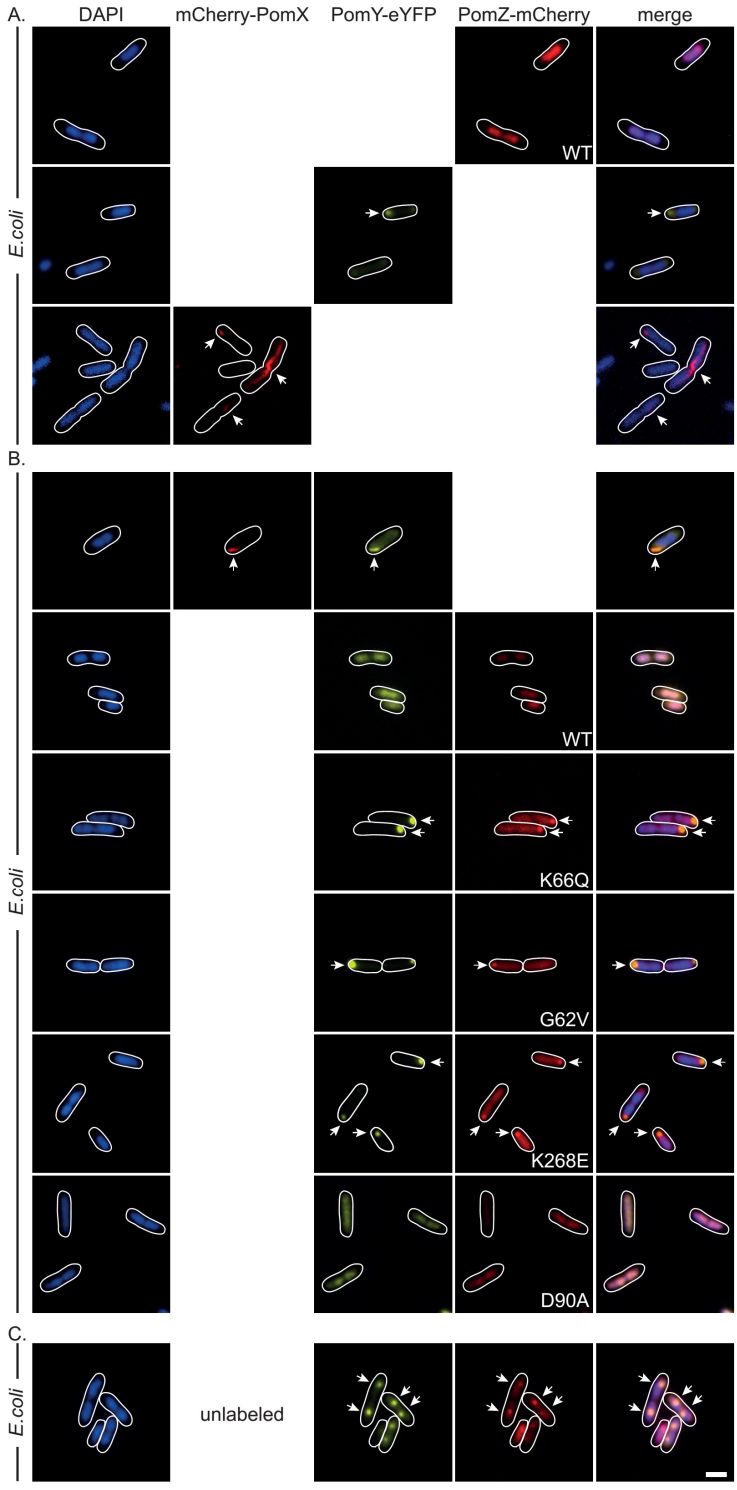

Figure 47: PomXYZ interact in *E. coli* and form nucleoid associated clusters.
(A) Fluorescence microscopy of mCherry-PomX, PomY-eYFP and PomZ-mCherry expressed in *E. coli*. Expression of *pomY-eYFP* and *pomZ-mCherry* was induced in exponentially growing cells with low amounts of IPTG (0.05 mM) for 2 h at 37 °C in LB. Expression of *mCherry-pomX* was induced similarly for 1 h. Cells were treated with 30 µg/ml chloramphenicol for 30 min at 25 °C and nucleoids were stained with DAPI prior to micrsocopy. Cells were imaged on 1 % agarose buffered with TPM at 25 °C. Cell outlines were obtained from DIC pictures. Scale bar: 2 µm **(B)** Coexpression of *pomY-eyfp* with *mCherry-pomX* and *pomZ-mCherry* and ist variants. *mCherry-pomX* and *pomZ-mCherry* were expressed as in (A). *pomY-eyfp* was expressed under regulation of arabinose. For microscopy cells were induced with 0.015% arabinose for 2 h at 37 °C. Cells were imaged as in (A). **(C)** Coexpression of PomXYZ in *E. coli*. *pomZ-mCherry* and *pomY-eyfp* were expressed in presence of 0.05 mM IPTG from the same plasmid for 2 h at 37 °C and expression of *pomX* was induced by addition of 0.015% arabinose for 30 min. Cells were otherwise treated and imaged as in (A).

5.3.6 PomZ ATPase activity is required for biased random motion of the PomXYZ complex to midcell

In *M. xanthus* the ATP-hydrolysis deficient form of PomZ, PomZ^{D90A}, formed a cluster that colocalized with the PomXY complex on the nucleoid. Because this cluster rarely localized at midcell, but predominantly in the off-centre position, we hypothesized that PomXYZ clusters in presence of PomZ^{D90A} are restricted in their dynamic translocation towards midcell. In order to investigate this idea a non-motile strain was created that expresses *pomZ*^{D90A} from the *mxan_0018* and *mxan_0019* intergenic region, under the control of its native promoter, as the only source of *pomZ*. Of note, PomZ^{D90A} accumulated slightly above WT-like levels, suggesting that observations made do not arise from aberrant protein levels (Figure 48 B). In this background PomY-mCherry was expressed, resulting in strain SA7027 (Δ*mglA*; Δ*pomZ*/*pomZ*^{D90A}; *pomY*$^{+}$/*pomY-mCherry*+++), to assay cluster localization and dynamics of the PomXYZ complex. Time-lapse microscopy was performed in 30 sec intervals for 20 minutes (Figure 48 A). PomY-mCherry clusters were observed in the off-centre position and at midcell, but midcell clusters were detected only in rare cases (5% of cells). Independently of their localization and distance to midcell, clusters displayed only little motion and were essentially stalled at their position, showing a CD_{20} of 0.19 ± 0.13 µm², which was strikingly similar to clusters observed in the absence of PomZ. Equally, PomY cluster motion was strongly constrained at any position and showed a mean squared displacement of 0.05 ± 0.06 µm² after 20 min (n=39) (Figure 48 D). In summary these data demonstrate that the biased-random motion of PomXYZ clusters towards midcell and their constrained motion at midcell depends on ATP-hydrolysis by PomZ.

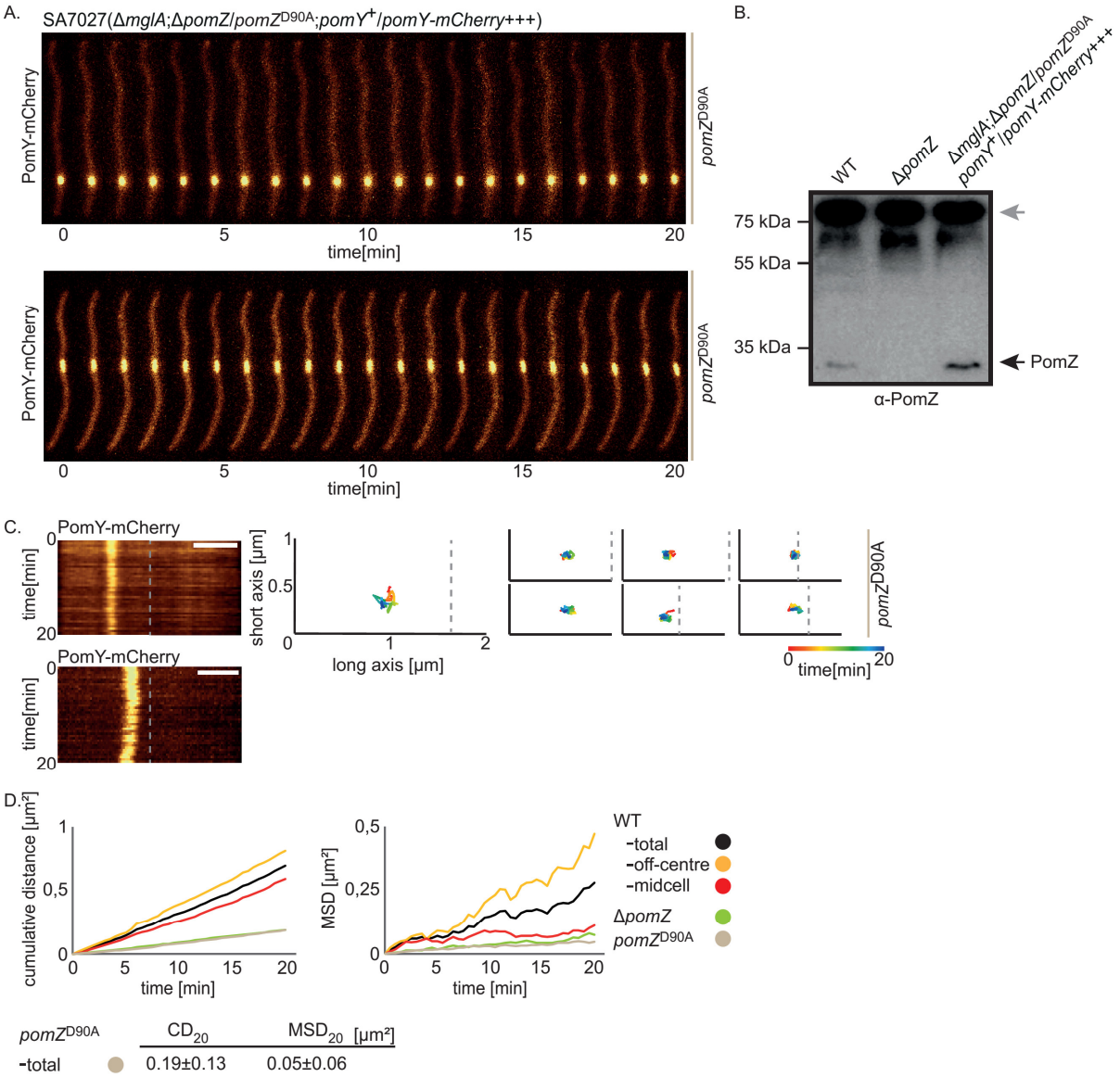

Figure 48: ATP-hydrolysis by PomZ is required for biased PomXYZ cluster motion towards midcell.
(A) Fluorescence microscopy of PomY-mCherry in strain SA7027 that expresses PomZ^{D90A} as the only source of PomZ. Cells were mixed with a 1:200 dilution TetraSpeck microspheres and imaged on 1 % agarose, buffered with TPM, supplemented with 0.25 % CTT at 32 °C in 30 seconds intervals for 20 minutes. Movies were aligned with Metamorph using the autoalignment function. Every 2nd picture is shown. Scale bar: 2 µm. **(B)** Immunoblot analysis of cell lysates of indicated strains for the presence of PomZ and PomZ^{D90A}. PomZ and PomZ^{D90A} were detected using α-PomZ antibodies. **(C)** Kymographs of PomY-mCherry in strain SA7027 were generated with Metamorph from linescans of cells along the long cell axis with a thickness of 10 pixels. Grey stippled line indicates midcell. Scale bar 2 µm. Representative XY-tracks were generated from the position of the centroid of the PomY-mCherry cluster at every timepoint during the time-lapse movies, as measured by Metamorph with the particle tracking plugin (8.6.6). X-axis corresponds to 2 µm distance along the long cell axis, Y-axis corresponds to 1 µm along the short cell axis. Grey stippled line indicates midcell. **(D)** Quantification of PomY-mCherry cluster motion in presence of PomZ^{D90A}, measured by cumulative distance and mean squared displacement. CD_{20} and MSD_{20} were calculated as described in 8.6.6 (n=39).

5.3.7 Overexpression of PomZ delocalizes PomY and slows down cluster motion

Overexpression of PomZ-mCherry leads to a cell division defect. However, PomZ-mCherry still formed clusters and a patchy localization on the nucleoid when overexpressed.

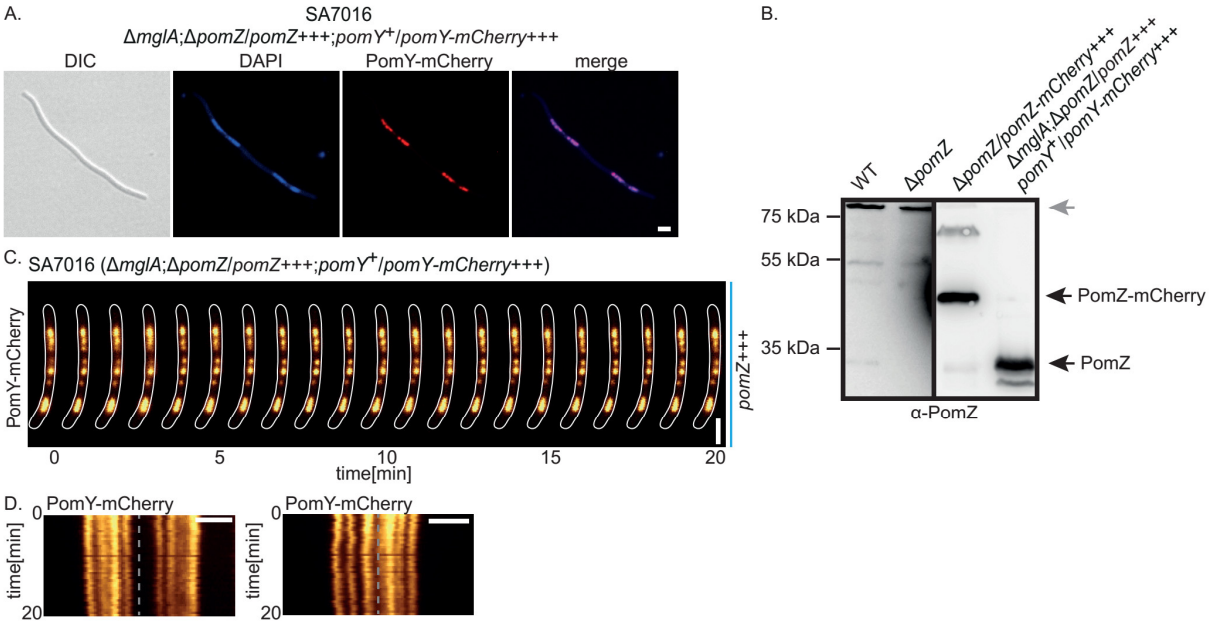

Figure 49 Overexpression of PomZ delocalizes PomY to cover the nucleoid.
(A) Fluorescence microscopy of PomY-mCherry in presence of high levels of PomZ in strain SA7016. Exponentially growing cells were collected and treated with DAPI before visualization by fluorescence microscopy on a 1 % TPM agarose pad. Merged pictures were created with Metamorph. Scale bar: 2 µm. **(B)** Immunoblot analysis of lysates of indicated strains for the accumulation of PomZ, using specific α-PomZ antibodies. Black arrows indicate PomZ and PomZ-mCherry. Note, that a faint band is visible in WT, corresponding to full-length PomZ. **(C)** Time-lapse recordings of SA7016. Pictures were acquired on 1% TPM agarose supplemented with 0.25 % CTT. Cells were imaged every 30 sec for 20 min. Every 2nd picture is shown. Cellular outline was obtained from DIC pictures. Movis were aligned using Metamorph. Scale bar: 2 µm. **(D)** Kymographs of PomY-mCherry signals in representative cells of SA7016 over 20 min. Kymographs were created with Metamorph from linescans on fluorescence images with a thickness of 10 pixels along the long cells axis. Grey stippled line indicates midcell. Scale bar 2µm.

Therefore we asked whether cluster translocation is affected by overexpression of PomZ. To this end, we analyzed PomXYZ cluster motion in cells that accumulated native PomZ at high levels (SA7016; Δ*mglA*; Δ*pomZ*/*pomZ*+++; *pomY*+/*pomY-mCherry*+++). This strain had a Δ*pomZ* phenotype with a mean cell length of 13.3 ± 7.4 µm and PomZ accumulated at approximately 50 - 100 x higher levels than under native expression conditions, as in SA3147 (Δ*pomZ*/*pomZ-mCherry*+++) (Figure 49 B) (see also Figure 45).

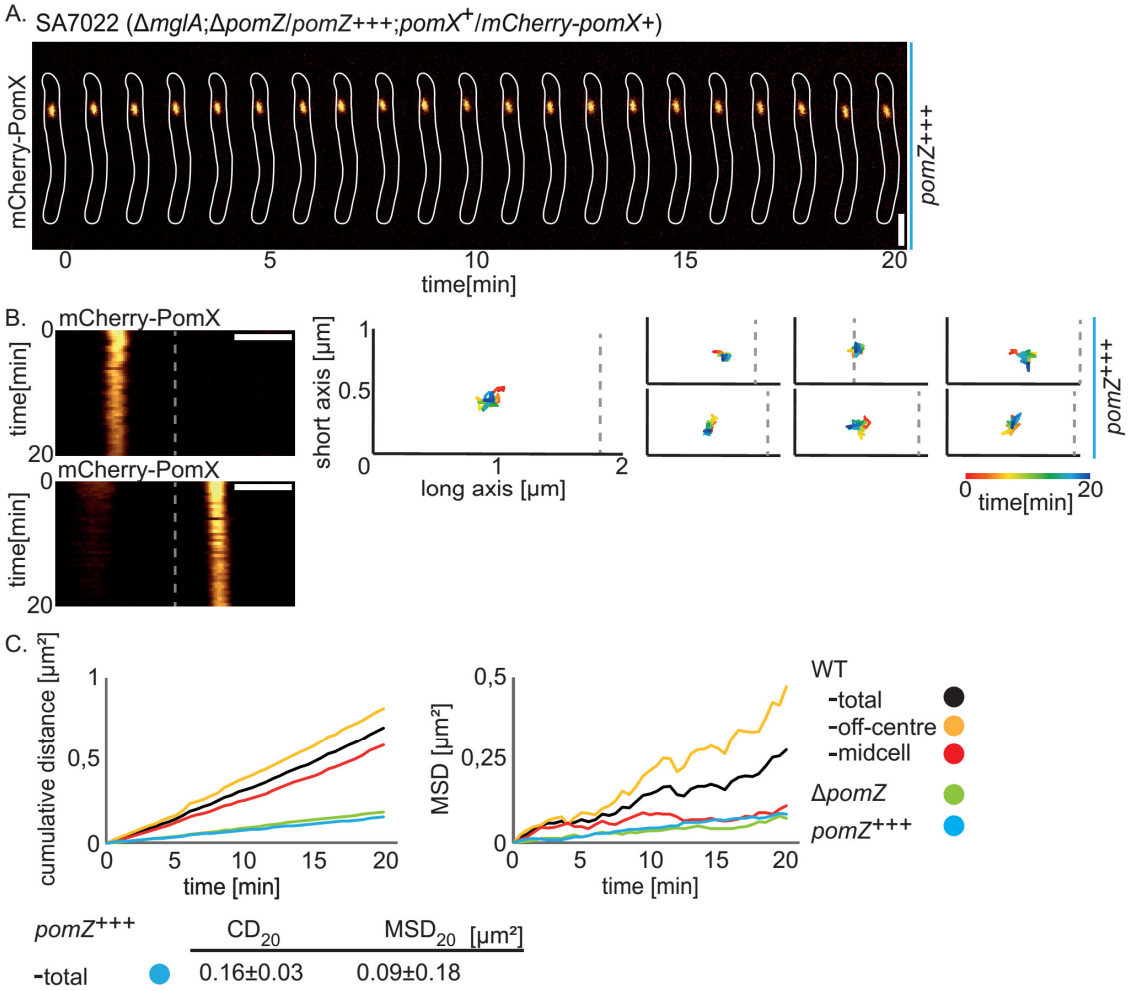

Figure 50: PomX cluster motion is reduced and clusters do not translocate to midcell upon PomZ overexpression.
(A) Fluorescence microscopy of mCherry-PomX in presence of high levels of PomZ in strain SA7022. Time-lapse recordings of SA7022 were performed on exponentially grown cells. Pictures were acquired on 1% TPM agarose supplemented with 0.25 % CTT at 32 °C. Cells were imaged every 30 sec for 20 min. Every 2nd picture is shown. Cellular outline was obtained from DIC pictures. Movies were aligned using the auto align plugin from Metamorph. Scale bar: 2 µm. **(B)** Kymographs of mCherry-PomX clusters in strain SA7022 were generated with Metamorph from linescans of cells along the long cell axis with a thickness of 10 pixels. Grey stippled lines indicate midcell. Scale bar 2 µm. Representative XY-tracks were generated from the position of the centroid of the mCherry-PomX cluster at every timepoint during the time-lapse movies, as measured by Metamorph with the particle tracking plugin (8.6.6). X-axis corresponds to 2 µm distance along the long cell axis, Y-axis corresponds to 1 µm along the short cell axis. Grey stippled lines indicate midcell. **(C)** Quantification of mCherry-PomX cluster motion in presence of high levels of PomZ, measured by cumulative distance and mean squared displacement. CD_{20} and MSD_{20} were calculated as described in 8.6.6 (n=50).

First, we analysed localization of PomY-mCherry to determine if overexpression of PomZ interferes with PomXY cluster recruitment to the DNA. Unexpectedly, single clusters of PomY-mCherry were not detectable. By contrast, several PomY-mCherry patches were observed that colocalized precisely with the DAPI-stained nucleoids (Figure 49 A). This observation was strikingly similar to the observation that PomZ recruits PomY to the nucleoids in *E. coli*. Because PomY on its own stimulates ATP-hydrolysis by PomZ in presence of DNA we next asked, if these PomY-mCherry patches were still dynamic and performed time-lapse microscopy in short intervals (30 sec). PomY-mCherry patches overall displayed only little motion, indicating that they are slightly dynamic on the nucleoid (Figure 49 C). However, in kymographs this motion was without any displacement towards midcell (Figure 49 D).

Because PomXYZ clusters were not observed under these conditions we conclude that PomXY complex formation is affected by overexpression of PomZ. Next, we analyzed localization of mCherry-PomX in the same strain background in SA7022 (Δ*mglA*; Δ*pomZ*/*pomZ*+++; *pomX*$^{+}$/*mCherry-pomX*+). Under these conditions mCherry-PomX formed one single cluster that was predominantly found in the off-centre position (Figure 50 A) and colocalized with the nucleoid (data not shown). This finding showed that cluster formation by PomX is unaffected by overaccumulation of PomZ and delocalization of PomY. Interestingly, these clusters did not show strong motion within a time frame of 20 min (Figure 50 A). mCherry-PomX clusters displayed a CD_{20} of 0.16 ± 0.03 µm² and a MSD_{20} of 0.09 ± 0.18 µm², strinkingly similar to cluster motion in the absence of PomZ (n=50). We conclude that PomZ levels are crucial for motion of the PomXYZ complex.

5.3.8 Lack of PomY reduces PomX cluster motion towards midcell

Based on our results we know that interference with ATP-hydrolysis by and accumulation of PomZ affects the PomXYZ cluster translocation towards midcell. Because PomX and PomY stimulate ATP-hydrolysis by PomZ *in vitro* in presence of DNA we predicted that lack of PomY would affect PomX cluster dynamics. In essence, lack of PomY would slow down biased PomX cluster motion to midcell. In fact in the absence of PomY, PomX clusters localize at midcell with a high frequency.

To test the prediction, mCherry-PomX cluster dynamics were analysed in non-motile cells lacking PomY (SA7008; Δ*mglA*; Δ*pomY*; *pomX*$^{+}$/*mCherry-pomX*+). These cells showed a cell length phenotype similar to a Δ*pomY* mutant, with an average cell length of 12.5 ± 6.4 µm. mCherry-PomX clusters were found in the off-centre position and at midcell (Figure 51 A), but the number of cells with a midcell cluster exceeded the number of cells with off-centre clusters. As expected both off-centre (CD_{20} 0.55 ± 0.12 µm²) and midcell clusters (CD_{20} 0.46 ± 0.10 µm²) of mCherry-PomX showed dynamic localization (Figure 51 B) (n=44). Moreover, cluster motion in absence of PomY was more constrained and off-centre clusters displayed a MSD_{20} of 0.22 ± 0.29 µm², which was around 50 % lower compared to clusters in PomY presence. Similarly, midcell clusters had an MSD_{20} of 0.09 ± 0.09 µm². Based on these data we conclude that lack of PomY reduces PomX cluster motion. However, the directional bias towards the mid-nucleoid at midcell still occured in the absence of PomY. In addition, these clusters showed a constrained motion at midcell in absence of PomY. Because PomY stimulates ATP-hydrolysis *in vitro,* we propose that lack of PomY affects cluster motion by reducing ATP-hydrolysis by PomZ, which in turn reduces cluster translocation speed.

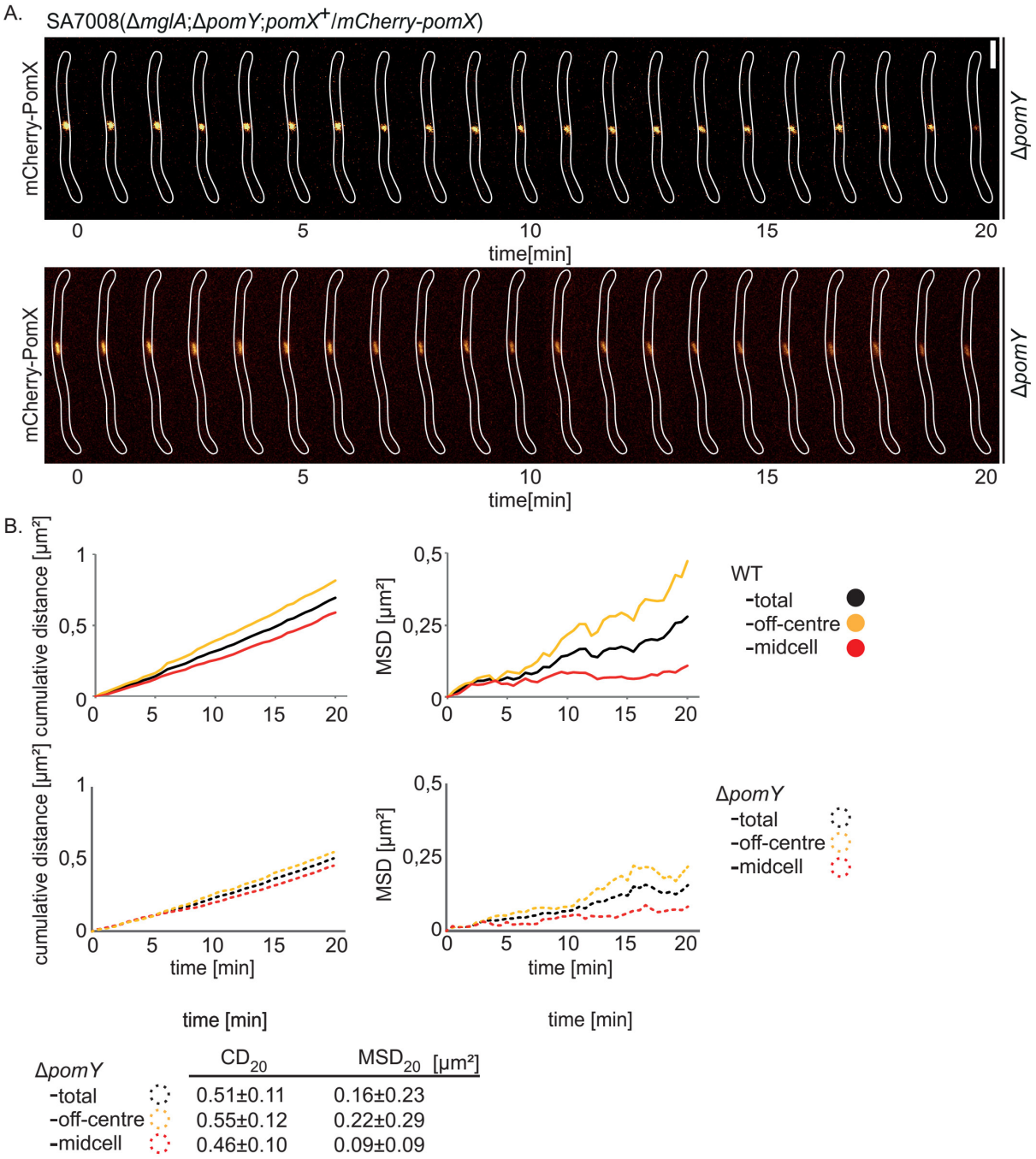

ΔpomY	CD_{20}	MSD_{20} [µm²]
-total	0.51±0.11	0.16±0.23
-off-centre	0.55±0.12	0.22±0.29
-midcell	0.46±0.10	0.09±0.09

Figure 51: Lack of PomY reduces cluster motion of PomX but not its directionality towards midcell.
(A) Time-lapse microscopy of mCherry-PomX clusters in non-motile cells lacking PomY. Time-lapse recordings of SA7008 were performed on exponentially grown cells. Pictures were acquired on 1 % TPM agarose, supplemented with 0.25 % CTT at 32 °C. Cells were imaged every 30 sec for 20 min. Every 2nd picture is shown. Cellular outline was obtained from DIC pictures. Movies were aligned using the auto align plugin of Metamorph. Scale bar: 2 µm. **(B)** Quantification of mCherry-PomX cluster motion in absence of PomY compared to the motion in its presence, measured by cumulative distance and mean squared displacement. CD_{20} and MSD_{20} were calculated from trajectories of single mCherry-PomX clusters as described in 8.6.6 (n=44).

5.3.9 PomZ is dynamic in the PomXYZ cluster and over the nucleoid

Our data provides strong evidence that a complex of PomXYZ localizes to the mid-nucleoid, which coincides with midcell, by a biased-random motion of the PomXYZ cluster along the nucleoid.

Moreover, this cluster translocation depends on ATP-hydrolysis by PomZ. Because PomZ on its own showed basically no ATPase activity *in vitro,* we predicted that ATP-hydrolysis only takes place in the PomXYZ complex on the nucleoid *in vivo*. If this prediction is correct, then PomZ-mCherry should show high exchange when interacting with the PomXY complex in the cluster. To test this prediction, **f**luorescence **r**ecovery **a**fter **p**hotoblaching (FRAP) experiments were performed with $PomZ^{WT}$-mCherry expressed at native levels. In these experiments labelled PomZ-mCherry in the cluster was photobleached with a laser and recovery of the signal was followed over time. Because PomZ-mCherry signals are weak, pictures were acquired every second with an acquisition time of 1 s. As predicted, after a short laser pulse of around 60 msec the PomZ cluster was bleached. 9 s after photobleaching, the PomZ-mCherry cluster fluorescence was completely restored. However, total cellular fluorescence was less than before (Figure 52 A). In particular, the patchy signal decreased simultaneously to the recovery of the cluster signal, indicating that the signal in the cluster recovered from the patchy PomZ signal. PomZ-mCherry clusters in total showed a half maximal recovery ($t_{1/2}$) of 1.2 ± 0.2 s (n=20) (Figure 52 A).

We observed that during the laser pulse some PomZ-mCherry signal away from the cluster was bleached too, suggesting that PomZ is not only dynamic in the PomXYZ complex but also away from the cluster. To analyse this, PomZ-mCherry signal was bleached over the nucleoid and signal recovery was followed over time. After the short laser pulse essentially the entire signal on the bleached side of the nucleoid was lost, whereas cluster intensity and the signal on the other nucleoid side showed little fluorescence loss. To quantify signal recovery of PomZ-mCherry, cells were divided into three parts. Fluorescence was measured on the bleached side and on the un-bleached side of the nucleoid as well as in the cluster. Similarly to the signal recovery in the PomZ-mCherry clusters described before, fluorescence was recovered fast and the pre-bleach situation was established with a half maximal recovery of 1.7 ± 0.4 s (n=18) (Figure 52 B). Concurrent with recovery of signal on the bleached side of the nucleoid a loss of signal was observed in the cluster and on the un-bleached side of the nucleoid (Figure 52 B), suggesting exchange of bleached PomZ molecules with unbleached molecules bound to the PomXYZ cluster and on the unbleached side of the nucleoid occurs.

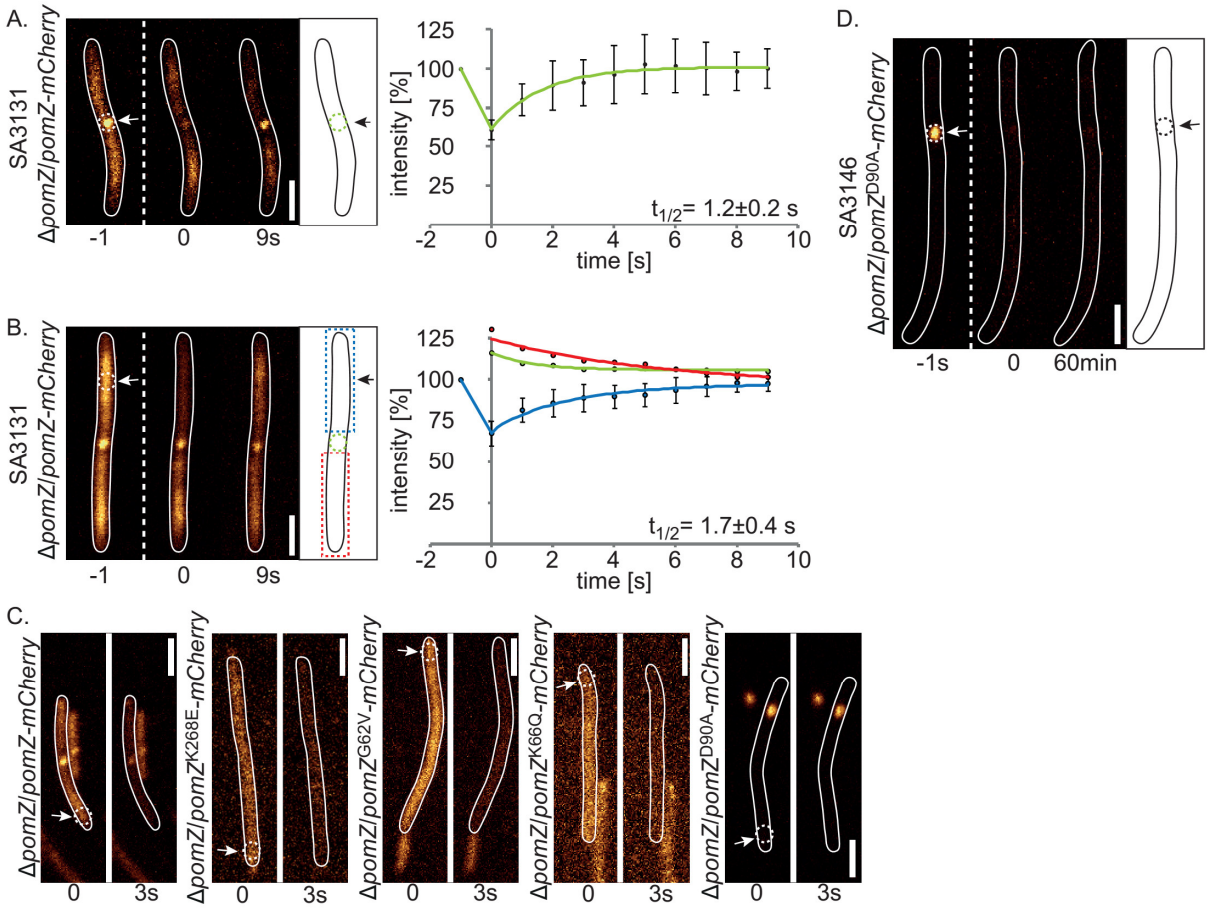

Figure 52: PomZ displays high turnover in the cluster and on the nucleoid.
(A) Measurement of *in vivo* recovery kinetics of PomZ-mCherry in the cluster by FRAP. FRAP experiments were performed as described in 8.6.4. Cells were exponentially grown and imaged on TPM-buffered 1 % agarose pads, supplemented with 0.25 % CTT. Cellular outline was obtained from DIC pictures. White arrow indicates the bleached region. Recovery was measured in the circular stippled region. White stippled line indicates bleaching event of around 60 msec. Recovery was followed in 1 s intervals with an acquisition time of 1 s. Mean intensity recovery was calculated from 20 independent bleaching events ± SD. Half maximal recovery was obtained from fitting the data to a single exponential equation with Origin6.2. Scale bar: 2 µm. **(B)** Measurement of *in vivo* recovery kinetics of PomZ-mCherry patchy pattern by FRAP. FRAP was performed as in (A). Cell was divided into three parts, bleached nucleoid side (blue), unbleached nucleoid side (red) and cluster (green) and signal intensity was measured as shown in the schematic. Mean intensity recovery was obtained from 18 independent bleaching experiments **(C)** Bleaching experiments with PomZ-mCherry and the four PomZ-mCherry variants. Cells were imaged before and after a 3 s bleaching event with the same laser intensity (8.6.4) as in (A) and (B) on the indicated area (white stippled circle). Cell outline was obtained from DIC picture. **(D)** FRAP experiments on PomZ^{D90A}-mCherry. PomZ^{D90A}-mCherry cluster was bleached as described in (A). White stippled line indicated a bleaching event of around 60 msec. Cell outline was obtained from DIC picture. Scale bar: 2 µm.

We wanted to examine if and how ATP-hydrolysis is required for the fast recovery of PomZ signals. To this end, a chromosomal area away from the PomZ cluster was photobleached for 3 seconds with the same laser intensity as before. We observed that the PomZ-mCherry signal in the cluster as well as the patchy signal were strongly decreased during this time, strengthening the idea that PomZ is highly dynamic on the nucleoid and in the cluster and that exchange between these two populations occurs within the 3 seconds of bleaching (Figure 52 C). Moreover, signal intensity of the PomZ^{D90A}-mCherry cluster was unaffected by the photobleaching approach, suggesting that PomZ^{D90A} is arrested in complex with PomX and PomY in the cluster and that release from the clusters depends on ATP-hydrolysis (Figure 52 C). In addition, the PomZ^{D90A}-mCherry cluster was bleached and

consistently, it did not recover, even after 60 min. This leads to the conclusion that most PomZ^{D90A}-mCherry molecules are stalled in the PomXYZ cluster and recovery of that cluster would rely on protein synthesis (Figure 52 D). As expected, the signal of PomZ^{K66Q}-, PomZ^{G62V}- and PomZ^{K268E}-mCherry was almost lost after 3 s of bleaching, indicating that nearly all molecules had passed the bleached area within 3 seconds (Figure 52 C).

In total these data show that PomZ exists in a dynamic interplay between a monomeric, diffuse phase and a dimeric phase. Importantly, in this dimeric phase PomZ shows fast dynamic localization on the nucleoid and exchanges molecules with the PomXYZ cluster. However, the exchange depends on ATP-hydrolysis. We hypothesize that PomZ in its dimeric state moves randomly over the nucleoid until it attaches to the cluster, where ATP-hydrolysis takes place. This ultimately leads to dissociation of PomZ from the nucleoid and the PomXY complex. The nucleoid bound, dimeric PomZ in turn refills from the cytosolic, monomeric PomZ after ATP-binding and dimerization.

5.3.10 PomZ moves over the nucleoid by ATP-hydrolysis-independent lateral diffusion

To obtain further insights into the mechanism of PomZ dynamics on the nucleoid, FRAP experiments were performed with strains expressing PomZ-mCherrry and the four PomZ-mCherry variants at high levels. For the analysis we made use of the fact that PomZ^{WT}-mCherry under high expression conditions colocalizes with the complete nucleoid (5.3.3). A small region over the nucleoid area was photobleached and signal recovery was followed at high resolution, with image acquisition every 250 msec. Within 30 s the PomZ-mCherry signal was completely recovered, restoring a pre-bleach situation. PomZ-mCherry showed a half maximal recovery of 5.3 ± 0.3 s (Figure 53 A). This recovery rate was slower than observed at native levels, indicating a physical block of PomZ molecules on the nucleoid, resulting in slower recovery rates. In a second experiment a similar region was photobleached in a strain expressing PomZ^{D90A}-mCherry at high levels. Strikingly, PomZ^{D90A}-mCherry showed only a slightly slower recovery rate with $t_{1/2}$ of 8.3 ± 0.4 s (Figure 53 B). As expected PomZ^{K66Q}-, PomZ^{G62V}- and PomZ^{K268E}-mCherry displayed a faster recovery than the WT protein although recovery rates were quite slow for diffuse proteins (n>12). Of note, in case of PomZ^{K66Q}-, PomZ^{G62V}- and PomZ^{K268E}-mCherry we were not able to bleach a defined spot, but instead created a gradient after the bleaching event. We therefore speculate that the actual recovery rate is way faster than measured, due to these technical problems (Figure 53 C, D, E).

The provided data strongly implies that the major part of the recovery is ATP-hydrolysis independent and comes from lateral diffusion of PomZ dimers on the nucleoid. However, PomZ-mCherry recovers faster than PomZ^{D90A}-mCherry on the DNA, indicating that ATP-hydrolysis and subsequent rebinding of freshly generated PomZ dimers also takes part in the dynamic behaviour of PomZ on the nucleoid. We conclude that PomZ dimers on the nucleoid undergo a diffusive random flux, which contributes to the signal recovery on the nucleoid and in the cluster.

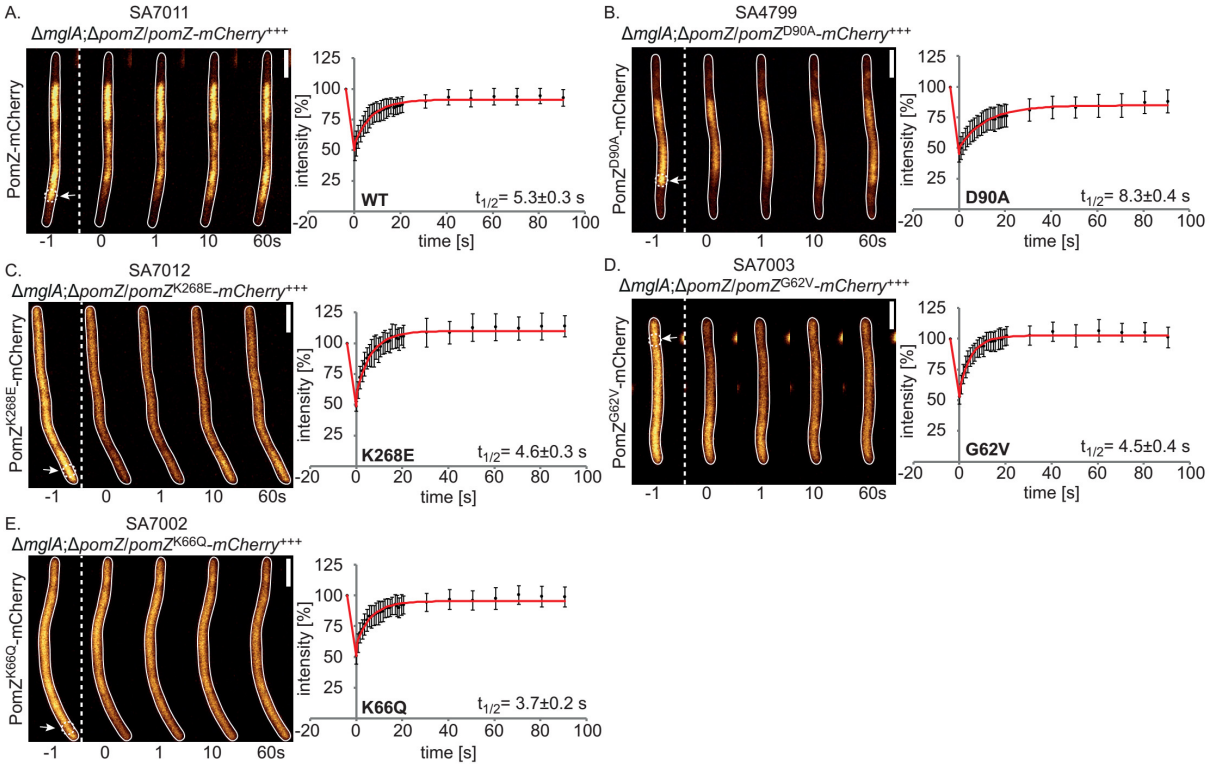

Figure 53: FRAP experiments with PomZ and its variants under overexpression conditions.
(A) Measurement of *in vivo* recovery kinetics of PomZ-mCherry under overexpression conditions in strain SA7011 (Δ*mglA*; Δ*pomZ*/*pomZ-mCherry*+++) by FRAP. FRAP experiments were performed as described in 8.6.4. Cells were exponentially grown and imaged in TPM-buffered 1 % agarose pads, supplemented with 0.25 % CTT. Cellular outline was obtained from DIC pictures. White arrow indicates the bleached region. Recovery was measured in the circular stippled region. White stippled line indicates bleaching event of around 160 msec. Recovery was followed over 90 s with an acquisition time of 300 msec. Mean intensity recovery was calculated from independent bleaching events ± SD (n=18). Half maximal recovery was obtained from fitting the data to a single exponential equation with Origin6.2. Scale bar: 2 µm. **(B)**, **(C)**, **(D)**, **(E)** Measurement of *in vivo* recovery kinetics of PomZ-mCherry variants under overexpression conditions in strain SA4799 (n=14), SA7012 (n=10), SA7003 (n=12) and SA7002 (n=12). FRAP experiments were performed as described in (A).

5.3.11 Perturbation of chromosome structure interferes with PomXYZ cluster motion

Because the PomXYZ cluster moves over the nucleoid towards midcell, with PomZ associating the cluster to the nucleoid, we hypothesized that interference with nucleoid structure or geometry would affect its translocation towards the mid-nucleoid.

To address this idea we added Hydroxyurea, a compound that interferes with the ribonucleotide reductase and therefore affects chromosome replication (Krakoff *et al.*, 1968), to the cells. Based on growth experiments we determined a minimal inhibitory concentration of 50 mM, which was used in the assays (Figure 54 A). To check if treatment of HU alters the recruitment of the PomXYZ cluster to the nucleoid, strain SA4712 (Δ*pomY*/*pomY-mCherry*+++) was treated with HU for 16 h prior to DAPI stain and subsequent microscopy. We first noticed that cluster formation by PomY-mCherry was unaffected, since all cells showed a PomY cluster either in the off-centre position or at midcell. The DAPI-stained nucleoids were generally more condensed along the long cell axis and sometimes misplaced. In general, these nucleoids were more shifted towards one cell pole, increasing the nucleoid-free sub-polar region on the other side (Figure 54 B). Nevertheless, in all observed cases

PomY-mCherry clusters colocalized with the DAPI-stained nucleoid, confirming that the PomZ-dependent recruitment to the DNA is unaffected in presence of 50 mM HU (Figure 54 B).

Before treatment with HU 21 % of cells displayed a diffuse localization of PomY-mCherry, while 79 % of cells presented a PomY-mCherry cluster. Of these clusters, 56 % were found a midcell and 23 % in the off-centre position. During the time course experiment cells slightly elongated, suggesting that cells had a defect in cell division in presence of HU. After 16 h essentially all cells displayed a PomY-mCherry cluster, 60 % of which were found at midcell, while 40 % were observed in the off-centre position. This suggests that clusters overall can translocate to midcell in presence of HU.

Next, we analyzed the PomY cluster localization in comparison to the nucleoid length. As mentioned before nucleoids condensed during the treatment from 4.8 ± 1.3 µm to 4.2 ± 1.1 µm. Mainly the fraction of cells with off-centre clusters increased, most likely these cluster were produced in cells with a diffuse PomY-mCherry signal over time, whereas mid-nucleoid clusters only slightly increased (Figure 54 C). Based on these findings we conclude that clusters are recruited to the nucleoid and are translocated to the mid-nucleoid.

To analyze cluster motion PomY-mCherry clusters dynamics were analyzed in time-lapse recordings at 30 s intervals in strain SA4746 (Δ*mglA*; *pomY*$^{+}$/*pomY-mCherry*+++), treated with 50 mM HU for 16 h before image acquisition (Figure 54 C). In these movies PomY-mCherry clusters displayed a dynamic localization, both in the off-centre and at midcell (Figure 54 E), giving rise to a CD_{20} of 0.37 ± 0.10 µm² and 0.32 ± 0.05 µm² after 20 min, respectively (Figure 54 F). This showed that both types of clusters moved similar distances in the same time period, but their motion was significantly reduced by treatment with HU in comparison to untreated cells (5.2.10). While midcell clusters generally moved around the midcell area, off-centre clusters showed a biased motion towards midcell, suggesting that overall, the positioning mechanism worked in the HU treated cells, but off-centre clusters showed a decreased MSD_{20} (0.26 ± 0.30 µm²) in presence of HU then compared to untreated cells.

In total these data show that the underlying mechanism for cluster translocation to midcell does not only depend on PomZ and its associated ability to hydrolyse ATP and to interact with the nucleoid, but also depends on the nucleoid structure.

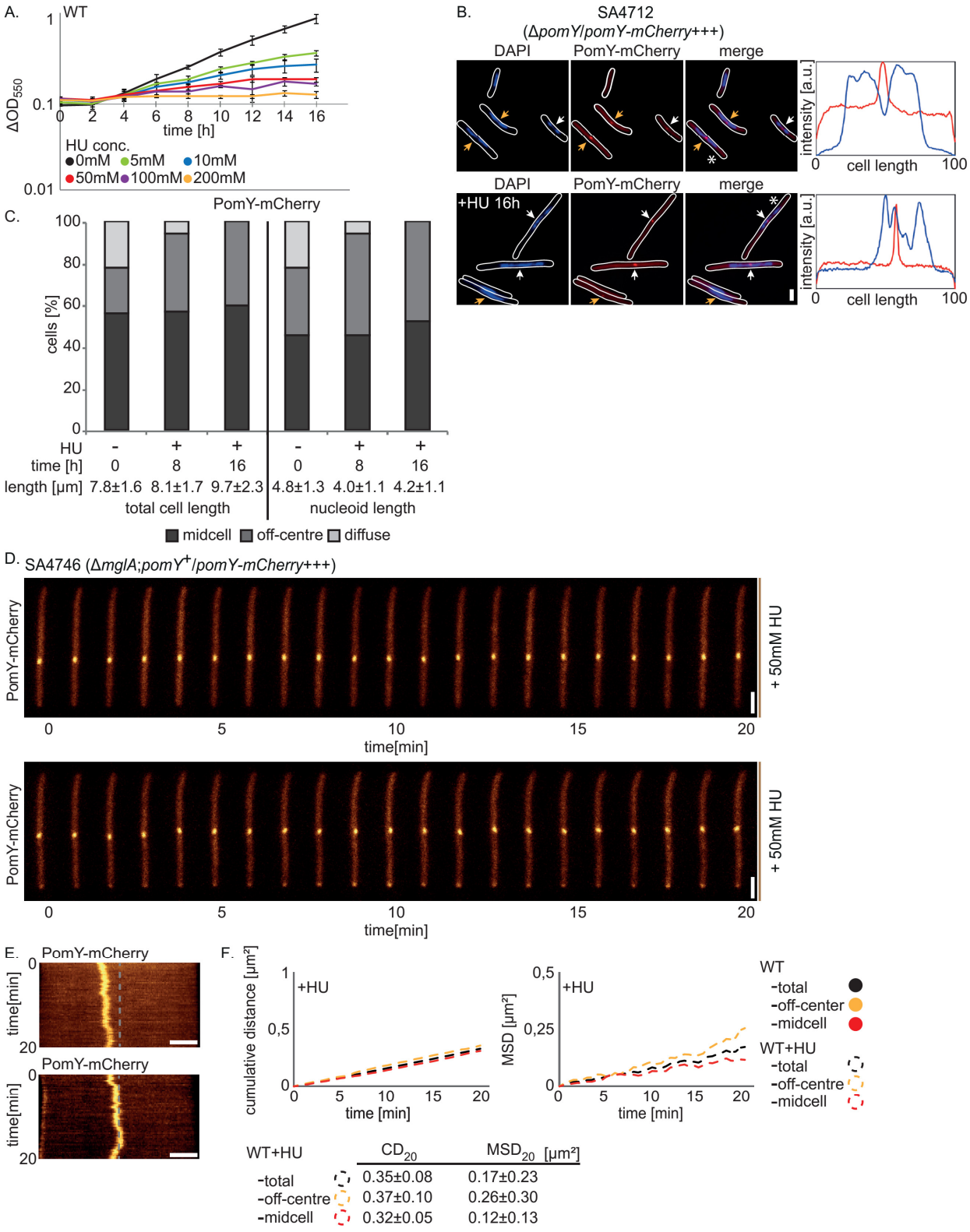

Figure 54: Nucleoid geometry is important for the positioning mechanism of PomXYZ clusters.
(A) Effect of hydroxyurea on growth of *M. xanthus* cells. Exponentially grown cells were diluted into fresh CTT containing different concentrations of HU to an OD_{550} of 0.1. Growth was followed at 32°C for 16 h in 2 h intervals. Growth experiments were performed in triplicates. **(B)** Fluorescence microscopy of PomY-mCherry in strain SA4712 (Δ*pomY*/*pomY-mCherry*+++) after growth in presence and absence of 50 mM HU for 16 h. Cells were treated with DAPI prior to micrscopy on 1 % agarose pads, buffered with TPM at 32 °C. Cellular outline was obtained from DIC pictures. Merged images were created with Metamorph. Linescans were produced with Metamorph on fluorescence signal of DAPI (blue) and PomY-mCherry (red) along long cell axis. **(C)** Quantification of PomY-mCherry localization before and after HU treatment for 8 h and 16 h. Localization was quantified in correlation to total cell length (left) and to nucleoid length (right). **(D)** Time-lapse microscopy of

PomY-mCherry in strain SA4746 (Δ*mglA*; *pomY*$^{+}$/*pomY-mCherry*+++). Images were acquired from cells that were exponential grown in presence of 50 mM HU for 16 h on a 1 % agarose pad, buffered with TPM and supplemented with 0.25 % CTT at 32 °C. Movies were aligned with Metamorph. Scale bar: 2 µm. **(E)** Representative kymographs of PomY-mCherry clusters in movies of (D). Scale bar: 2 µm. **(F)** Quantification of PomY-mCherry cluster motion in presence of 50 mM HU as measured by CD_{20} and MSD_{20}.

5.3.12 PomY aligns PomX clusters with cell division constrictions

To begin to understand how PomXYZ stimulate Z-ring formation and its correct localization at midcell, we performed time-lapse microscopy on cells expressing *mCherry-pomX* in non-motile Δ*pomY* and Δ*pomZ* mutants (SA7008 and SA7009, respectively). Cell growth was followed every 15 min for several hours on TPM agarose, containing 0.25 % CTT at 32 C, allowing cells to grow and divide normally. Consistent with the observations made earlier, in absence of PomY, mCherry-PomX clusters predominantly localized at midcell, while in the absence of PomZ they were found mostly in the off-centre position (data not shown). In cells lacking PomZ cell division constrictions colocalized with the mCherry-PomX cluster and during cell division the mCherry-PomX cluster was asymmetrically split and translocated into the two daughter cells, as similarly observed in presence of PomZ (Figure 55) (see also 5.2.9). In 93 % of cells (n=26) cell divisions occurred on the PomX cluster, while in 7% of cells cell divisions did not colocalize with the cluster but occurred in close proximity. In the daughter cells the mCherry-PomX cluster did not translocate to midcell but localized close to the cell pole during the experiment.

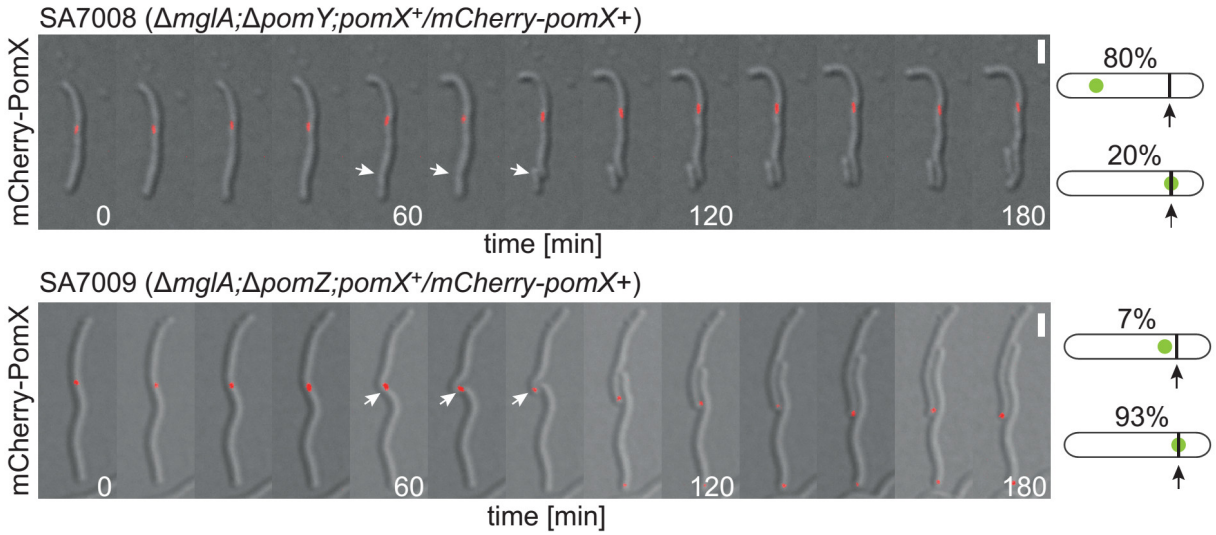

Figure 55: PomX clusters are aligned with cell division constrictions by PomY but not PomZ.
Time-lapse microscopy of mCherry-PomX in strains SA7008 (Δ*mglA*; Δ*pomY*; *pomX*$^{+}$/*mCherry-pomX*+) and SA7009 (Δ*mglA*; Δ*pomZ*; *pomX*$^{+}$/*mCherry-pomX*+). Cells were imaged on 1 % agarose pads, buffered with TPM and supplemented with 0.25 % CTT at 32 °C. Images were acquired every 15 min. Shown are merged pictures of mCherry-PomX fluorescence and DIC. White arrows indicate cell division events. Numbers in schematics were obtained from individual cell division events (n=26, SA7009; n=25, SA7008). Green spots indicates PomX clusters, black line and arrow indicate the cell division event. Scale bar 2 µm.

Unexpectedly, cell divisions rarely colocalized with the PomX cluster in absence of PomY (20 % of cells) (n=26) (Figure 55). This was surprising and led to the conclusion that first, PomX and PomZ alone are not able to recruit FtsZ towards midcell in absence of PomY and secondly that PomZ is not

required for recruitment of FtsZ to the PomXY cluster. Finally, these data strongly suggest that PomY by a yet unknown mechanism aligns cell division with PomXYZ clusters, indicating that PomY interacts with FtsZ *in vivo*.

5.4 PomX serves as an ATPase activating partner for PomZ

ParA-like ATPases often work together with an ATPase activating protein (AAP). In case of ParA's that are involved in chromosome segregation this function is fullfiled by ParB, and similarly in case of Soj by the ParB-homolog Spo0J. In more distantly related P-loop ATPases like MinD or PpfA ATP-hydrolysis is stimulated by proteins, completely unrelated to ParB and Spo0J. In case of MinD, ATPase activity is stimulated by the coiled-coil protein MinE and in case of PpfA, ATP-hydrolysis is suggested to be stimulated by TlpT, a soluble chemoreceptor (Hu & Lutkenhaus, 2001, Leonard *et al.*, 2005, Lim *et al.*, 2014, Roberts *et al.*, 2012).

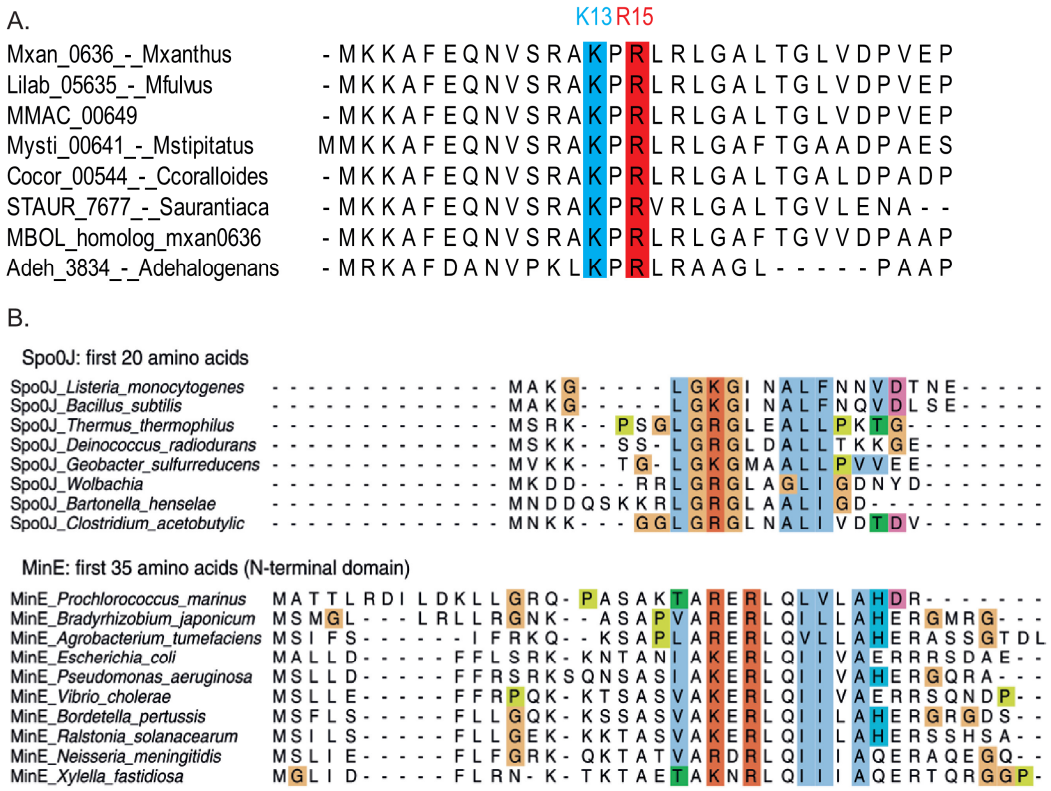

Figure 56: Alignment of the N-termini of the AAP's PomX, Spo0J and MinE.
(A) Partial sequence alignment of PomX and its homologs in other myxobacteria. Alignment was performed with the MAFFT algorithm on full length proteins sequences. Lysine 13 is shownlight blue and arginine 15 is indicated in red. (B) Partial alignments of the N-termini of Spo0J and MinE. Alignments were adapted from Leonard *et al*., 2005.

In the PomXYZ system PomX and PomY stimulate ATP-hydrolysis of PomZ in presence of DNA *in vitro*. This led to the idea that both of them are ATPase activating proteins for PomZ. Consistently, lack of PomY was shown to affect PomX cluster motion in the presence of PomZ *in vivo* most likely due to reduced ATP-hydrolysis by PomZ. In a previous study, a *pomX*$^{K13A;R15A}$ mutation was created based on an alignment of the N-terminal part of PomX in comparison with MinE and Spo0J (Figure 56)

(Huneke, 2013). These two substitutions resulted in a cell division defect, although PomX$^{K13A;R15A}$ accumulated at WT-like levels as observed by immunoblot analysis. Because the N-terminal region Spo0J is required for the stimulation of ATPase activity of its cognate ParA-like partner Soj (Leonard *et al.*, 2005) we hypothesized that the PomX^{K13A,R15A} variant affects ATP-hydrolysis by PomZ.

5.4.1 PomX$^{K13A;R15A}$ substitutions do not interfere with PomXYZ cluster formation but with stimulation of ATP-hydrolysis by PomZ

PomX is at the basis of cluster formation of the PomXYZ complex *in vivo*. To investigate the defect of the *pomX*$^{K13A;R15A}$ mutation, we first determined if the protein still interacts with PomY, PomZ and itself. For this purpose strains were created, expressing *pomY-mCherry* (SA6105; *pomX*::*pomX*$^{K13A;R15A}$; *pomY*$^{+}$/*pomY-mCherry*+++) or *pomZ-mCherry* (SA6106; *pomX*::*pomX*$^{K13A;R15A}$; *pomZ*$^{+}$/*pomZ-mCherry*) in presence of PomX$^{K13A;R15A}$ as the only source of PomX. PomY-mCherry localized in three different patterns. In 14 % of cells PomY-mCherry was diffuse throughout the cell. Nearly 80 % of cells presented a PomY-mCherry cluster at midcell while around 20 % displayed it in the off-centre position (Figure 57 A). This suggests that first, PomY can still associate with PomX$^{K13A;R15A}$ in the cluster and secondly, clusters find midcell as efficient as in the presence of PomX^{WT}.

By contrast, PomZ-mCherry showed reduced cluster formation, with only 27 % of cells showing a cluster. One third of these localized at midcell. PomZ-mCherry predominantly displayed a patchy localization (Figure 57 B), suggesting that ATP-binding, dimerization and DNA-binding by PomZ were not affected *in vivo*. Based on these findings we conclude that PomX$^{K13A;R15A}$ -PomYcluster formation is normal, but interaction between PomZ and PomX$^{K13A;R15A}$ is affected.

To test if the interaction between PomX$^{K13A;R15A}$, PomY and PomZ is impaired, a BACTH assay was performed with PomX^{WT} and PomX$^{K13A;R15A}$ to test for interaction with PomY and PomZ. Additionally, we also tested for interaction with PomZ^{D90A} and for self-interaction of PomX^{WT} and PomX$^{K13A;R15A}$. In this assay PomX^{WT} as well as PomX$^{K13A;R15A}$ interacted with PomY, reflecting the *in vivo* data. We observed an interaction between PomX^{WT} and PomZ but not between PomX$^{K13A;R15A}$ and PomZ, indicating that the PomX-PomZ interaction is affected by the two substitutions. Because PomZ^{D90A} strongly interacts with PomX in a BACTH assay and because its cluster formation depends on PomX *in vivo,* we tested PomX$^{K13A;R15A}$ for interaction to PomZ^{D90A} and observed that the two proteins interact (Figure 57 C). This suggested that the PomX$^{K13A;R15A}$-PomY interaction is unaffected but the N-terminal substitutions reduced the affinity to PomZ. However, if PomZ is kept in the dimeric ATP-bound form by the D90A substitution the two proteins interact.

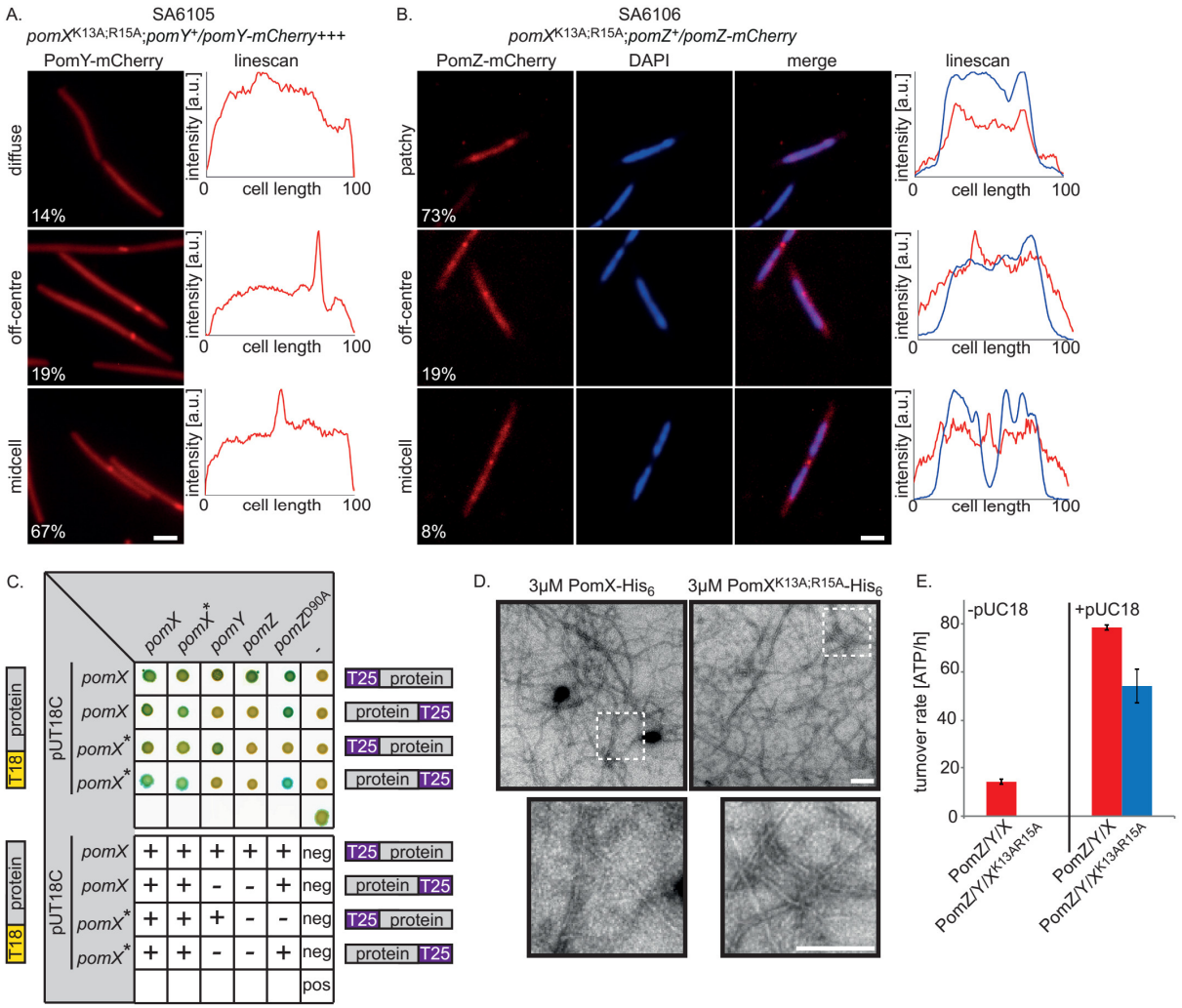

Figure 57: PomX$^{K13A;R15A}$ substitution affects PomX-PomZ interaction and ATP-hydrolysis by PomZ.
(A) Subcellular localization of PomY-mCherry in strain SA6105 (*pomX*::*pomX*$^{K13A;R15A}$; *pomY*$^{+}$/*pomY-mCherry*+++) expressing *pomX*$^{K13A;R15A}$. Exponentially grown cells were imaged on 1 % agarose, buffered with TPM. Numbers indicate localization patterns observed, in % of cells. Linescans were produced with Metamorph on fluorescence signal of PomY-mCherry along long cell axis. Scale bar: 2 µm. **(B)** Subcellular localization of PomZ-mCherry in strain SA6106 (*pomX*::*pomX*$^{K13A;R15A}$; *pomZ*$^{+}$/*pomZ-mCherry*) expressing *pomX*$^{K13A;R15A}$. Cells were imaged as in (A) but treated with DAPI prior to picture acquisition. Merged pictures were created with Metamorph. Linescans were made with Metamorph on fluorescence signal of PomZ-mCherry (red) and DAPI signal (blue) along long cell axis. Scale bar: 2 µm. **(C)** BACTH assay to test for interactions of PomX$^{K13A;R15A}$ in comparison to native PomX. BACTH assay was performed as described in 8.3.5. „+“ indicates interaction of two interaction partners as observed by the blue colony color on indicator agar plates, „-“ indicates no interaction. „pos“ marks the positive control and „neg“ indicates the negative controls. Picture shows one representative assay and all colonies were grown on the same plate at 30 °C. **(D)** Negative stain transmission electron microscopy of PomX-His$_6$ and PomX$^{K13A;R15A}$-His$_6$. Proteins were visualized with 1% uranyl acetate. Scale bar: 100 nm. **(E)** Specific ATPase activity of 2 µM His$_6$-PomZ in presence of PomY and PomX$^{K13A;R15A}$ was determined by a colorimetric malachite green assay in presence of 1 mM ATP. Proteins were mixed in equimolar ratio. If DNA was added to the reaction it was added at a final concentration of 5 nM. Bars represent the mean ± SD of 3 assays.

Because PomX$^{K13A;R15A}$ showed the ability to self-interact in a BACTH screen, we tested if the substituted PomX was still able to form filaments *in vitro* as PomX does. Therefore 3 µM PomX$^{K13A;R15A}$-His$_6$, which was purified as PomX-His$_6$ was purified by Andrea Harms, was used for negative stain transmission electron microscopy. PomX$^{K13A;R15A}$-His$_6$ formed filaments reminiscent of the filaments observed by PomX-His$_6$ (Figure 57 D). If PomX$^{K13A;R15A}$ structures are still bundled by PomY *in vitro* needs to be tested. In conclusion these data showed that the two substitutions in the N-

terminal part of PomX do not interfere with the interaction to PomY, nor with the ability of PomX to self-assemble into filamentous structures *in vitro*.

However, the data indicate that the interaction of PomX$^{K13A;R15A}$ with PomZ is affected *in vivo*, leading to the hypothesis that PomX-dependent ATP-hydrolysis by PomZ is diminished by the substitutions. To test this hypothesis an ATPase assay was performed with PomZ to determine the effect of PomX$^{K13A;R15A}$ on ATP-hydrolysis by PomZ *in vitro*. As reported PomZ-His$_6$ showed ATP-hydrolysis in presence of PomX and PomY and had a turnover rate of 14 ± 1 ATP*h^{-1}, which was elevated to 79 ± 2 ATP*h^{-1} in presence of pUC18 DNA. As expected, PomZ-His$_6$ showed no ATP-hydrolysis when PomX^{K13A,R15A}-His$_6$ was added to the reaction together with PomY, without addition of DNA. If DNA was added to the reaction, the turnover rate of PomZ-His$_6$ was reduced by 30 % to 54 ± 7 ATP*h^{-1}, compared to its turnover rate in presence of PomX^{WT} (Figure 57 E). In total these data demonstrate that PomX serves as ATPase activating protein for PomZ and stimulation of ATP-hydrolysis may occur via the N-terminal region of PomX.

5.4.2 PomX$^{K13A;R15A}$ substitutions slow down PomY cluster motion

We predicted that PomXYZ clusters in presence of PomX$^{K13A;R15A}$ are dynamic and overall translocate towards midcell by random biased motion, but their dynamic behavior should be reduced compared to clusters in presence of native PomX. To test our hypothesis time-lapse microscopy was performed with 30 s intervals on non-motile cells, expressing *pomY-mCherry* in presence of PomX$^{K13A;R15A}$ as the only source of PomX in strain SA7025 (Δ*mglA*; *pomX*::*pomX*$^{K13A;R15A}$; *pomY*$^{+}$/*pomY-mCherry*+++). Overall clusters were dynamic both in the off-centre and at midcell and showed motion along long and short cell axes (Figure 58 A). Importantly, off-centre clusters displayed a random biased motion towards midcell. Expectedly, PomY-mCherry clusters in presence of PomX$^{K13A;R15A}$ showed a CD$_{20}$ of 0.29 ± 0.06 µm² which was 60 % reduced compared to in the presence of native PomX (Δ*mglA*;*pomY*$^{+}$/*pomY-mCherry*+++: 0.70 ± 0.14 µm²) (Figure 58 C). Notably, cluster motion was neither abolished nor did it drop as observed in absence of PomZ. Similarly, PomY-mCherry clusters overall displayed a strongly constrained motion with an MDS$_{20}$ of 0.06 ± 0.06 µm² (Figure 58 C). We conclude that cluster motion is strongly affected by the two N-terminal substitutions in PomX. In addition to the data described above it demonstrates that ATP-hydrolysis by PomZ triggers clusters dynamics and interference with ATP-hydrolysis by substitutions in PomX slows down cluster motion and affects cell division. Moreover this provides evidence that PomX is an ATPase activating partner for PomZ and that ATP-hydrolysis by PomZ depends at least partially on the N-terminal region of PomX in addition to PomY and DNA.

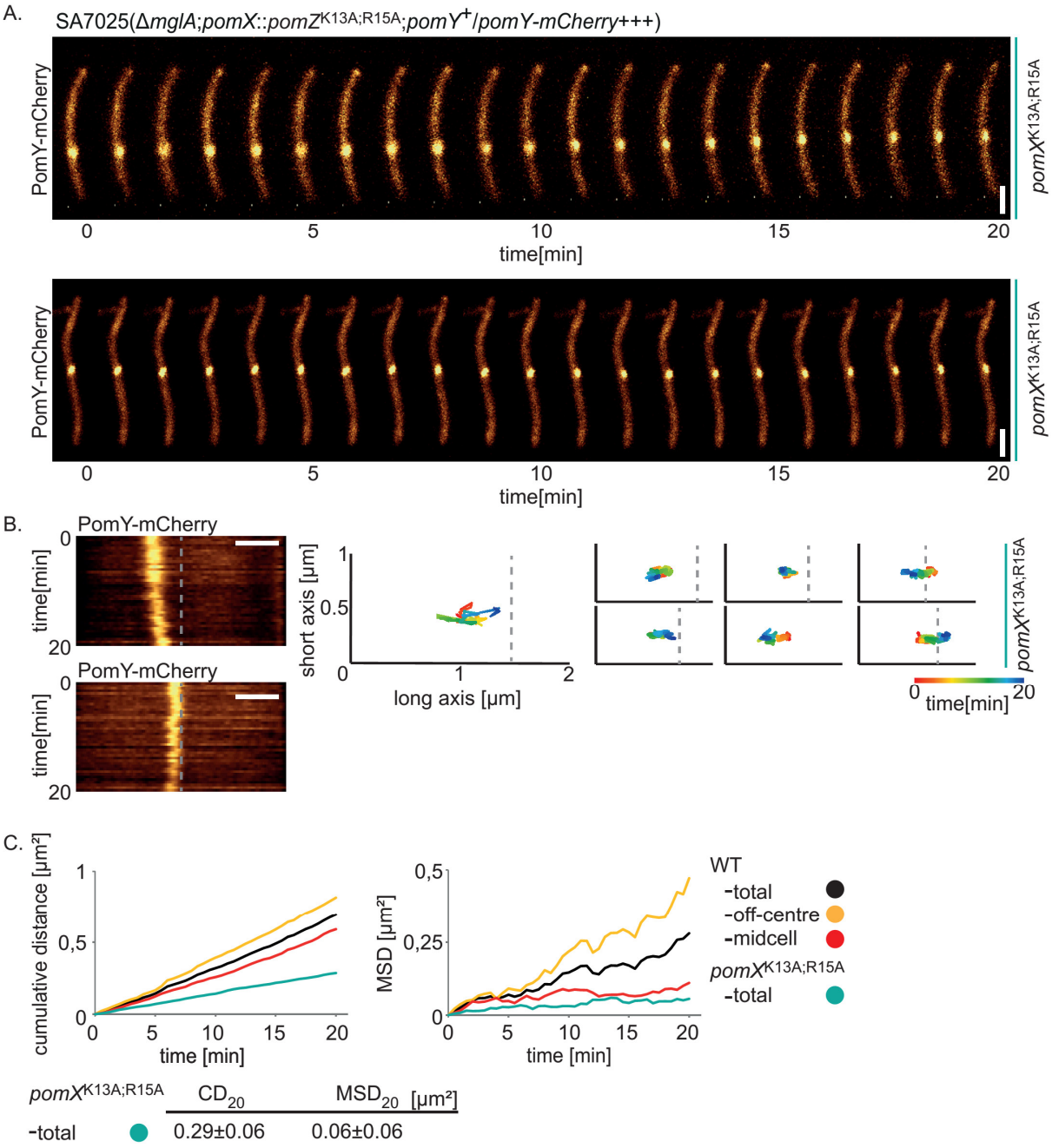

Figure 58: PomX$^{K13A;R15A}$ reduces PomXYZ cluster motion towards midcell *in vivo*.
(A) Time-lapse microscopy of PomY-mCherry in strain SA7025 (Δ*mglA*; *pomX*::*pomX*$^{K13A;R15A}$; *pomY*$^{+}$/*pomY-mCherry*+++) expressing *pomX*$^{K13A;R15A}$. Images were acquired from exponential grown cells on a 1 % agarose pad, buffered with TPM and supplemented with 0.25 % CTT at 32 °C. Movies were aligned with Metamorph. Scale bar: 2 µm. **(B)** Kymographs of PomY-mCherry clusters were generated with Metamorph from linescans of cells along the long cell axis with a thickness of 10 pixels. Grey stippled line indicates midcell. Scale bar 2 µm. Representative XY-tracks were generated from the position of the centroid of the PomY-mCherry cluster at every timepoint during the time-lapse movies, as measured by Metamorph with the particle tracking plugin (8.6.6). X-axis corresponds to 2 µm distance along the long cell axis, Y-axis corresponds to 1 µm along the short cell axis. Grey stippled line indicates midcell. **(C)** Quantification of PomY-mCherry cluster motion in presence of PomX$^{K13A;R15A}$ as measured by CD_{20} and MSD_{20}.

5.5 Supplementary results

5.5.1 Expression of mCherry-PomX and PomY-mCherry at higher levels

The phenotypes of a Δ*pomX* and a Δ*pomY* mutant could be rescued by expression of *mCherry-pomX* and *pomY-mCherry* from their putative native promoter from the *Mx8* attachment site. Under the control of these promoters mCherry-PomX and PomY-mCherry accumulated at native levels in strains SA4229 (Δ*pomX*/*mCherry-pomX*) and SA4713 (Δ*pomY*/*pomY-mCherry*) but their fluorescence signal was weak and therefore time-lapse microscopy could not be performed.

In order to enhance signal intensity of both fluorescent proteins *mCherry-pomX* and *pomY-mCherry* were expressed from stronger promoters. In case of *mCherry-pomX* the putative native promoter of *pomZ* was chosen and in case of *pomY-mCherry* the *pilA* promoter. Under the control of these promoters mCherry-PomX and PomY-mCherry accumulated at higher levels in strains SA4252 (Δ*pomX*/*mCherry-pomX*+) and SA4712 (Δ*pomY*/*pomY-mCherry*+++), respectively, but restored the WT phenotype (Figure 10 C; Figure 11 C). mCherry-PomX formed clusters at a higher frequency than when expressed from its native promoter, but generally localization patterns did not change. The majority of mCherry-PomX clusters were found at midcell (61 %), whereas off-centre clusters were observed in 1/3 of all cells. Similarly, PomY-mCherry localization did not change. PomY-mCherry clusters were formed in 71 % of cell, of which 2/3 localized at midcell and 1/3 in the off-centre position (Figure S 1 A, B). Importantly, mCherry-PomX and PomY-mCherry localization correlated to cell length as described earlier (Figure S 1 A, B). These data suggest that slight overexpression of mCherry-PomX as well as overexpression of PomY-mCherry in general has no effect on the localization of the fluorescently labelled proteins and furthermore on cell division. Therefore expression of both proteins at this level is a reasonable tool to investigate spatial localization of PomX and PomY by life cell imaging. Of importance, expression of mCherry-PomX under the control of the *pilA* promoter led to even higher accumulation of mCherry-PomX and resulted in strong degradation of the fluorescent fusion protein. Under these conditions mCherry-PomX formed long cell-spanning filaments and in cell division defects (Figure S 1 C). By addition cells did not divide over these filaments but produced constrictions in filament-free areas in the cell (Figure S 1 D). We conclude that accumulation of mCherry-PomX at too high levels interferes with cell division and cluster formation of the PomXYZ complex.

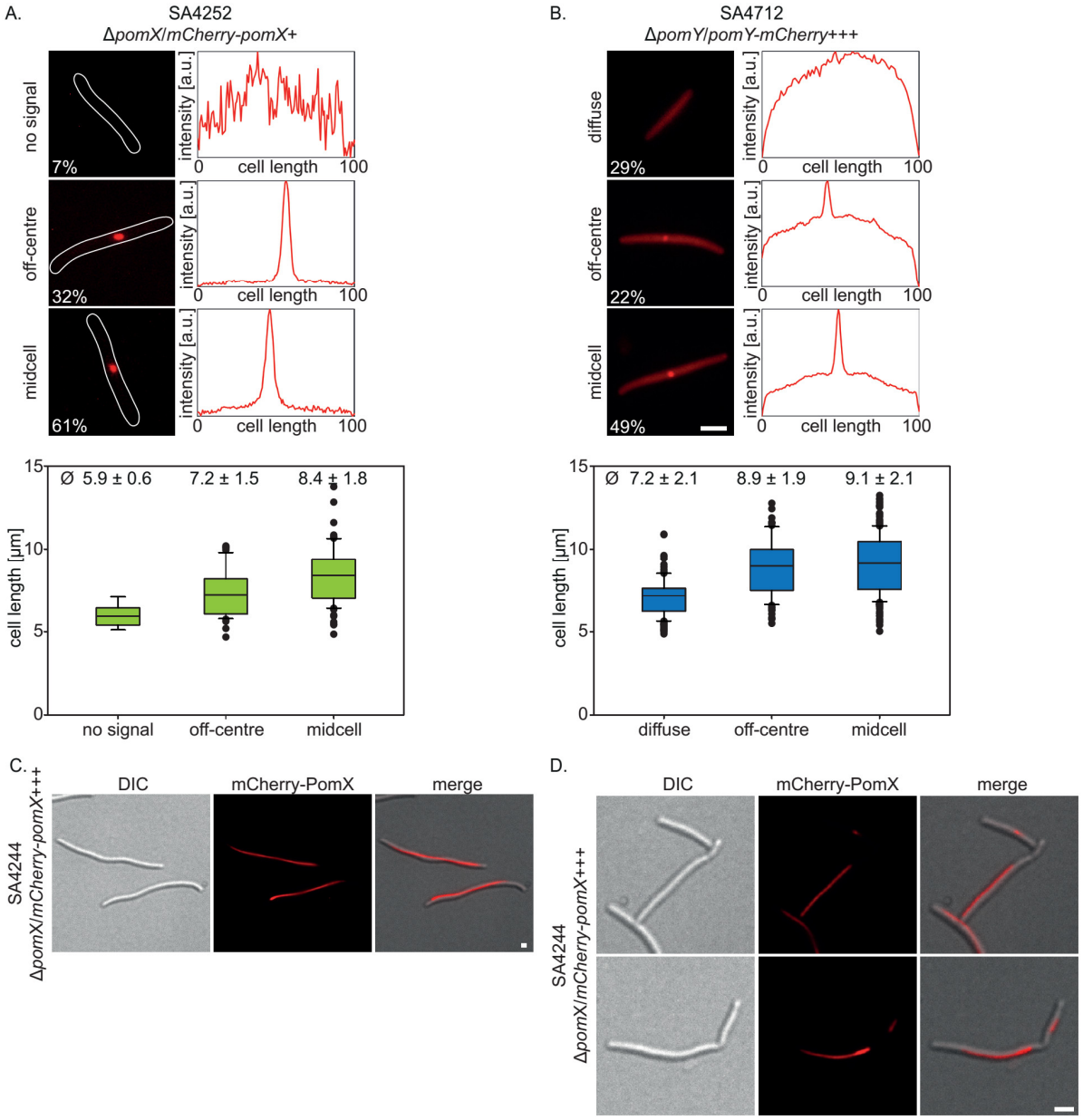

Figure S 1: Localization of mCherry-PomX and PomY-mCherry under high accumulation levels.
(A), **(B)** Localization of mCherry-PomX and PomY-mCherry in strain SA4252 (Δ*pomX*/*mCherry-pomX*+) and SA4712 (Δ*pomY*/*pomY-mCherry*+++), respectively. *mCherry-pomX* was expressed from the native *pomZ* promoter and *pomY-mCherry* form the *pilA* promoter. Both fluorescent proteins accumulated at higher levels then expressed from their native promoter (Figure 10; Figure 11). Numbers display frequency of observed localization patterns (n>200). Cells were imaged on 1 % agarose pads, buffered with TPM at 32 °C. Cellular outlines were obtained from DIC pictures. Linescans were made with Metamorph on fluorescence intensity of mCherry-PomX (A) and PomY-mCherry (B) signal along long cell axis. Box plots show localization patterns of both fluorescent proteins in correlation to cell length. Boxes enclose the 25th and 75th percentile, with the black line indicating the mean, that is also given in numbers above the boxes ± SD in µm. Whiskers enclose the 10th and 90th percentile and all outliers are shwon as black dots. Scale bar: 2 µm. **(C)** Localization of mCherry-PomX, expressed from the *pilA* promoter in strain SA4244 (Δ*pomX*/*mCherry-pomX*+++). Cells were imaged as in (A). Merge pictures were created with Metamorph. **(D)** Localization of mCherry-PomX filaments in strain SA4244 in cells with constrictions. Cells were imaged as in (A).

5.5.2 Cu^{2+} inducible expression of PomY-mCherry corrects the Δ*pomY* phenotype

For a variety of experiments *pomY-mCherry* had to be expressed under the control of a Cu^{2+} inducible promoter. All plasmids that express proteins under the control of a Cu^{2+} inducible promoter were integrated into the P_{cuoA} promoter in the native *cuoA* locus by homologous recombination. To investigate the accumulation level of PomY-mCherry when expressed from this promoter, in a first experiment expression of PomY-mCherry in strain SA4734 (Δ*pomY*/P_{cuoA}*pomY-mCherry*) was induced using different $CuSO_4$ concentration in the media. Cells were grown exponentially for 24 h in copper-free medium by dilution (approximately 5-6 doubling times) and diluted into medium, supplemented with $CuSO_4$ in the range from 0 µM – 300 µM and grown for additional 24 h at 32 °C. After induction cells were imaged on 1 % agarose pads, buffered with TPM and analyzed for their cell length phenotype. Without any copper PomY-mCherry signal was barely visible, suggesting that expression was not induced (Figure S 2 A). Cells displayed a Δ*pomY* phenotype with a mean cell length of 17.0 ± 9.0 µm and a constriction frequency of 2 % (Figure S 2 B). At around 100 µM Cu^{2+} PomY-mCherry clusters were visible and cells had a lenght of 9.3 ± 2.2 µm and produced 6 % constrictions. At 150 µM Cu^{2+} in the medium cells were on average even smaller, with 8.8 ± 1.6 µm and produced 10 % constrictions. Higher levels of copper had no effect on the signal intensity and on cell length phenotype (Figure S 2 A, B). Consistently, immunoblot analysis showed that PomY-mCherry did not accumulate when expressed in presence of less than 100 µM Cu^{2+} and reached its maximal accumulation at 150 µM. More copper had no effect on the accumulation of PomY-mCherry (Figure S 2 C). Based on these data we conclude that expression of *pomY-mCherry* from a Cu^{2+} inducible promoter corrected the Δ*pomY* phenotype at 100 - 150 µM Cu^{2+}. Because signals were slightly stronger when expressed in presence of 150 µM Cu^{2+}, this concentration was used in this study.

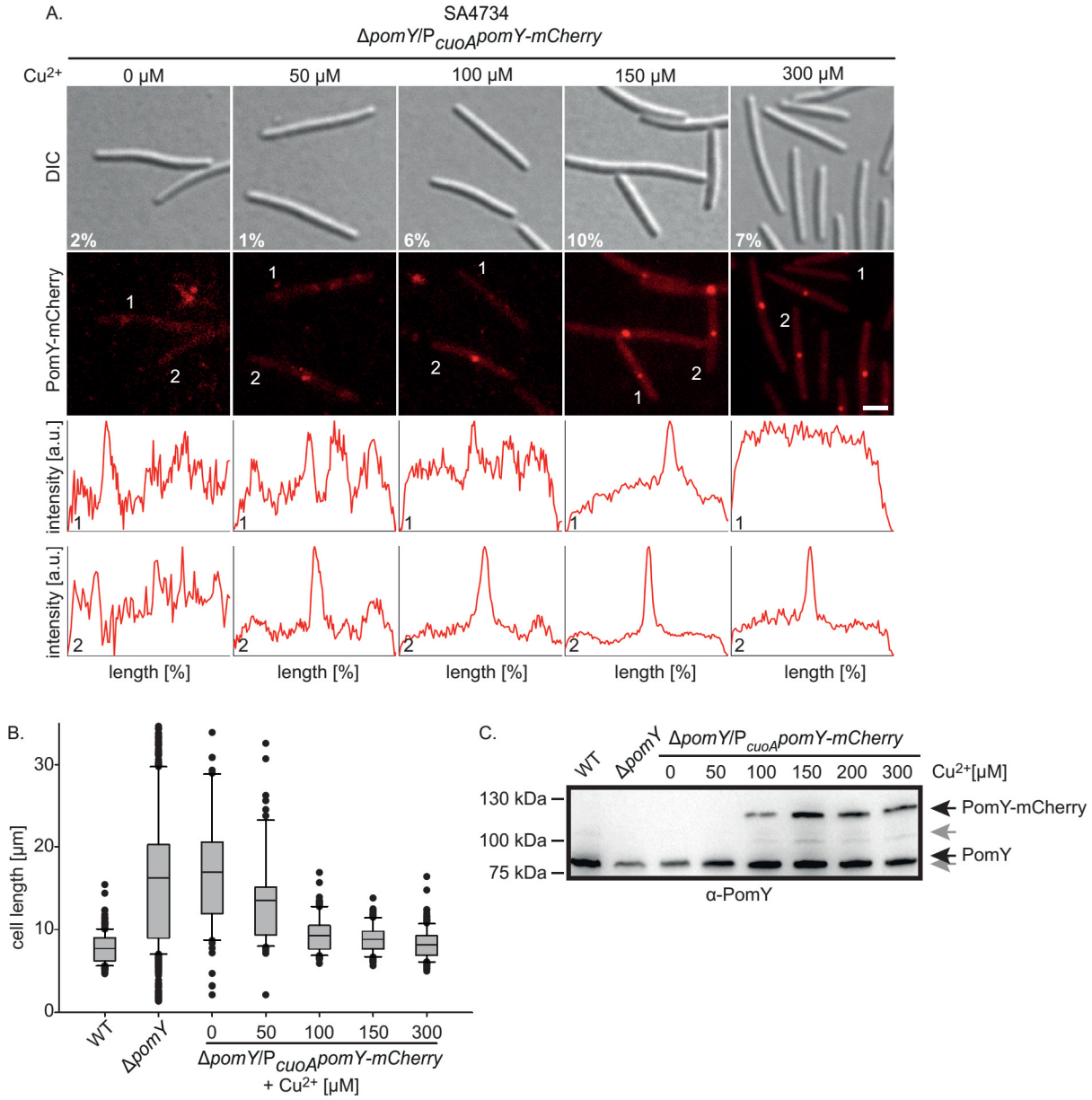

Figure S 2: Complementation of the Δ*pomY* phenotype by Cu^{2+}-dependent expression of *pomY-mCherry*. **(A)** Fluorescence microscopy of PomY-mCherry in SA4734 (Δ*pomY*/P$_{cuoA}$*pomY-mCherry*). Cells were exponentially grown in CTT medium supplemented with 0 - 300 µM $CuSO_4$ for 24 h. White numbers in the DIC pictures indicate constriction frequency under the tested conditions (n>100 cells per condition). Linescans were made with Metamorph on fluorescence intensity of PomY-mCherry signal along long cell axis. Numbers in the linescans correspond to the numbers in the fluorescence pictures, indicating selected cells. Scale bar: 2 µm. **(B)** Cell length distribution of strain SA4734 grown in presence of different concentrations of $CuSO_4$. Boxes enclose the 25th and 75th percentile, with the black line indicating the mean. Whiskers enclose the 10th and 90th percentile. Outliers smaller than 35 µm are depicted as black dots. Outliers bigger than 35 µm are not shown but are included for the calculation of the mean cell length. **(C)** Immunoblot analysis for the accumulation of PomY-mCherry when expressed under copper-dependent regulation in presence of different Cu^{2+} concentrations. Same amounts of total protein of each indicated strain were loaded per lane and PomY and PomY-mCherry were detected with specific α-PomY antibodies. Black arrows indicate PomY and PomY-mCherry, grey arrows indicate unspecific binding of the antibody.

5.5.3 Cu^{2+} inducible expression of *pomY-eyfp* corrects the Δ*pomY* phenotype

For the purpose of colocalization of PomY with PomX or PomZ in *M. xanthus* a differently labelled version of PomY was created. For most experiments *pomY-eyfp* was expressed under the control of a Cu^{2+}-regulated promoter P_{cuoA} from the native *cuoA* locus. Strain SA7024 (Δ*pomY*/P_{cuoA}*pomY-eyfp*) was exponentially grown in CTT media for 24 h and diluted into fresh CTT medium containing $CuSO_4$ in different concentrations, in a range from 0 – 300 µM $CuSO_4$. Induction was performed in an exponentially growth phase for 24 h at 32 °C. After that cells were applied to fluorescence microscopy and subsequently analyzed for their cell length phenotype. From this experiment accumulation level of PomY-eYFP was not determined.

If cells were grown in copper-free medium they showed a Δ*pomY* phenotype. Cells had an average cell length of 14.4 ± 8.2 µm and displayed constrictions with low frequency (<1%) (Figure S 1 B). Under these conditions cells displayed a weak diffuse fluorescence signal with tiny foci but these were way smaller than observed for PomY clusters under any other conditions (Figure S 3 A). We conclude that *pomY-eyfp* is expressed in small amounts even in absence of Cu^{2+}. With increasing concentrations of $CuSO_4$ in the media cells were on average smaller in length and produced more cell division constrictions. This effect was maximal at around 150 µM $CuSO_4$, which led to an average cell length of 7.2 ± 1.4 µm and a constriction frequency of 7 % which was similar to WT. Under these conditions PomY-eYFP displayed a diffuse localization throughout the cell with additional cluster formation in the off-centre position or at midcell (Figure S 3 A, B). Importantly, even higher concentration of Cu^{2+} in the medium had no additional effect on cell length and constriction frequency, but in contrast showed a similar cell length phenotype (7.1 ± 1.3 µm) and a similar constriction frequency (7 %) (Figure S 3 B). We conclude that expression of *pomY-eyfp* in presence of 150 µM $CuSO_4$ complements the Δ*pomY* phenotype and therefore was used in all assays.

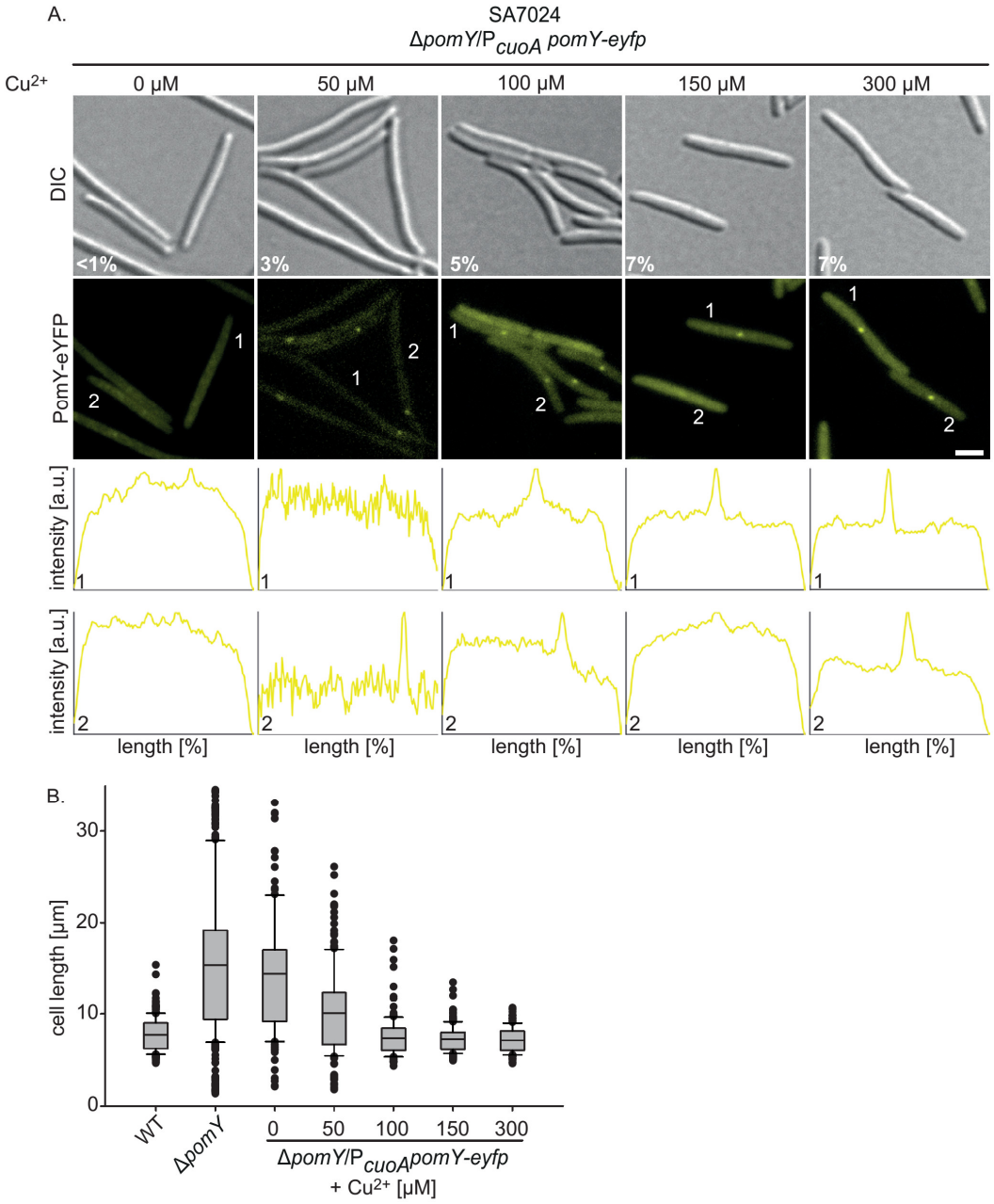

Figure S 3: Cu^{2+}-regulated expression of *pomY-eyfp* corrects a Δ*pomY* phenotype.
(A) Fluorescence microscopy of PomY-eYFP in SA7024 (Δ*pomY*/P_{cuoA}*pomY-eyfp*). Cells were exponentially grown in CTT medium supplemented with 0 - 300 µM $CuSO_4$ for 24 h. White numbers in the DIC pictures indicate constriction frequency under the tested conditions (n>100 cells per condition). Linescans were made with Metamorph on fluorescence intensity of PomY-eYFP signal along long cell axis. Numbers in the linescans correspond to the numbers in the fluorescence pictures, indicating selected cells. Scale bar: 2 µm. **(B)** Cell length distribution of strain SA7024 grown in presence of different concentrations of $CuSO_4$. Boxes enclose the 25th and 75th percentile, with the black line indicating the mean. Whiskers enclose the 10th and 90th percentile. Outliers smaller than 35 µm are depicted as black dots. Outliers bigger than 35 µm are not shown but are included for the calculation of the mean cell length.

5.5.4 Deletion of DNA-binding protein Mxan_0633 results in a cell division in *M. xanthus*

During the analysis of the genomic region of the *pomXYZ* gene cluster we observed that the gene upstream of *pomY*, *mxan_0633*, encodes for a DNA-binding protein. This gene is conserved in all myxobacteria that posses a *pomXYZ* gene cluster although it is not encoded directly upstream of *pomY* in more distantly related members of the family. In order to investigate if Mxan_0633 is somehow involved in the regulation of cell division, an in-frame deletion mutant was created (SA4759; Δ*mxan_0633*) and analyzed for its phenotype by microscopy. A Δ*mxan_0633* mutant displayed a weak cell length phenotype compared to WT and produced cells with an average length of 9.3 ± 3.5 µm (n=233) (Figure S 4 A, B), suggesting that this gene is also involved in cell division regulation in *M. xanthus*. In contrast to cells lacking one of the components of the Pom-system, a Δ*mxan_0633* mutant showed no strong reduction in constriction frequency (5%). In addition, all cell divisions observed in Δ*mxan_0633* were precisely at midcell with a mean localization of 50 ± 2 % (Figure S 4 C). Moreover, minicell formation was not observed in the absence of Mxan_0633.

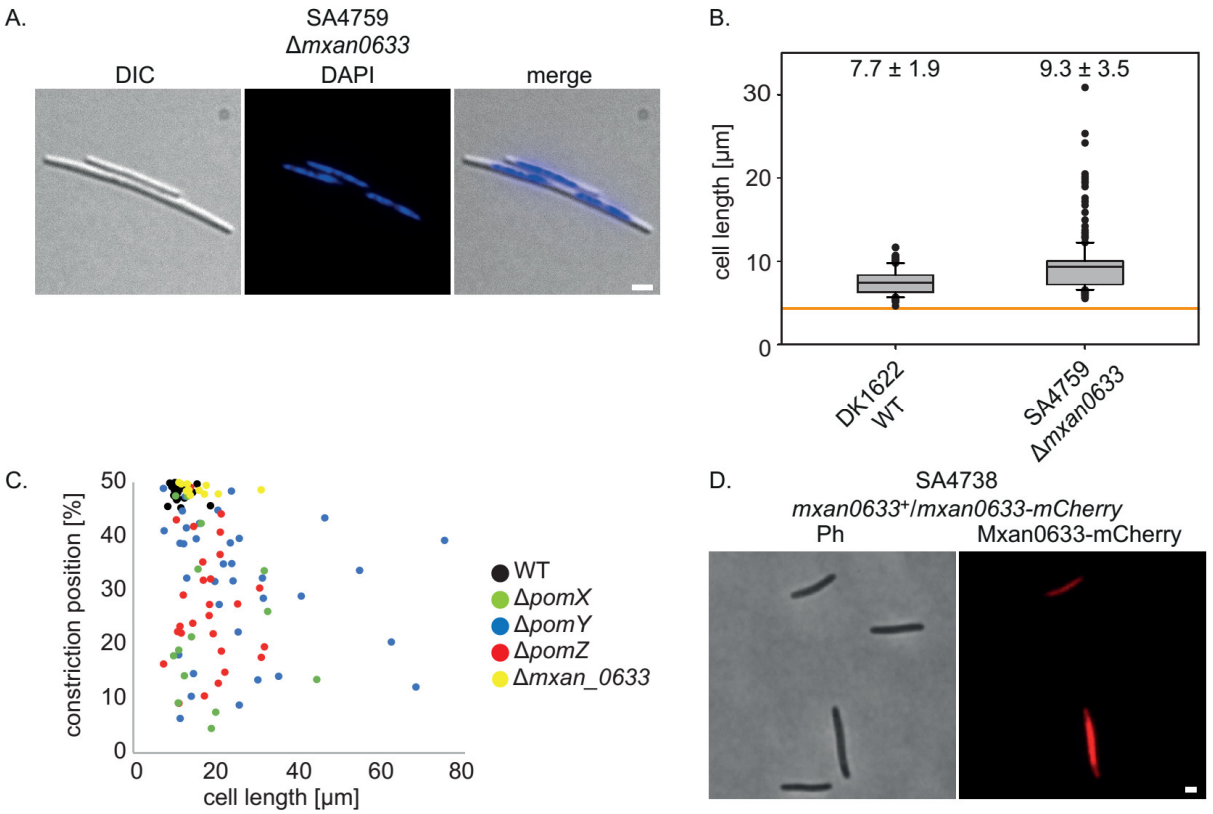

Figure S 4: A Δ*mxan_0633* mutant has a cell division defect.
(A) Fluorescence microscopy of DAPI-stained cells of SA4759 (Δ*mxan_0633*). Exponentially grown cells were imaged at 32 °C on 1 % agarose pads, buffered with TPM. Merged pictures were created with Metamorph. Scale bar: 2µm. **(B)** Cell length quantification of WT and a Δ*mxan_0633* mutant. Boxes enclose the 25th and 75th percentile with the black line showing the mean, which is also shown in numbers above the boxes ± SD in µm. Whiskers indicate 10th and 90th percentile and all outliers are shown as black dots (n=233). Cells below the orange line are counted as minicells as shown for mutant of the PomXYZ system. **(C)** Constriction positioning in strains of indicated genotypes shown in % of cell length as function of cell length. **(D)** Fluorescence microscopy of Mxan_0633-mCherry expressed from its putative native promoter in strain SA4738 (*mxan_0633*$^{+}$/*mxan_0633-mCherry*). Scale bar: 2 µm.

To investigate its localization, an Mxan_0633-mCherry fusion was created and expressed in WT background, resulting in strain SA4738 (*mxan_0633*$^{+}$/*mxan_0633-mCherry*). In this strain *mxan_0633-mCherry* was expressed under the control of its putative native promoter (300 bp in front of *mxan_0633*). For analysis, cells were exponentially grown at 32 °C and imaged on a 1 % agarose pad, buffered with TPM at 32 °C. In around 5 - 10 % of cells a fluorescence signal was detectable, whereas in all other cells no signal was observed. Interestingly, cells displayed a stronger signal of Mxan_0633-mCherry in the central part of the cell and less signal in the polar and subpolar regions. Because Mxan_0633 was identified as a DNA-binding protein by BlastP analysis this suggested that it colocalized with the nucleoid. Of note, this localization was similar to the patchy localization of PomZ-mCherry, but Mxan_0633-mCherry did not form clusters (Figure S 4 D). Furthermore, this localization was observed in cells with and without constrictions. Based on these observations, we conclude that Mxan_0633 could be involved in regulation of cell division by a yet unidentified mechanism. In contrast to the PomXYZ system Mxan_0633 does not affect correct positioning of the cell division site and also does not influence constriction frequency. On the other hand cells are elongated by the lack of Mxan_0633, indicating a defect in cell division. It has to be mentioned that *mxan_0633* is encoded on the strand opposite to *pomY* and their intergenic region is around 300 bp. Therefore deletion of *mxan_0633* could affect the expression of *pomY*, which also could result in a division defect. Because the analyzed cell division defect of a Δ*mxan_0633* mutant is different from a Δ*pomY* mutant, we speculate that Mxan_0633 has an additional PomXYZ-independent effect on cell division.

5.5.5 FtsZ of *M. xanthus* forms filaments in presence of GTP

PomZ was suggested to be a positive regulator for cell division at midcell, based on the finding that cell division frequency was reduced in absence of PomZ. Consistently, native $FtsZ_{mx}$ purified from *E. coli* showed cooperative GTP-hydrolysis, but did not form any filaments in presence of GTP, analyzed by right angle light scattering and negative stain transmission electron microscopy (Treuner-Lange *et al.*, 2013). To further investigate the interaction between PomXYZ and FtsZ the purification protocol for native $FtsZ_{mx}$, expressed in and purified from *E. coli* was changed together with Andrea Harms (8.5.4).

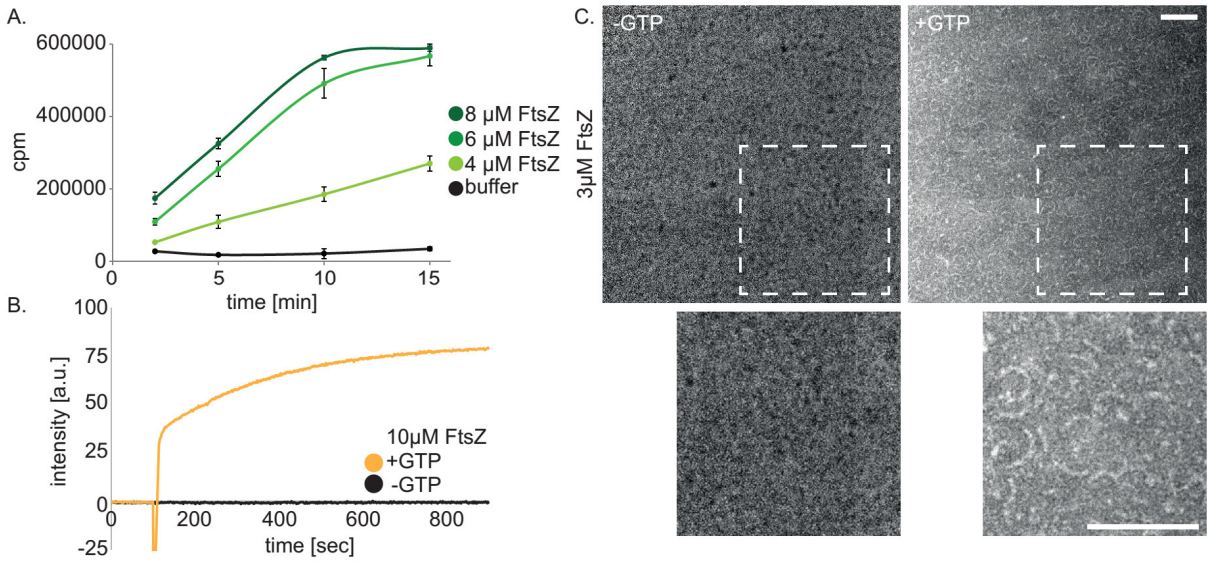

Figure S 5: $FtsZ_{mx}$ hydrolyses GTP and forms filaments in presence of GTP *in vitro*.
(A) GTP hydrolysis of indicated concentrations of $FtsZ_{mx}$, measured in a radioactive GTPase assay. Assays were performed in presence of 2.5 mM GTP, supplemented with 0.066 µM (gamma ^{32}P) GTP at 32 °C at pH 7.2 as described in 8.5.10. **(B)** $FtsZ_{mx}$ forms filaments in presence of GTP as observed by right angle light scattering. Experiments were performed with 10 µM $FtsZ_{mx}$ at 8 °C and pH 7.2 in presence of 10 mM $CaCl_2$. GTP was added at 100 s timepoint at a final concentration of 2.5 mM. The graphs show a representative curve of several assays. **(C)** Negative stain transmission electron microscopy with 3 µM $FtsZ_{mx}$ in presence and absence of GTP. Proteins were visualized by negative stain with 1 % uranyl acetate as described in 8.6.7. Scale bar: 100 nm.

In a first attempt purified $FtsZ_{mx}$ was analyzed for its GTPase activity to test for protein activity. Consistent with previous findings FtsZ showed GTPase activity *in vitro* as measured in a GTPase assay, using $\gamma^{32}P$ GTP by Andrea Harms (Figure S 5 A). From these curves the specific activity was calculated to be 1.4 GTP min^{-1} at a concentration of 4 µM $FtsZ_{mx}$. This activity increased to 3.6 GTP min^{-1} at 6 µM $FtsZ_{mx}$ and 3.2 GTP min^{-1} at 8 μM_{mx} FtsZ. We speculate that the increasing GTP-hydrolysis rate that reached a plateau after 6 µM $FtsZ_{mx}$ is an indication for a cooperative GTP-hydrolysis. Surprisingly, purified $FtsZ_{mx}$ showed a signal in right angle light scattering in presence of GTP (Figure S 5 B), suggesting that $FtsZ_{mx}$, purified under different conditions, showed GTP-dependent filament formation. To test this further, 3 µM $FtsZ_{mx}$ was incubated with and without 500 µM GTP for 5 min and applied to an EM grid and negatively stained with uranyl acetate. As shown in Figure S 5 C, $FtsZ_{mx}$ formed short curved filaments in presence of GTP whereas no structures were observed in the absence of GTP. In conclusion these data suggest that $FtsZ_{mx}$ can form filaments in presence of GTP.

6 Discussion

Positioning of the cell division site is a key process that is precisely controlled in a spatio-temporal manner and this control is essential for the generation of appropriately sized daughter cells with the correct chromosome content. In bacteria, cell division initiates with the assembly of the tubulin homolog FtsZ into a circumferencial ring-like structure, the Z-ring, at the incipient cell division site (Bi & Lutkenhaus, 1991). This Z-ring acts as a scaffold for direct and indirect recruitment of the cytokinetic machinery that performes cell division. Generally, positioning of the Z-ring dictates the localization of the cell division site and therefore systems that determine cell division site position regulate Z-ring formation and position (Rothfield *et al.*, 2005). While the core components of the cell division machinery are conserved among bacteria, the systems that regulate the spatio-temporal positioning of the cell division site are diverse and poorly understood.

Here we report on the identification of two novel cell division regulators PomX and PomY that function together with the ParA ATPase PomZ to regulate cell division by stimulation of Z-ring formation and correct positioning at midcell. We further found that a dynamically localized complex of PomXYZ translocates to the mid-nucleoid, which coincides with midcell before cell division, in a PomZ ATP-hydrolysis-dependent manner. This dynamically localized complex of PomXYZ serves as a landmark to guide Z-ring localization, connecting chromosome organization with the positioning of the cell division site in *M. xanthus*. Open questions, related to the connection between the PomXYZ system and FtsZ, the identification of midcell as the side of cell division and how PomXYZ cluster motion is accomplished will be discussed below.

6.1 The PomXYZ system serves as a positive and spatial regulator for Z-ring formation at midcell

Here we demonstrate that the combined work of PomX and PomY together with the ParA ATPase PomZ results in the correct spatial and temporal localization of the Z-ring at correct frequency. In the absence of PomZ cells are viable but display an increased cell length and a reduced cell division frequency, observed by less cell division constrictions. Concurrent with that Z-rings are also produced at lower frequency (Treuner-Lange *et al.*, 2013). Similarly, cells lacking PomX or PomY are viable and display cell division defects observed by an increasing cell length, a reduction in cell division contrictions by two-fold and compromised Z-ring production, suggesting that they promote efficient Z-ring production or stimulate Z-ring stability in the same way as observed for PomZ. In addition, a Δ*pomX* or Δ*pomY* phenotype is further characterized by the formation of minicells. Moreover, we observe that the few cell divisions formed are formed away from midcell in a nucleoid free area, suggesting that PomX and PomY are required for the correct localization of the Z-ring and cell division. Similarly, the Z-rings formed are also misplaced and positioned away from midcell in a Δ*pomZ* mutant, too. It is important to notice that a *Δpom* phenotype is neither characterized by aberrant replication nor by inappropriate segregation of the chromsome, as it was shown that defects in both may result in minicell formation as by the lack of the Smc homolog in *E. coli* (Niki *et al.*, 1991) or by lack of ParA and ParB in *C. glutamicum* (Donovan *et al.*, 2013, Donovan *et al.*, 2010). This implies that the resulting phenotypes are solely due to deregulated Z-ring formation and placement. These data suggest that that PomX, PomY and PomZ work in the same system. Three lines of

evidence support this hypothesis. First, all three genes are encoded in one gene cluster that is conserved among several myxobacteria that do not possess the members of the Min-system. Additionally, PomX, PomY and PomZ accumulate independently of each other showing that all three proteins have a distinct function in the Pom-system. Finally, all possible double mutants, as well as a triple mutant are viable and phenocopy the single *pomX*, *pomY* and *pomZ* mutant. Taken together, we conclude that PomX, PomY and PomZ function as one system to regulate cell division in *M. xanthus* and positioning the Z-ring at midcell at correct frequency.

Two different ways of restricting Z-ring formation to midcell are described. On the one hand negative regulation systems inhibit cell division all over the cell body but are restricted in their function to sites where cell division is non-permissive. On the other hand, systems were identified that recruit FtsZ to a certain location, serving as landmarks for Z-ring formation (Rothfield *et al.*, 2005). One major question for all systems that position cell division is how the negative or positive regulators impact on FtsZ and Z-ring formation. Based on our data, we propose that the PomXYZ system is a positive regulation system that directly affects FtsZ localization and stimulates assembly into the Z-ring. Therefore the PomXYZ system integrates different features of other positive regulation systems that position cell division.

Cell division site placement during vegetative growth in *S. pneumoniae* is regulated by a novel membrane protein MapZ (or LocZ). Cells lacking MapZ are viable, but show a growth defect and misshaped Z-rings that are tilted compared to its normal position. In this system MapZ, anchored in the membrane, interacts with FtsZ via its N-terminal cytoplasmic part. MapZ localizes at the incipient cell division site before FtsZ by a passive, cell growth-dependent mechanism, creating a landmark for FtsZ recruitment (Fleurie *et al.*, 2014, Holeckova *et al.*, 2015). Analogously, SsgB in *S. coelicolour* is suggested to recruit FtsZ to the incipient cell division site during sporulation-dependent cell division. SsgB forms SsgA-dependent ladder-like patterns throughout the aerial hyphae which is followed by the ladder-like localization of FtsZ. Like MapZ, SsgA and SsgB localize in the same position in absence of FtsZ and further interact with FtsZ via SsgB (Willemse *et al.*, 2011). By a yet unidentified mechanism SsgA/B localize at the site of cell division also, serving as landmarks for Z-ring position.

Several lines of evidence suggest that PomXYZ function as positive regulators like MapZ and SsgB. First, PomXYZ form a big cluster at midcell before cell division is initiated and consistently, cell division constrictions take place on the PomXYZ cluster. Secondly, they localize at midcell before and in the absence of FtsZ and colocalize with FtsZ during cell division, suggesting that they mark midcell and then become integral part of the divisome. Third, PomX, PomY and PomZ stimulate Z-ring formation and cell division. Similarly a Δ*ssgAB* mutant cannot divide but forms long unseparated cell filaments, indicating that presence of SsgA and SsgB promotes Z-ring production and cell division *in vivo* (Willemse *et al.*, 2011). By constrast, Z-rings form in the absence of MapZ at normal frequency, but they are incorrectly localized, indicating that MapZ has no stimulating effect on Z-ring formation, only serving as beacon to guide FtsZ localization (Fleurie *et al.*, 2014, Holeckova *et al.*, 2015). Finally, PomXYZ are required to position FtsZ at midcell, suggesting that the PomZ system guides Z-ring formation to midcell. Thus the PomXYZ system integrates several features of positive regulation mechanisms that serve as guides to recruit FtsZ to midcell and stimulate Z-ring formation.

E. coli and *B. subtilis* and *C. crescentus* by comparison make use of negative regulation systems to position cell division that share some similarities with the PomXYZ system. Similary to the Min-system in *E. coli,* as well as the MipZ/ParB system in *C. crescentus,* the PomXYZ system incorporates a ParA ATPase, PomZ, to position cell division at midcell (de Boer *et al.*, 1991, Thanbichler & Shapiro, 2006, Treuner-Lange *et al.*, 2013). The *E. coli* Min-system self-organizes to undergo MinD-ATP-hydrolysis-dependent oscillations from pole to pole, induced by MinE (Hu & Lutkenhaus, 1999, Hu & Lutkenhaus, 2001, Raskin & de Boer, 1999a). This membrane-localized pattern formation over time results in the highest concentration of the Z-ring inhibitor MinC at the poles, while the lowest concentration is at midcell (Castaing *et al.*, 2008, Raskin & de Boer, 1999a, Raskin & de Boer, 1999b). Similarly, in *C. crescentus* the ParA ATPase MipZ together with ParB forms a self-organized, bi-directional gradient with the highest concentration of MipZ restricted to the cell poles. However, the mechanism that brings MipZ to the poles is different compared to MinD in *E. coli*. MipZ is recruited to the poles by ParB that is thought to stimulate dimer-formation of MipZ. (Thanbichler & Shapiro, 2006). However, the PomXYZ systems shows that ParA-ATPases can be involved in negative and positive regulation systems. All three systems incorporate ParA ATPases that binds to a cellular surface in an ATPase-cycle dependent manner. In case of MipZ and PomZ it is the nucleoid structure and in case of MinD it is the membrane (Kiekebusch *et al.*, 2012, Szeto *et al.*, 2003, Szeto *et al.*, 2002). This self-organization, observed by the Min-system and MipZ could also be observed by the PomXYZ system, but the outcome is different. PomXYZ self-organizes on the nucleoid to localize at midcell and to stimulate cell divisions. Consistently, MipZ and MinCD serve as negative regulators for Z-ring formation and they are titrated away from the side of cell division, whereas the PomXYZ system is brought up to midcell. In addition, deletion or depletion of MinCD and MipZ results in the formation of multiple Z-rings or multiple FtsZ clusters all over the cell (de Boer *et al.*, 1992, Thanbichler & Shapiro, 2006). By contrast, deletion of PomXYZ shows a reduction in Z-ring formation. Thus the PomXYZ system incorporates the function of a ParA ATPase for the positioning of cell division at midcell like MinD and MipZ but shows a completely different cellular localization. Whereas the negative regulators of the Min system and MipZ are sequestered away from the side of cell division, the PomXYZ system brings a stimulation complex to midcell. A ParA ATPase (MinD/PomZ) recruits the inhibitor/stimulator complex (MinC/PomXY) to a cellular surface the membrane, or the nucleoid. This complex is given specificity by a topology factor MinE, sequestering MinCD to the poles, or PomX that forms the cluster at midcell. Importantly, MinE and PomX give local information to the system by stimulation of ATP-hydrolysis in their cognate ParA partner. In conclusions this shows that two different concepts for the positioning of cell division can have the same outcome.

Besides a variety of indirect evidence that the PomXYZ systems stimulates Z-ring formation and cell division the precise mode of action is still elusive. PomX, PomY and PomZ do not interact with FtsZ in a BACTH assay, but colocalize with Z-rings and cell division constrictions and up until now, no direct interaction could be observed between PomXYZ and FtsZ *in vitro*. However, PomY is a good candidate to further investigate for direct interaction with FtsZ. A Δ*pomY* mutant has the strongest effect on cell length and in combination with a Δ*pomX* mutant the strongest impact on Z-ring formation. Interestingly, cell division takes place on the PomXYZ cluster in WT, but cells do not divide on the

PomXZ cluster in the absence of PomY. In comparison, cell division takes place on the PomXY cluster in the absence of PomZ. This raises the hypothesis that PomY connects the PomXYZ complex with FtsZ and cell division and it further suggests that PomY interact with FtsZ.

In conclusion we propose that the PomXYZ system is a positive regulation system that guides Z-ring formation at midcell by first, localizing at midcell to mark it for the recruitment of FtsZ and secondly, stimulation of Z-ring formation and stability.

6.2 PomX and PomY are two ATPase activating proteins that regulate the PomZ ATPase cycle

The spatio-temporal organization of cellular processes is a fundamental problem for all unicellular organisms, as they have to regulate different functions within the same cellular compartment. Bacteria have evolved a variety of regulation mechanisms that spatially restrict the activity of these processes. Proteins of the ParA ATPases are known to regulate spatial and temporal localization of different cellular functions, such as motility (Schuhmacher *et al.*, 2015), plasmid and chromosome partitioning (Lim *et al.*, 2014, Ptacin *et al.*, 2010, Ringgaard *et al.*, 2009), carboxysome organization and localizations of chemotaxis proteins (Ringgaard *et al.*, 2011, Roberts *et al.*, 2012, Savage *et al.*, 2010) and cell division (Bowman *et al.*, 2010, de Boer *et al.*, 1989, Thanbichler & Shapiro, 2006, Treuner-Lange *et al.*, 2013). PomZ is a ParA ATPases and shares several characteristics with its members.

Based on alignments with other ParA ATPases PomZ shows all characteristic sequence motifs which are the deviant Walker A motif, a Walker B motif, the catalytic aspartate which is involved in ATP-hydrolysis and a positively charged amino acid in the C-terminal part that is involved in unspecific DNA-binding in Soj, ParA's of plasmid and chromosome partitioning systems and PpfA (Hester & Lutkenhaus, 2007, Lim *et al.*, 2014, Roberts *et al.*, 2012). We could show based on mutational analysis that PomZ binds DNA upon ATP-binding and dimerization and furthermore hydrolyzes ATP. Consistently, as a member of the ParA ATPases, PomZ shows low intrinsic ATPase activity *in vitro*, similar to ParA from the ParAB*S* system of *C. crenscentus* (Lim *et al.*, 2014) and SopA in the SopAB*C* system involved in F-plasmid stability (Ah-Seng *et al.*, 2009, Castaing *et al.*, 2008). However, ATPase activity by PomZ alone was within the range of the negative control, suggesting that it is basically inactive on its own. Generally, this associated ATPase activity of ParA ATPases is induced by AAP's (ATPase activating proteins) with the exception of MipZ. As MinE and ParB stimulate the ATPase activity of dimeric MinD and ParA, respectively and TlpT was suggested to have the same function for PpfA (Hu & Lutkenhaus, 2001, Lim *et al.*, 2014, Roberts *et al.*, 2012). Interestingly, none of the three proteins that were shown to stimulate ATP-hydrolysis in their cognate ParA ATPase partner shows any overall homology, suggesting that unrelated proteins with different functions *in vivo* can stimulate ATP-hydrolysis of ParA ATPases.

Like MinD, ParA and PpfA, PomZ ATPase activity is regulated by its interaction partners. PomX and PomY equally stimulate ATP hydrolysis by PomZ alone in presence of DNA. In complex however, they synergistically stimulate its ATPase activity. Based on these data we conclude that PomZ has two

AAP's that alone and in complex stimulate ATPase activity by PomZ. As far as we know this is the first known ParA ATPase that employs two AAP's to regulate ATPase activity.

In addition PomZ localizes to the nucleoid and this localization is ATP-dependent, since only dimeric PomZ localizes to the nucleoid in *M. xanthus*, as well as in the unrelated *E. coli.* Binding to different surfaces which are then used as a scaffold for function is a well described property of ParA-like ATPases and can be required for efficient stimulation of ATP-hydrolysis (Hester & Lutkenhaus, 2007, Kiekebusch *et al.*, 2012, Murray & Errington, 2008, Ringgaard *et al.*, 2011, Ringgaard *et al.*, 2009, Roberts *et al.*, 2012). In *E. coli*, MinD recruits the FtsZ inhibitor MinC and uses the membrane as a surface for this recruitment event. An N-terminal amphipathic helix interacts with the membrane in response to ATP binding and dimerization (Szeto *et al.*, 2003, Szeto *et al.*, 2002). Importantly, interaction of MinD with MinE and phospholipids stimulates ATP-hydrolysis by MinD (Hu & Lutkenhaus, 2001, Park *et al.*, 2012). This amphipathic helix however, is absent in ParA's that are involved in plasmid partitioning or chromosome segregation like SopA from the F-plasmid or ParA from *C. crescentus*. Large ParA's in contrast have a specific DNA-binding domain, which precedes the Walker A box, together with conserved positively charged residues that are involved in non-specific DNA-binding as in the case of SopA, while small ParA's lack the preceding DNA-binding domain, but instead only have the positively charged amino acids for unspecific DNA-binding (Gerdes *et al.*, 2000). Interestingly, MipZ from *C. crescentus* uses the chromosome as a surface to build the bi-directional protein gradient from the poles but lacks both conserved motifs which are required for DNA-binding. However, DNA stimulates ATP-hydrolysis by MipZ and is required for gradient formation (Kiekebusch *et al.*, 2012). Therefore the mode of DNA-binding is still unresolved.

PomZ does not localizes to the membrane and lacks the amphipathic helix of MinD. We suggest that membrane binding is not part of the ATPase cycle of PomZ. In contrast PomZ binds non-specifically to DNA *in vivo* and *in vitro*. Based on the mutational analysis of PomZ we suggest that PomZ is more related to PpfA and other ParA ATPases that are involved in chromosome partitioning. Indeed, PomZ lacks a conserved DNA-binding domain of large ParA's like SopA, but exhibits a lysin at position 268 which equivalent is important for DNA-binding in Soj (Hester & Lutkenhaus, 2007), suggesting that PomZ uses the same residues for DNA-binding as Soj. PpfA lacks a DNA-binding domain too, but shares the positively charged arginine at position 167 and lysine at position 196 (corresponding to lysine-268 in PomZ) which are in concert important for DNA-binding (Roberts *et al.*, 2012).

But how does DNA-binding and interaction with PomX and PomY regulate ATP-hydrolysis in PomZ? Cluster formation of PomZ is abolished if PomZ is blocked in ATP-binding, dimerization and DNA-binding. Consistently, ATP-hydrolysis by PomZ can only be efficiently stimulated by PomX and PomY in presence DNA. This suggests that ATP-hydrolysis by PomZ depends on DNA-binding and that DNA-binding is a prerequisite for the interaction of PomZ with the AAP's PomX and PomY or a complex of both. Of note, DNA alone has only little effect on ATPase activity of PomZ. Similar observations were made for other ParA ATPases, which are Soj, SopA and ParA from *C. crescentus*. In Soj, ATP-hydrolysis is induced by the presence of Spo0J and *parS* DNA *in vitro*. In contrast to PomZ, Spo0J is able to stimulate Soj ATPase activity to a large extent even in absence of DNA (Leonard *et al.*, 2005), suggesting that Spo0J interacts with Soj in absence of DNA. Similar to PomZ,

ATPase activities of SopA and ParA are also strongly simulated by their AAP's in presence of DNA. In contrast to Spo0J, SopB and ParB do not show a stimulating effect in absence of DNA. Strikingly, ParA ATPase activity is induced more by DNA alone than by ParB (Lim *et al.*, 2014). We conclude that the dynamic localization as well as the ATPase cycle of PomZ is regulated by PomX, PomY and the ability of PomZ to bind to DNA.

Interaction and ATP-hydrolysis stimulation in Soj and MinD is mediated via the first 20-30 N-terminal amino acids of Spo0J and MinE, respectively and similarly the N-terminus of TlpT is suggested to simulate ATP-hydrolysis by PpfA (Leonard *et al.*, 2005, Roberts *et al.*, 2012, Hu & Lutkenhaus, 2001). It is consistent with this finding that lack of the N-terminal part of TlpT results in a loss of interaction with PpfA. Similarly an N-terminally truncated version of Spo0J and a MinE with N-terminal substitutions are unable to stimulate ATPase activity of Soj and MinD, respectively. Intriguingly, a peptide of the 20 N-terminal amino acids Spo0J stimulates ATP-hydrolysis by Soj like the full-length protein (Leonard *et al.*, 2005).

Alike Spo0J, MinE and TlpT the N-terminal region of PomX is required for interaction with PomZ and stimulation of ATP-hydrolysis by PomZ. Substitution of only two conserved, positively charged amino acids in PomX (K13 and R15 to alanine) interferes PomXYZ-dependent positioning of cell division at midcell. Several lines of evidence suggest that the mechanism for stimulation of ATP-hydrolysis by PomX is similar to that of Spo0J, and TlpT. First, substitution of K13 and R15 in PomX with alanine results in a cell division defect similar to, but milder than a Δ*pomX* mutant, suggesting that $PomX^{K13A;R15A}$ function is partially diminished compared to PomX *in vivo*, but not completely abolished. Consistently, substituted $PomX^{K13A;R15A}$ accumulates at WT levels *in vivo*, forms filaments and interacts with PomY like $PomX^{WT}$, but its interaction with PomZ is affected *in vivo* and in a BACTH assay. Secondly, $PomX^{K13A;R15A}$ has a reduced effect on stimulating ATPase activity by PomZ in presence of PomY and DNA and is unable to stimulate ATP-hydrolysis in presence of PomY only. Third, the N-terminal 25 amino acids of PomX are completely conserved among all identified PomX homologs, suggesting that the mechanism is shared with other myxobacteria. Finally, as a cellular readout for ATP-hydrolysis by PomZ, cluster motion of the PomXYZ complex to midcell is reduced by 30 % in presence of $PomX^{K13A;R15A}$ but not abolished. We conclude that PomX adopts a similar mechanism for stimulation of ATP-hydrolysis by its cognate ParA ATPase PomZ via the interaction with its N-terminal part. It has still to be tested, if deletion of this domain completely abolishes PomX function in ATP-hydrolysis stimulation and furthermore, if interaction between PomX and PomZ on a molecular level is really mediated by the N-terminus, because it was shown before that the PomX coiled-coil domain on its own also has affinity for PomZ and interacts with it in a BACTH assay (Huneke, 2013). At this moment it is still unclear how PomY stimulates PomZ ATP-hydrolysis on a molecular level, we however believe that the mechanism is different to that of PomX because the N-terminal region of PomY has no homologies to the PomX N-terminus and is furthermore not conserved among other myxobacteria that possess a PomXYZ system. We hypothesize that the stimulation effect of PomY does not function via PomX in the PomXYZ complex because it stimulates ATP-hydrolysis by PomZ on its own and stimulates ATP-hydrolysis by PomZ in presence of DNA more than synergistically.

6.3 A diffusive, random PomZ flux on the nucleoid creates a bias for PomXYZ complex translocation to the mid-nucleoid

Expression of PomXYZ in *E. coli* resulted in cluster formation on the nucleoids, which showed that these three proteins are sufficient and required to form DNA-associated clusters *in vivo*. In the PomXYZ complex, all three proteins have different functions. PomX alone forms a polymeric structure *in vivo* in absence of any co-factor, which recruits PomY for interaction. In this complex PomY bundles PomX filaments *in vitro* and has a condensation function on the polymeric PomX structure *in vivo,* which ultimately results in the formation of round-shaped PomXY clusters. Importantly, this complex is not associated with the DNA. PomZ binds to the nucleoid in the ATP-bound dimeric state and is able to tether PomXY clusters to the nucleoid. This leads to a complex formation of PomXYZ that all three colocalize in the observed cluster on the nucleoid.

In this complex with PomXY, ATP-hydrolysis by PomZ is stimulated. Monomeric ADP-bound PomZ dissociates from the PomXYZ complex and is released into the cytoplasmic space. Consistently, PomZ shows a fast turnover in this complex and exchanges molecules with the surrounding nucleoid. The complex itself, associated with the nucleoid, is dynamically localized and shows a biased-random motion towards the mid-nucleoid which coincides with midcell before the nucleoids finally segregate. At the mid-nucleoid, the complex switches from a biased-random motion to a constrained motion. As explained earlier our data suggest that PomZ uses the nucleoid as a surface for the positioning of the PomXYZ complex towards midcell, but our data does not explain why clusters first move towards midcell and then switch to a constrained motion. The question of how the PomXYZ system identifies midcell will be discussed below.

Based on our data we built a model together with Silke Bergeler and Erwin Frey (LMU Munich) for how the ParA ATPase PomZ integrates the local interaction with the PomXY complex and the nucleoid into a global pattern formation that relates the position of the PomXYZ complex to cellular space. For this model we made several critical observations.

First, PomXY and PomZ interact on the nucleoid and then the nucleoid is used as a surface for the positioning. Second, PomZ in the cluster hydrolyses ATP and shows a high turnover rate as observed by FRAP experiments. Third, PomZ is also highly dynamic on the nucleoid surface and move predominantly by lateral diffusion, giving rise to a diffusive and random flux of PomZ dimers on the nucleoid, similar to the observations made for SopA *in vitro* (Vecchiarelli *et al.*, 2010, Vecchiarelli *et al.*, 2013b, Vecchiarelli *et al.*, 2014a). Next, only 5 % - 10 % of total PomZ is in the cluster. Finally, ATP-bound PomZ can bind to the nucleoid anywhere, but its release depends on ATP-hydrolysis that is locally restricted within the PomXYZ cluster.

Based on these observations we proposed a model in which a diffusive flux of PomZ molecules on the nucleoid associates with the PomXY cluster. The model is inspired by Itsewaart *et al.,* 2014 and depends on the feature that PomZ is in a dynamic equilibrium between a monomeric ADP-bound and a dimeric ATP-bound phase.

In this model the diffusive PomZ flux on the nucleoid on either side of the cluster into the PomXYZ complex scales with the amount of PomZ on the nucleoid on each side of the cluster. Because PomZ is symmetrically distributed on the nucleoid in this model, the asymmetry of the PomXYZ off-centre cluster scales with a difference in the PomZ flux on either side of the cluster into

the cluster. In the cluster, PomZ undergoes ATP-hydrolysis, stimulated by PomXY and as a consequence PomZ is released from the PomXYZ complex. The difference of the diffusive flux of PomZ dimers into the cluster results in a local PomZ gradient on the PomXY complex, where the size of that local concentration gradient correlates with the PomXYZ cluster position on the nucleoid and thereby with the amount of PomZ on each side of the cluster on the nucleoid. In other words, if a PomXYZ cluster is not in the middle of the nucleoid, a local PomZ gradient on the cluster occurs with the higher concentration of PomZ on the side of the PomXYZ complex, which points towards midcell. The cluster then moves in the direction of the higher PomZ concentration, i.e. the cluster moves up the gradient, similarly to the observations made for other ParAB systems (Lim *et al.*, 2014, Vecchiarelli *et al.*, 2014a). Based on this model, off-centre cluster translocation is random, but biased in the direction of midcell.

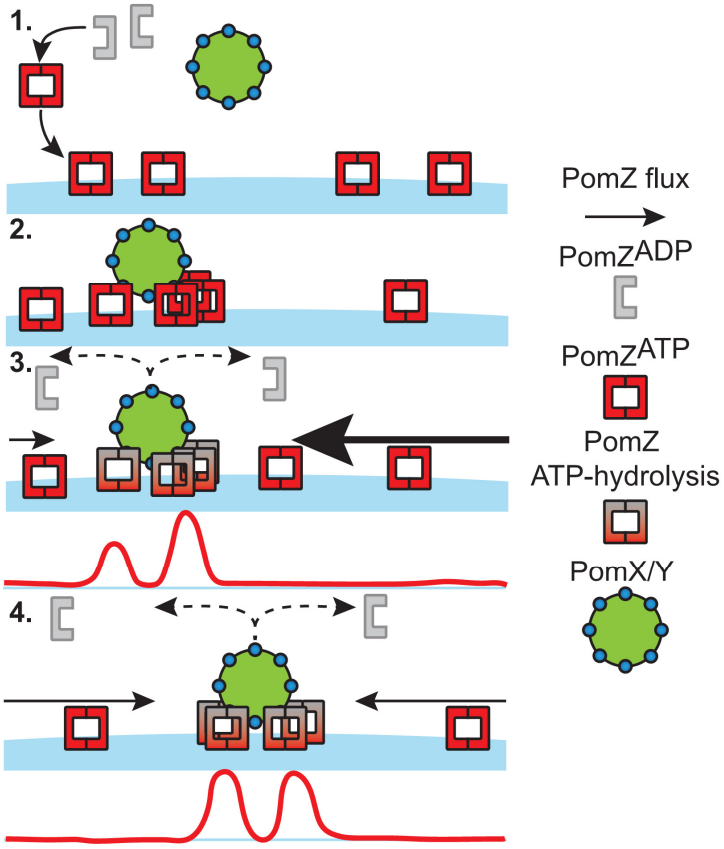

Figure 59: A diffusive flux of PomZ positiones the PomXYZ complex at the mid-nucleoid at midcell.
Model for PomZ-dependent positioning of the PomXYZ complex at the mid-nucleoid. (1) PomZ spontaneously dimerizes upon ATP-binding and associates randomly with the nucleoid (blue). (2) PomZ recruits the PomXY complex to the nucleoid. Because PomZ is dynamically localized on the nucleoid PomZ dimers can associate with the PomXY complex and accumulates at the interface of the PomXY cluster and the DNA. (3) Within the PomXYZ cluster ATP-hydrolysis by PomZ takes place and PomZ dissociates from the PomXY complex into the cytoplasm where is diffuses. More PomZ will attach to the cluster with the higher binding capacity of dimeric PomZ, which is in case of an off-centre cluster the side pointing towards midcell. This leads to a local gradient formation along the PomXYZ cluster with the higher concentration of PomZ at the side, pointing towards midcell. Based on ATP-hydrolysis the cluster moves preferentially towards the direction of higher PomZ concentration, towards midcell. (4) in the middle oft he nucleoid at midcell the diffusive PomZ fluxes equalize which in turn results in a diminishing PomZ gradient. Therefore cluster display random motion at midcell compared to a biased random motion in the off-centre position.

When a cluster at some point moves to the mid-nucleoid at midcell, the nucleoid mass on either side of the cluster and therefore the amount of nucleoid-bound PomZ equalizes. The diffusive flux into the PomXY cluster then also equalizes. The local gradient along the PomXYZ cluster in turn diminishes, resulting in a random-constrained motion around midcell. This system is furthermore self-correcting. If clusters accidentally move further than the mid-nucleoid, the gradient switches orientation and the bias targets clusters to the opposite direction. In summary the global cellular localization of the PomXYZ complex is integrated into a dynamic local protein gradient along the PomXYZ cluster that, as a result of its asymmetric position on the nucleoid compared to the nucleoid midpoint, experiences a bias for its motion along this gradient and therefore describes a biased or constrained motion depending on its position on the nucleoid.

We tested this model and identified different criteria that affect the function of the system to position the dynamically localized PomXYZ complex at midcell. As mentioned earlier a PomXY complex together with DNA stimulates ATP-hydrolysis by PomZ. Importantly, DNA on its own has no influence on ATP-hydrolysis in absence of PomX and PomY. This is required, because if DNA would have any effect on ATP-hydrolysis alone the diffusive flux of PomZ dimers on the nucleoid would be perturbed, since PomZ would leave the nucleoid independent of its association with the PomXY complex. In general, the dynamic equilibrium between monomeric and dimeric PomZ would be shifted towards the monomeric phase. In our model this would eventually lead to a strongly reduced cluster motion and moreover to a higher noise in the translocation mechanism, because attachment of PomZ to the cluster would be a rare event under these conditions.

The other way around we predicted that a too slow rate of ATP-hydrolysis would also lead to a break-down of the system, because PomZ would, based on its lateral diffusion on the nucleoid attach more and more to the PomXY complex, similarly to the PomZ^{D90A} situation, which stalls the cluster on the DNA. Any kind of perturbation of ATP-hydrolysis by PomZ, as observed in the absence of PomY and in the PomX^{K13A,R15A} substitution, results in slower cluster motion. Ultimately, a block in ATP-hydrolysis as observed by PomZ^{D90A} would tether the PomXY complex to the nucleoid at any position.However, ATP-hydrolysis by PomZ should generally be slower than observed in other ParAB*S* systems because PomZ shows some retention time, observed as the PomZ cluster, in the PomXYZ complex, whereas the *parS*-bound chromosomal ParB follows the retracting ParA cloud similarly to the plasmid ParAB*S* systems.

In addition, PomZ concentration on the nucleoid has to be tightly regulated because accumulation of too high levels of PomZ results in the saturation of the cluster and a strong accumulation of PomZ on the nucleoid, also leading to stalled clusters on the DNA. If levels of PomZ are too high then, based on our model, the system collapses. The effect of too much PomZ would be a too high flux of PomZ into the cluster, leading to saturation and a drop in the PomZ gradient on the cluster. This in turn diminishes the biased motion to midcell, stalling clusters after recruitment to the nucleoid.

Next the physical properties of the nucleoid seem to have an important role for the PomZ-dependent translocation mechanism. Condensation and decondensation of the nucleoid as well as missegregation of the DNA interferes with cluster translocation, indicating that the interaction to the nucleoid can be manipulated easily to diminish cluster motion. Similar to that, pB171 plasmid

positioning was affected in *E. coli* cells that were treated with nalidixic acid to inhibit gyrase function. In addition, lack of the condensation proteins MukE and MukF and the terminus organisator MatP resulted in aberrant chromosome organization and furthermore in mislocalization of pB171, even in presence of the ParAB*S* system (Ietswaart *et al.*, 2014).

Finally, the PomXYZ cluster on the nucleoid has to create a physical hinderance for the diffusive flux of PomZ on the nucleoid. If this was not the case the random PomZ fluxes would circumvent attachment to the PomXYZ cluster and therefore equalize the local PomZ gradient even if the PomXYZ cluster is in the off-centre position.

We conclude that function of the PomXYZ system depends on several properties, including the dynamic interplay of the three proteins, with its tightly regulated ATP-hydrolysis, their interaction with each other and the nucleoid and its structure and moreover its correct organization within the cellular space.

6.4 The Pom-system adopts features of other ParA partitioning systems in a novel fashion

In our model PomXY clusters follow a local dynamic PomZ gradient in a biased-random motion to the mid-nucleoid. However, how this PomXY cluster (the cargo complex in the PomXYZ) is translocated to midcell is unknown and different mechanisms have been suggested for how force is generated for the translocation of cellular cargo by ParA ATPases.

Based on the finding that certain ParA's form filamentous structures *in vitro* and sediment into the pellet fraction in polymerization assays upon ATP binding, a "filament-pulling" model was proposed (Ebersbach *et al.*, 2006, Ptacin *et al.*, 2010, Ringgaard *et al.*, 2009). In this model ParA's are suggested to polymerize in presence of ATP into long filaments that attach to the ParB-bound plasmids or ParB-bound chromosomal DNA. Because ParB stimulates ParA ATP-hydrolysis the filaments disassemble and "pull" on the ParB/DNA complex which in turn results in a translocation event (Ebersbach *et al.*, 2006, Ptacin *et al.*, 2010, Ringgaard *et al.*, 2009). The retraction of the filament applies a force on the ParB/DNA complex that moves in the direction of the retraction (Ebersbach *et al.*, 2006, Lim *et al.*, 2005).

In a different model a "diffusion-ratchet" mechanism was proposed. In this model ParA forms a surface on the DNA which recruits the cargo complex. In the SopAB*C* system the SopB-bound F-plasmid is recruited to the SopA-bound nucleoid. Binding of ParB to ParA results in ATP-hydrolysis and subsequent dissociation of monomeric ParA from the nucleoid. Because ParA needs time for the nucleotide exchange and dimerization, a temporal delay occurs that results in a concentration difference between the ParA "in front" of the cargo complex and "behind" the cargo complex, where a depletion zone is formed. After ATP-hydrolysis the ParB-plasmid cargo is not attached to the nucleoid-bound ParA and diffuses in the constrained space between membrane and nucleoid surface until it re-binds to nucleoid-bound ParA, preferentially where the concentration is higher. Overall this results in a unidirectional motion along a dynamic ParA gradient on the nucleoid till the cargo complex reaches the nucleoid end and moves in the opposite direction (Vecchiarelli *et al.*, 2010, Vecchiarelli *et al.*, 2013b, Vecchiarelli *et al.*, 2012).

Third, a DNA-relay mechanism was proposed. In the DNA-relay model ParB is recruited to nucleoid-bound ParA dimers and tethered to the DNA. The translocation mechanism utilizes the elastic capacity of DNA to relay the ParB-*parS* cargo complex from one nucleoid-bound ParA dimer to the next. Directionality in this system, which is based on the ParAB*S* system of *C. crescentus,* is given by a global ParA gradient that spans throughout the whole cell (Lim *et al.*, 2014).

Finally, a “Tarzan in the jungle” model was proposed for how dimers of MinE chases MinD on the membrane. In this model MinE dimers have two arms. One arm interacts with a MinD dimer to stimulate ATP-hydrolysis by MinD, while the other arm interacts with the membrane. After ATP-hydrolysis MinE either falls off the membrane or “swings” to the next MinD dimer on the membrane, thereby chasing MinD. Because higher local concentrations of MinD dimers on the membrane favor the “swinging” from one MinD dimer to the next, the MinE dimer will preferentially move towards higher concentrations of MinD (Park *et al.*, 2011).

Our described model explains how a complex of PomXYZ finds midcell to mark it as the incipient cell division site. It utilizes the dynamic fashion of a ParA ATPase with its associated ATP-hydrolysis and ability to interact with the nucleoid to generate a cellular localization pattern that localizes a cell division positioning complex at midcell. Hoewever, how force is generated to translocate the PomXYZ complex to midcell is unclear. The PomXYZ system displays strong similarities to the systems mentioned above. However, besides these similarities the PomXYZ system shows remarkable differences that need to be discussed further.

Under all tested conditions there is no evidence that PomZ forms filaments *in vivo* or *in vitro* (Treuner-Lange *et al.*, 2013), suggesting that the PomZ-mediated translocation mechanism does not depend on PomZ filaments that “pull” on the PomXY complex. Consistent with this idea PomZ forms a symmetric localization over the nucleoid which is in strong contrast to the observations made for pB171 ParA in *E. coli* and the chromosomal ParA from *C. crescentus* and *M. xanthus* (Harms *et al.*, 2013, Ptacin *et al.*, 2010, Ringgaard *et al.*, 2009). In all three cases a ParA cloud extents until it reaches the ParB-bound plasmid or *parS* sequences on the chromosome and subsequently retracts. This kind of global asymmetry is not observed for PomZ under any condition. Strikingly, this global asymmetry of ParA is achieved by an additional protein TipN in *C. crescentus* which sequesters ParA to the new pole (Huitema *et al.*, 2006, Lam *et al.*, 2006, Ptacin *et al.*, 2010). This is required to maintain directional *oriC* motion along the ParA gradient during the ParAB*S*-dependent translocation event (Ptacin *et al.*, 2010). In addition PomZ does not form filaments in presence of ATP as observed by TEM and does also not sediment by high speed centrifugation (personal communication A. Harms, MPI Marburg). Furthermore, a filament-pulling mechanism would not allow the cargo complex to stop at midcell, but would result in a more or less oscillatory motion between the nucleoid poles, as far as no second filament would pull from the other side, or the cargo gets immobilized similar to the PopZ-dependent immobilization in the case of ParB/*S* from *C. crescentus* or as in case of *M. xanthus* (Ebersbach *et al.*, 2008a, Harms *et al.*, 2013). We conclude that a filament-pulling mechanism seems not to be likely for the translocation of the PomXYZ cluster.

PomZ *in vivo* does not form a depletion zone “behind” the PomXY cluster during cluster motion, which was observed for SopA in *in vitro* reconstruction experiments with SopB*C* coated beads (Vecchiarelli *et al.*, 2014a). The highest local concentration of PomZ is observed within the PomXYZ

complex. We hypothesize, based on the symmetric localization of PomZ on the nucleoid and the FRAP experiments that PomZ is diffusing fast on the nucleoid. In the “diffusion-ratchet” model, a too fast recovery of ParA dimers would stall the cargo complex, because a ParA-gradient could not form. We hypothesize that the fast PomZ dynamics explain that the PomXYZ systems lacks a PomZ-depleted area behind the PomXY cluster (Vecchiarelli *et al.*, 2010, Vecchiarelli *et al.*, 2013a, Vecchiarelli *et al.*, 2013b). Similarly to the “filament-pulling” mechanism, a “diffusion ratchet” mechanism would also lead to directional motion to the end of the nucleoid and could not explain why a PomXYZ cluster shows a constrained motion around the midcell area.

The PomXY complex, like MinE follows the local concentration gradient of its cognate ParA ATPase, but colocalizes with it in the PomXYZ cluster. In theory the PomXY complex could be handed over from one PomZ dimer to the next on the nucleoid, reminiscent to the “Tarzan in the jungle” model for MinE chasing MinD on the membrane (Park *et al.*, 2011). However, binding to the membrane by MinE by a hidden membrane targeting sequence is part of the model, implicating that either PomX, or PomY would have to bind to DNA themselves to be transported from PomZ dimer to the next.

Finally, translocation of the PomXY complex could be executed as described in the DNA-relay model. The DNA-relay model does not implement any kind of polymeric structure of ParA but just relies on the capacity of a ParA dimer to bind to the supercoiled nucleoid and tether the cargo complex of ParB-*parS* (Lim *et al.*, 2014). This would fit with the observations made for PomZ. However, PomZ does not form a global gradient as described for the *C. crescentus* ParA, along the nucleoid, from one cell pole to the other (Lim *et al.*, 2014). Furthermore PomZ is highly dynamic on the DNA. If PomZ would transport the PomXY complex utilizing the elastic capacity of the nucleoid as described in this model, we would expect that the lateral PomZ diffusion on the nucleoid would have to be slower, since force could not be generated if PomZ-DNA interaction is transient. By addition in the “diffusion-ratchet” and the in the “DNA-relay” model the ParB/*S* complex is tethered to the nucleoid by single ParA dimers, which allows in case of the diffusion-ratchet model a phase of diffusion and in case of the DNA-relay model a reliable translocation from one nucleoid attached ParA dimer to the other. PomZ by contrast accumulates at the interphase of nucleoid and PomXY complex and shows the highest local concentration at this position, suggesting that several dimers are bound at any time. Based on calculations, 10 % of PomZ-mCherry signal in the cluster correspond to approximately 100-150 PomZ molecules (personal communication A.Treuner-Lange). Furthermore it is hard to believe that single ParA dimers, bound to the nucleoid are able to translocate a complex of hundreds of PomX and PomY molecules with the size of several megadalton (MDa). The actual force that is generated by the diffusive PomZ fluxes on the nucleoid must be a sum of several PomZ molecules in the PomXYZ complex. Because there is a continuous diffusive flux of PomZ on the nucleoids creating a local PomZ gradient along the PomXY cluster the net force of several PomZ-PomXY interactions translocates the PomXY cluster towards the higher concentration of PomZ (Figure 59). The idea that several PomZ molecules create a net force by an unknown mechanism would also explain the high level of precision in finding midcell and the relative low level of stochasticity in the cluster translocation towards midcell. We conclude that the mechanism by which cargo motion is braught about is unclear for the PomXYZ system with the only exception that a “filament pulling” mechanism is unlikely based on the lack of observable filaments by PomZ *in vivo* and *in vitro*.

Although the PomXYZ system is only conserved in close relatives of *M. xanthus* the ParA-like ATPases are highly versatile and can in orchestrated function with their AAP's produce different cellular patterns. We therefore think that although cell division might be regulated differently in other bacteria the mechanism by which PomZ positions a cellular protein complex at the mid-nucleoid might be used to position other cellular complexes or plasmids.

PpfA from *R. spaeroides* together with its AAP TlpT adopts a similar cellular pattern as the PomXYZ system. PpfA on its own associates with the nucleoid in an ATP-dependent manner and interacts with TlpT to form a visible complex in form of a cluster *in vivo* (Roberts *et al.*, 2012). Like the PomXYZ complex the PpfA/TlpT complex is positioned to the mid-nucleoid before cell division but by an unknown mechanism duplicates and moves to the ¼ and ¾ positions. We hypothesize that the relocalization mechanism depends on nucleoid duplication before cell division but chromosome organization has not been studied in *R. phaeroides* so far. By contrast the PomXYZ complex stays at the mid-nucleoid and we suggest that at some point it interacts with the cell division machinery. This leads to the conclusion that the positioning mechanism may be similar, but the function and the interaction partners are different. While PomXYZ position the cell division site at midcell, PpfA's function is to position and segregate chemoreceptors to allow that newborn cells are able to sense signals. However, like PpfA/TlpT also the PomXYZ complex duplicates and relocates to the new mid-nucleoid, but after cell division.

Furthermore it was recently been shown that *Streptococcus elongatus* PCC7942 positions caboxysomes in a ParA-dependent manner (Savage *et al.*, 2010). Like PpfA this ParA ATPase is required to reliably position carboxysomes and distribute them upon cell division. Deletion of ParA and the mis-segregation of the caboxysomes result in growth defects in *S. elongatus*. Although the mechanism for the positioning of carboxysomes is not understood tethering the carboxysomes to the nucleoids would allow faithful segregation of both important cellular structures upon cell division (Savage *et al.*, 2010). Generally, coupling of cellular processes to chromosome replication and segregation seems to be an easy way to synchronize important cellular functions with cell division and this is also done by the PomXYZ system in an elegant way.

6.5 PomXYZ system couples cell division to the end of chromosome replication and its segregation

In bacteria cell division is directly linked to the end of chromosome replication and its segregation as well as to cell growth to guarantee that daughter cells are of appropriate size and to protect genomic integrity upon proliferation. Based on these systems the question arises what couples chromosome segregation to the initiation of cell division in *M. xanthus*?

To couple initiation of cell division to cell cycle progression, *E. coli* and *B. subtilis* make usage of the combined function of the Min-system and the nucleoid occlusion effect facilitated by the two DNA-binding proteins SlmA and Noc, respectively (Bernhardt & de Boer, 2005, Wu & Errington, 2004). The Min-system inhibits cell division away from midcell, whereas the Noc and SlmA interfere with Z-ring formation over the nucleoid. Because SlmA and Noc bind to SBS and NBS away from the terminus region of the chromosome (Cho *et al.*, 2011, Tonthat *et al.*, 2013, Wu *et al.*, 2009) they enable cells to

initiate cell division at the end of chromosome segregation, giving a timing feature to the inhibition effect. Thus the orchestrated interplay of the Min-system and the nucleoid occlusion proteins SlmA and Noc allows cells to position Z-rings efficiently at midcell only in cells that have segregated nucleoids.

M. xanthus lacks a known homolog of SlmA or Noc that fulfills the same function. Therefore it is of debate if there is nucleoid occlusion. Interestingly, in cells of a Δ*pomXYZ* mutant, cell divisions do not take place over the multiple nucleoids, suggesting that nucleoid occlusion exists in *M. xanthus*. Similarly, to SlmA and Noc, PomZ binds to the nucleoid, potentially functioning as a protector for Z-ring formation over the DNA, but several lines of evidence suggest that PomZ has no function in nucleoid occlusion. First, lack of PomZ does not lead to cell divisions over the nucleoid. Secondly, purified His_6-PomZ has no effect on FtsZ filament formation in light-scattering assays (personal communication A. Harms, MPI Marburg) and finally, interference with chromosome replication (Huneke, 2013), chromosome segregation (Harms *et al.*, 2013) and chromosome structure, by deletion of *smc* (Stühn, 2013), results in cell division constrictions over the DNA even in the presence of PomZ, which contradicts that idea. This is consistent with the finding that cell division takes place over the nucleoids in absence of SlmA and Noc if chromosome metabolism is blocked (Bernhardt & de Boer, 2005, Wu & Errington, 2004). This strongly suggests that PomZ is not involved in any nucleoid occlusion function *in vivo* and furthermore that *M. xanthus* most likely does not utilize any nucleoid occlusion mechanism to position cell division.

C. crescentus utilizes the MipZ/ParB-system for efficient positioning of Z-rings at midcell. In contrast to the combined work of Min-system and nucleoid occlusion, MipZ alone organizes a spatial and temporal localization of FtsZ at midcell. Only after initiation of replication and spatial separation of the ParB-bound *ori*'s MipZ forms the bi-directional gradient in a PopZ-dependent manner, that allows Z-rings to form at midcell (Bowman *et al.*, 2008, Ebersbach *et al.*, 2008a, Thanbichler & Shapiro, 2006). *C. crescentus* was not shown to utilize a SlmA or Noc analogous protein but the coupling of chromosome segregation to cell division is only maintained by MipZ. However, why Z-rings do not constrict until nucleoids are finally fully separated is unknown. One could argue that *C. crescentus* either has a SlmA/Noc analogous protein that facilitates nucleoid occlusion or that cells have to acquire a certain length until the MipZ concentration at midcell is low enough to allow for Z-ring formation and constriction.

But what coordinates cell division with chromosome segregation in *M. xanthus*? The PomXYZ system brings up the cell division stimulating complex to the mid-nucleoid at midcell, early during chromosome replication and chromosome segregation. One possibility would be that recruitment of FtsZ to this complex is prohibited until chromosomes are segregated, because the nucleoid itself has influence on Z-ring formation. Alternatively, the PomXYZ complex could have to be released from the nucleoid before recruitment of FtsZ takes place. This would fit the notion that PomXYZ localize in between nuceloids in 10 % of cells. However, our data suggest that FtsZ is recruited to midcell before the end of replication. First, Z-rings form while replication is still ongoing, suggesting that chromosome segregation is not finished in these cell. Interestingly, constrictions are not observed over the nucleoids in *M. xanthus*, indicating a delay between FtsZ recruitment and cell constriction. Secondly, Z-rings form over the nucleoid if chromosome metabolism is perturbed as mentioned earlier, excluding

that the nucleoid has influence on Z-ring formation and that the PomXYZ complex has to leave the nucleoid before the recruitment event. It would therefore be possible that FtsZ is recruited to the PomXYZ complex while it is still over the nucleoid, but the divisome switches from assembly to constriction only if the PomXYZ complex is released from the nucleoid in WT cells.

Because perturbation of chromosome replication, segregation and condensation results in cell division defects and cell divisions over the nucleoid the perfectly timed interplay between the ParABS mediated segregation and cell division could be another possible link between both processes. However, how these two systems are linked is not known.

7 Conclusion

In this study we analyzed the regulation of PomZ-dependent cell division and positioning of the cell division site in *M. xanthus*. More precisely, we identified PomX and PomY, two additional regulators for correct cell division and analyzed their function in PomZ-dependent regulation of cell division. We showed that PomX, PomY and PomZ interact *in vitro* and *in vivo*, where they associate into a cluster on the nucleoid. We demonstrated that ATP-binding and ATP-hydrolysis by PomZ is required for its dynamic association with the nucleoid and the PomXY complex and furthermore this DNA association is necessary for the recruitment of the complex to the DNA and for its dynamic relocation to the mid-nucleoid. We could show that PomZ is an active ATPase *in vivo* and *in vitro* and its ATP-hydrolysis is activated by both PomX and PomY and furthermore even elevated by a complex of both in presence of DNA. This shows that PomZ is the first ParA ATPase that is regulated by two AAP's at the same time. We further showed that the N-terminal region of PomX mediates interaction to PomZ and thereby stimulates ATP-hydrolysis. This ATP-hydrolysis is required for the dynamic translocation by biased random motion towards the mid-nucleoid, which coincides with midcell before chromosomes have been segregated and its constrained motion at the mid-nucleoid.

Based on our data we proposed a model in which a diffusive flux of PomZ on the nucleoid into the PomXY complex scales with the amount of nucleoid-bound PomZ on either side of the cluster. This PomZ flux on either side of the cluster is different if the cluster is in the off-centre position. The flux difference creates a local PomZ gradient on the cluster-DNA interface which leads to the preferential motion towards the higher concentration of PomZ. We tested this model by analyzing the PomXYZ cluster motion towards midcell under different conditions and could elucidate different prerequisites for the PomXYZ system to function properly.

First, the cycling of PomZ between an ATP-bound dimeric and an ADP-bound monomeric phase is required for the dynamic motion of the PomXYZ cluster on the DNA. Secondly, the nucleoid geometry is required for the cluster motion towards midcell. Third, PomZ is highly dynamic in the cluster where ATP-hydrolysis takes place, as well as on the nucleoid giving strong evidence for the diffusive PomZ flux on the DNA. Finally, the system finds the mid-nucleoid independently of *M. xanthus* cells, as PomXYZ form DNA-associated clusters in *E. coli* which does not possess the PomXYZ system but uses the Min-system instead for regulation of cell division site placement.

In conclusion, we identified a completely novel system for regulation of cell division and cell division site placement at midcell in the rod-shaped soil bacterium *M. xanthus*. This system incorporates PomZ a member of the highly diverse class of ParA-ATPases that localizes a cell division regulator complex at midcell by finding the middle of the nucleoid. At midcell we propose that PomXYZ recruit FtsZ and by addition stimulate Z-ring formation. With this system, we hypothesize, *M. xanthus* cells coordinate chromosome segregation with cell division positioning. However, it is still elusive what PomXYZ do to FtsZ and how Z-ring formation is stimulated and furthermore how they dissociate from the nucleoid at midcell, to form a complex in between the segregated chromosomes. This will be analyzed in the future.

8 Material and Methods

8.1 Chemicals, equipment and software

All chemicals (Table 1), enzymes (Table 2) and kits (Table 3) used in this study are listed in 8.1 together with their suppliers. Technical equipment, as well as their providing companies, is listed in Table 4. Specific software used for data analysis is listed in Table 5 with their suppliers.

Table 1: Reagents and antibiotics used in this study

Reagents	Supplier
Chemicals	Carl Roth GmbH u. Co KG (Karlsruhe) Millipore Merck Chemicals GmbH (Schwalbach) Sigma-Aldrich (Taufkirchen)
Media components, agar	Carl Roth GmbH u. Co KG (Karlsruhe) Millipore Merck Chemicals GmbH (Schwalbach) BD Difco (Heidelberg) Invitrogen™ life technologies (Karlsruhe)
Oligonucleotides	Eurofins MWG Operon (Ebersberg) Invitrogen™ life technologies (Karlsruhe)
Rabbit antisera	Eurogentec (Seraing, Belgium)
Sterile filters (0.22 µm/0.45 µm)	Millipore Merck Chemicals GmbH (Schwalbach)
Uranyl acetate	Plano GmbH (Wetzlar)
Electron microscopy grids	Plano GmbH (Wetzlar)
96-well plates	Greiner Bio-One GmbH, Frickenhausen
Radioactive ATP/GTP	Hartmann Analytic GmbH (Braunschweig)
PVDF membrane	GE Healthcare Europe GmbH (Freiburg)
Anti-GFP monoclonal antibody	Roche Diagnostics GmbH (Mannheim)
Luminata Western HRP Substrate	Millipore Merck Chemicals GmbH (Schwalbach)
Goat anti-rabbit IgG	Pierce™ Thermo Scientific™ (Darmstadt)
Instant Blue	expedeon (Cambridgeshire, UK)
Protino® Ni-NTA agarose	Macherey-Nagel (Düren)
SDS gel electrophoresis size standards	
Pageruler™ Plus Prestained Protein Ladder	Pierce™ Thermo Scientific™ (Darmstadt)
Agarose gel electrophoresis size standards	
2nd-log DNA Ladder	New England Biolabs (Frankfurt a. M.)
Antibiotics	
Kanamycin sulfate	Carl Roth GmbH u. Co KG (Karlsruhe)
Chloramphenicol	
Ampicillin sodiumsulfate	
Gentamycin sulfate	
Oxytetracycline dehydrate	
Tetracycline hydrochloride	

Cephalexin hydrate	Sigma-Aldrich (Taufkirchen)
Hydroxy-urea	

Table 2: Enzymes used in this study

Enzymes	Supplier
Restriction endonucleases	New England Biolabs (Frankfurt a. M.)
Antarctic Phosphatase	
T4-DNA Ligase	
5 PRIME Master Mix	5 PRIME GmbH (Hilden)
Phusion High-Fidelity DNA Polymerase	Thermo Scientific™ (Darmstadt)

Table 3: Kits used in this study

Kits	Supplier
NucleoSpin® Gel and PCR Clean-up Kit	Macherey-Nagel (Düren)
Qiaquick Gel Extraction Kit	Qiagen (Hilden)
NucleoSpin® Plasmid Kit	Macherey-Nagel (Düren)
QIAprep Spin Miniprep Kit	Qiagen (Hilden)
MasterPure DNA purification kit	Epicentre Biotechnologies® Biozym (Oldendorf)
QuickChange II XL site directed mutagenesis kit	Stratagene Agilent Technologies (Waldbronn)
Bacterial Two Hybrid Kit	Euromedex (Souffelweyersheim, France)

Table 4: Equipment used in this study

Device	Application	Manufacturer
Branson Sonifier	Cell disruption	Heinemann (Schwäbisch Gmünd)
MasterCycler personal **MasterCycler epigradient**	Polymerase Chain Reaction	Eppendorf (Hamburg)
Thermomixer Compact **Thermomixer Comfort**	Incubation of small reaction volumes	Eppendorf (Hamburg)
Multifunktionsreader Infini te M200 Pro with Monochromatoroptics	Detection of color changes in colorimetric enzyme assays.	Tecan Deutschland GmbH (Crailsheim)
GenePulser Xcell	Elektroporation of bacterial cells	Bio-Rad (München)
Mini-PROTEAN® 3 cell **Mini-PROTEAN® TetraCell**	Protein Gelelectrophoresis	Bio-Rad (München)
Fuji Photo Film FPM 100A **Luminescent image analyser LAS-4000**	Chemiluminescence detection	Fujifilm (Düsseldorf)

Ultrospec 2100 pro Sprectrophotometer **Nanodrop ND-1000 UV-Vis spectrophotometer**	Determination of optical densities Nucleic acid quantification	GE Healthcare Europe GmbH (Freiburg) Nanodrop (Wilmington)
TransBlot® Turbo™Transfer System	Western blotting	Bio-Rad (München)
Airfuge™	Ultracentrifugation of proteins in small volumes	Beckman Coulter (Krefeld)
Eppendorf Centrifuge 5424 **Eppendorf Centrifuge 5424 R**	Centrifugation of small reaction volumes	Eppendorf (Hamburg)
Thermo Scientific Heraeus Multifuge 1S-R	Centrifugation 15 ml and 50 ml Falcon Tubes	Thermo Scientific™ (Darmstadt)
Optima™ L-90K Ultracentrifuge	Separation of soluble and insoluble cellular parts after cell disruption	Beckman Coulter (Krefeld)
Avanti® J-26 XP Centrifuge	Harvesting of big cell cultures	Beckman Coulter (Krefeld)
E-BOX VX2 imaging system	Illumination of DNA in agarose gels	PeqLab (Erlangen)
ÄKTA pure with Fraction collector F9-C **- 5 ml HiTrap Q HP** **- 5 ml HiTrap Chelating HP** **-HiLoad 16/600 Superdex 200 pg** **- 5 ml HiTrap SP HP**	Size exclusion chromatography, anion-, cation-exchange chromatography, affinity purification of recombinant proteins	GE Healthcare Europe GmbH (Freiburg)
4800 plus MALDI TOF/TOF Analyzer	Identification of proteins	Applied Biosystems (Darmstadt)
DMI6000B microscope with adaptive focus control (AFC) **- temperature control** **- HCX PL APO 100x/1.47 oil Corr TIRF objective** **- Hamamatsu Flash 4.0 camera**	Fluorescence microscopy	Leica (Wetzlar) Hamamatsu Photonics (Hersching)
Nikon Ti-E microscope with Perfect Focus System (PFS) **- temperature control** **- CFI PL APO 100x/1.45 Lambda oil** **- Hamamatsu Flash 4.0 camera**	Fluorescense recovery after photobleaching (FRAP) experiments	Nikon GmbH (Düsseldorf) Hamamatsu Photonics (Hersching)

JEM-1400 Plus Electron Microscope	Transmission electron microscopy	Jeol GmbH (Freising)

Table 5: Software used for data analysis

Software	Application	Supplier
Metamorph® v 7.5	Data analysis of microscopy pictures	Molecular Devices (Union City, CA)
Leica MM AF	Image acquisition and data analysis of microscopy pictures	Leica (Wetzlar)
NIS Elements AR 2.30 software	Image acquisition for FRAP microscopy	Nikon
Vector NTI advance software, suite 11	Checking of DNA and proteins sequences, *in silico* cloning of plasmids and data management of DNA, protein and plasmid sequences.	Invitrogen™ life technologies (Karlsruhe)

8.2 Media

Depending on the bacteria and the purpose, different media were used for cultivation. *E. coli* cells were predominantly grown in LB medium and on LB agar plates. For expression of proteins sometimes 2 x YT was used. *M. xanthus* cells were grown in 1 % CTT medium or on 1 % CTT agar plates. The media used in this study and their composition is listed in Table 6.

Table 6: Media used for bacterial growth

Medium	Composition	Usage
Luria-Bertani (LB)	1 % (w/v) tryptone, 0,5 % (w/v) yeast extract, 1 % (w/v) NaCl	Cultivation of *E. coli* strains.
LB agar plates	LB medium 1 % (w/v) agar	Cultivation of *E. coli* strains.
LB agar plates for blue-white screening	LB medium 1 % (w/v) agar 40 µg/ml Xgal	Cultivation of *E. coli* BTH101 cells for analysis of Bacterial Two Hybrid assay.
2 x YT	16 g Bacto tryptone, 5 g yeast extract, 5 g NaCl, pH 7.2	Cultivation of *E. coli* strains for heterologous expression of proteins.

1 % CTT	1 % (w/v) BactoTM casitone, 10mM Tris-HCl pH 8.0, 1mM potassium phosphate buffer pH 7.6, 8mM MgSO4	Cultivation medium of *M. xanthus* strains.
1 % CTT agar plates	1 % CTT medium 1.5 % (w/v) agar	Cultivation medium of *M. xanthus* strains.
1 % CTT soft agar	1 % CTT medium 0.5 % (w/v) agar	This medium was used for recovery of transformed *M. xanthus* strains.
1 % CTT galactose plates	1 % CTT medium 1.5 % (w/v) agar 2 % - 3 % (w/v) galactose	Media for selection of 2nd homologous recombination of *galK* containing plamids
TPM buffer	10 mM Tris-HCl pH 7.6 1 mM KH2PO4 pH 7.6 8 mM MgSO4	*M. xanthus* starvation assay medium
TPM agarose	10 mM Tris-HCl pH 7.6 1 mM KH2PO4 pH 7.6 8 mM MgSO4 1 % (w/v) SeaKem LE agarose (Cambrex)	Medium for microscopy of bacterial cells on agar surface for snapshots.
TPM-CTT agarose	10 mM Tris-HCl pH 7.6 1 mM KH2PO4 pH 7.6 8 mM MgSO4 1 % (w/v) SeaKem LE agarose (Cambrex) 0.25 % CTT	Medium for time-lapse microscopy of bacterial cells. Enables cells to grow and divide without creating much background fluorescence.

Table 7: Media additives and their concentrations used for bacterial growth media

Additive	Final concentration	Stock concentration	Dissolved in
E. coli			
Ampicillin sodium salt	100 µg/ml	100 mg/ml	H2O
Carbenicillin sodium salt	100 µg/ml	100 mg/ml	H2O
Chloramphenicol	50 µg/ml	50 mg/ml	99.99 % EtOH
Kanamycin sulfate	100 µg/ml	100 µg/ml	H2O
Tetracycline	15 µg/ml	15 mg/ml	99.99 % EtOH
Isopropyl β-D-1-thiogalactopyranoside (IPTG)	0.1 mM-1 mM	1 M	H2O

5-Brom-4-chlor-3-indoxyl-β-D-galactopyranosid (X-gal)	40 µg/ml	20 mg/ml	Dimethylformamid
M. xanthus			
Kanamycin sulfate	50 µg/ml	50 mg/ml	H2O
Oxytetracycline	10 µg/ml	10 mg/ml	100 mM HCl
Gentamycin sulfate	10 µg/ml	10 mg/ml	H2O
Cephalexin	35 µg/ml	5 mg/ml	H2O
CuSO4	400 mM	150 µM	H2O

8.3 Microbiological methods

8.3.1 *E. coli* strains used in this study

Table 8: *E. coli* strains used in this study

Strain	Genotype	Reference
TOP10	F$^-$ *mcr*A Δ(*mrr-hsdRMS-mcrBC*) Φ80*lac*ZΔM15 Δ*lac*X74 *rec*A1 *ara*D139 Δ(*ara leu*) 7697 *gal*U *gal*K *rps*L (Str^R) *end*A1 *nup*G	Invitrogen™ life technologies (Karlsruhe)
BTH101	F$^-$ *cya-99 araD139 galE15 galK16 rpsL1* (Str^R) *hsdR2 mcrA1 mcrB1*	Euromedex, (Souffelweyersheim, France)
Rosetta™2(DE3)	F$^-$ *ompT hsdS$_B$* (r$_B$- m$_B$-) *gal dcm* (DE3) pRARE2 (Cam^R)	Novagene® Merck (Darmstadt)
NEB Turbo	F$^-$ *proA$^+$B$^+$ lacI^q lacZM15 / fhuA2 (lac-proAB) glnV galK16 galE15 R(zgb-210::Tn10)*Tet^S *endA1 thi-1 (hsdS-mcrB)5*	New England Biolabs (Frankfurt a. M.)
Mach1	F$^-$ Φ80*lac*ZΔM15 Δ*lac*X74 *hsd*R(rK$^-$, mK$^+$) Δ*rec*A1398 *end*A1 *ton*A	Invitrogen™ life technologies (Karlsruhe)
BL21(DE3)	F$^-$ *ompT hsdS*$_B$ (r$_B^-$ m$_B^-$) *gal dcm* (DE3)	Invitrogen™ life technologies (Karlsruhe)
ArcticExpress(DE3)RP	*E. coli* B F$^-$ *ompT hsdS*(r$_B^-$ m$_B^-$) *dcm*$^+$ (Tet^R) *gal endA* Hte [*cpn10 cpn60* (Gent^R)] [*argU proL* (Str^R)]	Agilent Technologies (Waldbronn)
NiCo21(DE3)	*can::CBD fhuA2 [lon] ompT gal (λ DE3) [dcm] arnA::CBD slyD::CBD glmS6Ala hsdS λ DE3 = λ sBamHIo EcoRI-B int::(lacI::PlacUV5::T7 gene1) i21 nin5*	New England Biolabs (Frankfurt a. M.)

8.3.2 *M. xanthus* strains used in this study

Table 9: *M. xanthus* strains used in this study

Strain	Genotype	Reference
DK1622	Wild type	(Kaiser *et al.*, 1979)
SA3108	Δ*mxan_0635* (Δ*pomZ)*	(Treuner-Lange *et al.*, 2013)
SA3131	Δ*pomZ*/*attB*::P_{nat} *pomZ-mCherry* (pKA28), Tc^R	(Treuner-Lange *et al.*, 2013)
SA3139	*ftsZ*$^+$/*attB*::P_{nat} *ftsZ-mCherry* (pKA32), Tc^R	(Treuner-Lange *et al.*, 2013)
SA3142	Δ*pomZ*, *ftsZ*$^+$/*attB*::P_{nat} *ftsZ-mCherry* (pKA32), Tc^R	(Treuner-Lange *et al.*, 2013)
SA3146	Δ*pomZ*/*attB*::P_{nat} *pomZ*^{D90A}*-mCherry* (pKA43), Tc^R	(Treuner-Lange *et al.*, 2013)
SA3147	Δ*pomZ*/*attB*::P_{pilA} *pomZ-mCherry* (pKA45), Km^R	(Aguiluz Fabian, 2009)
SA3155	*ftsZ*$^+$/*attB*::P_{nat} *ftsZ-gfp* (pKA51), Tc^R	(Aguiluz Fabian, 2009)
SA3174	*pomX*$^+$/*attB*::P_{nat} *mCherry-PomX* (pKA46), Tc^R	(Aguiluz Fabian, 2009)
SA4202	*parB*$^+$/*attB*::P_{nat} *parB-eyfp* (pAH7), Tc^R	(Harms *et al.*, 2013, Treuner-Lange *et al.*, 2013)
SA4219	Δ*pomX*, *parB*$^+$/*attB*::P_{nat} *parB-eyfp* (pAH7), Tc^R	A. Harms (MPI, Marburg)
SA4223	Δ*mxan_0636* (Δ*pomX)*	A. Harms (MPI, Marburg)
SA4228	Δ*pomX*, *ftsZ*$^+$/*attB*::P_{nat} *ftsZ-mCherry* (pKA32), Tc^R	A. Harms (MPI, Marburg)
SA4229	Δ*pomX*/*attB*::P_{nat} *mCherry-pomX* (pKA46), Tc^R	A. Harms (MPI, Marburg)
SA4232	Δ*pomX*, *pomZ*$^+$/*attB*::P_{nat} *pomZ-mCherry* (pKA28), Tc^R	A. Harms (MPI, Marburg)
SA4244	Δ*pomX*/*attB*::P_{pilA} *mCherry-PomX* (pAH35), Km^R	A. Harms (MPI, Marburg)
SA4252	Δ*pomX*/*attB*::$P_{nat\,pomZ}$ *mCherry-pomX* (pAH53), Km^R	A. Harms (MPI, Marburg)
SA4254	Δ*mxan_0635*, Δ*mxan_0636* (Δ*pomZ,* Δ*pomX*)	A. Harms (MPI, Marburg)
SA4279	Δ*pomX*/P_{cuoA}::P_{cuoA} *mCherry-pomX* (pAH52), Km^R	A. Harms (MPI, Marburg)
SA4295	Δ*pomX*/P_{cuoA}::P_{cuoA} *mCherry-pomX*, *ftsZ*$^+$/*attB*::P_{nat} *ftsZ-gfp* (pAH52/ pKA51), Km^R, Tc^R	A. Harms (MPI, Marburg)
SA4297	*pomX*$^+$/*attB*::$P_{nat\,pomZ}$ *mCherry-pomX* (pAH53), Km^R	A. Harms (MPI, Marburg)
SA4703	Δ*mxan_0634* (Δ*pomY*)	(Schumacher, 2011)
SA4706	Δ*pomY, pomZ*$^+$/*attB*::P_{nat} *pomZ-mCherry* (pKA28), Tc^R	This study
SA4707	Δ*pomY*, *ftsZ*$^+$/*attB*::P_{nat} *ftsZ-mCherry* (pKA32), Tc^R	(Schumacher, 2011)
SA4709	Δ*pomY, parB*$^+$/*attB*::P_{nat}*parB-eyfp* (pAH7), Tc^R	(Schumacher, 2011)
SA4712	Δ*pomY*/*attB*::P_{pilA} *pomY-mCherry* (pDS7), Km^R	(Schumacher, 2011)
SA4713	Δ*pomY*/*attB*::P_{nat} *pomY-mCherry* (pDS8), Tc^R	(Schumacher, 2011)
SA4714	*pomY*$^+$/*attB*::P_{nat} *pomY-mCherry* (pDS8), Tc^R	This study
SA4718	*pilQ1*, Δ*ftsZ*/P_{cuoA}::P_{cuoA}*ftsZ*, *pomY*$^+$/*attB*::P_{pilA}*pomY-mCherry* (pNG10A*ftsZ*/ pDS7), Km^R, Tc^R, 300 µM $CuSO_4$	This study
SA4720	Δ*pomZ, pomY*$^+$/*attB*::P_{pilA} *pomY-mCherry* (pDS7), Km^R	This study
SA4722	Δ*mxan_0634-0636* (Δ*pomY,* Δ*pomZ,* Δ*pomX*)	This study
SA4725	*pomY*$^+$/*attB*::P_{pilA} *pomY-mCherry* (pDS7), Km^R	This study
SA4728	Δ*pomY*/*attB*::P_{nat} *pomY-eyfp* (pDS18), Tc^R	This study

SA4729	Δ*pomX*/P*cuoA*::P*cuoA mCherry-pomX*, *pomY*$^{+}$/*attB*::P$_{nat}$ *pomY-eyfp* (pAH52,pDS18), Km^{R}, Tc^{R}	This study
SA4734	Δ*pomY*/P*cuoA*::P*cuoA pomY-mCherry* (pDS21), Km^{R}	This study
SA4736	Δ*pomY*/P*cuoA*::P*cuoA pomY-mCherry*, *ftsZ*$^{+}$/*attB*::P$_{nat}$ *ftsZ-gfp* (pDS21, pKA51), Km^{R}, Tc^{R}	This study
SA4737	Δ*pomX*, *pomY*$^{+}$/*attB*::P*pilA pomY-mCherry* (pDS7), Km^{R}	This study
SA4738	*mxan_0633*$^{+}$/*attB*::P$_{nat}$ *mxan_0633-mCherry* (pDS24), Tc^{R}	This study
SA4739	Δ*pomY*, *pomX*$^{+}$/*attB*::P$_{nat}$*pomZ mCherry-pomX* (pAH53), Km^{R}	This study
SA4743	Δ*mxan_0634-0635* (Δ*pomY,* Δ*pomZ*)	This study
SA4420	Δ*mglA*	(Miertzschke *et al.*, 2011)
SA4746	Δ*mglA*, *pomY*$^{+}$/*attB*::P*pilA pomY-mCherry* (pDS7), Km^{R}	This study
SA4755	Δ*pomYZX*, *ftsZ*$^{+}$/*attB::ftsZ-mCherry* (pKA32), Tc^{R}	This study
SA4756	Δ*pomYZX*, *parB*$^{+}$/*attB*::P$_{nat}$ *parB-eyfp* (pAH7), Tc^{R}	This study
SA4758	Δ*pomZ*/*attB*::P$_{nat}$ *pomZ*^{D90A}*-mCherry*, *pomY*$^{+}$/P*cuoA*::P*cuoA pomY-eyfp* (pKA43, pDS22), Tc^{R}, Km^{R}	This study
SA4759	Δ*mxan_0633*	This study
SA4760	Δ*pomZ*/*attB*::P*pilA pomZ*^{K268A}*-mCherry* (pAH103), Km^{R}	This study
SA4761	Δ*pomZ*/*attB*::P*pilA pomZ*^{K268E}*-mCherry* (pAH104), Km^{R}	This study
SA4772	Δ*mglA,* Δ*pomZ*	This study
SA4777	Δ*mglA,* Δ*pomX*	This study
SA4779	Δ*mglA,* Δ*pomY*	This study
SA4796	Δ*mglA,* Δ*pomZ*, *pomY*$^{+}$/*attB*::P*pilA pomY-mCherry* (pDS7), Km^{R}	This study
SA4797	Δ*mglA,* Δ*pomX*/*attB*::P$_{nat}$*pomZ mCherry-pomX* (pAH53), Km^{R}	This study
SA4798	Δ*mglA,* Δ*pomZ*/*attB*::P$_{nat}$ *pomZ-mCherry* (pKA28), Tc^{R}	This study
SA4799	Δ*mglA*, Δ*pomZ*/*attB*::P*pilA pomZ*^{D90A}*-mCherry* (pEB13), Km^{R}	This study
SA5000	Δ*pomZ*/*attB*::P$_{nat}$ *pomZ*^{G62V}*-mCherry* (pEB16), Tc^{R}	E. Butaite (MPI, Marburg)
SA5001	Δ*pomZ*/*attB*::P$_{nat}$ *pomZ*^{K66Q}*-mCherry* (pKA55), Tc^{R}	E. Butaite (MPI, Marburg)
SA5003	Δ*pomZ*/*attB*::P*pilA pomZ*^{G62V}*-mCherry* (pEB10), Km^{R}	E. Butaite (MPI, Marburg)
SA5004	Δ*pomZ*/*attB*::P*pilA pomZ*^{K66Q}*-mCherry* (pEB11), Km^{R}	E. Butaite (MPI, Marburg)
SA5006	Δ*pomZ*/*attB*::P*pilA pomZ*^{D90A}*-mCherry* (pEB13), Km^{R}	E. Butaite (MPI, Marburg)
SA5802	*pomZ*$^{+}$/*attB*::P*pilA pomZ-mCherry* (pKA45), Km^{R}	A. Harms (MPI, Marburg)
SA5821	Δ*pomZ*, *pomX*$^{+}$/*attB*::P$_{nat}$*pomZ mCherry-pomX* (pAH53), Km^{R}	A. Harms (MPI, Marburg)
SA5836	Δ*pomZ*/*attB*::P$_{nat}$ *pomZ*^{K268A}*-mCherry* (pAH99), Tc^{R}	A. Harms (MPI, Marburg)
SA5837	Δ*pomZ*/*attB*::P$_{nat}$ *pomZ*^{K268E}*-mCherry* (pAH100), Tc^{R}	A. Harms (MPI, Marburg)
SA6100	*pomX*::*pomX*$^{K13A;R15A}$	(Huneke, 2013)
SA6130	Δ*mxan_0634*, Δ*mxan_0635* (Δ*pomY,* Δ*pomX*)	(Huneke, 2013)
SA6757	Δ*mglA, mxan4000::tetO-array, mxan18-19*::P$_{van}$ *tetR-eyfp* (pMAT13, pMAT112)	A. Treuner-Lange (MPI, Marburg)
SA7000	Δ*mglA,* Δ*pomY*/*attB*::P*pilA pomY-mCherry* (pDS7), Km^{R}	This study

SA7002	Δ*mglA,* Δ*pomZ*/*attB*::P_{pilA} *pomZ*^{K66Q}-*mCherry* (pEB11), Km^R	This study
SA7003	Δ*mglA,* Δ*pomZ*/*attB*::P_{pilA} *pomZ*^{G62V}-*mCherry* (pEB10), Km^R	This study
SA7008	Δ*mglA,* Δ*pomY*, *pomX*$^+$/*attB*::$P_{nat pomZ}$ *mCherry-pomX* (pAH53), Km^R	This study
SA7009	Δ*mglA,* Δ*pomZ*, *pomX*$^+$/*attB*::$P_{nat pomZ}$ *mCherry-pomX* (pAH53), Km^R	This study
SA7010	Δ*pomY*, Δ*pomZ*/*attB*::P_{nat} *pomZ*^{D90A}-*mCherry* (pKA43),Tc^R	This study
SA7011	Δ*mglA*, Δ*pomZ*/*attB*::P_{pilA} *pomZ-mCherry* (pKA45), Km^R	This study
SA7012	Δ*mglA,* Δ*pomZ*/*attB*::P_{pilA} *pomZ*^{K268E}-*mCherry* (pAH104), Km^R	This study
SA7014	Δ*pomX,* Δ*pomZ*/*attB*::P_{nat} *pomZ*^{D90A}-*mCherry*, (pKA43), Tc^R	This study
SA7015	Δ*mglA,* Δ*pomZ*/*mxan18-19*::P_{pilA} *pomZ* (pDS75), Tc^R	This study
SA7016	Δ*mglA,* Δ*pomZ*/*mxan18-19*::P_{pilA} *pomZ*, *pomY*$^+$/*attB*::P_{pilA} *pomY-mCherry* (pDS75, pDS7), Tc^R, Km^R	This study
SA7020	Δ*pomZ*/*attB*::P_{nat} *pomZ-mCherry*, *pomY*$^+$/P_{couA}::P_{couA} *pomY-eyfp* (pKA28, pDS22), Tc^R, Km^R	This study
SA7021	Δ*mglA*, *pomX*::*pomX*$^{K13A;R15A}$	This study
SA7022	Δ*mglA,* Δ*pomZ*/*mxan18-19*::P_{pilA} *pomZ*, *pomX*$^+$/*attB*::$P_{nat pomZ}$ *mCherry-pomX* (pDS75, pAH53), Tc^R, Km^R	This study
SA7024	Δ*pomY*/P_{cuoA}::P_{cuoA} *pomY-eyfp* (pDS22), Km^R	This study
SA7025	Δ*mglA*, *pomX*::*pomX*$^{K13A;R15A}$, *pomY*$^+$/*attB*::P_{pilA} *pomY-mCherry* (pDS7), Km^R	This study
SA7026	Δ*mglA,* Δ*pomZ*/*mxan18-19*::P_{nat} *pomZ*^{D90A} (pDS80), Tc^R	This study
SA7027	Δ*mglA,* Δ*pomZ*/*mxan18-19*::P_{nat} *pomZ*^{D90A}, *pomY*$^+$/*attB*::P_{pilA} *pomY-mCherry* (pDS80, pDS7), Tc^R, Km^R	This study
SA7039	Δ*pomX*/*attB*::$P_{nat pomZ}$ *mCherry-pomX* (pAH96), Tc^R	This study
SA7040	Δ*pomY*/*attB*::P_{pilA} *pomY-mCherry* (pDS19), Tc^R	This study
SA7041	Δ*pomY*/P_{cuoA}::P_{cuoA} *pomY-eyfp*, *pomX*$^+$/*attB*::$P_{nat pomZ}$mCherry-*pomX* (pDS22, pAH96), Km^R, Tc^R	This study
SA7042	Δ*pomX*/*attB*::$P_{nat pomZ}$ *mCherry-pomX*, *ssB*$^+$/P_{nat}*ssB*::P_{nat} *ssB-eyfp* (pAH96, pAH83), Tc^R, Km^R	This study
SA7043	Δ*pomY*/*attB*::P_{pilA} *pomY-mCherry*, *ssB*$^+$/P_{nat} *ssB*::P_{nat} *ssB-eyfp* (pDS19, pAH83), Tc^R, Km^R	This study

[1] Km^R and Tc^R indicate kanamycin and tetracycline resistance, respectively

[2] Plasmids in brackets contain indicated genes or gene fusions for integration at indicated sites on the genome. Fusions at the *attB* site and the *mxan18-19* intergenic region were expressed from the *pilA* promoter (P_{pilA}), their native promoter (P_{nat}) or the native promoter of *pomZ* ($P_{nat pomZ}$). Plasmids containing the *cuoA* promoter (P_{cuoA}) were under copper regulated gene expression and were integrated into the P_{cuoA}.

[3] + indicates that strains contained a native copy of the corresponding gene

[4] Δ indicates that a strain contains an in-frame deletion of the corresponding gene. Gene deletions were constructed as described in 8.4.3.

8.3.3 Cultivation of bacterial strains

All media and solutions were autoclaved for 20 min, 121 °C and 1 bar over-pressure. Antibiotics and other media additives were filtered using sterile 0.22 µm pore-size filters (Millipore Merck, Schwalbach) and were added to pre-cooled media at around 55 °C.

E. coli strains were used for cloning and propagation of plasmids as well as for heterologous expression of proteins and fluorescence microscopy. *E. coli* cells were grown aerobically on LB agar plates at 37 °C. *E. coli* liquid cultures were incubated aerobically on horizontal shakers at 37 °C and 230 rpm if not mentioned differently in the experimental procedure. If necessary, growth was followed by determination of the optical density at 600 nm (OD_{600}). *M. xanthus* cells were grown aerobically on 1 % CTT agar plates, containing selective antibiotics, at 32 °C in the dark. *M. xanthus* liquid cultures were grown in 1 % CTT liquid media, containing corresponding antibiotics, at 32 °C and 230 rpm in the dark in Erlenmeyer flasks in 1/10 of the total flask volume. Optical density was determined at 550 nm (OD_{550}). In general all media used for growing *M. xanthus* strains contained 10 µg/ml Gentamycin to prohibit contamination.

8.3.4 Short- and long-term storage of bacterial strains

E. coli and *M. xanthus* cultures on solid media were stored up to four weeks at 4 °C and 18 °C, respectively. For longer storage glycerol stocks were prepared. *E. coli* glycerol stocks were prepared from overnight cultures by addition of 333 µl 40 % (v/v) glycerol to 1 ml of culture in cryo-tubes. For *M. xanthus* stocks cells were grown to an OD_{550} of 0.8 - 1.0. 1 ml of the culture was then mixed with 333 µl 40 % (v/v) glycerol to a final concentration of 10 % (v/v). In both cases stocks were immediately frozen in liquid nitrogen and stored at -80 °C.

8.3.5 Bacterial Two Hybrid Assay (BACTH)

The Bacterial Two Hybrid system (Karimova *et al.*, 2005) was used in this study to detect direct interactions between two proteins of interest in a heterologous system in *E. coli.* Plasmids containing the T18 (pUT18 and pUT18C) and the T25 (pKT25 and pKNT25) fragment of the *Bordetella pertussis* adenylate cyclase gene were provided by the manufacturer (Euromedex, Souffelweyersheim, France). Plasmids were cloned containing N-terminal or C-terminal fusions of genes of interest to the T18 or T25 fragment of the adenylate cyclase. For the assay electro-competent cells of strain BTH101, lacking the *cyaA* gene, encoding the catalytic domain of the adenylate cyclase, were transformed with two plasmids as described by the manufacturer. Cells of strain BTH101 do not produce cyclic adenosine monophosphate (cAMP). If two hybrid proteins are expressed from the transformed plasmids and interact in this assay the parts of the catalytic domains of the *B. pertussis* adenylate cyclase come close. Hetero dimers of the hybrid proteins result in functional complementation of the T18 and the T25 fragment complementing the *cyaA*$^-$ phenotype of strain BTH101 and produce cAMP. cAMP production in term activates the expression of the *lac*-operon to produce β-galactosidase. The

enzyme cleaves X-gal, provided by the growth medium, which allows for blue-white screening of colonies. To test for functional complementation plasmids containing the gene of interest to T18 fragment were used as bait and co-transformed with a plasmid containing the second gene of interest fused to the T25 fragment. For transformation 10 ng – 25 ng of plasmid DNA were used. Co-transformed cells were spread on selective LB agar plates containing 100 µg/ml ampicillin, 50 µg/ml kanamycin, 0.5 mM IPTG and 40 µg/ml X-gal as indicator. Plates were incubated on 30 °C for 48 h. Pictures were acquired before and after additional incubation of the plates at 4 °C for 24 h to enhance the blue color of positive colonies. For comparison, for each screen the plasmids pUT18C-Zip and pKNT25-Zip were co-transformed as a positive control. Additionally each bait plasmid used in the screen was co-transformed with an empty pKT25 and pKNT25 plasmid as a negative control. For direct comparison 3 corresponding colonies and a "smear" of each co-transformation plate were inoculated into 1 ml LB medium containing 100 µg/ml ampicillin, 50 µg/ml kanamycin and 0.5 mM IPTG and incubated for 2 h shaking at 30 °C. After incubation 2 µl of each interaction pair to test were spot with all the controls on the same selective LB agar plate containing the same additives as described before and were incubated and imaged as described above.

8.4 Molecular biological methods

8.4.1 Plasmids and oligonucleotides

Primers that were used in this study together with their sequences are listed in Table 10. Blue sequences indicate recognition sites for restriction endonucleases, whereas red sequences indicate start and stop codons in the primer sequence. Orange sequences mark additional nucleotides that were used as linker sequences.

Table 10: List of primers used for cloning and sequencing in this study

Primer name	Description	Sequence 5' - 3'
Primers for generation of in-frame deletion of *mxan_0634* (*pomY*)		
KA-371	primer A fwd	CCGGAATTCCGACGAGCAGTTGAGCACCAG
MXAN_0634-5	primer B rev	GCGTCTAGAGAGCAGCGCGTCCGGACGCTC
KA-373	primer C fwd	GCGTCTAGAGTCACCCCAAGCCATTCC
KA-374	primer D rev	GCGAAGCTTCCTTGAAGTTCAGGAAGAGC
KA-375	primer E fwd	GGGTCTCCGCTGTATCGC
KA-376	primer F rev	GGCAGCGAGGACTTCTGG
KA-377	primer G fwd	GGAACCAGATGATGGACAAGC
KA-378	primer H rev	TCGTGGATGGCTTCCTCG
Primers for generation of in-frame deletion of *mxan_0636* (*pomX*)		
KA-224	primer A fwd	GCGGGATCCTCCACGTCCTACGCCTGG
MXAN0636-1	primer B rev	GCGTCTAGAGGACACGTTCTGTTCAAAGGC
MXAN0636-2	primer C fwd	GCGTCTAGACACCGGGCCCTGAGTCAGGCC
MXAN0636-3	primer D rev	GCCAAGCTTCAACGCGATGTCCGCGCCC
KA-284	primer E fwd	GCTCCAGACGCACTATCCG
KA-285	primer F rev	AGGACGGGAAGTAGCCAGG

Primers for generation of in-frame deletion of *mxan_4901* (*smc*)		
Mxan_4901-A	primer A fwd	GCGAAGCTTCTTCGCTGCGGGCGACCCGCG
Mxan_4901-B	primer B rev	GCGTCTAGAGCCGGTGATGTCCAACCGCTTG
Mxan_4901-C	primer C fwd	GCGTCTAGAGCCAACGACGACAAGGTGACG
Mxan_4901-D	primer D rev	GCGGGATCCGTCCGCGCCGGACGCCGCGTC
Mxan_4901-E	primer E fwd	GTGGCGAAGCGGGTGGAGGAC
Mxan_4901-F	primer F rev	GACCCGGGTGATGCGCGTCTC
Mxan_4901-G	primer G fwd	GACACGCTGCGGCTCGACATG
Mxan_4901-H	primer H rev	GGTCCCGCCGCCGCTGACGGC
Primers for generation of in-frame deletion of *mxan_0633*		
Mxan_0633-1	primer A fwd	GCGAAGCTTCGGACCTCCAGCTCCGCGACC
Mxan_0633-2	primer B rev	GCGTCTAGATGTCGAAAAGAGGGCTTCGTC
Mxan_0633-3	primer C fwd	GCGTCTAGAGGGCAGGTGGCGAACGCGCTC
Mxan_0633-4	primer D rev	GCGGAATTCCTGCCAGACCTGGCCCAGCGTC
Mxan_0633-5	primer E fwd	GGATGCGCCCCACGTCCAGCAG
Mxan_0633-6	primer F rev	CAGCGCGGGCTTCCACACGATG
Mxan_0633-7	primer G fwd	CGCACGCCATGGAACAACGAC
Mxan_0633-8	primer H rev	GTTCGCCACCTGCCCCAACAG
Primer for checking in-frame deletion of *mglA*		
mglA-E	primer E fwd	GTCGGAAGGGCTCTTTCAG
mglA-F	primer F rev	GACGTCTTCCCCGGCTCC
mglA-G	primer G fwd	GGCCCGGGCTCTGCGGGAAG
mglA-H	primer H rev	GCGTGTCGAAGACGCCCACGC
Primers for cloning of pDS24, containing P_{nat} *mxan_0633-mCherry*		
0633-1 fwd Pnat EcoRI	fwd	GCGGAATTCGGACAGCTCCGCGTGCTGCGC
0633-2 rev BglII	rev, w/o stop codon	GCGAGATCTCGTCTCGAGCGCGTTCGCCAC
Primers to check for Mx8 *attB* integration of plasmids		
attB left		CGGCACACTGAGGCCACATC
attB right		GGAATGATCGGACCAGCTGAA
attP left		GGGAAGCTCTGGGTGACGAA
attP right		GCTTTCGCGACATGGAGGA
Primers for cloning of plasmids containing *ftsZ* used in BACTH assay		
Mxan_5597 ftsZ XbaI	fwd, w. start codon	GCGTCTAGAGATGGACCAGTTCGATCAG
Mxan_5597 ftsZ KpnI	rev	GCGGGTACCCGCGGCAGTTCCGTCTGGCC
Primers for cloning of plasmids containing *pomX* and *pomX*^{K13A,R15A} used in BACTH assay		
Mxan_0636-1 pomX fwd	fwd, w. start codon	GCGTCTAGAGATGAAGAAAGCCTTTGAAC
Mxan_0636-2 pomX rev	rev	GCGGGTACCCGGCGCACCGTGGCCTGAC
Primers for cloning of plasmids containing *pomZ* used in BACTH assay		
Mxan_0635-4 pomZ fwd	fwd, w. start codon	GCGTCTAGAGATGGAAGCGCCGACGTAC
Mxan_0635-5 pomZ rev	rev	GCGGGTACCCGGCCGGCCTGCTGGGTGCC

Primers for cloning of plasmids containing *pomY* used in BACTH assay		
Mxan_0634-16 pomY fwd	fwd, w. start codon	GCGTCTAGAGGTGAGCGACGAGCGTCCG
Mxan_0634-17 pomY rev	rev	GCGGGTACCCGAGCGGCGAAGTATTTGTG
Primers for cloning pDS3, containing *pomY* for expression of *pomY-His$_6$* in *E. coli*		
Mxan_0634-11	fwd, w/o. start codon	GCGGAATTCGAGCGACGAGCGTC
Mxan_0634-12	rev, w/o. stop codon	CGCAAGCTTAGCGGCGAAGTATTTG
Primers for cloning pEMR3, containing *pomX* for expression of *pomX-His$_6$* in *E. coli*		
NdeI-pomX fwd		GGAATTCCATATGAAGAAAGCCTTTGAACAG
pomX c-term His rev		GCCAAGCTTGCGCACCGTGGCCTGACTCAGG
Primers for cloning pDS7, containing *pomY-mCherry*		
Mxan_0634-6	fwd, w. start codon	GCGTCTAGAGTGAGCGACGAGCGTCCG
mCherry stop rev HinDIII	rev, w. stop codon	GGGAAGCTTTTACTTGTACAGCTCGTC
Primers for cloning pDS8, containing P$_{nat}$*pomY-mCherry*		
KA-371	fwd	CCGGAATTCCGACGAGCAGTTGAGCACCAG
Mxan_0634-4	rev, w/o. stop	GGAAGATCTGGCGGAAGCGGCGAAGTATTTGTGCC
Primers for cloning pDS16, in-frame construct for deletion of *pomY* and *pomZ*		
Mxan_0635-1	fwd	GCGTCTAGACAGACGAAGGGCACCCAGCAG
Mxan_0635-2	rev	GCCAAGCTTCCGCTGCACCTCCACCTCGG
Primers for cloning pMAT12, in-frame construct for deletion of *pomX* and *pomZ*		
KA-200	fwd	CCGGAATTCCCTGCGCCAACTCCTCAG
Mxan_0635-3	rev	GCGTCTAGAAATCTGCTTCGGGGACACGCC
Primers for cloning pDS17, cloning vector for C-terminal e*yfp* fusions		
KA-396	fwd, 5 AA linker, w. start codon	GCGGGATCCGCCGCCGGCTCCGGCATGGTGAGCAAGGGCGAGG
KA-397	rev, w. stop codon	GCCAAGCTTTCACTTGTACAGCTCGTCCATGCC
Primers for cloning pDS18, containing P$_{nat}$*pomY-eyfp*		
KA-371	fwd, P$_{nat}$	CCGGAATTCCGACGAGCAGTTGAGCACCAG
Mxan0634 rev BglII+3AA linker	rev, w/o stop, 3 AA linker	GCGAGATCTGGCGGAGCCAGCGGCGAAGTATTTGTG
Primers for cloning pDS22, containing P$_{cuoA}$*pomY-eyfp*		
Mxan-0634-6	fwd w. start codon	GCGTCTAGAGTGAGCGACGAGCGTCCG
KA-397	rev, w. stop codon	GCCAAGCTTTCACTTGTACAGCTCGTCCATGCC

Primers for cloning pDS75, containing *mxan_0018-0019* intergenic region instead of *attB*		
Mxan18-19 fwd BsrDI	fwd	GCGATCATTGCGCGCCAGACGATAACAGGC
Mxan18-19 rev BlpI	rev	GCGGCTGAGCCCGCGCCGACAACCGCAACC
Primers for checking integration of pDS75 and its derivatives into *mxan_0018-0019* intergenic region		
18-19 int p75 fwd	fwd primer binding on plasmid	TTACTCTAGCTTCCCGGC
18-19 int p75 rev	rev primer binding on plasmid	GTCTGACGCTCAGTGGAAC
18-19 C fwd	fwd primer binding on chromosome	CCCACGGAGAGCTGCGTGAC
18-19 C rev	rev primer binding on chromosome	GAGAAGGGTGCCGTCACGTC
Primer for site directed mutagenesis of *pomZ*		
KA-413	*pomZ*^{G62V} fwd	TCCTGAACTTCAAGGTTGGCACCGGCAAGAC
KA-414	*pomZ*^{G62V} rev	GTCTTGCCGGTGCCAACCTTGAAGTTCAGGA
KA-417	*pomZ*^{K66Q} fwd	GGTGGCACCGGCCAGACGTCGCTGT
KA-418	*pomZ*^{K66Q} rev	ACAGCGACGTCTGGCCGGTGCCACC
KA-419	*pomZ*^{D90A} fwd	CTCATCGACCTCGCCAGCCAGGGCCAC
KA-420	*pomZ*^{D90A} rev	GTGGCCCTGGCTGGCGAGGTCGATGAG
AH-93	*pomZ*^{K268A} fwd	ATCCGGCAGTGCACCGCGTTCGCGCAGGCCTCC
AH-94	*pomZ*^{K268A} rev	GGAGGCCTGCGCGAACGCGGTGCACTGCCGGAT
AH-91	*pomZ*^{K268E} fwd	ATCCGGCAGTGCACCGAGTTCGCGCAGGCCTCC
AH-92	*pomZ*^{K268E} rev	GGAGGCCTGCGCGAACTCGGTGCACTGCCGGAT
Primers for cloning plasmids for expression of *pomY-eyfp* in *E. coli* (pRSFDuet-1 MCS1; pBAD24)		
Mxan_0634-18	fwd, BspHI (NcoI compatible)	GCGTCATGAGCGACGAGCGTCCGGAC
Mxan_0634-15	rev e*yfp*, stop codon	GCGAAGCTTTCACTTGTACAGCTCGTCCAT
Primers for cloning plasmids for expression of *mCherry-pomX* and *pomX* in *E. coli* (pRSFDuet-1 MCS1; pBAD24)		
mCherry BspHI fwd	fwd, BspHI (NcoI compatible), start codon	GCGTCATGAGCAAGGGCGAGGAGGATAAC
Mxan_0636 BspHI fwd	fwd, BspHI (NcoI compatible), start codon	GCGTCATGAAGAAAGCCTTTGAACAGAACG
Mxan_0636-3 HindIII rev stop	rev, stop codon	GCGAAGCTTTCAGCGCACCGTGGCCTGAC

Primers for cloning plasmids for expression of *pomZ-mCherry* in *E. coli* (pRSFDuet-1 MCS1; pBAD24)		
Mxan_0635 BspHI fwd	fwd, BspHI (NcoI compatible), start codon	GCGTCATGATGGAAGCGCCGACGTACAGC
KA-478	rev mCherry, stop codon	GCCAAGCTTTCATTACTTGTACAGCTCGTCCAT
Primers for cloning plasmids for expression of *pomZ-mCherry* in *E. coli* (pRSFDuet-1 MCS2)		
Mxan_0635 NdeI fwd	fwd, start codon	GCGCATATGGAAGCGCCGACGTACAGCTCC
mCherry rev stop PacI	rev, stop codon	GCCTTAATTAATCACTTGTACAGCTCGTCCATG
Primers for cloning plasmids for expression of *ftsZ-gfp* in *E. coli* (pRSFDuet-1 MCS2)		
AH-113	fwd, start codon	GGAATTCCATATGGACCAGTTCGATCAGAACAAG
AH-115	rev, stop codon	GCGATATCTTACTTGTACAGCTCGTCCATGCC

Table 11: List of plasmids used in this study and their description

Plasmid	Description	Reference
pSW105	Vector containing *Mx8 attP* fragment for integration into genomic *Mx8 attB* site, contains P_{pilA}, Km^R	S. Weiss (MPI Marburg)
pSWU30	Vector containing *Mx8 attP* fragment for integration into genomic *Mx8 attB* site, Tc^R	(Wu *et al.*, 1997)
pBJ114	Vector containing Km^R and *galK* gene, used for in-frame deletion of genes and native site integration of plasmid DNA.	(Julien *et al.*, 2000)
pUT18	Vector containing T18 fragment of *B. pertussis* adenylate cyclase. Used for N–terminal fusions to T18 fragment in BACTH assay, Amp^R	Euromedex (France)
pUT18C	Vector containing T18 fragment of *B. pertussis* adenylate cyclase. Used for C–terminal fusions to T18 fragment in BACTH assay, Amp^R	Euromedex (France)
pKT25	Vector containing T25 fragment of *B. pertussis* adenylate cyclase. Used for C–terminal fusions to T25 fragment in BACTH assay, Km^R	Euromedex (France)
pKNT25	Vector containing T25 fragment of *B. pertussis* adenylate cyclase. Used for N–terminal fusions to T25 fragment in BACTH assay, Km^R	Euromedex (France)
pET-24b+	Vector for cloning C-terminal *His6*-tag fusions for heterologous expression in *E. coli*, Km^R	Millipore Merck (Schwalbach)

pRSFDuet™-1	Vector for the expression of up to two genes at the same time under the regulation of an IPTG-inducible T7 promoter with a *lac* operator. Km^R	Millipore Merck (Schwalbach)
pBAD24	Vector with an arabinose-inducible expression system for *E. coli*, Amp^R	(Guzman *et al.*, 1995)
pUC18	General cloning vector, Amp^R	Thermo Scientific™ (Darmstadt)
pNG10A	Vector containing P_{couA} for integration into P_{couA} genomic region, Tc^R	(Gomez-Santos *et al.*, 2012)
pNG10A*ftsZ*	pNG10A, *ftsZ,* Tc^R	(Treuner-Lange *et al.*, 2013)
pMAT11	Vector containing P_{couA} for integration into P_{couA} genomic region, Km^R	A. Treuner-Lange (MPI Marburg)
pMR3691	Vector for expression of genes under regulation of a vanillate-inducible promoter for integration into the *mxan0018-0019* intergenic region. Tc^R	(Iniesta *et al.*, 2012)
pKA1	pBJ114 with up and downstream fragment for in-frame deletion of *mxan_0635*, Km^R	(Treuner-Lange *et al.*, 2013)
pKA3	pET-24b$^+$ with *pomZ* for expression of *pomZ-His$_6$*, Km^R	(Treuner-Lange *et al.*, 2013)
pKA19	pSW105, *pomZ,* Km^R	(Treuner-Lange *et al.*, 2013)
pKA28	pSWU30, P_{nat}*pomZ-mCherry*, Tc^R	(Treuner-Lange *et al.*, 2013)
pKA32	pSWU30, P_{nat}*ftsZ-mCherry*, Tc^R	(Treuner-Lange *et al.*, 2013)
pKA43	pSWU30, P_{nat}*pomZ*^{D90A}*-mCherry*, Tc^R	(Treuner-Lange *et al.*, 2013)
pKA45	pSW105, *pomZ-mCherry*, Km^R	K. Aguiluz-Fabian (MPI Marburg)
pKA46	pSWU30, P_{nat}*mCherry-pomX*, Tc^R	K. Aguiluz-Fabian (MPI Marburg)
pKA51	pSWU30, P_{nat}*ftsZ-gfp*, Tc^R	(Treuner-Lange *et al.*, 2013)
pKA55	pSWU30, P_{nat}*pomZ*^{K66Q}*-mCherry*, Tc^R	K. Aguiluz-Fabian (MPI Marburg)
pKA70	pET45b+, with *ftsZ* for expression of native *ftsZ*, Amp^R	(Treuner-Lange *et al.*, 2013)
pEB10	pSW105, *pomZ*^{G62V}*-mCherry*, Km^R	E. Butaite (MPI Marburg)
pEB11	pSW105, *pomZ*^{K66Q}*-mCherry*, Km^R	E. Butaite (MPI Marburg)
pEB13	pSW105, *pomZ*^{D90A}*-mCherry*, Km^R	E. Butaite (MPI Marburg)
pEB16	pSWU30, P_{nat} *pomZ*^{G62V}*-mCherry*, Tc^R	E. Butaite (MPI Marburg)
pAH7	pSWU30, P_{nat} *parB-eyfp*, Tc^R	(Harms *et al.*, 2013)
pAH35	pSW105, *mCherry-pomX*, Km^R	A. Harms (MPI Marburg)
pAH52	pMAT11, *mCherry-pomX*, Km^R	A. Harms (MPI Marburg)
pAH53	pSW105, $P_{nat_{pomZ}}$ *mCherry-pomX*, Km^R	A. Harms (MPI Marburg)
pAH83	pBJ114, P_{nat}*ssb-eyfp*	A. Harms (MPI Marburg)

pAH96	pSWU30, P_{nat}*pomZ* *mCherry-pomX*, Tc^R	A. Harms (MPI Marburg)
pAH99	pSWU30, P_{nat} *pomZ*^{K268A}*-mCherry*, Tc^R	A. Harms (MPI Marburg)
pAH100	pSWU30, P_{nat} *pomZ*^{K268E}*-mCherry*, Tc^R	A. Harms (MPI Marburg)
pAH103	pSW105, *pomZ*^{K268A}*-mCherry*, Km^R	A. Harms (MPI Marburg)
pAH104	pSW105, *pomZ*^{K268E}*-mCherry*, Km^R	A. Harms (MPI Marburg)
pAH106	pRSFDuet™-1, *pomZ*^{G62V}*-mCherry*, Km^R	A. Harms (MPI Marburg)
pAH107	pRSFDuet™-1, *pomZ*^{K66Q}*-mCherry*, Km^R	A. Harms (MPI Marburg)
pAH108	pRSFDuet™-1, *pomZ*^{D90A}*-mCherry*, Km^R	A. Harms (MPI Marburg)
pAH109	pRSFDuet™-1, *pomZ*^{K268A}*-mCherry*, Km^R	A. Harms (MPI Marburg)
pAH110	pRSFDuet™-1, *pomZ*^{K268E}*-mCherry*, Km^R	A. Harms (MPI Marburg)
pMAT12	pBJ114 with up- and downstream fragment for in-frame deletion of *mxan_0635-0636*	A. Treuner-Lange (MPI Marburg)
pSL16	pBJ114 with up- and downstream fragment for in-frame deletion of *mglA*	(Miertzschke *et al.*, 2011)
pDS1	pBJ114 with up- and downstream fragment for in-frame deletion of *mxan_0634*, Km^R	(Schumacher, 2011)
pDS3	pET-24b$^+$ with *pomY* for expression of *pomY-His$_6$*, Km^R	(Schumacher, 2011)
pDS7	pSW105, *pomY-mCherry*, Km^R	(Schumacher, 2011)
pDS8	pSWU30, P_{nat}*pomY-mCherry*, Tc^R	(Schumacher, 2011)
pDS12	pBJ114 with up- and downstream fragment for in-frame deletion of *mxan_0634-0636*	This study
pDS16	pBJ114 with up- and downstream fragment for in-frame deletion of *mxan_0634-0635*	This study
pDS17	pSWU30, (3 AA linker)-e*yfp*, Tc^R	This study
pDS18	pSWU30, P_{nat}*pomY-eyfp*, Tc^R	This study
pDS19	pSWU30, P_{pilA}*pomY-mCherry*, Tc^R	This study
pDS21	pMAT11, *pomY-mCherry*, Km^R	This study
pDS22	pMAT11, *pomY-eyfp*, Km^R	This study
pDS23	pBJ114 with up- and downstream fragment for in-frame deletion of *mxan_0633*	This study
pDS24	pSWU30, P_{nat}*mxan_0633-mCherry*, Tc^R	This study
pDS27	pBJ114 with up- and downstream fragment for in-frame deletion of *mxan_4901* (*smc*)	This study
pDS37	pRSFDuet™-1, *mCherry-pomX*, Km^R	This study
pDS38	pBAD24, *pomX*, Amp^R	This study
pDS43	pRSFDuet™-1, *pomZ-mCherry*, Km^R	This study
pDS45	pBAD24, *pomY-eyfp*, Amp^R	This study
pDS46	pRSFDuet™-1, *pomY-eyfp*, Km^R	This study

pDS68	pRSFDuet™-1, *pomY-eyfp* (MCS1), *pomZ-mCherry* (MCS2), Km^R	This study
pDS69	pRSFDuet™-1, *mCherry-pomX* (MCS1), *ftsZ-gfp* (MCS2), Km^R	This study
pDS74	pSWU30, P_{pilA}*pomZ*, Tc^R	This study
pDS75	pDS74, containing *mxan_0018-0019* intergenic region fragment for integration into genome, P_{pilA}*pomZ,* Tc^R	This study
pDS80	pDS75, P_{nat}*pomZ*^{D90A} , Tc^R	This study
pDS52	pKNT25, *pomZ*^{G62V} (N-terminal fusion to T25 fragment), Km^R	This study
pDS53	pKT25, *pomZ*^{G62V} (C-terminal fusion to T25 fragment), Km^R	This study
pDS54	pUT18, *pomZ*^{G62V} (N-terminal fusion to T18 fragment), Amp^R	This study
pDS55	pUT18C, *pomZ*^{G62V} (C-terminal fusion to T18 fragment), Amp^R	This study
pDS56	pKNT25, *pomZ*^{K66Q} (N-terminal fusion to T25 fragment), Km^R	This study
pDS57	pKT25, *pomZ*^{K66Q} (C-terminal fusion to T25 fragment), Km^R	This study
pDS58	pUT18, *pomZ*^{K66Q} (N-terminal fusion to T18 fragment), Amp^R	This study
pDS59	pUT18C, *pomZ*^{K66Q} (C-terminal fusion to T18 fragment), Amp^R	This study
pDS60	pKNT25, *pomZ*^{K268A} (N-terminal fusion to T25 fragment), Km^R	This study
pDS61	pKT25, *pomZ*^{K268A} (C-terminal fusion to T25 fragment), Km^R	This study
pDS62	pUT18, *pomZ*^{K268A} (N-terminal fusion to T18 fragment), Amp^R	This study
pDS63	pUT18C, *pomZ*^{K268A} (C-terminal fusion to T18 fragment), Amp^R	This study
pDS64	pKNT25, *pomZ*^{K268E} (N-terminal fusion to T25 fragment), Km^R	This study
pDS65	pKT25, *pomZ*^{K268E} (C-terminal fusion to T25 fragment), Km^R	This study
pDS66	pUT18, *pomZ*^{K268E} (N-terminal fusion to T18 fragment), Amp^R	This study

pDS67	pUT18C, *pomZ*^{K268E} (C-terminal fusion to T18 fragment), Amp^{R}	This study
pDS115	pUT18C, *pomZ*^{D90A} (C-terminal fusion to T18 fragment), Amp^{R}	This study
pDS117	pUT18, *pomZ*^{D90A} (N-terminal fusion to T18 fragment), Amp^{R}	This study
pDS118	pKT25, *pomZ*^{D90A} (C-terminal fusion to T25 fragment), Km^{R}	This study
pDS119	pKNT25, *pomZ*^{D90A} (N-terminal fusion to T25 fragment), Km^{R}	This study
pDS105	pKT25, *pomZ* (C-terminal fusion to T25 fragment), Km^{R}	This study
pDS113	pKNT25, *pomZ* (N-terminal fusion to T25 fragment), Km^{R}	This study
pDS109	pUT18, *pomZ* (N-terminal fusion to T18 fragment), Amp^{R}	This study
pDS100	pUT18C, *pomZ* (C-terminal fusion to T18 fragment), Amp^{R}	This study
pDS106	pKT25, *pomX* (C-terminal fusion to T25 fragment), Km^{R}	This study
pDS114	pKNT25, *pomX* (N-terminal fusion to T25 fragment), Km^{R}	This study
pDS110	pUT18, *pomX* (N-terminal fusion to T18 fragment), Amp^{R}	This study
pDS103	pUT18C, *pomX* (C-terminal fusion to T18 fragment), Amp^{R}	This study
pDS120	pUT18C, *pomY* (C-terminal fusion to T18 fragment), Amp^{R}	This study
pDS121	pKT25, *pomY* (C-terminal fusion to T25 fragment), Km^{R}	This study
pDS122	pUT18, *pomY* (N-terminal fusion to T18 fragment), Amp^{R}	This study
pDS123	pKNT25, *pomY* (N-terminal fusion to T25 fragment), Km^{R}	This study
pDS108	pKT25, *ftsZ* (C-terminal fusion to T25 fragment), Km^{R}	This study
pDS116	pKNT25, *ftsZ* (N-terminal fusion to T25 fragment), Km^{R}	This study
pDS112	pUT18, *ftsZ* (N-terminal fusion to T18 fragment), Amp^{R}	This study

pDS101	pUT18C, *ftsZ* (C-terminal fusion to T18 fragment), Amp^R	This study
pSH36	pKNT25, *pomX*^{K13A,R15A} (N-terminal fusion to T25 fragment), Km^R	S. Huneke (MPI Marburg)
pSH37	pKT25, *pomX*^{K13A,R15A} (C-terminal fusion to T25 fragment), Km^R	S. Huneke (MPI Marburg)
pSH38	pUT18, *pomX*^{K13A,R15A} (N-terminal fusion to T18 fragment), Amp^R	S. Huneke (MPI Marburg)
pSH39	pUT18C, *pomX*^{K13A,R15A} (C-terminal fusion to T18 fragment), Amp^R	S. Huneke (MPI Marburg)
pEMR3	pET-24b$^+$ with *pomX* for expression of *pomX-His$_6$*, Km^R	A. Harms (MPI Marburg)

8.4.2 Construction of plasmids

Purified *M. xanthus* genomic DNA as well as plasmids were used as template to amplify genes of interest and genomic regions. Plasmid DNA was used as template to amplify genes coding for *eyfp*, *mCherry*, e*gfp*. *E. coli* TOP10, Mach1 or NEB Turbo were used for all cloning steps. Sequencing was performed by Eurofins MWG Operon (Ebersberg) using custom made primers. Sequencing reactions were analyzed with the help of ContigExpress of VectorNTI advance suite 11 (Invitrogen™ life technologies, Karlsruhe).

Plasmids pDS1, pDS12, pDS16, pDS23, pDS27; pMAT12, pAH27 (constructed for in-frame deletions): The mentioned plasmids are all derivatives of pBJ114 and were used to construct markerless in-frame deletions of single genes or multiple genes at the same time as described in 8.4.3. For **pDS1** up- (“KA-371/Mxan_0634-5”) and downstream fragment (“KA-373/KA-374”) were amplified from genomic *M. xanthus* DNA and digested EcoRI+XbaI and XbaI+HindIII, respectively. Fragments were cloned separately into pBJ114 and sequenced. For **pAH27** up- (“KA-224/Mxan_0636-1”) and downstream fragment (“Mxan_0636-2/ Mxan_0636-3”) were amplified from genomic *M. xanthus* DNA and digested EcoRI+XbaI and XbaI+HindIII, respectively. Fragments were cloned separately into pBJ114 and sequenced. **pMAT12** is a derivative of pAH27. Upstream fragment (“KA-200/Mxan_0635-3”) was amplified from genomic DNA, digested with EcoRI+XbaI and cloned into pAH27 that was digested EcoRI+XbaI before. **pDS12** is a derivative of pDS1. For construction of pDS12, pAH27 was digested XbaI+HindIII and downstream fragment was cloned into pDS1 that was digested with the same enzymes before. **pDS16** is a derivative of pDS1 in which the downstream fragment (XbaI+HindIII) was replaced with another downstream fragment (“Mxan0635-1+Mxan0635-2”) that was digested in the same way. For cloning of **pDS23** upstream (“Mxan_0633-1/ Mxan_0633-2”) and downstream fragment (“Mxan_0633-3/ Mxan_0633-4”) were amplified from genomic *M. xanthus* DNA and digested EcoRI+XbaI and XbaI+HindIII, respectively. Fragments were cloned separately into pBJ114 before plasmid was sequenced. Finally, for the in-frame deletion of *smc* plasmid **pDS27** was constructed. pDS27 is a derivative of pBJ114. For pDS27 upstream and downstream fragment were amplified using the primer pairs “Mxan_4901-1/Mxan_4901-2” and

"Mxan_4901-3/Mxan_4901-4", respectively. Upstream fragment (EcoRI+XbaI) and downstream fragment (XbaI+HindIII) were digested and cloned separately into pBJ114 that was digested with the same restriction enzymes before.

Plasmids pDS120, pDS121, pDS122, pDS123 (constructed for BACTH assays): For all four plasmids *pomY* was amplified from genomic *M. xanthus* DNA using the primers "Mxan_0634-16" and "Mxan_0634-17". Amplified by these primers *pomY* contains no stop codon because it is provided by the vector. To be translated in the correct frame *pomY* contains one additional amino acid at the beginning and the end which additionally serves as a part of the linker for both *T18* and *T25* fragment fusions.

Plasmids pDS101, pDS108, pDS112, pDS116 (constructed for BACTH assays): For all four plasmids *ftsZ* was amplified from genomic *M. xanthus* DNA using the primers "Mxan_5597 ftsZ XbaI" and "Mxan_5597 ftsZ KpnI". Amplified by these primers *ftsZ* contains no stop codon because it is provided by the vector. To be translated in the correct frame *ftsZ* contains one additional amino acid at the beginning and the end which additionally serves as a part of the linker for both *T18* and *T25* fragment fusions.

Plasmids pDS100, pDS105, pDS109, pDS113 (constructed for BACTH assays): For all four plasmids *pomZ* was amplified from genomic *M. xanthus* DNA using the primers "Mxan_0635-4 pomZ fwd" and "Mxan_0635-5 pomZ rev". Amplified by these primers *pomZ* contains no stop codon because it is provided by the vector. To be translated in the correct frame *pomZ* contains one additional amino acid at the beginning and the end which additionally serves as a part of the linker for both *T18* and *T25* fragment fusions.

Plasmids pDS103, pDS106, pDS110, pDS114 (constructed for BACTH assays): For all four plasmids *pomX* was amplified from genomic *M. xanthus* DNA using the primers "Mxan_0636-1 pomX fwd" and "Mxan_0636-2 pomX rev". Amplified by these primers *pomX* contains no stop codon because it is provided by the vector. To be translated in the correct frame *pomX* contains one additional amino acid at the beginning and the end which additionally serves as a part of the linker for both *T18* and *T25* fragment fusions.

Bacterial Two Hybrid plasmids containing *pomZ*^{K66Q}, *pomZ*^{G62V}, *pomZ*^{D90A}, *pomZ*^{K268A}, *pomZ*^{K268E}: *pomZ*^{G62V} was amplified from pEB10, *pomZ*^{K66Q} was amplified from pEB11, *pomZ*^{D90A} was amplified from pKA43 and *pomZ*^{K268A} and *pomZ*^{K268E} from pAH99 and pAH100, respectively, using the primers "Mxan_0635-4 pomZ fwd" and "Mxan_0635-5 pomZ rev". Amplified by these primers the PCR products do not contain a stop codon but it is provided by the vector. To be translated in the correct frame *the pomZ* derivatives contain one additional amino acid at the beginning and the end which additionally serves as a part of the linker for both *T18* and *T25* fragment fusions.

Plasmids pDS7 and pDS8 (constructed to express *pomY-mCherry* for fluorescence microscopy): pDS8 is a derivative of pKA28. A PCR fragment, containing *pomY* and its putative native promoter (P_{nat}, 611 bp), was amplified with "KA-371" and "Mxan_0634-4" from genomic DNA and digested with the restriction endonucleases EcoRI+BglII. pKA28 served as a backbone and was digested EcoRI and BamHI. Ligation of insert and vector resulted in pDS8. BglII and BamHI have compatible restriction recognition sites, however if ligation takes place the restriction site is not recognised anymore by both of them. **pDS7** is a derivative of pSW105 digested with XbaI and HindIII. *pomY-mCherry* was amplified from pDS8 with primers "Mxan_0636-6" and "mCherry stop rev HindIII" and digested the same way. Ligation of vector backbone and *pomY-mCherry* fragment results in pDS7.

Plasmid pDS18 (constructed to express *pomY-eyfp* for fluorescence microscopy): To clone pDS18 first pDS17 had to be constructed. **pDS17** is a derivative of pSWU30 containing a BamHI+ HindIII cloned e*yfp* gene with a N-terminal linker amplified with "KA-396" and "KA-397". After sequencing pDS17, *pomY* was cloned into pDS17 with EcoRI and BglII using a PCR fragment amplified by "KA-371" and "Mxan0634 rev BglII+3AA linker", resulting in **pDS18**.

Plasmids pDS21 and pDS22 (constructed for expression of *pomY-mCherry* and *pomY-eyfp* under regulation of P_{cuoA}): pDS21 is a derivative of pMAT11. Insert from pDS7 was excised with XbaI and HindIII and ligated into pMAT11 which was digested with the same restriction enzymes before. pDS22 is also a derivative of pMAT11. For **pDS22** *pomY-eyfp* was amplified from pDS18 with primers "KA-397" and "Mxan_0634-6". The PCR product was digested with XbaI and HindIII prior to ligation into pMAT11, digested with the same restriction endonucleases.

Plasmid pDS75 (constructed for expression of genes under regulation of their native promoter (P_{nat}) and P_{pilA} from *mxan_0018-0019* site): pDS75 is a derivative of **pDS74**, containing *pomZ* expressed from P_{pilA}. pDS74 in turn was received from pSWU30 (Tc^R). For **pDS75** *attB* locus was excised from pDS74 using BsrDI and BlpI. This was replaced by the *mxan_0018-0019* intergenic region amplified from pMR3691 using the primers "Mxan18-19 fwd BsrDI" and "Mxan18-19 rev BlpI".

Plasmids pDS37, pDS43, pDS46 (constructed for expression of fluorescently tagged *pomY*, *pomZ* and *pomX* in *E. coli*): pDS37, **pDS43** and **pDS46** are derivatives of pRSFDuet-1. To construct **pDS37** *mCherry-pomX* was amplified from pAH53 with "mCherry BspHI fwd" and "Mxan_0636-3 HindIII rev stop" and cloned into pRSFDuet-1 multiple cloning site 1 (MCS1) that was digested with NcoI and HindIII before. For **pDS43** *pomZ-mCherry* was amplified from pKA28 with primers "Mxan_0635 BspHI fwd" and "KA-478" and cloned into pRSFDuet-1 the same way. For **pDS46** *pomY-eyfp* was amplified from pDS18 using "Mxan_0634-18" and "Mxan_0634-15" and cloned into pRSFDuet-1 as described before.

Plasmids pDS68, pDS69 (constructed for co-expression of *pomY-eyfp* and *pomZ-mCherry* as well as *mCherry-pomX* and *ftsZ-gfp*): pDS68 is a derivative of **pDS46** containing *pomY-eyfp* in MCS1. To construct pDS68, *pomZ-mCherry* was amplified from pKA28 with "Mxan_0635 start NdeI" and "mCherry stop PacI" and cloned into MCS2 of pDS46 using the indicated restriction enzymes. **pDS69** is a derivative of pDS37 containing *mCherry-pomX* in MCS1. To clone pDS69 *ftsZ-gfp* was amplified from pKA51 with primers "AH-113" and "AH-115". PCR product was digested with NdeI and EcoRV and ligated into pRSFDuet-1 MCS2.

Plasmids pDS38, pDS45 (constructed for expression of *pomX* and *pomY-eyfp* in *E. coli*): pDS38 and pDS45 are derivatives of pBAD24. For pDS38 *pomX* was amplified from genomic DNA using the primers "Mxan_0636 BspHI fwd" and "Mxan_0636-3 HindIII rev stop" and cloned into pBAD24 using the indicated restriction sites. To construct pDS45, *pomY-eyfp* was amplified with primers "Mxan_0634-18" and "Mxan_0634-15" and ligated into pBAD24 using BspHI and HindIII restriction sites.

Plasmids pAH99, pAH100, pAH103 and pAH104 (expression of *pomZ*^{K268A}*-mCherry* and *pomZ*^{K268E}*-mCherry* from P_{nat} and P_{pilA}): To create pAH99 and pAH100, plasmid pKA28, carrying *pomZ-mCherry* under the regulation of its native promoter, was subjected to site directed mutagenesis with primers "AH-93" + "AH-94" (exchange of K268 to A) and "AH-91" + "AH-92" (exchange of K268 to E), respectively. To receive pAH103 and pAH104 site directed mutagenesis with the same primer pairs was performed on pKA45, carrying *pomZ-mCherry* under the regulation of P_{pilA}.

Plasmid pDS80 (expression of *pomZ*^{D90A} from *mxan_0018-0019* intergenic region): pDS80 is a derivative of pDS75. To create **pDS80**, P_{nat}*pomZ*^{D90A} together with a short part of the vector backbone was excised from pKA43 with NdeI and HindIII. This fragment was cloned into pDS75 that was digested with NdeI and HindIII and replaced P_{pilA}*pomZ* and a short sequence of the vector.

8.4.3 Generation of *M. xanthus* in-frame deletions

In-frame deletions of specific genomic regions were generated as described previously with small modifications (Shi *et al.*, 2008) In brief, two DNA fragments of approximately 500 bp length were amplified by PCR using the primers AB and CD. These fragments encoded a DNA sequence directly upstream (fragment AB; upstream-fragment) and downstream (fragment CD; downstream-fragment) of the region to be deleted. For in-frame deletion of genes upstream- and downstream-fragment contained 30 bp of the beginning and the end of the gene. First the upstream-fragment was cloned into pBJ114 (Km^R) using the restriction enzymes EcoRI and XbaI, followed by the downstream-fragment using XbaI and HindIII. Plasmids, proved to be correct in sequence, by sequencing the manipulated regions with specific primers, were used for transformation of corresponding *M. xanthus* strains. The plasmid pBJ114 cannot replicate autonomously but confers kanamycin resistance when integrated into the genome by homologous recombination along the upstream- or downstream-fragment. Transformants were selected by kanamycin resistance on CTT plates containing 50 µg/ml kanamycin. Single transformants were picked and integration of the plasmid was mapped by PCR

using the primer combinations M13 fwd/E and M13 rev/F. If possible both clones with an upstream and a downstream integration of the plasmid were isolated. To obtain a marker-less in-frame deletion mutation a second homologous recombination has to take place in order to excise the plasmid with its kanamycin resistance. For counter-selection plasmid pBJ114 contains the selection marker *galK* (gene encoding for the galactokinase from *E. coli*). The gene product GalK converts galactose into galactose-1-phosphate. *M. xanthus* cannot metabolize galactose-1-phosphate, that accumulates up to toxic levels when cells are grown on galactose-containing media, resulting in growth defects. Therefore, only cells that undergo a second homologous recombination to excise the plasmid are able to grow under these conditions. After excision of the plasmid only 50% of the transformants will contain an in-frame deletion of the specific genomic region, whereas another 50% will restore the original (WT) genomic situation, if the genomic region is not important for viability. For the second homologous recombination event cells were grown in liquid cultures without kanamycin to exponential growth-phase to allow for plasmid excision. Cells were spread in dilution-series on CTT plates containing 10 µg/ml gentamycin and 2.5% galactose. Obtained colonies were transferred in parallel on CTT plates containing 50 µg/ml kanamycin and CTT plates containing galactose. Colonies that show growth on CTT plates with galactose but not on plates containing kanamycin were used to test for in-frame deletion by PCR using the primer combinations E/F and G/H.

8.4.4 Preparation of DNA from *M. xanthus* and *E. coli*

Plasmid DNA was amplified in and extracted from *E. coli* Top10, NEB Turbo or MachI. For extraction of plasmid DNA either QIAprep Spin Miniprep Kit (Qiagen, Hilden) or NucleoSpin® Plasmid Kit (Macherey-Nagel, Düren) was used. Genomic *M. xanthus* DNA was isolated using MasterPure DNA preparation Kit (Epicentre® Biozym, Oldendorf) according to manufacturer's instructions. Quality and concentration of DNA was determined by the Nanodrop ND-1000 sprectrophotometer (Nanodrop, Wilmington). Crude genomic DNA extracts to verify genomic integration of plasmids was obtained by boiling cells in 30 µl H_2O for 10 min at 95 °C. Before use of DNA extracts cell debris was sedimented for 2 min at 13000 rpm.

8.4.5 Polymerase chain reaction (PCR) for amplification of DNA fragments

Amplification of specific DNA fragments by polymerase chain reaction was performed using Phusion High-Fidelity DNA Polymerase (Thermo Scientific™ (Darmstadt)) in a total reaction volume of 20 µl as described in Table 12.

Table 12: General PCR reaction mix for amplification of DNA with Phusion polymerase

Component	Volume	Final concentration
Genomic or plasmid DNA	1 µl	40-100 ng
10 µM primer A	0,5 µl	0,25 µM
10 µM primer B	0,5 µl	0,25 µM
10 mM dNTP mix	0,4 µl	0,2 mM
5 x Phusion GC buffer	4 µl	1 x
5 x enhancer	4 µl	1 x
Phusion DNA Polymerase	0,2 µl	1 unit/50 µl PCR
HPLC H_20	9,4 µl	

For PCR's with Phusion High-Fidelity Polymerase the following PCR program was used and modified depending on GC content of primers and length of the DNA fragment to be amplified.

Table 13: General program for Phusion PCR

Step	Temperature	Time
Initial denaturation	95 °C	3 min
Denaturation	95 °C	30 sec
Annealing	5 °C below melting temperature (mostly 55 °C - 60 °C)	30 sec
Elongation	72 °C	30 sec/1000 bp
Final elongation	72 °C	10 min

PCR products were separated by agarose gel electrophoresis and analysed for correct size. Correct DNA fragments were either directly purified using the NucleoSpin® Gel and PCR Clean-up Kit (Macherey-Nagel, Düren) or isolated from the agarose gel by excision of the correct fragment-containing gel piece and subsequent purification with the Qiaquick Gel Extraction Kit (Qiagen, Hilden) and eluted in 30 µl of elution buffer.

8.4.6 Check PCR for plasmid integration or gene deletion

To test for plasmid integration into the *M. xanthus* genome, or to test for gene deletion, check PCR's were performed in a 25 µl reaction volume using the 5 PRIME Master Mix (5 PRIME GmbH, Hilden), containing Taq polymerase, as described in Table 14.

Table 14: General program for test PCR's with 5 PRIME Master Mix

Step	Termperature	Time
Initial denaturation	95 °C	3 min
Denaturation	95 °C	30 sec
Annealing	60 °C	30 sec
Elongation	72 °C	1 min/1000 bp
Final elongation	72 °C	10 min

PCR products were separated by agarose gel electrophoresis and analyzed for correct size by correlation to a DNA size standard.

8.4.7 Site-directed mutagenesis of plasmids

For site-directed mutagenesis of plasmid DNA the Quickchange II XL site directed mutagenesis kit (Stratagene, Agilent Technologies, Waldbronn) was used according to manufacturer's advice. Primers for site-directed mutagenesis were designed as described by the manufacturer.

8.4.8 Agarose gel electrophoresis

PCR reactions and digested plasmids were visualized via agarose gel electrophoresis. DNA samples were mixed with 10 x DNA loading buffer (New England Biolabs, Frankfurt a. M.) and separated on 1 % agarose gels with 0.01 % (v/v) ethidium bromide in 1 x TBE buffer (life technologies GmbH, Karlsruhe) at 100-120 V. As size standard the 2-log DNA ladder (New England Biolabs, Frankfurt a. M.) was used. Gels were documented with the E-BOX VX2 imaging system (PeqLab, Erlangen).

8.4.9 Restriction and ligation of DNA fragments

For cloning of plasmids, vector backbones and PCR fragments had to be digested in order to make them compatible for ligation. For cloning, 2-3 µg of plasmid DNA was digested by endonucleases from New England Biolabs according to manufacturer's instruction for 3 h in a 50 µl volume. After heat inactivation of the restriction endonucleases for 10 min at 65 °C restriction mix was cooled on ice. The digest was mixed with 6 µl 10 x Antarctic Phosphatase buffer, 3 µl HPLC H_2O and 1 µl of Antarctic Phosphatase (New England Biolabs, Frankfurt a. M.). Reaction was carried out at 37 °C for 1 h. After dephosphorylation, digest was separated by agarose gel electrophoresis and DNA fragments of correct size were excised from gel and purified with the Qiaquick Gel Extraction Kit (Qiagen, Hilden). Purified PCR fragments were digested by endonucleases from New England Biolabs according to manufacturer's instruction for 3 h in a 50 µl volume. After heat inactivation of the restriction endonucleases for 10 min at 65 °C (or after manufacturer's instructions) restriction mix was cooled on ice and purified with NucleoSpin® Gel and PCR Clean-up Kit (Macherey-Nagel, Düren).

Ligation of DNA fragments and plasmid DNA was performed with T4 DNA Ligase (New England Biolabs, Frankfurt a. M.) in a reaction volume of 20 µl according to manufacturer's instructions. Ligation reactions were either incubated at 37 °C for 1 h or overnight at room-temperature. PCR fragments were ligated into vectors using a 3- to 5-fold molar excess of insert DNA.

8.4.10 Preparation and transformation of chemically competent *E. coli* cells

For cloning of plasmids or heterologous gene expression *E. coli* strains had to be made competent. An overnight culture of *E. coli* TOP10, NEB Turbo, MachI, BL21(DE3), Rosetta™2(DE3) or ArcticExpress(DE3)RP was diluted 1: 200 into 100 ml fresh LB medium and incubated at 37 °C for approximately 2 h to an OD_{600} of 0.6 - 0.8. Cells were harvested in falcon tubes for 15 min at 4700 rpm at 4 °C. Cell pellets were resuspended in buffer TFB1 in a total volume of 20 ml and incubated on ice for 10 min. Cells were harvested a second time for 15 min at 4700 rpm and 4 °C and subsequently resuspended in buffer 2 ml TFB2. Cells were incubated for up to 1 h on ice. After incubation 50 µl aliquots of cells in reaction tubes were frozen in liquid nitrogen and kept at -80 °C until used.

For transformation 50 µl of cells were thawed on ice and mixed carefully with 10 µl ligation reaction or 1 µl of plasmid DNA. Mixture was incubated on ice for 20 min and then heat-shocked for 2 min at 42 °C in a water bath. After cooling 5 min on ice, cells were mixed with 1 ml LB medium and incubated for 45 min at 37 °C, shaking. Then, cells were pelleted for 2 min at 13.000 rpm at room temperature, resuspended in residual LB medium and spread on LB agar plates with corresponding antibiotics. Transformations plates were incubated at 37 °C over night. Ligated plasmids were checked for correct inserts by test restrictions followed by sequencing.

Table 15: Composition of TFB buffers for preparation of chemically competent *E. coli* cells

Buffer	Composition
TFB1	30 mM potassium acetate
	10 mM $CaCl_2$
	50 mM $MnCl_2$
	100 mM RbCl
	15 % glycerol (v/v)
	pH 5.8 (adjusted with 1 M acetic acid)
TFB2	10 mM MOPS pH 6.5 (adjusted with KOH)
	75 mM $CaCl_2$
	10 mM RbCl
	15 % glycerol (v/v)

8.4.11 Preparation and transformation of electrocompetent *E. coli* cells

In order to perform a Bacterial Two Hybrid assay (BACTH) cells of the strain BTH101 (Euromedex, Souffelweyersheim, France) had to be prepared. An overnight culture of BTH101 was diluted 1: 200 into 100 ml fresh LB medium. Cells were grown at 37 °C, shaking on a rotary shaker at 230 rpm up to an OD_{600} of 0.6-0.8 and harvested by centrifugation at 4700 rpm for 15 min at 4 °C in falcon tubes. Cell pellets were resuspended in 50 ml ice cold, sterile 10 % (v/v) glycerol. The washing step was repeated twice. Finally, cell pellets were resuspended in 2 ml sterile 10 % glycerol and shock-frozen in 50 µl aliquots in liquid nitrogen. Cells were stored for later usage at -80 °C.

For transformation of electrocompetent *E. coli* 50 µl cells were thawed on ice and mixed with 1-2 µl (10-25 ng) plasmid DNA. The mixture was transferred into a sterile 0.1 cm electroporation cuvette (Bio-Rad, München) and pulsed with 1.8 kV, 25µF and 200 Ω. Subsequently, 1 ml LB medium was added and the mixture was transferred into a sterile reaction tube and incubated at 37 °C for 1 h shaking at 230 rpm. Cells were harvested by centrifugation at 13.000 rpm for 2 min at room temperature. Supernatant was discarded and cells were resuspended in 100 µl LB medium and spread on LB agar plates containing corresponding selective antibiotics. Plates were incubated overnight at 37 °C or at 30 °C for 48 h for the BACTH assay.

8.4.12 Preparation and transformation of electrocompetent *M. xanthus* cells

M. xanthus cells were inoculated initially from a single colony in 5 ml CTT medium in a 50 ml Erlen-Meyer flask and incubated overnight at 32 °C shaking in the dark. Cultures for transformation were scaled up to 20 ml, depending on the amount of transformations that had to be performed. Exponentially growing cultures were harvested in falcon tubes at 4700 rpm for 10 min at room temperature and resuspended in sterile ddH_2O to the original volume. Cells were pelleted again as described before and washed again twice. In the last washing step cells were resuspended in 80 µl-400 µl of sterile ddH_2O (80 µl per transformation). 80 µl cells were transferred into a sterile 0.1 cm electroporation cuvette (Bio-Rad, München) and mixed with 5 µl - 10 µl of plasmid DNA (1 µg - 2 µg DNA). Mixture was pulsed with 0.65 kV, 25 µF and 400 Ω. Subsequently, 1 ml CTT was added to the electroporated cells and transferred into a 25 ml Erlen-Meyer flask to a total volume of 2.5 ml culture. Transformations were incubated 6 h - 8 h at 32 °C, shaking at 230 rpm in the dark. For sensitive transformations recovery time was prolonged for additional 10 h. Cells were harvested at 8000 rpm in a table-top centrifuge at room temperature for 5 min. Supernatant was discarded and pellets were resuspended in 100 µl fresh CTT medium. Cells were spread on CTT agar plates with corresponding antibiotics in dilution series. Agar plates were incubated at 32 °C in the dark for several days. Grown colonies were transferred onto fresh CTT agar plates with antibiotics and checked for plasmid insertion into the genome by PCR.

8.5 Biochemical methods

8.5.1 Purification of PomY-His_6 from *E. coli* ArcticExpress(DE3)RP

To overexpress His_6-tagged PomY, plasmid pDS3 was propagated in *E. coli* ArcticExpress(DE3)RP cells (Agilent Technologies, Waldbronn). To overexpress PomY-His_6, 50 ml LB medium containing 50 µg/ml kanamycin were inoculated with a single colony from freshly transformed Arctic Express DE3 RP cells containing pDS3. Cells were grown over night at 30 °C shaking at 230 rpm. This overnight culture was diluted the next day 1:200 into fresh LB medium without antibiotics and grown to an OD_{600} of 0.6 – 0.7. Cultures were pre-cooled and shifted to 18 °C prior to induction of *pomY-His_6* expression with 1 mM IPTG. Cells were incubated overnight at 18 °C shaking at 230 rpm. Cells were harvested by centrifugation at 6000 x g for 20 min at 4 °C. Pellets were washed in lysis buffer 1 (50 mM NaH_2PO_4; 300 mM NaCl; 10 mM imidazole; pH 8.0 (adjusted with NaOH)), harvested again at 6000 x g for 20 min at 4 °C and then resuspended in 50 ml lysis buffer 2 (50 mM NaH_2PO_4; 300 mM NaCl; 10 mM imidazole; pH 8.0 (adjusted with NaOH); 0.1 mM EDTA; 1 mM β-mercaptoethanol; 100 µg/ml PMSF; 1 x complete protease inhibitor (Roche Diagnostics GmbH, Mannheim); 10 U/ml DNase 1; 0.1 % Triton X-100). To lyse cells, resuspended pellets were sonicated 3 x for 5 min with a Branson Sonifier (Duty cycle 4; Output control 40 %; Heinemann, Schwäbisch Gmünd) on ice. To pellet cell debris, lysates were cleared at 4700 rpm for 20 min at 4 °C. The resulting supernatant was additionally filtered using a 0.45 µm sterile filter (Millipore Merck, Schwalbach). To purify PomY-His_6 only the soluble cell fraction was used. Cleared soluble fraction was loaded onto a 5 ml HiTrap Chelating HP column, preloaded with $NiSO_4$ and equilibrated with lysis buffer 1. Proteins were eluted with elution buffer (50 mM NaH_2PO_4; 300 mM NaCl; 500 mM imidazole;

pH 8.0 (adjusted with NaOH)) along a gradient of 20 column volumes (CV). Elution fractions containing PomY-His_6 were loaded onto a HiLoad 16/600 Superdex 200 pg column that was equilibrated with dialysis buffer (50 mM Hepes/NaOH pH 7.2; 50 mM KCl; 0.1 mM EDTA; 1 mM β-mercaptoethanol; 10 % (v/v) glycerol) before. Collected fractions containing PomY-His_6 after gel filtration were pooled and loaded onto a 5 ml HiTrap SP HP column, equilibrated with dialysis buffer, for concentration of the protein. PomY-His_6 was eluted from the column with cation-exchange buffer (50 mM Hepes/NaOH pH 7.2; 2 M KCl; 0.1 mM EDTA; 1 mM β-mercaptoethanol; 10 % (v/v) glycerol) along a gradient of 2 CV. Elution fractions from the ion-exchange chromatography were dialyzed 3 x against 2 l dialysis buffer at 4 °C. Aliquots of 100 µl were snap-frozen in liquid nitrogen and stored at -80 °C until usage.

Table 16: Buffers used for purification of PomY-His_6

Buffer	Composition
Buffers for purification of PomY-His_6	
Lysis buffer 1	50 mM NaH_2PO_4 300 mM NaCl 10 mM imidazole pH 8.0 (adjusted with NaOH)
Lysis buffer 2	50 mM NaH_2PO_4 300 mM NaCl 10 mM imidazole pH 8.0 (adjusted with NaOH) 0.1 mM EDTA 1 mM β-mercaptoethanol 100 µg/ml Phenylmethylsulfonylfluorid (PMSF) 1 x complete protease inhibitor (Roche, Mannheim) 10 U/ml DNase 1 0.1 % Triton X-100
Elution buffer	50 mM NaH_2PO_4 300 mM NaCl 500 mM imidazole pH 8.0 (adjusted with NaOH)
Dialysis buffer	50 mM Hepes/NaOH pH 7.2 50 mM KCl 0.1 mM EDTA 1 mM β-mercaptoethanol 10 % (v/v) glycerol

Cation-exchange buffer	50 mM Hepes/NaOH pH 7.2 2 M KCl 0.1 mM EDTA 1 mM β-mercaptoethanol 10 % (v/v) glycerol

8.5.2 Purification of PomX-His$_6$ from *E. coli* NiCo21(DE3)

To overexpress His$_6$-tagged PomX, plasmid pEMR3 was propagated in *E. coli* NiCo21 DE3 cells (New England Biolabs, Frankfurt a. M.). For expression of *pomX-His$_6$* 50 ml LB medium containing 50 µg/ml kanamycin were inoculated with a single colony from freshly transformed NiCo21 DE3 cells containing pEMR3. Cells were grown over night at 30 °C, shaking at 230 rpm. This overnight culture was diluted the next day 1:200 into fresh LB medium supplemented with 50 µg/ml kanamycin and grown at 30 °C to an OD_{600} of 0.6 – 0.7. Prior to induction cells were cooled and shifted to 18 °C. *pomX-His$_6$* expression was induced by addition of IPTG to a final concentration of 0.4 mM. Expression was carried out overnight at 18 °C shaking at 230 rpm. The next day cells were harvested by centrifugation at 5000 x g for 20 min at 4 °C. Pellet was washed in lysis buffer 1 (50 mM NaH_2PO_4; 300 mM NaCl; 10 mM imidazole; pH 8.0 (adjusted with NaOH)), harvested again at 5000 x g for 20 min at 4 °C and then resuspended in 50 ml lysis buffer 2 (50 mM NaH_2PO_4; 300 mM NaCl; 10 mM imidazole; pH 8.0 (adjusted with NaOH); 0.1 mM EDTA; 1 mM β-mercaptoethanol; 100 µg/ml PMSF; 1 x complete protease inhibitor (Roche Diagnostics GmbH, Mannheim); 10 U/ml DNase 1). Cells were lysed by sonication on ice (3 x 5 min; Duty cycle 4; Output control 40 %) with a Branson Sonifier (Heinemann, Schwäbisch Gmünd). To separate soluble fraction from cell debris, cells were applied to centrifugation at 20000 x g for 20 min at 4 °C. Only the supernatant was used for further purification of PomX-His$_6$. PomX-His$_6$ was purified using 10 ml Protino® Ni-NTA resin (Macherey-Nagel, Düren) that was equilibrated with lysis buffer 1. Supernatant from centrifugation was mixed with 10 ml resin and incubated for 1 h at 4°C on a rotary shaker. PomX-His$_6$ was purified from batch by consecutive centrifugation steps instead of using a flow column. Mixed Ni-NTA resin was pelleted at 500 x g for 5 min at 4 °C. Supernatant was removed to eliminate all protein that is not bound to the Ni-NTA resin. Resin was washed with 6 x 50 ml wash buffer (50 mM NaH_2PO_4; 300 mM NaCl; 20 mM imidazole; pH 8.0 (adjusted with NaOH)) and in between applied to centrifugation as described before. PomX-His$_6$ was eluted from the resin by washing 1 x with 5 ml elution buffer 1 containing 50 mM imidazole (50 mM NaH_2PO_4; 300 mM NaCl; 50 mM imidazole; pH 8.0 (adjusted with NaOH)) and 3 x with 5 ml elution buffer 2 containing 250 mM imidazole (50 mM NaH_2PO_4; 300 mM NaCl; 250 mM imidazole; pH 8.0 (adjusted with NaOH)). In between resin was applied to centrifugation as described before and supernatant was collected, as it contained purified PomX-His$_6$. Purified PomX-His$_6$ was dialyzed 4 x against 2 l dialysis buffer (50 mM Hepes/NaOH pH 7.2; 50 mM KCl; 0.1 mM EDTA; 1 mM β-mercaptoethanol; 10 % (v/v) glycerol) to remove residual phosphate and imidazole. Aliquots were snap-frozen in liquid nitrogen and stored at -80 °C until usage.

Table 17: Buffer used for purification of PomX-His$_6$

Buffer	Composition
Buffers for purification of PomX-His$_6$	
Lysis buffer 1	50 mM NaH_2PO_4 300 mM NaCl 10 mM imidazole pH 8.0 (adjusted with NaOH)
Lysis buffer 2	50 mM NaH_2PO_4 300 mM NaCl 10 mM imidazole pH 8.0 (adjusted with NaOH) 0.1 mM EDTA 1 mM β-mercaptoethanol 100 µg/ml Phenylmethylsulfonylfluorid (PMSF) 1 x complete protease inhibitor (Roche, Mannheim) 10 U/ml DNase 1
Wash buffer	50 mM NaH_2PO_4 300 mM NaCl 20 mM imidazole pH 8.0 (adjusted with NaOH)
Elution buffer 1	50 mM NaH_2PO_4 300 mM NaCl 50 mM imidazole pH 8.0 (adjusted with NaOH)
Elution buffer 2	50 mM NaH_2PO_4 300 mM NaCl 250 mM imidazole pH 8.0 (adjusted with NaOH)
Dialysis buffer	50 mM Hepes/NaOH pH 7.2 50 mM KCl 0.1 mM EDTA 1 mM β-mercaptoethanol 10 % (v/v) glycerol

8.5.3 Purification of His$_6$-PomZ from *E. coli* Rosetta™2(DE3)

Overexpression and purification of His$_6$-PomZ was performed as described before (Treuner-Lange *et al.*, 2013). In short, plasmid pKA3 was propagated in *E. coli* Rosetta™2(DE3) cells (Novagen® Merck, Darmstadt). To overexpress His$_6$-PomZ, 50 ml 2 x YT medium, containing 100 µg/ml ampicillin and 0.2 % glucose were inoculated with a single colony from freshly transformed Rosetta™2(DE3) cells harboring pKA3. Cells were grown over night at 37 °C shaking at 230 rpm.

Cells were diluted into fresh 2 x YT medium containing 100 µg/ml ampicillin the next day and cultivated to an OD_{600} of 0.6 – 0.7 at 37 °C. Overexpression was induced with 0.5 mM IPTG followed by further cultivation for 2 h at 37 °C shaking at 230 rpm. Cells were washed once and then resuspended in lysis buffer 1 (50 mM Hepes/NaOH pH 7.2; 50 mM KCl; 0.1 mM EDTA; 10 % (v/v) glycerol; 1 mM β-mercaptoethanol; 10 mM imidazole; 5 mM $MgCl_2$) After cell lysis by French press (16000 psi) the lysate was applied to centrifugation at 30000 x g for 30 min at 4 °C. Cleared supernatant was used for further purification of His_6-PomZ. The cleared soluble fraction was loaded onto a 5 ml HiTrap Chelating HP column preloaded with $NiSO_4$ and equilibrated with lysis buffer. Proteins were eluted with elution buffer (50 mM Hepes/NaOH pH 7.2; 50 mM KCl; 0.1 mM EDTA; 10 % (v/v) glycerol; 1 mM β-mercaptoethanol; 500 mM imidazole; 5 mM $MgCl_2$) along a gradient of 20 CV from 50 mM to 500 mM imidazole. Elution fractions containing His_6-PomZ were loaded onto a HiLoad 16/600 Superdex 200 pg column that was equilibrated with dialysis buffer (50 mM Hepes/NaOH pH 7.2; 50 mM KCl; 0.1 mM EDTA; 10 % (v/v) glycerol; 1 mM β-mercaptoethanol) before. Fractions with His_6-PomZ were pooled, snap-frozen in liquid nitrogen and stored at -80 °C until used.

Table 18: Buffers for purification of His6-PomZ

Buffer	Composition
Buffers for purification of His_6-PomZ	
Lysis buffer	50 mM Hepes/NaOH pH 7.2 50 mM KCl 0.1 mM EDTA 10 % (v/v) glycerol 1 mM β-mercaptoethanol 10 mM imidazole 5 mM $MgCl_2$
Elution buffer	50 mM Hepes/NaOH pH 7.2 50 mM KCl 0.1 mM EDTA 10 % (v/v) glycerol 1 mM β-mercaptoethanol 500 mM imidazole 5 mM $MgCl_2$
Dialysis buffer	50 mM Hepes/NaOH pH 7.2 50 mM KCl 0.1 mM EDTA 10 % (v/v) glycerol 1 mM β-mercaptoethanol

8.5.4 Purification of native FtsZ without affinity tag from *E. coli* Rosetta™2(DE3)

To overexpress native FtsZ from *M. xanthus* in *E. coli* plasmid pKA70 was propagated in Rosetta™2(DE3) (Novagen® Merck, Darmstadt). 50 ml 2 x YT medium containing 100 µg/ml ampicillin were inoculated with a single colony from freshly transformed Rosetta™2(DE3) cells harboring pKA70 and cultivated overnight. Cells were diluted 1:200 into fresh 2 x YT medium containing 100 µg/ml ampicillin the next day and grown at 37 °C to an OD_{600} of 0.6 – 0.7. Expression of *ftsZ* was induced by addition of IPTG to a final concentration of 0.5 mM and cells were cultivated for additional 3 h at 37 °C shaking at 230 rpm. Cells from 1 l culture were harvested by centrifugation at 6000 x g for 20 min at 4 °C, washed once in lysis buffer 1 (50 mM Tris-HCl pH 7.9; 50 mM KCl; 1 mM EDTA; 1 mM β-mercaptoethanol; 10 % (v/v) glycerol) and then resuspended in 100 ml lysis buffer 2 (50 mM Tris-HCl pH 7.9; 50 mM KCl; 1 mM EDTA; 1 mM β-mercaptoethanol; 10 % (v/v) glycerol; 1 x complete protease inhibitor (Roche Diagnostics GmbH, Mannheim); 10 U/ml DNase 1). Cells were lysed by sonication on ice with a Branson Sonifier (3 x 5 min; Duty cycle 4; Output control 40 %; Heinemann). To separate soluble fraction from cell debris, lysate was applied to centrifugation at 20000 x g for 20 min at 4 °C. Supernatant was used for ammonium sulfate precipitation by adding ammonium sulfate to 33 % of saturation at 4 °C to precipitate native FtsZ protein and separate it from contaminating proteins. Precipitate was collected by centrifugation at 20000 x g for 20 min at 4 °C. Pellet was dissolved in 80 ml lysis buffer 1 and filtered with a 0.45 µm sterile filter (Millipore Merck, Schwalbach). Protein mixture was loaded onto a 5 ml HiTrap Q HP column, equilibrated in lysis buffer 1. Proteins were eluted with elution buffer (50 mM Tris-HCl pH 7.9; 1 M KCl; 1 mM EDTA; 1 mM β-mercaptoethanol; 10 % (v/v) glycerol) along a gradient of 20 CV from 50 mM to 500 mM KCl. Fractions containing FtsZ were pooled and diluted 1:5 with dilution buffer (50 mM Tris-HCl pH 7.9; 1 mM EDTA; 1 mM β-mercaptoethanol; 10 % (v/v) glycerol) to dilute KCl concentration back to 50 mM. This diluted protein mixture was loaded onto a 5 ml HiTrap Q HP column, equilibrated with lysis buffer 1. Proteins were eluted again with elution buffer as described before along a shorter gradient of 4 CV. Fractions containing FtsZ were snap-frozen in liquid nitrogen and stored at -80 °C until used.

Table 19: Buffers for purification of native FtsZ

Buffer	Composition
Buffers for purification of FtsZ	
Lysis buffer 1	50 mM Tris-HCl pH 7.9 50 mM KCl 1 mM EDTA 1 mM β-mercaptoethanol 10 % (v/v) glycerol
Lysis buffer 2	50 mM Tris-HCl pH 7.9 50 mM KCl 1 mM EDTA 1 mM β-mercaptoethanol 10 % (v/v) glycerol 1 x complete protease inhibitor (Roche, Mannheim) 10 U/ml DNase 1
Elution buffer	50 mM Tris-HCl pH 7.9 1 M KCl 1 mM EDTA 1 mM β-mercaptoethanol 10 % (v/v) glycerol
Dilution buffer	50 mM Tris-HCl pH 7.9 1 mM EDTA 1 mM β-mercaptoethanol 10 % (v/v) glycerol

8.5.5 Determination of protein concentrations by Bradford assay

To determine protein concentrations the Bio-Rad proteins assay kit was used according to the manufacturer's recommendations. In short, 20 µl of protein sample were mixed with 980 µl 1:5 diluted Bradford reagent and incubated 5 min at room temperature in the dark. In the same way, different dilutions of BSA were added, to create a standard curve showing protein versus measured absorbance. Absorbance was measured at 595 nm with an Ultrospec 2100 pro spectrophotometer (GE Healthcare Europe GmbH, Freiburg).

8.5.6 Determination of total protein content in cell extracts

To determine the total protein content of a *M. xanthus* lysate sample the Bio-Rad proteins assay kit was used according to the manufacturer's recommendations. In order to create a standard curve 50 µg/µl BSA was dissolved in H_2O and diluted in a series of steps of 1:2 in H_2O. One volume of BSA dilutions (50 µg/µl; 25 µg/µl; 12.5 µg/µl; 6.25 µg/µl; 3.125 µg/µl) was diluted into three volumes of H_2O and one volume of 5 x SDS sample buffer. These resulting dilutions (10 µg/µl; 5 µg/µl; 2.5 µg/µl; 1.25

µg/µl; 0.625 µg/µl) were diluted again 1:25 in H_2O and 20 µl of these samples were mixed with 980 µl 1:5 diluted Bradford reagent and incubated 5 min at room temperature in the dark. Absorbance was measured at 595 nm as described before. *M. xanthus* cell lysates were prepared by dissolving a pellet of cells in 1 x SDS sample buffer followed by incubation at 95 °C for 10 min. Insoluble cell material was sedimented for 2 min at room-temperature at 13.000 rpm. Lysates were diluted the same way as described before and also mixed with Bradford reagent. Protein concentration was calculated from the standard curve by the Ultrospec 2100 pro spectrophotometer (GE Healthcare Europe GmbH, Freiburg).

8.5.7 SDS polyacrylamide gel electrophoresis (SDS-PAGE)

To separate proteins by size SDS polyacrylamide gel electrophoresis (Laemmli, 1970) was performed with SDS gels with acrylamide concentration in the range of 7 % - 12 % (Table 20). To denature proteins, they were mixed with 5 x SDS sample buffer (50 % (v/v) glycerol, 225 mM Tris-HCl pH 6.8, 10 mM EDTA, 10% (w/v) SDS, 0.5 M DTT, 1% (w/v) bromphenol blue) and incubated at 95 ˚C for 10 min before centrifugation for 2 min at room temperature at 13.000 rpm. Gels were run in a Bio-Rad MiniPROTEAN 3 Cell or MiniPROTEAN TetraCell at 120 V in 1 x Tris Glycin SDS (TGS) buffer from BioRad (Bio-Rad, München). As protein standard PageRuler Prestained Protein Ladder from Pierce/Thermo Scientific was used. Proteins, separated by SDS-PAGE were stained with Instant Blue™ (expedeon, Cambridgeshire, UK) for 10 min.

Table 20: Composition of SDS-gels

Reagent	7 %	8 %	10 %	12 %	Stacking gel
Resolving gel buffer	2.5 ml	2.5 ml	2.5 ml	2.5 ml	-
Stacking gel buffer	-	-	-	-	2.5 ml
Acrylamide (30 %)	2.35 ml	2.70 ml	3.36 ml	4.03 ml	1.10 ml
ddH_2O	5.15 ml	4.80 ml	4.14 ml	3.47 ml	6.50 ml
TEMED	0.02 ml	0.02 ml	0.02 ml	0.02 ml	0.05 ml
APS (10 %)	0.05 ml	0.05 ml	0.05 ml	0.05 ml	0.08 ml

Table 21: Composition of buffers used for SDS-gels

Buffer	Composition
Resolving gel buffer	1.5 M Tris-HCl pH 8.8 0.4 % (w/v) SDS
Stacking gel buffer	0.5 M Tris-HCl pH 6.8 0.4 % (w/v) SDS

8.5.8 Immunoblot analysis and antibody production

Immunoblot analysis was performed to detect proteins of interest with specific antibodies. First proteins from cell lysates (8.5.6) or purified proteins were separated by SDS-PAGE as described before (8.5.7). For this purpose equal amounts of proteins in between 15 mg and 30 mg were loaded per lane. Proteins were transferred to a methanol-activated 0.2 µm PVDF membrane (GE healthcare Europe GmbH) using the semi-dry Trans-Blot Turbo™ Transfer System (BioRad, München) with a buffer containing 300 mM glycine and 300 mM Tris base with a pH around 9-10. Transfer was performed using 1.3 A, 25 V for 30 min. Membranes were transferred into a clean plastic container and blocked overnight in 5 % dried non-fat milk powder (w/v) in 1 x TBS (50 mM Tris-HCl pH 7.5; 150 mM NaCl) at 4 °C shaking. After blocking the membrane, primary antibody was added to the blot in 1 % dried non-fat milk powder (w/v) in 1 x TBS at the corresponding dilution (Table 22) and incubated overnight, shaking at 4 °C. After washing 3 x with 1 x TBST (50 mM Tris-HCl pH 7.5; 150 mM NaCl; 0.1 % Tween-20 (v/v)) the horseradish peroxidase-coupled goat α-rabbit immunoglobulin G secondary antibody was applied to the blot at a given dilution in 1 % dried non-fat milk powder (w/v) in 1 x TBS for 2 h at room-temperature shaking. Before detecting the signals, the membrane was washed again with 1 x TBST. Then, the blot was developed with the Luminata Western HRP Substrate (Millipore Merck, Schwalbach) and visualized with the luminescent image analyzer LAS-4000 (Fujifilm, Düsseldorf). Protein specific primary antibodies were produced by Eurogentec (Seraing, Belgium), using rabbits as production host. Antibodies were produced from His_6-tagged full length PomY, PomZ and PomX and from native full length FtsZ purified from *E. coli*. If multiple antibodies were produced production number of used antibody is indicated in Table 22.

Table 22: Antibodys used in this study with their corresponding dilution used for detection

Antibody	Dilution
a-PomZ (No. 492)	1 : 10.000
a-PomY (No. 1411)	1 : 10.000
a-PomX (No. 948)	1 : 5.000
a-FtsZ (No. 852)	1 : 25.000
a-mCherry	1 : 10.000
a-GFP	1 : 2.000
Goat a-rabbit IgG	1 : 25.000
Sheep a-mouse IgG	1 : 5.000

8.5.9 Protein pelleting assay

To investigate protein-protein interaction *in vitro* sedimentation assays were performed with purified proteins. Before sedimentation a clear spin was performed with proteins to be tested in the sedimentation assay at 20000 g for 5 min at 4 °C. For sedimentation assays proteins were mixed and pre-incubated for 2 min at 32°C in a total volume of 20 µl mixed with 8 x reaction buffer to a final concentration of 1 x (Table 23). If necessary, 1 mM ATP were added to the mixture and together incubated for additional 10 min at 32 C. Protein mixtures were then transferred into centrifugation tubes and spun down with a Beckman® Airfuge™ at 29 psi (~ 160.000 g). Supernatant was carefully

removed and used as the soluble fraction for SDS-PAGE analysis. The pellet fraction was resolved in the same volume as the supernatant and also used for SDS-PAGE analysis. Proteins from supernatant and pellet fraction were separated by SDS-PAGE and stained with Instant Blue™ (expedeon, Cambridgeshire, UK) for 10 min.

8.5.10 Radioactive GTPase assay with FtsZ

GTP-hydrolysis by FtsZmx was measured at different protein concentrations in the range between 4 µM - 8 µM in a radioactive GTPase assay. For the assay FtsZ was mixed with 8 x reaction buffer diluted with ddH2O to a final concentration of 1 x in 97 µl total volume. Protein was incubated at 32 °C for 2 min to adapt for termperature and reaction was started by addition of 3 µl GTP mix of 1 µl 50 mM GTP and 2 µl (gamma-^{32}P) GTP. Final concentration of (gamma-^{32}P) GTP was 0.066 µM. After 2, 5, 10 and 15 min 10 µl sample were collected and mixed with 400 µl charcoal solution (50 g/l charcoal in 20 mM phosphoric acid). Solution was pelleted for 2 min at 13000 rpm at room temperature. 100 µl of the supernatant were mixed with 3 ml Quick Safe A. and measured by scintillation counting to determine the amount of free $^{32}P_i$ in solution. To determine turnover rate of GTP measured counts per minute (cpm) were plotted as function of time. Turnover rate of GTP was calculated at different protein concentrations from values in the linear range of the assay.

8.5.11 Right angle light scattering

Right angle light scattering was performed with 10 µM FtsZ in 8 x reaction buffer, filled up with ddH_2O to a final concentration of 1 x (Table 23) on a temperature-controlled ISS PC1 spectrofluorometer with a cooled photomultiplier. The excitation and emission wavelength were set to 350 nm. Assays were performed at 8 °C. FtsZ was preincubated in the cuvette to adapt for termperture. Measurement was initiated and after 100 s filament formation was started by addition of GTP to final concentration of 250 µM. Light scattering was followed for 900 s. As negative control light scattering of FtsZ alone in absence of GTP was measured for 900 s.

8.5.12 Electrophoretic mobility shift assay (EMSA)

To test the ability of purified His_6-PomZ to interact with double stranded plasmid DNA *in vitro* electrophoretic mobility shift assays were performed. For the assay His_6-PomZ was dialysed against EMSA buffer (50 mM Tris-HCl pH 8.5, 5 mM $MgSO_4$). DNA-binding of His_6-PomZ was assayed in presence of 200 fmol purified pUC18 plasmid DNA. To assay binding kinetics 0 pmol -100 pmol His_6-PomZ was preincubated with pUC18 DNA for 10 min at 25 °C. If ATP was necessary it was added at a final concentration of 0.75 mM. After 10 min, reactions were mixed with loading dye and separated on, 1 % agarose gel buffered in 0.5 x TB buffer with $MgSO_4$ (45 mM Tris base, 45 mM boric acid, 1mM $MgSO_4$) and stained with ethidium bromide.

8.5.13 ATPase assay with malachite green

To determine the turnover rate of ATP by PomZ a colorimetric malachite green assay was performed. Malachite green is an indicator for inorganic phosphate and turns from yellow to green, depending on the amount of inorganic phosphate in solution (Lanzetta *et al.*, 1979). For the malachite green assay proteins of interest, in general His_6-PomZ was incubated in a 96-well plate (Greiner Bio-

One GmbH, Frickenhausen). Protein was mixed in triplicate with 8 x reaction buffer (400 mM Hepes/NaOH pH 7.2; 400 mM KCl; 80 mM $MgCl_2$; 8 mM β-mercaptoethanol) supplemented with 8 mM ATP and filled up with ddH_2O to a final concentration of 1 x to start the reaction and keep reaction volumes the same. Reaction was performed at 37 °C for 30 min. After incubation each reaction was supplemented with 250 µl malachite green reagent and incubated for additional 5 min. To stop the reaction and the color development of the malachite green reagent, 50 µl of 34 % (v/v) citric acid was added to the reaction. After 15 min the developed color was measured with an Infini te M200 Pro plate-reader at 660 nm. In order to elucidate the effect of PomX-His_6 and PomY-His_6 on His_6-PomZ the proteins were pre-mixed prior to reaction start with ATP. To determine if DNA has any effect on His_6-PomZ ATPase activity, pUC18 plasmid DNA was added to the proteins to a final concentration of 5 nM. To avoid contaminating phosphate from pUC18 purification and storage, plasmid DNA was dialyzed against dialysis buffer (50 mM Hepes/NaOH pH 7.2; 50 mM KCl; 0.1 mM EDTA; 1 mM β-mercaptoethanol; 10 % (v/v) glycerol). For each assay a 6-point phosphate standard curve was measured. The inorganic phosphate released from hydrolyzed ATP by His_6-PomZ was obtained from the regression of the standard curve. The turnover rate of ATP per molecule His_6-PomZ per hour was calculated.

Table 23: Buffers and solutions with their composition, needed for malachite green assay

Solution	Composition
8 x reaction buffer	400 mM Hepes/NaOH pH 7.2 400 mM KCl 80 mM $MgCl_2$ 8 mM β-mercaptoethanol 8 mM ATP
Malachite green solution	170 mg malachite green (Sigma-Aldrich, Taufkirchen) in 23,5 ml ddH_2O 5,25 g ammonium molybdate in 125 ml of 4 M HCl Both components are mixed and filled up to 500 ml with ddH_2O on ice. Mixture is cooled on ice for 1 h and then filtered.

8.6 Microscopy

8.6.1 Fluorophores and filter sets for fluorescence microscopy

Fluorophores which were used in this study are listed in Table 24. To activate and follow the localization of fluorescently tagged proteins the filter systems listed in Table 25 were used in this study.

Table 24: Fluorophores for fluorescence microscopy used in this study

Fluorophore	Specification
mCherry	Monomeric fluorophore Excitation maximum: 578 nm Emission maximum: 610 nm
GFP	Codon optimized sequence for high GC content Excitation maximum: 395 nm Emission maximum: 509 nm
eYFP	Excitation maximum: 514 nm Emission maximum: 527 nm

Table 25: Filtersets used for the DMI 6000 B microscope (Leica)

Filter	Excitations	Emission
A4 (DAPI)	360/40	470/40
L5 (GFP)	480/40	527/30
TX2 (mCherry)	560/40	645/75
YFP	500/20	535/30

Numbers of excitation and emission wavelength are given in nm.

8.6.2 Live cell imaging

To perform fluorescence microscopy with *M. xanthus* strains, liquid cultures were inoculated and grown for 48 h in an exponential growth phase. To allow cells to grow exponentially for 48 h cultures were inoculated from one single colony in 5 ml CTT medium with corresponding antibiotics in the morning of day 1 and diluted twice a day to an OD_{550} of 0.1. On day 3 cells were imaged at an OD_{550} of 0.3 - 0.6 on TPM agarose slides (Table 6). 10 µl of culture were mounted onto the TPM agarose patch and incubated for 5 min at RT in the dark to let the cells attach to the surface. Cells were covered with a 0.17 mm coverslip before microscopy. If necessary 390 µl culture was pre-mixed with 10 µl of 40 µg/ml DAPI and incubated 5 min at 32 °C shaking in the dark before 10 µl were applied to the TPM agarose patch. Cells were imaged if not mentioned differently with a DMI 6000 B microscope (Leica, Wetzlar) with a HCX PL APO 100x/1.47 oil objective corrected for TIRF (Table 4) at 32 °C in the dark and recorded with a Hamamatsu Flash 4.0 sCMOS camera. Images were acquired with Leica MM AF and processed Metamorph® v 7.5 (Molecular Devices).

8.6.3 Time-lapse microscopy

If cells were imaged to follow growth and localization of fluorescent proteins over time, cells were treated differently to allow bacteria to grow normally under these conditions. 10 µl of exponentially growing cells (8.6.2) were spotted on a 0.17 mm thick and 22 x 60 mm glass coverslip that was attached to a plastic slide with a hole in the middle. On these cells a thin layer of TPM agarose with 0.25 % CTT and antibiotics was applied which was covered with parafilm to prevent drying. Cells were imaged from the bottom through the hole with the same setup as described in 8.6.2.

8.6.4 Fluorescence recovery after photobleaching (FRAP)

To follow the *in vivo*-dynamics of PomX, PomY and PomZ and its derivatives we performed fluorescence recovery after photobleaching experiments on their fluorescently labeled fusion-proteins. Photobleaching was exclusively performed on the mCherry-labelled versions of PomX, PomY and PomZ. For these experiments cells were grown in CTT medium and diluted twice a day to keep them exponentially growing for 48 h as described in 8.6.2 and were prepared for microscopy as described in 8.6.3. FRAP experiments were performed on a Nikon Ti-Eclipse microscope with Perfect Focus System (PFS), with a CFI PL APO 100 x / 1.45 oil objective at 32 °C in the dark. Pictures were recorded with a Hamamatsu Flash 4.0 sCMOS camera (Table 4) using the NIS Elements AR 2.30 software (Nikon). After initial calibration of the lasers, according to manufacturer's advice, for photobleaching a 651 nm laser beam was focused on the central part of the image plane. After acquisition of an initial pre-bleach picture, cells of interest were bleached using a single 5 x 5 pixel circular shaped region. Laser intensities had to be adjusted according to Table 26. Directly after bleaching and in different intervals pictures were acquired to follow cellular fluorescence (Table 26). Data analysis, in particular quantification of fluorescence intensities, was performed with Metamorph® v 7.5 (Molecular Devices Union City, CA). For every timepoint, a pictures was aquired, total integrated cellular fluorescence in a region of interest (ROI) within the outline of the cell was measured together with total integrated background fluorescence of a ROI of same size placed on the background. Additionally, fluorescence intensity was measured in the bleached region together with background fluorescence or a ROI of same size placed on the background. After background correction, corrected fluorescence intensity of the bleached area (or area of interest) was divided by total corrected cellular fluorescence, which in term corrects for bleaching effects during picture acquisition. This relative fluorescence was correlated to the initial fluorescence in the bleached area (or area of interest). The mean relative fluorescence of several cells was plotted as function of time [sec]. To get a recovery rate for the tested fluorescent protein (t_1), the plotted data was fitted to an "*Expdec 1*" function ($y = y_0 + A * e^{-x/t}$) using Origin8.0. Half-maximal recovery ($t_{1/2}$) was calculated from the recovery rate (t_1) by $t_{1/2} = \ln(2) * t_1$.

Table 26: Laser adjustments for FRAP experiments

Strain	FRAP conditions
SA3131	Laser 561 nm, 1 x 5 % laser power, 500 µsec dwelling time (approx. 32 msec); Acquisition 1000 msec
SA3147	Laser 561 nm, 1 x 5 % laser power, 500 µsec dwelling time (approx. 32 msec); Acquisition 1000 msec
SA4799	Laser 561 nm, 10 x 10 % laser power, 500 µsec dwelling time (approx.. 160 msec); Acquisition 300 msec
SA7003	Laser 561 nm, 10 x 10 % laser power, 500 µsec dwelling time (approx.. 160 msec); Acquisition 300 msec
SA7004	Laser 561 nm, 10 x 10 % laser power, 500 µsec dwelling time (approx.. 160 msec); Acquisition 300 msec

SA7011	Laser 561 nm, 10 x 10 % laser power, 500 µsec dwelling time (approx.. 160 msec); Acquisition 300 msec
SA7012	Laser 561 nm, 10 x 10 % laser power, 500 µsec dwelling time (approx.. 160 msec); Acquisition 300 msec

8.6.5 Measuring cell length

Deletion of *pomX*, *pomY* and *pomZ* results in cell division phenotype. One way to characterize the cell division phenotype is the analysis of the cell length in a population of cells. For analysis the traced line tool of Metamorph® v 7.5 was used and cell length was measured along the long axes of the cell by placing the traced line through the middle of the cell.

8.6.6 Image alignment and particle tracking

In order to quantify dynamics of the PomX-PomY cluster *in vivo*, time-lapse movies were recorded as described in 8.6.3. Exponentially growing cells of non-motile strains, obtained by deletion of *mglA*, were imaged by DIC microscopy together with fluorescence microscopy every 30 sec for 30 min. To reduce artificial cluster motion, cells were excluded that showed any kind of cellular motility. Additionally, movies were aligned using the Metamorph® v 7.5 auto-alignment tool. As a reference point for movie auto-alignment a 1:100 dilution of TetraSpeck™ 0.5 µm fluorescently labelled beads (Molecular probes™ life technologies,Karlsruhe) was mixed in a 1:1 ratio prior to application of cells to the agar pad. In general, this leads to 1 TetraSpeck™ bead per frame, which is enough for precise picture alignment. For each cell to be analyzed cell length as well as cluster position in % of cell length was measured. Additionally, for later analysis, cells were oriented that off-centre clusters were always left of midcell and on a tangent that was horizontally in case the cell was curved. To obtain data the Metamorph® v 7.5 particle tracking tool was used. For our analysis the maximum identity method was chosen, with a minimal identity of 60 % from frame to frame and a maximal displacement of 50 pixel in between frames. Tracks of all cells were manually inspected afterwards.

To obtain the cumulative distance [µm²] the distance a cluster moved within two timepoints was squared. A mean squared distance was calculated from multiple cells for each timepoint. Mean squared distance was added up from 0 - 20 min, resulting in the cumulative distance. For Mean Squared Displacement (MSD) analysis the distance of the cluster at t_x to the cluster position at t_0 was squared for each cell and timepoint and a mean was calculated from all cells analyzed. The data was plotted as function of time to give information about the MSD at a given timepoint.

8.6.7 Transmission electron microscopy

Transmission electron microscopy (TEM) was performed to test if PomX-His_6, PomY-His_6 and $FtsZ_{mx}$ form higher-ordered structures, interact and have any function on each other *in vitro* that is observable under these conditions. Experiments were performed at the MPI for Biophysics (Frankfurt) in close collaboration with Dr. Janet Vonck or with Andrea Harms at the MPI for Terrestrial Microbiology (Marburg). In order to do electron microscopy proteins of interest had to be applied on an electron microscopy grid, fixed and stained using the negative stain method with uranyl acetate. In

brief, uranyl acetate solution was prepared by solving 4 % (w/v) uranyl acetate in ddH_2O. When uranyl acetate was solved, solution was diluted to 2 % with ddH_2O. 2 % uranyl acetate solution was spun down prior to usage for 10 min at 20000 g at room temperature. Uranyl acetate solution was stored at room temperature in the dark for several months. For fixation and negative stain of protein samples, 10 µl of a protein sample of interest were applied on one side of the EM grid and incubated for 1 min at room temperature. Liquid was blotted through the grid by applying the unused side of the grid on a Whatman paper. Grid was washed twice with ddH_2O and once with 1 % Uranyl acetate solution with the same technique. Then uranyl acetate was applied on the grid for 20 sec and dried by blotting the liquid through the grid with a Whatman paper. Finished grids were stored in a grid holder for several months at room temperature. Electron microscopy was performed by Dr. Janet Vonck with a CM120 (FEI) at 120 KV or with Andrea Harms with a JEM-1400 Plus (Jeol).

8.7 Bioinformatical analysis

M. xanthus genes and protein sequences were obtained from NCBI (http://www.ncbi.nlm.nih.gov/). To search for homologous protein sequences Blastp and Blastx searches were performed (NCBI) using a protein query or a nucleotide query, respectively (http://blast.ncbi.nlm.nih.gov/Blast.cgi). Protein sequences were further analyzed using the SMART algorithm (http://smart.embl-heidelberg.de/). Protein sequences were aligned using MAFFT (**M**ultiple **A**lignment using **F**ast **F**ourier **T**ransform) (http://www.ebi.ac.uk/Tools/msa/mafft/) and further analysed with iTOl (**I**nteractive **T**ree **O**f **L**ife) (http://itol.embl.de/upload.cgi). To identify global similarity and identity between two proteins of interest the EMBOSS Needle algorithm was used (http://www.ebi.ac.uk/Tools/psa/emboss_needle/).

8.8 List of protein sequences used for phylogenetic analysis

ArsA proteins

Escherichia coli (gi|501622470), *Klebsiella pneumonae* (gi|505445306), *Acidovorax ebreus* (gi|506393889), *Ralstonia pickettii* (gi|502315734), *Gallionella capsiferriformans* (gi|503059344), *Mycobacterium gilvum* (gi|500222446), *Rhodococcus opacus* (gi|501996657), *Rhizobium leguminosarum* (gi|499973157), *Magnetospirillum magneticum* (gi|499703504), *Planctopirus limnophila* (gi|502873491), *Rhodospirillum rubrum* (gi|499708467)

MinD proteins

Bordetella petrii (gi|501204886), *Neisseria menengitidis* (gi|488144255), *Brucella* (gi|492971474), *Bradyrhizobium* (gi|499399518), *Rhodopseudomonas palustris* (gi|499983816), *Bacillus subtilis* (gi|490533452), *Synechocystis sp*. PCC6803 (gi|499176303), *Shewanella oneidensis* (gi|499385037), *Azotobacter vinelandii* (gi|502035008), *Klebsiella pneumoniae* (gi|523671144), *Escherichia coli* (gi|766633109)

MipZ proteins

Magnetospirillum gryphiswaldense MSR-1 (gi|144898536), *Caulobacter vibrioides* (gi|499222486), *Rhodospirillum rubrum* (gi|499709233), *Bradyrhizobium* (gi|499400452), *Phenylobacterium zucineum* (gi|501513915), *Rickettsia bellii* (gi|499796306), *Rickettsia canadensis* (gi|501098386), *Zymomonas mobilis* (gi|499559478), *Ruegeria pomeroyi* (gi|499358130), *Caulobacter crescentus* (gi|501244156), *Hyphomonas neptunium* (gi|499965430), *Maricaulis maris* (gi|499962939)

MotR proteins

Pseudomonas aeruginosa (gi|5902661), *Campylobacter jejunii* (gi|488943616), *Aliivibrio fischeri* (gi|491562734), *Cellvibiro japonicus* Ueda107 (gi|190686710), *Helicobacter pylori* (gi|446987226), *Zymomonas mobilis* (gi|502557115), *Brachyspira pilosicoli* (gi|503010145), *Sulforospirillum deleyianum* (gi|502619237)

Mrp proteins

Escherichia coli (gi|26108894), *Synechocystis sp*. 6803 (gi|499175937), *Rhodopseudomonas palustris* (gi|499791786), *Clostridium botulinum* (gi|501312451), *Myxococcus xanthus* (gi|499873081), *Sinorhizobium fredii* (gi|502091604), *Wollinella succinogenes* (gi|499452267), *Klebsiella pneumoniae* (gi|520902047), *Paenibacillus sp*. (gi|506217839), *Ruegeria sp*. TM1040 (gi|499857009), *Synechococcus sp*. (gi|499561973), *Nostoc punctiforme* (gi|501379885)

NifH proteins

Anabaena variabilis (gi|1236929), *Acidithiobacillus ferrivorans* (gi|737207928), *Bradyrhizobium diazoefficiens* (gi|648510467), *Frankia alni* ACN14a (gi|111153677), *Klebsiella pneumoniae* (gi|927659270), *Denitrovibrio acetiphilus* (gi|502775377), *Burkholderia vietnamiensis* (gi|134148332), *Desulfitobacterium hafniense* (gi|492336898), *Allochromatium vinosum* (gi|502736094), *Azotobacter vinelandii* (gi|502027635), *Leptothrix cholodnii* (gi|501314825)

ParC proteins

Pseudomonas aeruginosa (gi|730349669), *Cellvibrio japonicas* (gi|501464291), *Shewanella denitrificans* (gi|499815059), *Saccharophagus degradans* (gi|499787901), *Alteromonas macleodii* (gi|501509749), *Marinobacter santoriniensis* (gi|4962247599, *Pseudoalteromonas atlantica* (gi|499895041), *Teredinibacter turnerae* (gi|506298550), *Colwellia* psychrerythraea (gi|499353461), *Idiomarina loihiensis* (gi|499553580), *Vibrio cholera* (gi|446560322), *Vibrio vulnificus* (gi|499392389), *Vibrio parahaemolyticus* (gi|491621921), *Vibrio campbellii* (gi|498329250), *Aliivibrio fischeri* (gi|491562721), *Photobacterium profundum* (gi|499536907), *Halorhodospira* halophile (gi|500137278), *Alkalilimnicola ehrlichii* (gi|499948004), *Thioalkalivibrio sulfidiphilus* (gi|501779816), *Halothiobacillus neapolitanus* (gi|502585830), *Marinomonas sp.* MWYL1 (gi|501018411), *Hahella chejuensis* (gi|499718173), *Aeromonas hydrophila* (gi|500024576), *Rhodospirillum rubrum* (gi|499709348), *Aliivibrio wodanis* (gi|769986628)

ParA proteins

Caulobacter crescentus (gi|16127983), *Thermus thermophilus* (gi|499487336), *Bacillus subtilis* (gi|16081149), *Streptomyces coelicolor* A3(2) (gi|6539745), *Enterococcus faecalis* (gi|488335554), *Bordetella pertussis* (gi|565689132), *Magnetospirillum magneticum* (gi|499701719), *Phenylobacterium zucineum* (gi|501516131), *Rickettsia canadensis* (gi|501098296), *Rhodopseudomonas palustris* (gi|499981121), *Hyphomonas neptunium* (gi|114739091), *Neisseria meningitidis* (gi|488148987), *Paracoccus denitrificans* (gi|500070033)

PpfA

Rhodobacter sphaeroides (gi|488807787)

SopA

Escherichia coli (gi|693074657)

***Anaeromyxobacter dehalogenans* 2CP-C ParA-like ATPases**

Adeh_4355 (gi|85777281), Adeh_3835 (gi|499742149), Adeh_0930 (gi|499739254), Adeh_3274 (gi|85776205), Adeh_1356 (gi|499739679)

***Corallococcus coralloides* DSM 2259 ParA-like ATPases**

COCOR_08074 (gi|504213744), COCOR_00543 (gi|504206293), COCOR_06325 (gi|504212011), COCOR_04050 (gi|380734363)

***Haliangium ochraceum* DSM 14365 ParA-like ATPases**

Hoch_4591 (gi|502592088), Hoch_4669 (gi|502592167), Hoch_0095 (gi|262076767), Hoch_6822 (gi|262083317), Hoch_4486 (gi|262081010)

***Myxococcus fulvus* HW-1 ParA-like ATPases**

LILAB_08935 (gi|337257538), LILAB_05640 (gi|337256889), LILAB_17170 (gi|337259177), LILAB_27830 (gi|337261293)

***Myxococcus stipitatus* DSM 14675 ParA-like ATPases**

MYSTI_08118 (gi|441492689), MYSTI_00640 (gi|441485295), MYSTI_06407 (gi|441490985), MYSTI_03965 (gi|441488576), MYSTI_01518 (gi|441486163)

***Myxococcus xanthus* DK1622 ParA-like ATPases**

MXAN_5815 (gi|108464137), MXAN_7477 (ParA) (gi|108467427), MXAN_0635 (PomZ) (gi|27804832), MXAN_3920 (gi|108463317)

***Stigmatella aurantiaca* DW4/3-1 ParA-like ATPases**

STIAU_3067 (gi|115368893), STIAU_5794 (gi|115369324), STIAU_7860 (gi|115367687), STIAU_2218 (gi|115364878)

***Sorangium cellulosum* So0157-2 ParA-like ATPases**

SCE1572_18980 (gi|520999385), SCE1572_19025 (gi|520999390), SCE1572_41305 (gi|521007379), SCE1572_23930 (gi|521004257), SCE1572_45000 (gi|520999880), SCE1572_45945 (gi|521008194), SCE1572_20405 (gi|521003646)

8.8.1 ParA/MinD ATPases from unpublished genomes

Cystobacter fuscus

CFUS_00887:

MDAPTYSPKQVAEMLGVPLKSLTPALEQDSYTGAEVWALRERLGVFPAPLGRRKQLFLNFKGGTGKT
SLSTSYAWRLAELGYTVLIIDLDSQGHATKCLGYEGEDFDQTLLNVLVRKAPLSEVIQKTSLPNLDFVP
SNLTMSTVDLALMPMAGREFKLRNALKEVEGRYDVIVFDAPPSFGLLNLNALMAANDLFVPVLADFLS
FHGLKLLFETVQGLDEDLNHVLDHVFIVVNSFNATFRLAKEALEALQTHYPEYLLPTIIRQCTKFAQAAS
EGRPIFVADPSSKGATDIESLIQHVLPRLRAGAAPGSDTGAQQAG

Melittangium boletus

Mbol_XXXX:

MDAPTYSPKQVAELLGLPLKSFTPALKQDSYTGAEVWALREQLGRFPEPIGRRKQLFLNFKGGTGKT
SLSTSYAWRLAELGFTVLIIDLDSQGHATKCLGYEGEDFDQTLLNVLVRKVPLSEVIQKTSLPNLDFVP
SNLTMSTVDLALMPMAGREFKLRNALKEVEGRYDVIVFDAPPSFGLLNLNALMAANDLFVPVLADFLS
FHGLKLLFETVQGLDEDLNHVLDHVFIVVNSFNATFRLAKEALEALQTHYPEYLLPTIIRQCTRFAQAAS
EGRPIFAADPGSKGATDIESLIQHVLPRLRAGSAPGSGTDAQQAG

Myxococcus macrosporus

MMAC_00648:

MEAPTYSSKQVAEMLGVSPKQIPEESRKDAYTPDDIWELRATLDRFPARLGHRRQLFLNFKGGTGKT
SLSTSYAWRLAELGYAVLLIDLDSQGHATKCLGYEGEDFEKTLLDVLVRKTPLAKVIQKSSLPNLDFVP
SNLTMSTVDLALMPMAGREFKLRNALKDVEAQYDVVVFDAPPSFGLLNLNALMAANDLFVPVLADFLS
FHGLKLLFETVQSLEEDLNHVLDHVFIVVNSFNATFKLAKEALEALQTHYPEFLLPTIIRQCTKFAQASS
EGRPVFVADPSSKGANDIQAMIDNILPRLVAAAAAAQTKGTQQAG

9 References

Aarsman, M.E., A. Piette, C. Fraipont, T.M. Vinkenvleugel, M. Nguyen-Disteche & T. den Blaauwen, (2005) Maturation of the *Escherichia coli* divisome occurs in two steps. *Molecular microbiology* **55**: 1631-1645.

Adams, D.W., L.J. Wu & J. Errington, (2015) Nucleoid occlusion protein Noc recruits DNA to the bacterial cell membrane. *The EMBO journal* **34**: 491-501.

Addinall, S.G. & J. Lutkenhaus, (1996) FtsA is localized to the septum in an FtsZ-dependent manner. *Journal of bacteriology* **178**: 7167-7172.

Aguiluz Fabian, K., (2009) The ParA-protein AgmE positively regulates cell division in *Myxococcus xanthus*. Doctoral Thesis. Philipps-Universität Marburg, Marburg, Germany.

Ah-Seng, Y., F. Lopez, F. Pasta, D. Lane & J.Y. Bouet, (2009) Dual role of DNA in regulating ATP hydrolysis by the SopA partition protein. *The Journal of biological chemistry* **284**: 30067-30075.

Altschul, S.F., W. Gish, W. Miller, E.W. Myers & D.J. Lipman, (1990) Basic local alignment search tool. *Journal of molecular biology* **215**: 403-410.

Anderson, D.E., F.J. Gueiros-Filho & H.P. Erickson, (2004) Assembly dynamics of FtsZ rings in *Bacillus subtilis* and *Escherichia coli* and effects of FtsZ-regulating proteins. *Journal of bacteriology* **186**: 5775-5781.

Andrade, M.A. & P. Bork, (1995) HEAT repeats in the Huntington's disease protein. *Nature genetics* **11**: 115-116.

Artimo, P., M. Jonnalagedda, K. Arnold, D. Baratin, G. Csardi, E. de Castro, S. Duvaud, V. Flegel, A. Fortier, E. Gasteiger, A. Grosdidier, C. Hernandez, V. Ioannidis, D. Kuznetsov, R. Liechti, S. Moretti, K. Mostaguir, N. Redaschi, G. Rossier, I. Xenarios & H. Stockinger, (2012) ExPASy: SIB bioinformatics resource portal. *Nucleic acids research* **40**: W597-603.

Balaban, M. & D.R. Hendrixson, (2011) Polar flagellar biosynthesis and a regulator of flagellar number influence spatial parameters of cell division in *Campylobacter jejuni*. *PLoS pathogens* **7**: e1002420.

Barilla, D., E. Carmelo & F. Hayes, (2007) The tail of the ParG DNA segregation protein remodels ParF polymers and enhances ATP hydrolysis via an arginine finger-like motif. *Proceedings of the National Academy of Sciences of the United States of America* **104**: 1811-1816.

Barilla, D., M.F. Rosenberg, U. Nobbmann & F. Hayes, (2005) Bacterial DNA segregation dynamics mediated by the polymerizing protein ParF. *The EMBO journal* **24**: 1453-1464.

Berger, J.M., S.J. Gamblin, S.C. Harrison & J.C. Wang, (1996) Structure and mechanism of DNA topoisomerase II. *Nature* **379**: 225-232.

Bernander, R. & T.J. Ettema, (2010) FtsZ-less cell division in archaea and bacteria. *Current opinion in microbiology* **13**: 747-752.

Bernhardt, T.G. & P.A. de Boer, (2003) The *Escherichia coli* amidase AmiC is a periplasmic septal ring component exported via the twin-arginine transport pathway. *Molecular microbiology* **48**: 1171-1182.

Bernhardt, T.G. & P.A. de Boer, (2005) SlmA, a nucleoid-associated, FtsZ binding protein required for blocking septal ring assembly over chromosomes in *E. coli*. *Molecular cell* **18**: 555-564.

Bi, E. & J. Lutkenhaus, (1993) Cell division inhibitors SulA and MinCD prevent formation of the FtsZ ring. *Journal of bacteriology* **175**: 1118-1125.

Bi, E.F. & J. Lutkenhaus, (1991) FtsZ ring structure associated with division in *Escherichia coli*. *Nature* **354**: 161-164.

Bigot, S., O.A. Saleh, C. Lesterlin, C. Pages, M. El Karoui, C. Dennis, M. Grigoriev, J.F. Allemand, F.X. Barre & F. Cornet, (2005) KOPS: DNA motifs that control *E. coli* chromosome segregation by orienting the FtsK translocase. *The EMBO journal* **24**: 3770-3780.

Bouet, J.Y., Y. Ah-Seng, N. Benmeradi & D. Lane, (2007) Polymerization of SopA partition ATPase: regulation by DNA binding and SopB. *Molecular microbiology* **63**: 468-481.

Bourne, H.R., D.A. Sanders & F. McCormick, (1991) The GTPase superfamily: conserved structure and molecular mechanism. *Nature* **349**: 117-127.

Bowman, G.R., L.R. Comolli, G.M. Gaietta, M. Fero, S.H. Hong, Y. Jones, J.H. Lee, K.H. Downing, M.H. Ellisman, H.H. McAdams & L. Shapiro, (2010) Caulobacter PopZ forms a polar subdomain dictating sequential changes in pole composition and function. *Molecular microbiology* **76**: 173-189.

Bowman, G.R., L.R. Comolli, J. Zhu, M. Eckart, M. Koenig, K.H. Downing, W.E. Moerner, T. Earnest & L. Shapiro, (2008) A polymeric protein anchors the chromosomal origin/ParB complex at a bacterial cell pole. *Cell* **134**: 945-955.

Boyle, D.S., M.M. Khattar, S.G. Addinall, J. Lutkenhaus & W.D. Donachie, (1997) ftsW is an essential cell-division gene in *Escherichia coli*. *Molecular microbiology* **24**: 1263-1273.

Bramkamp, M., R. Emmins, L. Weston, C. Donovan, R.A. Daniel & J. Errington, (2008) A novel component of the division-site selection system of *Bacillus subtilis* and a new mode of action for the division inhibitor MinCD. *Molecular microbiology* **70**: 1556-1569.

Breier, A.M. & A.D. Grossman, (2007) Whole-genome analysis of the chromosome partitioning and sporulation protein Spo0J (ParB) reveals spreading and origin-distal sites on the *Bacillus subtilis* chromosome. *Molecular microbiology* **64**: 703-718.

Buddelmeijer, N. & J. Beckwith, (2004) A complex of the *Escherichia coli* cell division proteins FtsL, FtsB and FtsQ forms independently of its localization to the septal region. *Molecular microbiology* **52**: 1315-1327.

Bulyha, I., C. Schmidt, P. Lenz, V. Jakovljevic, A. Hone, B. Maier, M. Hoppert & L. Sogaard-Andersen, (2009) Regulation of the type IV pili molecular machine by dynamic localization of two motor proteins. *Molecular microbiology* **74**: 691-706.

Camberg, J.L., J.R. Hoskins & S. Wickner, (2009) ClpXP protease degrades the cytoskeletal protein, FtsZ, and modulates FtsZ polymer dynamics. *Proceedings of the National Academy of Sciences of the United States of America* **106**: 10614-10619.

Campos-Garcia, J., R. Najera, L. Camarena & G. Soberon-Chavez, (2000) The *Pseudomonas aeruginosa motR* gene involved in regulation of bacterial motility. *FEMS microbiology letters* **184**: 57-62.

Campos, M., I.V. Surovtsev, S. Kato, A. Paintdakhi, B. Beltran, S.E. Ebmeier & C. Jacobs-Wagner, (2014) A constant size extension drives bacterial cell size homeostasis. *Cell* **159**: 1433-1446.

Castaing, J.P., J.Y. Bouet & D. Lane, (2008) F plasmid partition depends on interaction of SopA with non-specific DNA. *Molecular microbiology* **70**: 1000-1011.

Cho, H., H.R. McManus, S.L. Dove & T.G. Bernhardt, (2011) Nucleoid occlusion factor SlmA is a DNA-activated FtsZ polymerization antagonist. *Proceedings of the National Academy of Sciences of the United States of America* **108**: 3773-3778.

Cordell, S.C., E.J. Robinson & J. Lowe, (2003) Crystal structure of the SOS cell division inhibitor SulA and in complex with FtsZ. *Proceedings of the National Academy of Sciences of the United States of America* **100**: 7889-7894.

Crooks, G.E., G. Hon, J.M. Chandonia & S.E. Brenner, (2004) WebLogo: a sequence logo generator. *Genome research* **14**: 1188-1190.

Daniel, R.A., E.J. Harry & J. Errington, (2000) Role of penicillin-binding protein PBP 2B in assembly and functioning of the division machinery of *Bacillus subtilis*. *Molecular microbiology* **35**: 299-311.

Davis, M.A., K.A. Martin & S.J. Austin, (1992) Biochemical activities of the ParA partition protein of the P1 plasmid. *Molecular microbiology* **6**: 1141-1147.

de Boer, P.A., R.E. Crossley, A.R. Hand & L.I. Rothfield, (1991) The MinD protein is a membrane ATPase required for the correct placement of the *Escherichia coli* division site. *The EMBO journal* **10**: 4371-4380.

de Boer, P.A., R.E. Crossley & L.I. Rothfield, (1989) A division inhibitor and a topological specificity factor coded for by the *minicell* locus determine proper placement of the division septum in *E. coli*. *Cell* **56**: 641-649.

de Boer, P.A., R.E. Crossley & L.I. Rothfield, (1992) Roles of MinC and MinD in the site-specific septation block mediated by the MinCDE system of *Escherichia coli*. *Journal of bacteriology* **174**: 63-70.

Donovan, C., A. Schauss, R. Kramer & M. Bramkamp, (2013) Chromosome segregation impacts on cell growth and division site selection in *Corynebacterium glutamicum*. *PloS one* **8**: e55078.

Donovan, C., A. Schwaiger, R. Kramer & M. Bramkamp, (2010) Subcellular localization and characterization of the ParAB system from *Corynebacterium glutamicum*. *Journal of bacteriology* **192**: 3441-3451.

Ebersbach, G., A. Briegel, G.J. Jensen & C. Jacobs-Wagner, (2008a) A self-associating protein critical for chromosome attachment, division, and polar organization in caulobacter. *Cell* **134**: 956-968.

Ebersbach, G., E. Galli, J. Moller-Jensen, J. Lowe & K. Gerdes, (2008b) Novel coiled-coil cell division factor ZapB stimulates Z ring assembly and cell division. *Molecular microbiology* **68**: 720-735.

Ebersbach, G. & K. Gerdes, (2001) The double *par* locus of virulence factor pB171: DNA segregation is correlated with oscillation of ParA. *Proceedings of the National Academy of Sciences of the United States of America* **98**: 15078-15083.

Ebersbach, G. & K. Gerdes, (2004) Bacterial mitosis: partitioning protein ParA oscillates in spiral-shaped structures and positions plasmids at mid-cell. *Molecular microbiology* **52**: 385-398.

Ebersbach, G., S. Ringgaard, J. Moller-Jensen, Q. Wang, D.J. Sherratt & K. Gerdes, (2006) Regular cellular distribution of plasmids by oscillating and filament-forming ParA ATPase of plasmid pB171. *Molecular microbiology* **61**: 1428-1442.

Edwards, D.H. & J. Errington, (1997) The *Bacillus subtilis* DivIVA protein targets to the division septum and controls the site specificity of cell division. *Molecular microbiology* **24**: 905-915.

Enenkel, C., N. Schulke & G. Blobel, (1996) Expression in yeast of binding regions of karyopherins alpha and beta inhibits nuclear import and cell growth. *Proceedings of the National Academy of Sciences of the United States of America* **93**: 12986-12991.

Fink, G. & J. Lowe, (2015) Reconstitution of a prokaryotic minus end-tracking system using TubR*C* centromeric complexes and tubulin-like protein TubZ filaments. *Proceedings of the National Academy of Sciences of the United States of America* **112**: E1845-1850.

Fleming, T.C., J.Y. Shin, S.H. Lee, E. Becker, K.C. Huang, C. Bustamante & K. Pogliano, (2010) Dynamic SpoIIIE assembly mediates septal membrane fission during Bacillus subtilis sporulation. *Genes & development* **24**: 1160-1172.

Fleurie, A., C. Lesterlin, S. Manuse, C. Zhao, C. Cluzel, J.P. Lavergne, M. Franz-Wachtel, B. Macek, C. Combet, E. Kuru, M.S. VanNieuwenhze, Y.V. Brun, D. Sherratt & C. Grangeasse, (2014) MapZ marks the division sites and positions FtsZ rings in *Streptococcus pneumoniae*. *Nature* **516**: 259-262.

Fogel, M.A. & M.K. Waldor, (2006) A dynamic, mitotic-like mechanism for bacterial chromosome segregation. *Genes & development* **20**: 3269-3282.

Friedman, S.A. & S.J. Austin, (1988) The P1 plasmid-partition system synthesizes two essential proteins from an autoregulated operon. *Plasmid* **19**: 103-112.

Friedrich, C., I. Bulyha & L. Sogaard-Andersen, (2014) Outside-in assembly pathway of the type IV pilus system in *Myxococcus xanthus*. *Journal of bacteriology* **196**: 378-390.

Galkin, V.E., A. Orlova, C. Rivera, R.D. Mullins & E.H. Egelman, (2009) Structural polymorphism of the ParM filament and dynamic instability. *Structure* **17**: 1253-1264.

Gamba, P., J.W. Veening, N.J. Saunders, L.W. Hamoen & R.A. Daniel, (2009) Two-step assembly dynamics of the Bacillus subtilis divisome. *Journal of bacteriology* **191**: 4186-4194.

Garner, E.C., C.S. Campbell, D.B. Weibel & R.D. Mullins, (2007) Reconstitution of DNA segregation driven by assembly of a prokaryotic actin homolog. *Science* **315**: 1270-1274.

Gerdes, K., M. Howard & F. Szardenings, (2010) Pushing and pulling in prokaryotic DNA segregation. *Cell* **141**: 927-942.

Gerdes, K., J.E. Larsen & S. Molin, (1985) Stable inheritance of plasmid R1 requires two different loci. *Journal of bacteriology* **161**: 292-298.

Gerdes, K. & S. Molin, (1986) Partitioning of plasmid R1. Structural and functional analysis of the parA locus. *Journal of molecular biology* **190**: 269-279.

Gerdes, K., J. Moller-Jensen & R. Bugge Jensen, (2000) Plasmid and chromosome partitioning: surprises from phylogeny. *Molecular microbiology* **37**: 455-466.

Gerding, M.A., B. Liu, F.O. Bendezu, C.A. Hale, T.G. Bernhardt & P.A. de Boer, (2009) Self-enhanced accumulation of FtsN at Division Sites and Roles for Other Proteins with a SPOR domain (DamX, DedD, and RlpA) in *Escherichia coli* cell constriction. *Journal of bacteriology* **191**: 7383-7401.

Gerding, M.A., Y. Ogata, N.D. Pecora, H. Niki & P.A. de Boer, (2007) The trans-envelope Tol-Pal complex is part of the cell division machinery and required for proper outer-membrane invagination during cell constriction in *E. coli*. *Molecular microbiology* **63**: 1008-1025.

Goehring, N.W. & J. Beckwith, (2005) Diverse paths to midcell: assembly of the bacterial cell division machinery. *Current biology : CB* **15**: R514-526.

Goehring, N.W., M.D. Gonzalez & J. Beckwith, (2006) Premature targeting of cell division proteins to midcell reveals hierarchies of protein interactions involved in divisome assembly. *Molecular microbiology* **61**: 33-45.

Goldman, B.S., W.C. Nierman, D. Kaiser, S.C. Slater, A.S. Durkin, J.A. Eisen, C.M. Ronning, W.B. Barbazuk, M. Blanchard, C. Field, C. Halling, G. Hinkle, O. Iartchuk, H.S. Kim, C. Mackenzie, R. Madupu, N. Miller, A. Shvartsbeyn, S.A. Sullivan, M. Vaudin, R. Wiegand & H.B. Kaplan, (2006) Evolution of sensory complexity recorded in a myxobacterial genome. *Proceedings of the National Academy of Sciences of the United States of America* **103**: 15200-15205.

Goley, E.D., N.A. Dye, J.N. Werner, Z. Gitai & L. Shapiro, (2010) Imaging-based identification of a critical regulator of FtsZ protofilament curvature in *Caulobacter*. *Molecular cell* **39**: 975-987.

Goley, E.D., Y.C. Yeh, S.H. Hong, M.J. Fero, E. Abeliuk, H.H. McAdams & L. Shapiro, (2011) Assembly of the *Caulobacter* cell division machine. *Molecular microbiology* **80**: 1680-1698.

Gomez-Santos, N., A. Treuner-Lange, A. Moraleda-Munoz, E. Garcia-Bravo, R. Garcia-Hernandez, M. Martinez-Cayuela, J. Perez, L. Sogaard-Andersen & J. Munoz-Dorado, (2012) Comprehensive set of integrative plasmid vectors for copper-inducible gene expression in *Myxococcus xanthus*. *Applied and environmental microbiology* **78**: 2515-2521.

Gregory, J.A., E.C. Becker & K. Pogliano, (2008) *Bacillus subtilis* MinC destabilizes FtsZ-rings at new cell poles and contributes to the timing of cell division. *Genes & development* **22**: 3475-3488.

Groves, M.R., N. Hanlon, P. Turowski, B.A. Hemmings & D. Barford, (1999) The structure of the protein phosphatase 2A PR65/A subunit reveals the conformation of its 15 tandemly repeated HEAT motifs. *Cell* **96**: 99-110.

Gueiros-Filho, F.J. & R. Losick, (2002) A widely conserved bacterial cell division protein that promotes assembly of the tubulin-like protein FtsZ. *Genes & development* **16**: 2544-2556.

Guzman, L.M., D. Belin, M.J. Carson & J. Beckwith, (1995) Tight regulation, modulation, and high-level expression by vectors containing the arabinose PBAD promoter. *Journal of bacteriology* **177**: 4121-4130.

Haeusser, D.P., A.C. Garza, A.Z. Buscher & P.A. Levin, (2007) The division inhibitor EzrA contains a seven-residue patch required for maintaining the dynamic nature of the medial FtsZ ring. *Journal of bacteriology* **189**: 9001-9010.

Haeusser, D.P., A.H. Lee, R.B. Weart & P.A. Levin, (2009) ClpX inhibits FtsZ assembly in a manner that does not require its ATP hydrolysis-dependent chaperone activity. *Journal of bacteriology* **191**: 1986-1991.

Haeusser, D.P., R.L. Schwartz, A.M. Smith, M.E. Oates & P.A. Levin, (2004) EzrA prevents aberrant cell division by modulating assembly of the cytoskeletal protein FtsZ. *Molecular microbiology* **52**: 801-814.

Hale, C.A. & P.A. de Boer, (1997) Direct binding of FtsZ to ZipA, an essential component of the septal ring structure that mediates cell division in *E. coli*. *Cell* **88**: 175-185.

Hale, C.A. & P.A. de Boer, (1999) Recruitment of ZipA to the septal ring of *Escherichia coli* is dependent on FtsZ and independent of FtsA. *Journal of bacteriology* **181**: 167-176.

Hamoen, L.W., J.C. Meile, W. de Jong, P. Noirot & J. Errington, (2006) SepF, a novel FtsZ-interacting protein required for a late step in cell division. *Molecular microbiology* **59**: 989-999.

Harms, A., A. Treuner-Lange, D. Schumacher & L. Sogaard-Andersen, (2013) Tracking of chromosome and replisome dynamics in *Myxococcus xanthus* reveals a novel chromosome arrangement. *PLoS genetics* **9**: e1003802.

Hester, C.M. & J. Lutkenhaus, (2007) Soj (ParA) DNA binding is mediated by conserved arginines and is essential for plasmid segregation. *Proceedings of the National Academy of Sciences of the United States of America* **104**: 20326-20331.

Hirano, M., H. Mori, T. Onogi, M. Yamazoe, H. Niki, T. Ogura & S. Hiraga, (1998) Autoregulation of the partition genes of the mini-F plasmid and the intracellular localization of their products in *Escherichia coli*. *Molecular & general genetics : MGG* **257**: 392-403.

Hirota, Y., A. Ryter & F. Jacob, (1968) Thermosensitive mutants of *E. coli* affected in the processes of DNA synthesis and cellular division. *Cold Spring Harbor symposia on quantitative biology* **33**: 677-693.

Hodgkin, J. & D. Kaiser, (1977) Cell-to-cell stimulation of movement in nonmotile mutants of *Myxococcus*. *Proceedings of the National Academy of Sciences of the United States of America* **74**: 2938-2942.

Holden, S.J., T. Pengo, K.L. Meibom, C. Fernandez Fernandez, J. Collier & S. Manley, (2014) High throughput 3D super-resolution microscopy reveals *Caulobacter crescentus in vivo* Z-ring organization. *Proceedings of the National Academy of Sciences of the United States of America* **111**: 4566-4571.

Holeckova, N., L. Doubravova, O. Massidda, V. Molle, K. Buriankova, O. Benada, O. Kofronova, A. Ulrych & P. Branny, (2015) LocZ is a new cell division protein involved in proper septum placement in *Streptococcus pneumoniae*. *mBio* **6**: e01700-01714.

Hu, Z. & J. Lutkenhaus, (1999) Topological regulation of cell division in *Escherichia coli* involves rapid pole to pole oscillation of the division inhibitor MinC under the control of MinD and MinE. *Molecular microbiology* **34**: 82-90.

Hu, Z. & J. Lutkenhaus, (2001) Topological regulation of cell division in *E. coli*. spatiotemporal oscillation of MinD requires stimulation of its ATPase by MinE and phospholipid. *Molecular cell* **7**: 1337-1343.

Hu, Z., A. Mukherjee, S. Pichoff & J. Lutkenhaus, (1999) The MinC component of the division site selection system in *Escherichia coli* interacts with FtsZ to prevent polymerization. *Proceedings of the National Academy of Sciences of the United States of America* **96**: 14819-14824.

Huisman, O. & R. D'Ari, (1981) An inducible DNA replication-cell division coupling mechanism in *E. coli*. *Nature* **290**: 797-799.

Huisman, O., R. D'Ari & S. Gottesman, (1984) Cell-division control in *Escherichia coli*: specific induction of the SOS function SfiA protein is sufficient to block septation. *Proceedings of the National Academy of Sciences of the United States of America* **81**: 4490-4494.

Huitema, E., S. Pritchard, D. Matteson, S.K. Radhakrishnan & P.H. Viollier, (2006) Bacterial birth scar proteins mark future flagellum assembly site. *Cell* **124**: 1025-1037.

Huneke, S., (2013) Untersuchung der Regulierung der Zellteilung in *Myxococcus xanthus*. Master Thesis. Philipps-Universität Marburg, Marburg, Germany.

Hwang, L.C., A.G. Vecchiarelli, Y.W. Han, M. Mizuuchi, Y. Harada, B.E. Funnell & K. Mizuuchi, (2013) ParA-mediated plasmid partition driven by protein pattern self-organization. *The EMBO journal* **32**: 1238-1249.

Ietswaart, R., F. Szardenings, K. Gerdes & M. Howard, (2014) Competing ParA structures space bacterial plasmids equally over the nucleoid. *PLoS computational biology* **10**: e1004009.

Iniesta, A.A., F. Garcia-Heras, J. Abellon-Ruiz, A. Gallego-Garcia & M. Elias-Arnanz, (2012) Two systems for conditional gene expression in *Myxococcus xanthus* inducible by isopropyl-beta-D-thiogalactopyranoside or vanillate. *Journal of bacteriology* **194**: 5875-5885.

Ireton, K. & A.D. Grossman, (1994) DNA-related conditions controlling the initiation of sporulation in *Bacillus subtilis*. *Cellular & molecular biology research* **40**: 193-198.

Ireton, K., N.W.t. Gunther & A.D. Grossman, (1994) *spo0J* is required for normal chromosome segregation as well as the initiation of sporulation in *Bacillus subtilis*. *Journal of bacteriology* **176**: 5320-5329.

Jakimowicz, D., B. Gust, J. Zakrzewska-Czerwinska & K.F. Chater, (2005) Developmental-stage-specific assembly of ParB complexes in *Streptomyces coelicolor* hyphae. *Journal of bacteriology* **187**: 3572-3580.

Jensen, R.B. & K. Gerdes, (1997) Partitioning of plasmid R1. The ParM protein exhibits ATPase activity and interacts with the centromere-like ParR-*parC* complex. *Journal of molecular biology* **269**: 505-513.

Julien, B., A.D. Kaiser & A. Garza, (2000) Spatial control of cell differentiation in *Myxococcus xanthus*. *Proceedings of the National Academy of Sciences of the United States of America* **97**: 9098-9103.

Justice, S.S., J. Garcia-Lara & L.I. Rothfield, (2000) Cell division inhibitors SulA and MinC/MinD block septum formation at different steps in the assembly of the *Escherichia coli* division machinery. *Molecular microbiology* **37**: 410-423.

Kaiser, D., C. Manoil & M. Dworkin, (1979) Myxobacteria: cell interactions, genetics, and development. *Annual review of microbiology* **33**: 595-639.

Karimova, G., N. Dautin & D. Ladant, (2005) Interaction network among *Escherichia coli* membrane proteins involved in cell division as revealed by bacterial two-hybrid analysis. *Journal of bacteriology* **187**: 2233-2243.

Katoh, K. & H. Toh, (2008) Recent developments in the MAFFT multiple sequence alignment program. *Briefings in bioinformatics* **9**: 286-298.

Kiekebusch, D., K.A. Michie, L.O. Essen, J. Lowe & M. Thanbichler, (2012) Localized dimerization and nucleoid binding drive gradient formation by the bacterial cell division inhibitor MipZ. *Molecular cell* **46**: 245-259.

Kim, H.J., M.J. Calcutt, F.J. Schmidt & K.F. Chater, (2000) Partitioning of the linear chromosome during sporulation of *Streptomyces coelicolor* A3(2) involves an *oriC*-linked *parAB* locus. *Journal of bacteriology* **182**: 1313-1320.

Koch, M.K., C.A. McHugh & E. Hoiczyk, (2011) BacM, an N-terminally processed bactofilin of *Myxococcus xanthus*, is crucial for proper cell shape. *Molecular microbiology* **80**: 1031-1051.

Krakoff, I.H., N.C. Brown & P. Reichard, (1968) Inhibition of ribonucleoside diphosphate reductase by hydroxyurea. *Cancer research* **28**: 1559-1565.

Kusumoto, A., K. Kamisaka, T. Yakushi, H. Terashima, A. Shinohara & M. Homma, (2006) Regulation of polar flagellar number by the *flhF* and *flhG* genes in *Vibrio alginolyticus*. *Journal of biochemistry* **139**: 113-121.

Laemmli, U.K., (1970) Cleavage of structural proteins during the assembly of the head of bacteriophage T4. *Nature* **227**: 680-685.

Lam, H., W.B. Schofield & C. Jacobs-Wagner, (2006) A landmark protein essential for establishing and perpetuating the polarity of a bacterial cell. *Cell* **124**: 1011-1023.

Lanzetta, P.A., L.J. Alvarez, P.S. Reinach & O.A. Candia, (1979) An improved assay for nanomole amounts of inorganic phosphate. *Analytical biochemistry* **100**: 95-97.

Larsen, R.A., C. Cusumano, A. Fujioka, G. Lim-Fong, P. Patterson & J. Pogliano, (2007) Treadmilling of a prokaryotic tubulin-like protein, TubZ, required for plasmid stability in *Bacillus thuringiensis*. *Genes & development* **21**: 1340-1352.

Le Quere, B. & J.M. Ghigo, (2009) BcsQ is an essential component of the *Escherichia coli* cellulose biosynthesis apparatus that localizes at the bacterial cell pole. *Molecular microbiology* **72**: 724-740.

Lee, P.S. & A.D. Grossman, (2006) The chromosome partitioning proteins Soj (ParA) and Spo0J (ParB) contribute to accurate chromosome partitioning, separation of replicated sister origins, and regulation of replication initiation in *Bacillus subtilis*. *Molecular microbiology* **60**: 853-869.

Leipe, D.D., Y.I. Wolf, E.V. Koonin & L. Aravind, (2002) Classification and evolution of P-loop GTPases and related ATPases. *Journal of molecular biology* **317**: 41-72.

Lenarcic, R., S. Halbedel, L. Visser, M. Shaw, L.J. Wu, J. Errington, D. Marenduzzo & L.W. Hamoen, (2009) Localisation of DivIVA by targeting to negatively curved membranes. *The EMBO journal* **28**: 2272-2282.

Leonard, T.A., P.J. Butler & J. Lowe, (2005) Bacterial chromosome segregation: structure and DNA binding of the Soj dimer--a conserved biological switch. *The EMBO journal* **24**: 270-282.

Letek, M., M. Fiuza, E. Ordonez, A.F. Villadangos, A. Ramos, L.M. Mateos & J.A. Gil, (2008a) Cell growth and cell division in the rod-shaped actinomycete *Corynebacterium glutamicum*. *Antonie van Leeuwenhoek* **94**: 99-109.

Letek, M., E. Ordonez, J. Vaquera, W. Margolin, K. Flardh, L.M. Mateos & J.A. Gil, (2008b) DivIVA is required for polar growth in the MreB-lacking rod-shaped actinomycete *Corynebacterium glutamicum*. *Journal of bacteriology* **190**: 3283-3292.

Letunic, I. & P. Bork, (2007) Interactive Tree Of Life (iTOL): an online tool for phylogenetic tree display and annotation. *Bioinformatics* **23**: 127-128.

Letunic, I. & P. Bork, (2011) Interactive Tree Of Life v2: online annotation and display of phylogenetic trees made easy. *Nucleic acids research* **39**: W475-478.

Letunic, I., T. Doerks & P. Bork, (2015) SMART: recent updates, new developments and status in 2015. *Nucleic acids research* **43**: D257-260.

Levin, P.A., I.G. Kurtser & A.D. Grossman, (1999) Identification and characterization of a negative regulator of FtsZ ring formation in *Bacillus subtilis*. *Proceedings of the National Academy of Sciences of the United States of America* **96**: 9642-9647.

Lewis, R.A., C.R. Bignell, W. Zeng, A.C. Jones & C.M. Thomas, (2002) Chromosome loss from *par* mutants of *Pseudomonas putida* depends on growth medium and phase of growth. *Microbiology* **148**: 537-548.

Li, W., A. Cowley, M. Uludag, T. Gur, H. McWilliam, S. Squizzato, Y.M. Park, N. Buso & R. Lopez, (2015) The EMBL-EBI bioinformatics web and programmatic tools framework. *Nucleic acids research* **43**: W580-584.

Li, Y., J. Hsin, L. Zhao, Y. Cheng, W. Shang, K.C. Huang, H.W. Wang & S. Ye, (2013) FtsZ protofilaments use a hinge-opening mechanism for constrictive force generation. *Science* **341**: 392-395.

Li, Z., M.J. Trimble, Y.V. Brun & G.J. Jensen, (2007) The structure of FtsZ filaments *in vivo* suggests a force-generating role in cell division. *The EMBO journal* **26**: 4694-4708.

Lim, G.E., A.I. Derman & J. Pogliano, (2005) Bacterial DNA segregation by dynamic SopA polymers. *Proceedings of the National Academy of Sciences of the United States of America* **102**: 17658-17663.

Lim, H.C., I.V. Surovtsev, B.G. Beltran, F. Huang, J. Bewersdorf & C. Jacobs-Wagner, (2014) Evidence for a DNA-relay mechanism in ParAB*S*-mediated chromosome segregation. *eLife* **3**: e02758.

Lin, D.C. & A.D. Grossman, (1998) Identification and characterization of a bacterial chromosome partitioning site. *Cell* **92**: 675-685.

Lindas, A.C., E.A. Karlsson, M.T. Lindgren, T.J. Ettema & R. Bernander, (2008) A unique cell division machinery in the Archaea. *Proceedings of the National Academy of Sciences of the United States of America* **105**: 18942-18946.

Livny, J., Y. Yamaichi & M.K. Waldor, (2007) Distribution of centromere-like *parS* sites in bacteria: insights from comparative genomics. *Journal of bacteriology* **189**: 8693-8703.

Loose, M. & T.J. Mitchison, (2014) The bacterial cell division proteins FtsA and FtsZ self-organize into dynamic cytoskeletal patterns. *Nature cell biology* **16**: 38-46.

Lowe, J. & L.A. Amos, (1998) Crystal structure of the bacterial cell-division protein FtsZ. *Nature* **391**: 203-206.

Lutkenhaus, J., (2012) The ParA/MinD family puts things in their place. *Trends in microbiology* **20**: 411-418.

Malik, H.S., T.H. Eickbush & D.S. Goldfarb, (1997) Evolutionary specialization of the nuclear targeting apparatus. *Proceedings of the National Academy of Sciences of the United States of America* **94**: 13738-13742.

Margolin, W., (2005) FtsZ and the division of prokaryotic cells and organelles. *Nature reviews. Molecular cell biology* **6**: 862-871.

Marston, A.L., H.B. Thomaides, D.H. Edwards, M.E. Sharpe & J. Errington, (1998) Polar localization of the MinD protein of *Bacillus subtilis* and its role in selection of the mid-cell division site. *Genes & development* **12**: 3419-3430.

Matroule, J.Y., H. Lam, D.T. Burnette & C. Jacobs-Wagner, (2004) Cytokinesis monitoring during development; rapid pole-to-pole shuttling of a signaling protein by localized kinase and phosphatase in *Caulobacter*. *Cell* **118**: 579-590.

McCormick, J.R. & R. Losick, (1996) Cell division gene *ftsQ* is required for efficient sporulation but not growth and viability in *Streptomyces coelicolor* A3(2). *Journal of bacteriology* **178**: 5295-5301.

McCormick, J.R., E.P. Su, A. Driks & R. Losick, (1994) Growth and viability of *Streptomyces coelicolor* mutant for the cell division gene *ftsZ*. *Molecular microbiology* **14**: 243-254.

Melby, T.E., C.N. Ciampaglio, G. Briscoe & H.P. Erickson, (1998) The symmetrical structure of structural maintenance of chromosomes (SMC) and MukB proteins: long, antiparallel coiled coils, folded at a flexible hinge. *The Journal of cell biology* **142**: 1595-1604.

Miertzschke, M., C. Koerner, I.R. Vetter, D. Keilberg, E. Hot, S. Leonardy, L. Sogaard-Andersen & A. Wittinghofer, (2011) Structural analysis of the Ras-like G protein MglA and its cognate GAP MglB and implications for bacterial polarity. *The EMBO journal* **30**: 4185-4197.

Mohl, D.A., J. Easter, Jr. & J.W. Gober, (2001) The chromosome partitioning protein, ParB, is required for cytokinesis in *Caulobacter crescentus*. *Molecular microbiology* **42**: 741-755.

Mohl, D.A. & J.W. Gober, (1997) Cell cycle-dependent polar localization of chromosome partitioning proteins in *Caulobacter crescentus*. *Cell* **88**: 675-684.

Moll, A. & M. Thanbichler, (2009) FtsN-like proteins are conserved components of the cell division machinery in proteobacteria. *Molecular microbiology* **72**: 1037-1053.

Moller-Jensen, J., J. Borch, M. Dam, R.B. Jensen, P. Roepstorff & K. Gerdes, (2003) Bacterial mitosis: ParM of plasmid R1 moves plasmid DNA by an actin-like insertional polymerization mechanism. *Molecular cell* **12**: 1477-1487.

Moller-Jensen, J., R.B. Jensen, J. Lowe & K. Gerdes, (2002) Prokaryotic DNA segregation by an actin-like filament. *The EMBO journal* **21**: 3119-3127.

Monahan, L.G., I.V. Hajduk, S.P. Blaber, I.G. Charles & E.J. Harry, (2014) Coordinating bacterial cell division with nutrient availability: a role for glycolysis. *mBio* **5**: e00935-00914.

Mosyak, L., Y. Zhang, E. Glasfeld, S. Haney, M. Stahl, J. Seehra & W.S. Somers, (2000) The bacterial cell-division protein ZipA and its interaction with an FtsZ fragment revealed by X-ray crystallography. *The EMBO journal* **19**: 3179-3191.

Mukherjee, A., C. Cao & J. Lutkenhaus, (1998) Inhibition of FtsZ polymerization by SulA, an inhibitor of septation in *Escherichia coli*. *Proceedings of the National Academy of Sciences of the United States of America* **95**: 2885-2890.

Mukherjee, A. & J. Lutkenhaus, (1994) Guanine nucleotide-dependent assembly of FtsZ into filaments. *Journal of bacteriology* **176**: 2754-2758.

Murray, H. & J. Errington, (2008) Dynamic control of the DNA replication initiation protein DnaA by Soj/ParA. *Cell* **135**: 74-84.

Murray, H., H. Ferreira & J. Errington, (2006) The bacterial chromosome segregation protein Spo0J spreads along DNA from *parS* nucleation sites. *Molecular microbiology* **61**: 1352-1361.

Niki, H. & S. Hiraga, (1997) Subcellular distribution of actively partitioning F plasmid during the cell division cycle in *E. coli*. *Cell* **90**: 951-957.

Niki, H., A. Jaffe, R. Imamura, T. Ogura & S. Hiraga, (1991) The new gene *mukB* codes for a 177 kd protein with coiled-coil domains involved in chromosome partitioning of *E. coli*. *The EMBO journal* **10**: 183-193.

Oliva, M.A., S.C. Cordell & J. Lowe, (2004) Structural insights into FtsZ protofilament formation. *Nature structural & molecular biology* **11**: 1243-1250.

Orlova, A., E.C. Garner, V.E. Galkin, J. Heuser, R.D. Mullins & E.H. Egelman, (2007) The structure of bacterial ParM filaments. *Nature structural & molecular biology* **14**: 921-926.

Osawa, M., D.E. Anderson & H.P. Erickson, (2008) Reconstitution of contractile FtsZ rings in liposomes. *Science* **320**: 792-794.

Osawa, M., D.E. Anderson & H.P. Erickson, (2009) Curved FtsZ protofilaments generate bending forces on liposome membranes. *The EMBO journal* **28**: 3476-3484.

Park, K.T., W. Wu, K.P. Battaile, S. Lovell, T. Holyoak & J. Lutkenhaus, (2011) The Min oscillator uses MinD-dependent conformational changes in MinE to spatially regulate cytokinesis. *Cell* **146**: 396-407.

Park, K.T., W. Wu, S. Lovell & J. Lutkenhaus, (2012) Mechanism of the asymmetric activation of the MinD ATPase by MinE. *Molecular microbiology* **85**: 271-281.

Patrick, J.E. & D.B. Kearns, (2008) MinJ (YvjD) is a topological determinant of cell division in *Bacillus subtilis*. *Molecular microbiology* **70**: 1166-1179.

Pichoff, S. & J. Lutkenhaus, (2002) Unique and overlapping roles for ZipA and FtsA in septal ring assembly in *Escherichia coli*. *The EMBO journal* **21**: 685-693.

Pichoff, S. & J. Lutkenhaus, (2005) Tethering the Z ring to the membrane through a conserved membrane targeting sequence in FtsA. *Molecular microbiology* **55**: 1722-1734.

Pogliano, J., K. Pogliano, D.S. Weiss, R. Losick & J. Beckwith, (1997) Inactivation of FtsI inhibits constriction of the FtsZ cytokinetic ring and delays the assembly of FtsZ rings at potential division sites. *Proceedings of the National Academy of Sciences of the United States of America* **94**: 559-564.

Popp, D., A. Narita, T. Oda, T. Fujisawa, H. Matsuo, Y. Nitanai, M. Iwasa, K. Maeda, H. Onishi & Y. Maeda, (2008) Molecular structure of the ParM polymer and the mechanism leading to its nucleotide-driven dynamic instability. *The EMBO journal* **27**: 570-579.

Pratto, F., A. Cicek, W.A. Weihofen, R. Lurz, W. Saenger & J.C. Alonso, (2008) *Streptococcus pyogenes* pSM19035 requires dynamic assembly of ATP-bound ParA and ParB on *parS* DNA during plasmid segregation. *Nucleic acids research* **36**: 3676-3689.

Ptacin, J.L., S.F. Lee, E.C. Garner, E. Toro, M. Eckart, L.R. Comolli, W.E. Moerner & L. Shapiro, (2010) A spindle-like apparatus guides bacterial chromosome segregation. *Nature cell biology* **12**: 791-798.

Raiborg, C. & H. Stenmark, (2009) The ESCRT machinery in endosomal sorting of ubiquitylated membrane proteins. *Nature* **458**: 445-452.

Raskin, D.M. & P.A. de Boer, (1997) The MinE ring: an FtsZ-independent cell structure required for selection of the correct division site in *E. coli*. *Cell* **91**: 685-694.

Raskin, D.M. & P.A. de Boer, (1999a) MinDE-dependent pole-to-pole oscillation of division inhibitor MinC in *Escherichia coli*. *Journal of bacteriology* **181**: 6419-6424.

Raskin, D.M. & P.A. de Boer, (1999b) Rapid pole-to-pole oscillation of a protein required for directing division to the middle of *Escherichia coli*. *Proceedings of the National Academy of Sciences of the United States of America* **96**: 4971-4976.

Reyes-Lamothe, R., T. Tran, D. Meas, L. Lee, A.M. Li, D.J. Sherratt & M.E. Tolmasky, (2014) High-copy bacterial plasmids diffuse in the nucleoid-free space, replicate stochastically and are randomly partitioned at cell division. *Nucleic acids research* **42**: 1042-1051.

Ringgaard, S., K. Schirner, B.M. Davis & M.K. Waldor, (2011) A family of ParA-like ATPases promotes cell pole maturation by facilitating polar localization of chemotaxis proteins. *Genes & development* **25**: 1544-1555.

Ringgaard, S., J. van Zon, M. Howard & K. Gerdes, (2009) Movement and equipositioning of plasmids by ParA filament disassembly. *Proceedings of the National Academy of Sciences of the United States of America* **106**: 19369-19374.

Ringgaard, S., M. Zepeda-Rivera, X. Wu, K. Schirner, B.M. Davis & M.K. Waldor, (2014) ParP prevents dissociation of CheA from chemotactic signaling arrays and tethers them to a polar anchor. *Proceedings of the National Academy of Sciences of the United States of America* **111**: E255-264.

Roberts, M.A., G.H. Wadhams, K.A. Hadfield, S. Tickner & J.P. Armitage, (2012) ParA-like protein uses nonspecific chromosomal DNA binding to partition protein complexes. *Proceedings of the National Academy of Sciences of the United States of America* **109**: 6698-6703.

Rodionov, O., M. Lobocka & M. Yarmolinsky, (1999) Silencing of genes flanking the P1 plasmid centromere. *Science* **283**: 546-549.

Rosen, B.P., (2002) Transport and detoxification systems for transition metals, heavy metals and metalloids in eukaryotic and prokaryotic microbes. *Comparative biochemistry and physiology. Part A, Molecular & integrative physiology* **133**: 689-693.

Rosen, B.P., U. Weigel, C. Karkaria & P. Gangola, (1988a) Molecular characterization of a unique anion pump: the ArsA protein is an arsenite(antimonate)-stimulated ATPase. *Progress in clinical and biological research* **273**: 105-112.

Rosen, B.P., U. Weigel, C. Karkaria & P. Gangola, (1988b) Molecular characterization of an anion pump. The arsA gene product is an arsenite(antimonate)-stimulated ATPase. *The Journal of biological chemistry* **263**: 3067-3070.

Rothfield, L., A. Taghbalout & Y.L. Shih, (2005) Spatial control of bacterial division-site placement. *Nature reviews. Microbiology* **3**: 959-968.

Salje, J. & J. Lowe, (2008) Bacterial actin: architecture of the ParMR*C* plasmid DNA partitioning complex. *The EMBO journal* **27**: 2230-2238.

Salje, J., B. Zuber & J. Lowe, (2009) Electron cryomicroscopy of *E. coli* reveals filament bundles involved in plasmid DNA segregation. *Science* **323**: 509-512.

Samson, R.Y., T. Obita, S.M. Freund, R.L. Williams & S.D. Bell, (2008) A role for the ESCRT system in cell division in archaea. *Science* **322**: 1710-1713.

Samson, R.Y., T. Obita, B. Hodgson, M.K. Shaw, P.L. Chong, R.L. Williams & S.D. Bell, (2011) Molecular and structural basis of ESCRT-III recruitment to membranes during archaeal cell division. *Molecular cell* **41**: 186-196.

Savage, D.F., B. Afonso, A.H. Chen & P.A. Silver, (2010) Spatially ordered dynamics of the bacterial carbon fixation machinery. *Science* **327**: 1258-1261.

Scheffers, D. & A.J. Driessen, (2001) The polymerization mechanism of the bacterial cell division protein FtsZ. *FEBS letters* **506**: 6-10.

Schofield, W.B., H.C. Lim & C. Jacobs-Wagner, (2010) Cell cycle coordination and regulation of bacterial chromosome segregation dynamics by polarly localized proteins. *The EMBO journal* **29**: 3068-3081.

Schuhmacher, J.S., F. Rossmann, F. Dempwolff, C. Knauer, F. Altegoer, W. Steinchen, A.K. Dorrich, A. Klingl, M. Stephan, U. Linne, K.M. Thormann & G. Bange, (2015) MinD-like ATPase FlhG effects location and number of bacterial flagella during C-ring assembly. *Proceedings of the National Academy of Sciences of the United States of America* **112**: 3092-3097.

Schultz, J., F. Milpetz, P. Bork & C.P. Ponting, (1998) SMART, a simple modular architecture research tool: identification of signaling domains. *Proceedings of the National Academy of Sciences of the United States of America* **95**: 5857-5864.

Schumacher, D., (2011) Analyse der Funktion von PomY während der Zellteilung von *Myxococcus xanthus*. Master Thesis. Philipps-Universität Marburg, Marburg, Germany.

Schwedock, J., J.R. McCormick, E.R. Angert, J.R. Nodwell & R. Losick, (1997) Assembly of the cell division protein FtsZ into ladder-like structures in the aerial hyphae of *Streptomyces coelicolor*. *Molecular microbiology* **25**: 847-858.

Shi, X., S. Wegener-Feldbrugge, S. Huntley, N. Hamann, R. Hedderich & L. Sogaard-Andersen, (2008) Bioinformatics and experimental analysis of proteins of two-component systems in *Myxococcus xanthus*. *Journal of bacteriology* **190**: 613-624.

Small, E., R. Marrington, A. Rodger, D.J. Scott, K. Sloan, D. Roper, T.R. Dafforn & S.G. Addinall, (2007) FtsZ polymer-bundling by the Escherichia coli ZapA orthologue, YgfE, involves a conformational change in bound GTP. *Journal of molecular biology* **369**: 210-221.

Stricker, J., P. Maddox, E.D. Salmon & H.P. Erickson, (2002) Rapid assembly dynamics of the *Escherichia coli* FtsZ-ring demonstrated by fluorescence recovery after photobleaching. *Proceedings of the National Academy of Sciences of the United States of America* **99**: 3171-3175.

Stühn, L., (2013) Analyse des ParA-like Proteins Mxan_3348 und des SMC-Proteins Mxan_4901 in *Myxococcus xanthus*. Bachelor of Science.

Szeto, T.H., S.L. Rowland, C.L. Habrukowich & G.F. King, (2003) The MinD membrane targeting sequence is a transplantable lipid-binding helix. *The Journal of biological chemistry* **278**: 40050-40056.

Szeto, T.H., S.L. Rowland, L.I. Rothfield & G.F. King, (2002) Membrane localization of MinD is mediated by a C-terminal motif that is conserved across eubacteria, archaea, and chloroplasts. *Proceedings of the National Academy of Sciences of the United States of America* **99**: 15693-15698.

Szwedziak, P., Q. Wang, T.A. Bharat, M. Tsim & J. Lowe, (2014) Architecture of the ring formed by the tubulin homologue FtsZ in bacterial cell division. *eLife* **3**: e04601.

Thanbichler, M., (2010) Synchronization of chromosome dynamics and cell division in bacteria. *Cold Spring Harbor perspectives in biology* **2**: a000331.

Thanbichler, M. & L. Shapiro, (2006) MipZ, a spatial regulator coordinating chromosome segregation with cell division in *Caulobacter*. *Cell* **126**: 147-162.

Thompson, S.R., G.H. Wadhams & J.P. Armitage, (2006) The positioning of cytoplasmic protein clusters in bacteria. *Proceedings of the National Academy of Sciences of the United States of America* **103**: 8209-8214.

Tisa, L.S. & B.P. Rosen, (1990) Molecular characterization of an anion pump. The ArsB protein is the membrane anchor for the ArsA protein. *The Journal of biological chemistry* **265**: 190-194.

Tonthat, N.K., S.L. Milam, N. Chinnam, T. Whitfill, W. Margolin & M.A. Schumacher, (2013) SlmA forms a higher-order structure on DNA that inhibits cytokinetic Z-ring formation over the nucleoid. *Proceedings of the National Academy of Sciences of the United States of America* **110**: 10586-10591.

Treuner-Lange, A., K. Aguiluz, C. van der Does, N. Gomez-Santos, A. Harms, D. Schumacher, P. Lenz, M. Hoppert, J. Kahnt, J. Munoz-Dorado & L. Sogaard-Andersen, (2013) PomZ, a ParA-like protein, regulates Z-ring formation and cell division in *Myxococcus xanthus*. *Molecular microbiology* **87**: 235-253.

Treuner-Lange, A. & L. Sogaard-Andersen, (2014) Regulation of cell polarity in bacteria. *The Journal of cell biology* **206**: 7-17.

Trudeau, K.G., M.J. Ward & D.R. Zusman, (1996) Identification and characterization of FrzZ, a novel response regulator necessary for swarming and fruiting-body formation in *Myxococcus xanthus*. *Molecular microbiology* **20**: 645-655.

Trusca, D., S. Scott, C. Thompson & D. Bramhill, (1998) Bacterial SOS checkpoint protein SulA inhibits polymerization of purified FtsZ cell division protein. *Journal of bacteriology* **180**: 3946-3953.

Typas, A., M. Banzhaf, C.A. Gross & W. Vollmer, (2012) From the regulation of peptidoglycan synthesis to bacterial growth and morphology. *Nature reviews. Microbiology* **10**: 123-136.

van Baarle, S. & M. Bramkamp, (2010) The MinCDJ system in *Bacillus subtilis* prevents minicell formation by promoting divisome disassembly. *PloS one* **5**: e9850.

Vecchiarelli, A.G., Y.W. Han, X. Tan, M. Mizuuchi, R. Ghirlando, C. Biertumpfel, B.E. Funnell & K. Mizuuchi, (2010) ATP control of dynamic P1 ParA-DNA interactions: a key role for the nucleoid in plasmid partition. *Molecular microbiology* **78**: 78-91.

Vecchiarelli, A.G., J.C. Havey, L.L. Ing, E.O. Wong, W.G. Waples & B.E. Funnell, (2013a) Dissection of the ATPase active site of P1 ParA reveals multiple active forms essential for plasmid partition. *The Journal of biological chemistry* **288**: 17823-17831.

Vecchiarelli, A.G., L.C. Hwang & K. Mizuuchi, (2013b) Cell-free study of F plasmid partition provides evidence for cargo transport by a diffusion-ratchet mechanism. *Proceedings of the National Academy of Sciences of the United States of America* **110**: E1390-1397.

Vecchiarelli, A.G., K. Mizuuchi & B.E. Funnell, (2012) Surfing biological surfaces: exploiting the nucleoid for partition and transport in bacteria. *Molecular microbiology* **86**: 513-523.

Vecchiarelli, A.G., K.C. Neuman & K. Mizuuchi, (2014a) A propagating ATPase gradient drives transport of surface-confined cellular cargo. *Proceedings of the National Academy of Sciences of the United States of America* **111**: 4880-4885.

Vecchiarelli, A.G., Y. Seol, K.C. Neuman & K. Mizuuchi, (2014b) A moving ParA gradient on the nucleoid directs subcellular cargo transport via a chemophoresis force. *Bioarchitecture* **4**: 154-159.

Vecchiarelli, A.G., J.A. Taylor & K. Mizuuchi, (2015) Reconstituting ParA/ParB-mediated transport of DNA cargo. *Methods in cell biology* **128**: 243-269.

Viollier, P.H., M. Thanbichler, P.T. McGrath, L. West, M. Meewan, H.H. McAdams & L. Shapiro, (2004) Rapid and sequential movement of individual chromosomal loci to specific subcellular locations during bacterial DNA replication. *Proceedings of the National Academy of Sciences of the United States of America* **101**: 9257-9262.

Weart, R.B., A.H. Lee, A.C. Chien, D.P. Haeusser, N.S. Hill & P.A. Levin, (2007) A metabolic sensor governing cell size in bacteria. *Cell* **130**: 335-347.

Weart, R.B., S. Nakano, B.E. Lane, P. Zuber & P.A. Levin, (2005) The ClpX chaperone modulates assembly of the tubulin-like protein FtsZ. *Molecular microbiology* **57**: 238-249.

Willemse, J., J.W. Borst, E. de Waal, T. Bisseling & G.P. van Wezel, (2011) Positive control of cell division: FtsZ is recruited by SsgB during sporulation of *Streptomyces*. *Genes & development* **25**: 89-99.

Williamson, M.P., (1994) The structure and function of proline-rich regions in proteins. *The Biochemical journal* **297 (Pt 2)**: 249-260.

Woldringh, C.L., E. Mulder, P.G. Huls & N. Vischer, (1991) Toporegulation of bacterial division according to the nucleoid occlusion model. *Research in microbiology* **142**: 309-320.

Woldringh, C.L., E. Mulder, J.A. Valkenburg, F.B. Wientjes, A. Zaritsky & N. Nanninga, (1990) Role of the nucleoid in the toporegulation of division. *Research in microbiology* **141**: 39-49.

Wu, L.J. & J. Errington, (1994) Bacillus subtilis SpoIIIE protein required for DNA segregation during asymmetric cell division. *Science* **264**: 572-575.

Wu, L.J. & J. Errington, (2004) Coordination of cell division and chromosome segregation by a nucleoid occlusion protein in *Bacillus subtilis*. *Cell* **117**: 915-925.

Wu, L.J., S. Ishikawa, Y. Kawai, T. Oshima, N. Ogasawara & J. Errington, (2009) Noc protein binds to specific DNA sequences to coordinate cell division with chromosome segregation. *The EMBO journal* **28**: 1940-1952.

Wu, S.S., J. Wu & D. Kaiser, (1997) The *Myxococcus xanthus pilT* locus is required for social gliding motility although pili are still produced. *Molecular microbiology* **23**: 109-121.

Yamaichi, Y., M.A. Fogel & M.K. Waldor, (2007) par genes and the pathology of chromosome loss in Vibrio cholerae. *Proceedings of the National Academy of Sciences of the United States of America* **104**: 630-635.

Yeh, Y.C., L.R. Comolli, K.H. Downing, L. Shapiro & H.H. McAdams, (2010) The *caulobacter* Tol-Pal complex is essential for outer membrane integrity and the positioning of a polar localization factor. *Journal of bacteriology* **192**: 4847-4858.

Yu, X.C., A.H. Tran, Q. Sun & W. Margolin, (1998a) Localization of cell division protein FtsK to the *Escherichia coli* septum and identification of a potential N-terminal targeting domain. *Journal of bacteriology* **180**: 1296-1304.

Yu, X.C., E.K. Weihe & W. Margolin, (1998b) Role of the C terminus of FtsK in Escherichia coli chromosome segregation. *Journal of bacteriology* **180**: 6424-6428.

Acknowledgment/Danksagung

Diese Dissertation wäre niemals entstanden ohne die Hilfe zahlreicher Menschen, die mich während der letzten Jahre unterstützt, mich in schweren und anstrengenden Zeiten aufgebaut und mir mein tägliches Leben auf verschiedene Arten erleichtert haben. Nachfolgend möchte ich diesen Menschen aus tiefstem Herzen dafür danken.

Zuerst möchte ich meinen herzlichen Dank an Lotte Søgaard-Andersen aussprechen. Sie hat mich seit mittlerweile fünf Jahren unterstützt und gefördert, motiviert neue Wege zu gehen und schwierige Dinge zu versuchen, mich kritisiert und gelehrt kritisch zu sein, aber auch wieder aufgebaut wenn ich Probleme in meinem Projekt hatte. Damit hat sie es mir ermöglicht mich wissenschaftlich aber auch persönlich weiterzuentwickeln. Aus all diesen Gründen möchte ich mich bei ihr für diese erfolgreiche und anstrengende, aber auch überraschende und interessante Reise bedanken.

Prof. Martin Thanbichler möchte ich dafür danken, dass auch er in den letzten Jahren stets mit Kritik und Rat zur Seite stand wenn Probleme zu lösen waren, oder einfach nur für Diskussionen, um im Labor und beim Schreiben des Papers weiterzukommen. Des Weiteren danke ich ihm für seine Arbeit als Zweitgutachter meine Dissertation.

Mein Dank gilt ebenfalls den weiteren Mitgliedern meiner Prüfungskommission Prof. Dr. Hans-Ulrich Mösch und Prof. Dr. Renate Renkawitz-Pohl, sowie den Mitgliedern meines IMPRS-Komitees Prof. Dr. Torsten Waldminghaus und Prof. Dr. Michael Bölker.

Andrea Harms möchte ich einen großen Dank aussprechen für die Mühen, die sie sich gemacht hat um mir im täglichen Labor-Alltag zu helfen. Für die Arbeit, die wir gemeinsam in den vielen Langzeitversuchen hatten, für die vielen Stunden, in denen wir gemeinsam in Frankfurt gearbeitet haben aber nicht zuletzt auch für die mentale Unterstützung ohne die ich das Projekt nicht so weit hätte vorantreiben können, so wie es jetzt ist.

Ich möchte weiter tiefen Dank an Anke Treuner-Lange, Susanne Kneip, Sabrina Huneke und Steffi Lindow aussprechen, die mich ebenfalls auf täglicher Basis im Laborleben sowie im privaten Leben unterstützt haben. Des Weiteren gilt mein Dank allen anderen Mitgliedern der Arbeitsgruppe für die vielen anstrengenden und fröhlichen Stunden, die wir zusammen verbracht haben.

Ich möchte mich bei meinen Freunden Manu, Désirée, Almuth, Kristina, Sabrina, Christoph und Isa dafür bedanken, dass sie für mich da waren während all der Zeit und sich immer mein Geheule angehört haben.

Zuletzt danke ich von ganzem Herzen meinen Eltern, sowie meiner Tante Beate und ihrem Mann Christian für die unendliche Unterstützung in allen Situationen der letzten Jahre, für ihr Interesse an meinem Leben und meiner Arbeit, für das immerwährende Verständnis und die vielen aufbauenden Worte. Ohne euch hätte diese Arbeit nicht gelingen können.

Danke!

Curriculum Vitae

Personal data

Name	Dominik Schumacher
Date of birth	01.05.1986
Place of birth	Arnsberg, Germany

Education

08/1996 – 06/2005 **Allgemeine Hochschulreife, Abitur**
Städtisches Gymnasium Laurentianum, Arnsberg

10/2006 – 07/2009 **Bachelor of Science - Biology**
Philipps-Universität Marburg

Bachelor Thesis: “Funktionelle Analyse des GbsR Repressors aus *Bacillus subtilis* durch ortsgerichtete Mutagenese”
Supervisor: Prof. Dr. Erhard Bremer

10/2009 – 09/2011 **Master of Science – Molecular and Cellular Biology**
Philipps-Universität Marburg

Master Thesis: “Analyse der Funktion von PomY während der Zellteilung von *Myxococcus xanthus*”
Supervisor: Prof. Dr. MD. Lotte Søgaard-Andersen

10/2011 – 08/2015 **PhD (Dr. rer. nat.)**
Philipps-Universität Marburg/ Max-Planck-Institut für terrestrische Mikrobiologie

PhD Thesis: “The PomXYZ cell division regulators self-organize on the nucleoid to position cell division at midcell in the rod-shaped bacterium *Myxococcus xanthus*”
Supervisor: Prof. Dr. MD. Lotte Søgaard-Andersen

Marburg, den _____._____._____ _____

Dominik Schumacher

List of publications:

Treuner-Lange, A., Aguiluz, K., van der Does, C., Gómez-Santos, N., Lenz, P., Harms, A., **Schumacher, D.**, Hoppert, M., Kahnt, J., Muñoz-Dorado, J. & Søgaard-Andersen, L. (2013). PomZ, a ParA-like protein, regulates Z-ring formation and cell division in *Myxococcus xanthus*. Mol. Microbiol. 87, 235-253.

Harms, A., Treuner-Lange, A., **Schumacher, D.** & Søgaard-Andersen, L. (2013). Tracking of chromosome and replisome dynamics in *Myxococcus xanthus* reveals a novel chromosome arrangement. PLoS Genet. 9, e1003802.

Schumacher, D., Bergeler, S., Harms, A., Vonck, J., Huneke, S., Frey, E., & Søgaard-Andersen, L. (2016). PomXYZ proteins self-organize on the nucleoid to regulate cell division (in preparation).

Erklärung

Hiermit versichere ich, dass ich die vorliegende Dissertation mit dem Titel

“The PomXYZ cell division regulators self-organize on the nucleoid to position cell division at midcell in the rod-shaped bacterium *Myxococcus xanthus*”

selbstständig verfasst, keine anderen als die im Text angegebenen Hilfsmittel verwendet und sämtliche Stellen, die dem Wortlaut oder dem Sinn nach aus anderen Werken entnommen sind, mit Quellenangabe kenntlich gemacht habe. Die Dissertation wurde in der jetzigen oder einer ähnlichen Form noch bei keiner anderen Hochschule eingereicht und hat noch keinem anderen Prüfungszweck gedient.

Marburg, den _____._____._____ _____

Dominik Schumacher

Einverständniserklärung

Hiermit erkläre ich mich einverstanden, dass die vorliegende Dissertation mit dem Titel

“The PomXYZ cell division regulators self-organize on the nucleoid to position cell division at midcell in the rod-shaped bacterium *Myxococcus xanthus*”

in Bibliotheken allgemein zugänglich gemacht wird. Dazu gehört, dass sie

- von der Bibliothek der Einrichtung, in der meine Dissertation angefertigt wurde, zur Benutzung in ihren Räumen bereitgehalten wird;
- in konventionellen und maschinenlesbaren Katalogen, Verzeichnissen und Datenbanken verzeichnet wird;
- im Rahmen der urheberrechtlichen Bestimmungen für Kopierzwecke benutzt werden kann.

Marburg, den _____._____._____ _____

Dominik Schumacher

_____

Prof. Dr. MD Lotte Søgaard-Andersen